

**Design, synthesis, and physicochemical characterization of
semifluorinated triphilic surfactants with applications for hydrophobic
drug delivery**

by

William Benjamin Tucker

A dissertation submitted in partial fulfillment of
the requirements for the degree of

Doctor of Philosophy

(Chemistry)

at the

UNIVERSITY OF WISCONSIN-MADISON

2015

Date of final oral examination: July 8, 2015

The dissertation is approved by the following members of the Final Oral Committee:

Sandro Mecozzi, Associate Professor, Department of Chemistry and School of Pharmacy
Robert J. McMahon, Professor, Department of Chemistry
Samuel H. Gellman, Professor, Department of Chemistry
Glen S. Kwon, Professor, School of Pharmacy
Charles T. Lauhon, Associate Professor, School of Pharmacy

**Design, synthesis, and physicochemical characterization of
semifluorinated triphilic surfactants with applications for hydrophobic
drug delivery**

William Benjamin Tucker

Under the supervision of Professor Sandro Mecozzi

At the University of Wisconsin-Madison

ABSTRACT

The use of PEGylated amphiphiles in drug-delivery systems has found widespread use in micelle and nanoemulsion formulations due to their unique benefits: drug solubilization above its aqueous solubility; the obviation of complex syntheses through the self-assembly; high-efficacy of drug delivery due to small average particles sizes. Despite the successes of micellar and nanoemulsion systems, stability remains an issue. Triphilic surfactants – those containing hydrophilic, lipophilic and fluorophilic moieties – have, to date, only been objects of peripheral interest to drug delivery. This work investigates triphilic design, behavior, and potential application in delivering hydrophobic pharmaceuticals.

The incorporation of fluorinated blocks can be accomplished by various means, with Williamson ether syntheses being common. Fluorotelomer alcohols $(F(CF_2)_x(CH_2)_2OH)$, however, show exceptional instability under basic conditions. An intramolecular hydrogen bond seems to dramatically increase the decomposition of fluorotelomer alcohols under basic conditions. Differences in decomposition among fluorotelomer alcohols of different lengths were found to depend on their respective solubility.

Syntheses for both linear and dibranched, triphilic surfactants were devised and carried out to prepare series of triphiles with various, terminal perfluoroalkoxy groups. The addition of terminal fluorinated substituents was found to lead to increases in thermodynamic (lower critical micelle concentration) and kinetic (increased resistance to dissociation) stability. These data suggest that the placement of fluorocarbons, not just their presence, is important in triphilic design. The ability of linear and dibranched triphiles to encapsulate paclitaxel (a model hydrophobic drug) was also shown to increase with the presence of and increasing size of fluorinated substituents.

Nanoemulsions are non-equilibrium drug delivery systems that can suffer from poor rapid particle size growth. The formulation of anesthetic nanoemulsions was studied to evaluate the effectiveness of triphilic surfactants in decreasing particle-size growth. A 30 vol% isoflurane formulation was developed, the highest concentration yet achieved in isoflurane emulsification; however, attempts to increase stability of this emulsion have so far proven unsuccessful. Triphilic surfactants proved successful at formulating highly stable, propofol nanoemulsions. Three propofol formulations were selected for *in vivo* evaluation in rat models, where efficacy similar to the clinically used Diprivan® formulation was observed.

ACKNOWLEDGMENTS

I would first like to thank my advisor Sandro Mecozzi for his encouragement, guidance, support, and patience over these last five years. I would also like to acknowledge the members of my thesis committee for their time and support in this process: Professors Bob McMahon, Sam Gellman, Glen Kwon and Chuck Lauhon. I would like to extend a thank you to the Kwon group for their assistance in these endeavors. Thank you to Dr. Robert Pearce, Dr. Colby Parks, Dr. Corey Amlong, and Mark Perkins for their support, collaboration, and insights.

I would like to acknowledge the faculty and staff at the Department of Chemistry and the School of Pharmacy here at the University of Wisconsin-Madison. Specifically, I would like to thank the Analytical Instrumentation Center at the School of Pharmacy, including the tireless efforts and invaluable aid of Dr. Tom Stringfellow, Dr. Cameron Scarlet, and Gary Girdaukas. I am also indebted to Dr. Martha Vestling in the Department of Chemistry for her considerable mass spectrometry work.

Thank you to the Mecozzi group, members current and former, for your helpful suggestions, great advice, fun work atmosphere, and innumerable small efforts you made to make graduate school better. I would like to extend a special thanks to Dr. Jun-Pil Jee, and Dr. Aaron McCoy for all of your help and assistance. I want to especially thank Dr. Sarah Decato for being an amazing friend, lab mate, and for being the Ashburn to my Mullins.

Finally, I am very grateful to my family. Without your ongoing and unconditional support over the years, I am very certain I would not be where I am today. Thank you, more than I can adequately express, for the intangible things you have always provided.

TABLE OF CONTENTS

ABSTRACT	i
ACKNOWLEDGMENTS	iii
TABLE OF CONTENTS	iv
LIST OF FIGURES AND TABLES	viii
LIST OF ABBREVIATIONS	xii
CHAPTER 1: Introduction	1
1.1 Introduction	2
<i>1.1.1 Perfluorocarbon physical properties</i>	<i>2</i>
<i>1.1.2 Fluorinated materials</i>	<i>3</i>
<i>1.1.3 Perfluorocarbons in medicine.....</i>	<i>5</i>
1.2 Micellar drug delivery	6
<i>1.2.1 Micelle structure and dynamics</i>	<i>6</i>
<i>1.2.2 Micelle drug delivery vehicles</i>	<i>11</i>
<i>1.2.3 Fluorosurfactants in micellar drug delivery.....</i>	<i>14</i>
<i>1.2.4 Micelle instability and triphilic surfactants.....</i>	<i>15</i>
1.3 Nanoemulsion drug delivery	16
<i>1.3.1 Nanoemulsion - formulation</i>	<i>16</i>
<i>1.3.2 Nanoemulsion - stability</i>	<i>18</i>
<i>1.3.3 Fluorinated anesthetic nanoemulsion.....</i>	<i>19</i>
<i>1.3.4 Hydrophobic-pharmaceutical nanoemulsions</i>	<i>21</i>
1.4 Thesis Objectives and Overview	21
1.5 References	22
CHAPTER 2: Synthetic challenges in fluorinated synthesis – decomposition of fluorotelomer alcohols	35

Abstract	36
2.1 Introduction	37
2.2 Results and Discussion	38
2.2.1 <i>Anomalous behavior of fluorotelomer alcohols in synthesis</i>	38
2.2.2 <i>Decomposition of fluorotelomer alcohols of different sizes</i>	39
2.2.3 <i>Fluorotelomer alcohol decomposition – mechanistic investigations</i>	42
2.2.4 <i>Alcohol and base – solubility and stability</i>	44
2.3 Conclusions	49
2.4 Experimental	49
2.4.1 <i>Materials</i>	49
2.4.2 <i>Methods</i>	50
2.5 References	50
CHAPTER 3: Relationship between structure and behavior of semifluorinated triphilic surfactants	54
Abstract	55
3.1 Introduction	56
3.2 Results and Discussion	58
3.2.1 <i>Design of triphilic surfactants</i>	58
3.2.2 <i>Synthesis of triphilic surfactants</i>	59
3.2.3 <i>Characterization of surfactants - MW, microviscosity, CMC</i>	62
3.2.4 <i>Characterization of triphilic micelles – kinetic stability</i>	68
3.2.5 <i>Characterization of triphilic micelles – hydrophobic-drug encapsulation</i>	70
3.3 Conclusions	73
3.4 Experimental	74
3.4.1 <i>Materials</i>	74
3.4.2 <i>mPEG mesylate (Mx-OMs) synthesis</i>	75

3.4.3 Linear and dibranched alcohol syntheses.....	76
3.4.4 Miktoarm alcohol syntheses.....	81
3.4.5 Linear and dibranched triphile syntheses.....	85
3.4.6 Miktoarm triphile syntheses.....	88
3.4.7 Physicochemical characterization.....	88
3.5 References	92
CHAPTER 4: Triphilic surfactant-based anesthetic nanoemulsions	97
Abstract	98
4.1 Introduction	99
4.2 Results and Discussion.....	103
4.2.1 Isoflurane nanoemulsion formulation.....	103
4.2.2 Propofol nanoemulsion formulation.....	106
4.2.3 Propofol in vivo testing	111
4.3 Conclusions	116
4.4 Experimental	117
4.4.1 Materials.....	117
4.4.2 Surfactant synthesis	118
4.4.3 Emulsion preparation	118
4.4.4 Animal Testing.....	119
4.4.5 Statistical Analysis.....	121
4.5 References	122
Appendix 1: Redesigned triphilic surfactants for hydrophobic pharmaceutical nanoemulsions	128
Abstract	129
A1.1 Introduction	130
A1.2 Results and Discussion.....	131

<i>A1.2.1 Redesigned triphilic synthesis and characterization</i>	131
<i>A1.2.2 Paclitaxel emulsion formulation</i>	132
A1.3 Conclusions	134
A1.4 Experimental.....	136
<i>A1.4.1 Materials</i>	136
<i>A1.4.2 M2F8-O-H18 synthesis</i>	136
<i>A1.4.3 M2F8-O-H18 characterization</i>	139
<i>A1.4.4 Emulsion preparation</i>	140
A1.5 References	141
Appendix 2: Supplementary Data	144
A2.1 Fluorotelomer alcohol decomposition data	145
A2.2 Triphilic surfactant data.....	167
<i>A2.2.1. NMR spectra</i>	167
<i>A2.2.2. MALDI spectra</i>	246
<i>A2.2.3. DLS data</i>	254
<i>A2.2.4. CMC data</i>	261
<i>A2.2.5. Microviscosity data</i>	277
<i>A2.2.6. FRET stability data</i>	279
<i>A2.2.7 Paclitaxel encapsulation data</i>	281
A2.3 Anesthetic emulsion data.....	283
<i>A2.3.1 Sevoflurane emulsions</i>	283
<i>A2.3.2 Isoflurane Emulsions</i>	283
<i>A2.3.3 Propofol Emulsions</i>	287
<i>A2.3.4 Propofol Emulsions – in vivo data</i>	298
<i>A2.3.5 Paclitaxel Emulsions</i>	303

LIST OF FIGURES AND TABLES

CHAPTER 1: Introduction	1
Figure 1.1. Phase separation of lipophilic, aqueous, and fluorous phases.	3
Table 1.1. Example of fluoropolymer materials and applications.....	4
Figure 1.2. Chemical structures of modern, fluorinated anesthetics.	5
Figure 1.3. Diagram showing the relationship between concentration, surface tension, and the critical micelle concentration.	6
Figure 1.4. Unimer-micelle equilibrium.....	7
Figure 1.5. Changes in observable physical properties as a function of surfactant concentration.	8
Figure 1.6. Structure of 1,3-bis(1'-pyrenyl)propane (P3P).	9
Table 1.2. CPP, general surfactant type, idealized surfactant shape, and expected aggregate type.	10
Figure 1.7. Structures of DSPE and MxDSPE.	11
Figure 1.8. Schematic representation of the EPR effect.....	13
Table 1.3. Polymeric micelle formulations of water-insoluble drugs approved for clinical use or under clinical trials.....	14
Figure 1.9. Schematic representation of the formation of an emulsion.....	16
Figure 1.10. Nanoemulsion destabilization process.....	18
Figure 1.11. Structure of fluorosurfactant M1diH3F8.	20
CHAPTER 2: Synthetic challenges in fluorinated synthesis – decomposition of fluorotelomer alcohols	35
Figure 2.1. Physical appearance of F6H2-OH after being heated in NaH/THF.....	39
Figure 2.2. ¹ H-NMR of F6H2-O-H5 before (top) and after (bottom) refluxing in NaH/THF for 24 h.	40
Figure 2.3. ¹ H-NMR spectra from top to bottom of neat F6H2-Oh (all starting fluorotelomer alcohols ¹ H-NMR are identical) and F4H2-OH, F6H2-OH, F8H2-OH and F10H2-OH after stability tests in NaH/THF.....	41

Figure 2.4. Intramolecular hydrogen-bond structure proposed by Ellis <i>et al.</i>	42
Figure 2.5. Appearance and disappearance of vinyl proton signals during timed stability test of F6H2-OH, times from top to bottom: 0 min, 15 min, 30 min, 1 h, 2 h, 24 h.....	43
Figure 2.6. Proposed decomposition pathway of fluorotelomer alcohols using sodium hydride as the base.....	44
Figure 2.7. Comparison of F6H2-OH decomposition under standard stability conditions (NaH/THF, Top) and less-soluble base conditions (NaH/BTF, Bottom).	45
Figure 2.8. Resulting ¹ H-NMR of F10H2-OH stability tested in NaH/DMF.	47
Figure 2.9. Change in CF ₃ chemical shift against concentration for F8H2-OH.....	48
Figure 2.10. Synthetic methodology for synthesis of semifluorinated ethers utilizing fluorotelomer alcohols devised by Zaggia <i>et al.</i>	49
CHAPTER 3: Relationship between structure and behavior of semifluorinated triphilic surfactants	54
Figure 3.1. A – Structure of MxDSPE, surfactants studied extensively by Torchilin <i>et al.</i> , and B – MxF10DSPE, triphilic surfactants studied previously in the Mecozzi laboratory.	56
Figure 3.2. Generalized structure of triphilic surfactants synthesized.	58
Figure 3.3. Radical synthesis of HO-H10F6 and HO-H10F8.	59
Figure 3.4. Anionic synthesis of HO-H10-O-F3 and HO-H10-O-F6.	60
Figure 3.5. Synthesis of linear surfactants M1H10, M1H10-O-F3, M1H10-O-F6, and M1H10F8.	60
Figure 3.6. Synthesis of dibranched surfactants M5diH10, M5diH10-O-F3, and M5diH10-O-F6.....	61
Figure 3.7. Synthesis of miktoarm surfactants M1 μ H10F8 and M2 μ H18F8	62
Table 3.1. Physicochemical data of comparison, linear, miktoarm, and dibranched surfactants	63
Figure 3.8. Relationship between number of fluorocarbons and pCMC (-log(M) \pm SD, $n = 4$) for the linear and dibranched amphiphiles.	64
Figure 3.9. Relationship between microviscosity (I_M/I_E ratio \pm SD, $n = 3$) and the number of fluorocarbons for linear and dibranched amphiphiles.....	66

Figure 3.10. Proposed core-shell-corona structure of linear and dibranched triphilic amphiphiles.	67
Figure 3.11. FRET stability profiles of representative micelles.....	68
Table 3.2. <i>In vitro</i> half-lives of comparison, linear, miktoarm, and dibranched surfactants ..	69
Figure 3.12. Structure of model hydrophobic drug paclitaxel.....	70
Figure 3.13. Percent weight encapsulation (mean \pm SD, $n = 3$) of paclitaxel (PTX) by linear and miktoarm surfactants.	71
Figure 3.14. Percent weight encapsulation (mean \pm SD, $n = 3$) of paclitaxel (PTX) by dibranched surfactants.....	72
CHAPTER 4: Triphilic surfactant-based anesthetic nanoemulsions	97
Figure 4.1 Structure of the volatile anesthetics sevoflurane, isoflurane, and halothane.	99
Figure 4.2. Structure of propofol and etomidate, non-volatile anesthetics commonly used to induce anesthesia.....	101
Figure 4.3. Structure of bupivacaine, a local anesthetic for which lipid rescue has been demonstrated.	102
Figure 4.4. Structure of MxH10F8 ($x = 1, 5$) triphilic surfactants used in isoflurane emulsions.....	103
Figure 4.5. Average particle size over time with SD given by error bars ($n = 3$) for 20 and 25 vol% isoflurane emulsions with M5H10F8 as the surfactant.	103
Figure 4.6. Structure of other surfactants investigated for isoflurane emulsions.....	104
Figure 4.7. Average particle size over time (error bars omitted for clarity) for 30 vol% isoflurane emulsions with Lipoid E80 as surfactant or co-surfactant.	105
Figure 4.8. Structure of some surfactants investigated for propofol emulsion formulations.	106
Figure 4.9. Average particle size over time with SD given by error bars ($n = 3$) for the linear M1H10-O-Fx ($x = 3, 6$), Lipoid E80, propofol emulsions.....	107
Figure 4.10. Effect of added Lipoid E80 co-surfactant on M1H10-O-F3/propofol emulsion A. initial diameter, B. initial particle size standard deviation, and C. initial particle size growth.	108
Figure 4.11. Average particle size over time with SD given by error bars ($n = 3$) for Lipoid E80 emulsions.	109
Figure 4.12. Average particle size over time with SD given by error bars ($n = 3$) for miktoarm surfactants M1 μ H10F8 (B8) and M2 μ H18F8.	110

Figure 4.13. Average particle size over time with SD given by error bars ($n = 3$) for the M1H10F8-based propofol emulsions with various concentrations of added perfluorooctyl bromide (PFOB).....	111
Figure 4.14. Average particle size over time (error bars omitted for clarity) for the four emulsions (B8, L3, F8, L80) tested against Diprivan.	111
Figure 4.15. Time to recovery of righting reflex (RORR) as a function of drug dose.....	112
Table 4.1. Threshold dose \pm SEM for each of the three emulsions L3, B8 and F8 and for Diprivan.....	112
Figure 4.16. Data for Diprivan and B8 with and without lipid bolus.....	113
Table 4.2. Slope \pm SEM of linear regression lines for Diprivan and B8 emulsion with and without lipid bolus injection.....	114
Figure 4.17. Time to return of righting reflex (RORR) v. lipid dose for Diprivan and B8. .	114
Appendix 1: Redesigned triphilic surfactants for hydrophobic pharmaceutical nanoemulsions	128
Figure A1.1. Hypothesized structure of redesigned triphilic surfactant emulsion.	131
Figure A1.2. Synthesis of M2F8-O-H18.....	132
Figure A1.3. Structure of paclitaxel (PTX) and 2-octyldodecan-1-ol.....	133
Figure A1.4. Average particle size over time with SD given by error bars ($n = 3$) for 100 mg PTX emulsion with M2F8-O-H18 as the surfactant and 2-octyl-dodecan-1-ol additive.	134
Figure A1.5. Structure of modified M2F8-O-H18 with pendent fluorophilic substituent ($y = 2-5$).	135

LIST OF ABBREVIATIONS

ACN	acetonitrile
BDE	bond dissociation energy
BTF	α,α,α -trifluorotoluene (benzotrifluoride)
CMC	critical micelle concentration
CPP	critical packing parameter
DCM	dichloromethane
DiI	1,1'-dioctadecyl-3,3,3',3'-tetramethylindocarbocyanine perchlorate
DiO	3,3'-dioctadecyloxacarbocyanine perchlorate
DLS	dynamic light scattering
DMF	<i>N,N</i> -dimethylformamide
DSPE	1,2-distearoyl- <i>sn</i> -glycero-3-phosphoethanolamine
E80	egg phospholipid from Lipoid GmbH containing at least 80% phosphatidylcholine
EPR	enhanced permeability and retention effect
FDA	Food and Drug Administration
FEP	copolymer of fluorinated ethylene and propylene
FRET	Förster Resonance Energy Transfer
HPLC	high performance liquid chromatography
IV	intravenous
LORR	loss of righting reflex
MALDI	matrix-assisted laser desorption/ionization

MxDSPE	1,2-distearoyl- <i>sn</i> -glycero-3-phosphoethanol-amine- <i>N</i> - [methoxy(polyethylene glycol)-x000], x = 1, 2, 5
mPEG	monomethoxy poly(ethylene glycol)
Ms	methanesulfonyl
NMR	nuclear magnetic resonance
o/w	oil-in-water (nanoemulsion)
P3P	1,3-bis-(1-pyrenyl)propane
PBS	phosphate buffered saline
PCTFE	polychlorotrifluoroethylene
PFA	perfluoroalkoxy alkane (copolymer of tetrafluoroethylene and perfluoropropylvinylether)
PFC	perfluorocarbon
PFOB	perfluorooctyl bromide
PFtB	perfluoro- <i>tert</i> -butyl
PTFE	polytetrafluoroethylene
PTX	paclitaxel
PVDF	polyvinylidene difluoride
RORR	recovery of righting reflex
THF	tetrahydrofuran
TLC	thin-layer chromatography
TMS	tetramethylsilane

CHAPTER 1:

Introduction

1.1 Introduction

1.1.1 Perfluorocarbon physical properties

The incorporation of fluorine atoms into organic molecules is of interest in the pharmaceutical,¹ materials,² and agrochemical fields³ because of the change in properties imparted by the C-F bond.⁴ The C-F bond – due to the strong Coulombic contribution arising from fluorine's high electronegativity – is a uniquely strong bond.⁵ The bond dissociation energy (BDE) for the C-F bond in fluoromethane (CH₃F) is 115 kcal mol⁻¹, compared to 104.9 kcal mol⁻¹ for the C-H bond in methane (CH₄).⁶ The high BDE of a C-F bond rises with increasing fluorination and in tetrafluoromethane (CF₄) reaches 130.5 kcal mol⁻¹.^{7,8} As a consequence of C-F bond strength, perfluorocarbons (PFCs, molecules of the formula C_nF_{2n+2}) have high thermal and chemical stability.⁹

In comparison to an aliphatic hydrogen atom, fluorine has a larger mean van der Waals radius (1.47 Å v. 1.20 Å),¹⁰ is more electronegative (3.98 v. 2.20 on the Pauling Scale),¹¹ and has a lower polarizability (0.557 Å³ v. 0.667 Å³ – as expressed as polarizability volumes).¹² Together these dissimilarities give PFCs very different physical properties than hydrocarbons. First, due to the steric repulsion between neighboring fluorines, PFCs adopt a rigid, helical structure rather than the more flexible, antiperiplanar structure of hydrocarbons.¹³ As a result, a perfluorocarbon has a larger cross sectional area (30 Å²) than does a hydrocarbon (20 Å²).¹⁴ Finally, the low polarizability of the fluorine atom and of the carbon-fluorine bond reduces the intermolecular van der Waals interactions of PFCs. This leads to low intermolecular cohesion, low surface tension, and high vapor pressure (relative to the molecular weight) of perfluorocarbons.¹⁵

The electrostatic potential surface of a perfluorocarbon is neutral, with no excess of electrical charge on any of the fluorine atoms. This effect, along with the very low polarizability of the fluorine atom and of the C-F bond, leads to reduced van der Waals interactions and extreme

hydrophobicity. In contrast to typical hydrophobic species however, the reduced van der Waals interactions of perfluorocarbons also cause them to be lipophobic.⁹ Together, the solvophobic exclusion of perfluorocarbons from both aqueous and organic liquid phases leads to the formation of a new liquid phase: the fluorous phase (**Figure 1.1**).¹⁶ Molecules that dissolve in the fluorous phase – PFCs or molecules incorporating perfluoroalkyl moieties – are thus termed fluorophilic.¹⁷ While PFCs will naturally phase segregate into the fluorous phase, there are several empirical rules for determining whether a non-PFC molecule will dissolve in a fluorous phase: a minimum fluorine content of 60 wt% (note: perfluorooctane (C_8F_{18}) is 78 wt% fluorine), the presence of one or more perfluoroalkyl moieties, and limited hydrogen bonding or polar groups.¹⁸

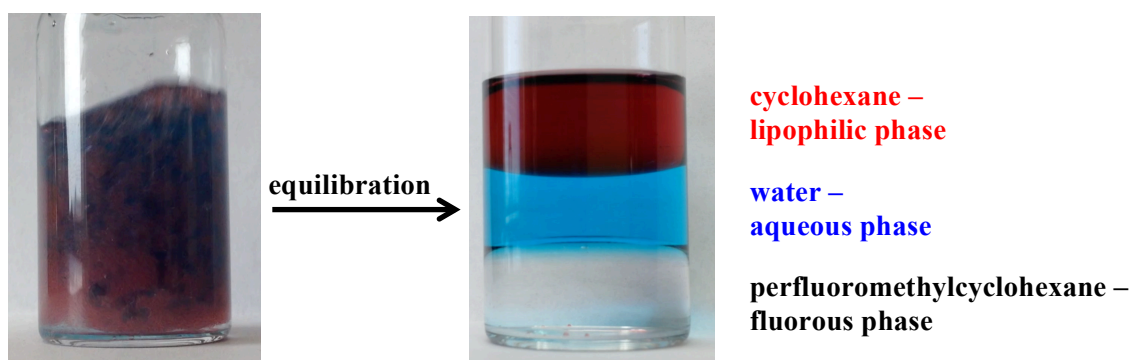


Figure 1.1. Phase separation of lipophilic, aqueous, and fluorous phases.

Example of the phase separation seen when water (dyed blue with $CuSO_4$), cyclohexane (dyed red with tetraphenylcyclopentadienone) and perfluoromethylcyclohexane (colorless) are mixed.

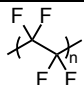

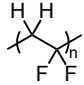
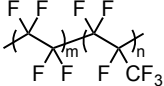
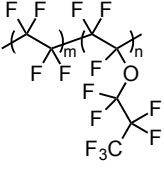
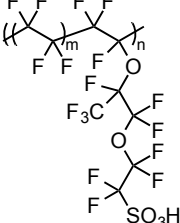
1.1.2 Fluorinated materials

Perfluorocarbons possess unique properties, including: high thermal stability, high chemical resistance, and oil and water repellence. These unique properties have made fluoropolymers – polymers containing a high percentage of fluorine in their structure – important materials in a number of industrial applications.¹⁹ The prototypical fluoropolymer is polytetrafluoroethylene (PTFE) – discovered serendipitously by Plunkett at DuPont in 1938.²⁰ Due to its excellent thermal and chemical stability, PTFE rose to prominence during the Manhattan Project as a coating for

systems involved in the purification of UF_6 . Despite its desirable properties, PTFE was found to be hard to process as a result of its high melting temperature and high melt viscosity.²¹ It was not until 62 years after its initial discovery that conditions were discovered that allowed PTFE to be more readily processed.²² Due to PTFE processing problems, other fluoropolymers were developed that were easier to process (**Table 1.1**) but at the expense of stability.²¹ Together the fluoropolymers in **Table 1.1** play important roles in the coatings, lubricants, chemicals and electronics industries.

Table 1.1. Example of fluoropolymer materials and applications.

Adapted from references 19 and 20.

Fluoropolymer	Repeating Unit	Applications
PTFE		Non-stick cookware, aerospace wiring, lubrication, corrosion-resistant containers, plumbing, biomedical devices
PCTFE		Barrier film, packaging, waterproof and cryogenic seals
PVDF		Coatings, wires, cables, electronics, solar panels, printing
FEP		Release film, cable insulation, plastic labware
PFA		Chemical-resistant tubing and components, semi-conductor manufacturing
Nafion		Fuel cells, batteries, ion-exchange membranes, fine-chemical synthesis

Nafion is an example of an important design philosophy: the incorporation of perfluorocarbons moieties into a structure for stability and other groups for functionality. Nafion (**Table 1.1**) is a unique perfluorinated ionomer – a polymer with ≤ 15 mol% pendant ionic groups.²³ As a perfluorinated ionomer, Nafion leverages the high stability afforded by a

perfluorocarbon backbone to make an ionomer that is stable for use as a thin-membrane ion exchange resin.²⁴ Structurally, Nafion exists as phase-segregated perfluorinated matrix (providing stability) surrounding clusters of hydrated sulfonates (providing functionality).²⁵ Nafion has found widespread applications in fine-chemical production,²⁶ ion-exchange resins,²⁵ and proton-exchange membranes for fuel cells.²⁰ The incorporation of fluorocarbons for stability will form the basis of the work discussed in this thesis.

1.1.3 Perfluorocarbons in medicine

Perfluorocarbons and fluorinated materials have been investigated for their potential application in medicine because of their high gas solubilization, spectroscopic properties, physical properties and biological inertness. PFCs and gases share similarly low intermolecular cohesion. This property allows gases, like oxygen, to dissolve at high concentrations in PFCs and has led to extensive investigation into the use of oxygenated PFC emulsions, including perfluorodecalin, perfluorooctylbromide (PFOB), and linear perfluorocarbons, as potential blood substitutes.^{27–30} Emulsified PFC nanodroplets have also been studied as ultrasound contrast agents and, in the case of perfluoro-15-crown-5 ether, as ¹⁹F-MRI contrast agents.^{15,29,31–35} Finally, the most indelible mark made on the medical field by fluorinated chemicals has been in modern inhaled anesthetics (**Figure 1.2**). Early anesthetics, diethyl ether and cyclopropane, were both fire and explosion hazards, while chloroform suffered from both hepatic and cardiac toxicity.³⁶ With the development of isoflurane, sevoflurane and desflurane, anesthesiology now has anesthetics that are neither flammable nor explosive and exhibit reduced toxicity.^{37–39}

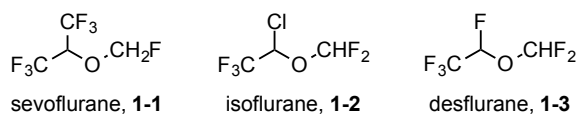


Figure 1.2. Chemical structures of modern, fluorinated anesthetics.

1.2 Micellar drug delivery

1.2.1 Micelle structure and dynamics

Micelles are colloidal nanoparticles, which form spontaneously through the non-covalent self-assembly of amphiphiles.⁴⁰ Amphiphiles are species that covalently link two immiscible components, hydrophilic and hydrophobic moieties. In aqueous solution, amphiphiles dissolved in bulk solution will minimize the free energy of the system through the equilibrium adsorption at the air-water interface.⁴¹ At the water surface amphiphiles direct hydrophobic moieties away from the water and hydrophilic groups into the water.⁴² This collection at the water surface leads to a change in the surface tension (**Figure 1.3**), and because of this amphiphiles are also known as surfactants (a portmanteau of surface-active agents).⁴³

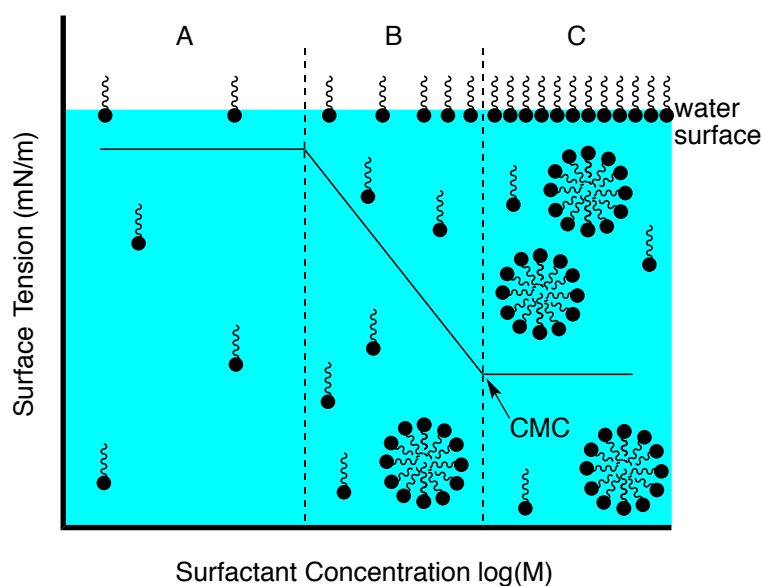


Figure 1.3. Diagram showing the relationship between concentration, surface tension, and the critical micelle concentration.

An important value for any surfactant is its critical micelle concentration (CMC), which can be determined by plotting surface tension against concentration. A corresponds to low adsorbed surfactant where surface tension is close to that of pure water. B is the regime where surface tension drops precipitously as adsorbed surfactant cooperatively increases and C is where surface tension plateaus at surface saturation.

As shown in **Figure 1.3**, the surface tension for surfactant solutions has three distinct regimes, designated as A, B and C.⁴⁴ At low surfactant concentrations (A in **Figure 1.3**), there is

an equilibrium between surfactants adsorbed at water surface and those dissolved in solution. At these low concentrations, the adsorbed surfactant content is low and surface tension is near that of pure water (72.8 mN/m).⁴¹ As the concentration increases (B in **Figure 1.3**), the adsorbed surfactant concentration increases cooperatively and the surface tension falls in proportion to concentration.⁴⁵ The fall in surface tension continues until adsorption at the water surface begins to saturate.⁴⁶ Near surface saturation, micelle formation becomes energetically equivalent to surfactant adsorption at the water surface. Thus the equilibrium between unimers (free surfactants) and micelles becomes dominant (**Figure 1.4**), and without new surfactants adsorbing at the surface the surface tension plateaus (C in **Figure 1.3**).⁴⁵ This disjunction between decreasing surface tension and unchanging surface tension (the crossover between B and C in **Figure 1.3**) is known as the critical micelle concentration (CMC). Above the CMC, increasing the surfactant concentration leads to an increase in the concentrations of micelles.⁴⁷

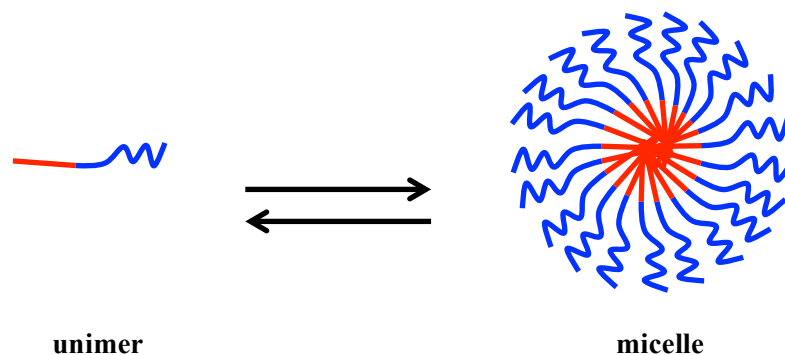


Figure 1.4. Unimer-micelle equilibrium.

Diagram showing the equilibrium that exists in solution between unimer (red- hydrophobic segment, blue – hydrophilic segment) and micelle (red – hydrophobic core, blue – hydrophilic corona).

As is exemplified in **Figure 1.5**, other physical properties aside from surface tension experience a disjunction as the surfactant concentration increases, indicating the CMC. The CMC can be determined graphically (**Figure 1.5**) by plotting changes in turbidity,⁴⁸ dye solubilization,⁴⁹ fluorescence solvatochromism,⁵⁰ or conductivity (for ionic surfactants)⁵¹ against

surfactant concentration. Different techniques can give moderately different values, which is the result of method-dependent properties.⁴¹

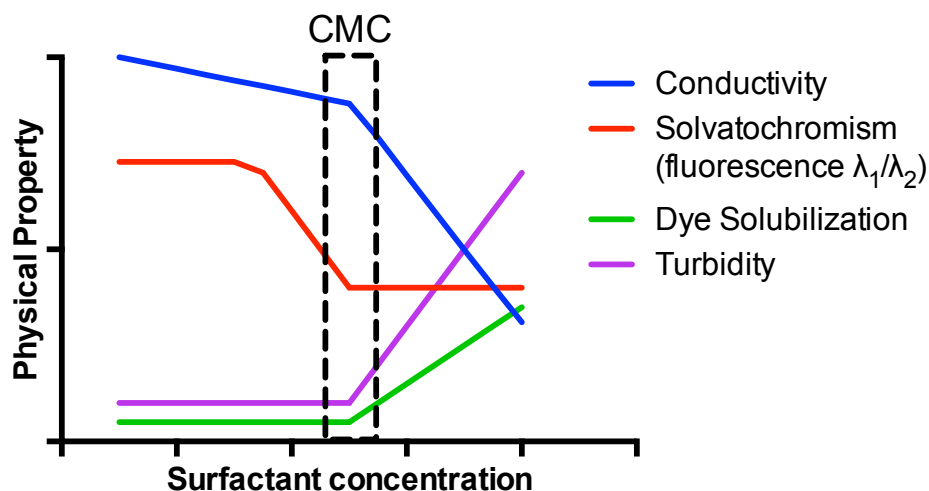


Figure 1.5. Changes in observable physical properties as a function of surfactant concentration.

Example plot showing the graphic discontinuity that occurs at the CMC for conductivity (for ionic surfactants), solvatochromism, dye solubilization, and turbidity. Adapted from reference 52.

Micelles are dynamic, equilibrium structures and the CMC is the measure of a micelle's thermodynamic stability.⁵² Micelle formation is driven almost exclusively by entropy, i.e. the hydrophobic effect. As the hydrophobic tails of surfactants are isolated from solution, highly-ordered water molecules are released into the bulk solvent.⁵³ Thus it follows that the larger the hydrophobic block the lower the CMC, with each additional unit in a linear chain decreasing the CMC logarithmically.^{54,55}

At concentrations above the CMC, surfactants will predominantly exist in micellar aggregates. As a micelle solution is diluted below its CMC, micelles will equilibrate towards a unimer-dominated regime. This dissociation of a micelle (by dilution or by the addition of dissociative media) is another important factor in micellar surfactant design. The resistance of a micelle to dissociation is known as kinetic stability.⁵⁶ Small molecule surfactants rapidly dissociate upon dilution because of their micelles' highly dynamic, rapidly exchanging

structure.⁴³ For polymeric surfactants it has been found that dissociation upon dilution will be slower – the extent to which is related to hydrophobic core dynamics.⁵⁷

Microviscosity is a measure of core dynamism, which can be determined through the fluorimetric measure of the rotational freedom of an encapsulated dye. A common method to determine microviscosity utilizes 1,3-bis-(1'-pyrenyl)propane (P3P, **Figure 1.6**). The fluorescence spectrum of P3P shows both excimer and non-excimer fluorescence signals. The ratio between excimer and non-excimer fluorescence is dependent upon the ability of P3P to rotate about the three-carbon linker between pyrenyl substituents. The more viscous a micellar core, the higher the non-excimer:excimer fluorescence ratio (I_M/I_E ratio).⁵⁸ Micelles with higher microviscosities have been shown to have greater kinetic stabilities, meaning that it takes longer for them to dissociate upon dilution.⁵⁹

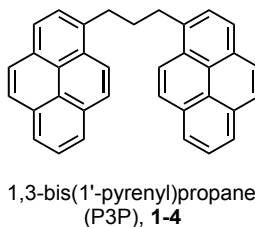


Figure 1.6. Structure of 1,3-bis(1'-pyrenyl)propane (P3P).


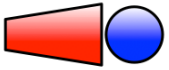
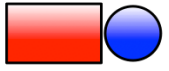
P3P is used to measure the microviscosity of colloidal aggregates. P3P exhibits two different fluorescence signals – excimer and non-excimer – the ratio of which is related to hydrophobic-core dynamics and kinetic stability.

Surfactants readily assemble in aqueous solution; however, not all amphiphiles assemble into spherical micelles. The type of aggregate formed will depend upon the architecture of the hydrated surfactant. The critical packing parameter (CPP), or shape factor, of the surfactant is a metric that relates surfactant structure to its expected aggregate type, e.g. spherical micelles, elongated/cylindrical micelles, or bilayers/vesicles.⁶⁰ The CPP is defined as $v/(a_0 l_c)$, where v and l_c are the volume and length, respectively, of the hydrophobic chain(s) and a_0 is the effective area per hydrophilic group.⁵² Spherical micelles result from the self-assembly of surfactants whose

head group area is significantly larger than the volume of the hydrophobic block, which can be envisioned as the packing of idealized cones (**Table 1.2**). A CPP value indicative of spherical micelles formation is less than 0.33. As the idealized conical surfactant becomes truncated – the volume of the hydrophobic block increases relative to the effective area of the hydrophilic block – the aggregates formed in solution go from spherical to oblong micelles (CPP closer to 0.33) to rod or cylinder-like micelles (CPP closer to 0.5). As the surfactant approaches a cylinder and hydrophilic domain size and hydrophobic domain sizes equalize (CPP approaches 1) vesicles and bilayers become the expected aggregates formed in solution (**Table 1.2**).⁶¹ In designing a surfactant for specific molecular architectures, the shape – or size relationship between hydrophilic and hydrophobic components – is an important factor to consider.

Table 1.2. CPP, general surfactant type, idealized surfactant shape, and expected aggregate type.

For the idealized surfactant shapes, v and l_c are represented by the volume and length of the red, hydrophobic, block and a_0 by the circumference of the blue, hydrophilic, block. Adapted from reference 60.

CPP	General Surfactant Type	Idealized Surfactant Shape	Expected Aggregate Type
≤ 0.33	Single hydrophobic chains and relatively large head groups		Spherical Micelles
$0.33 - 0.5$	Single hydrophobic chain with a relatively small head group		Oblong to Cylindrical Micelles
$0.5 - 1$	Double hydrophobic chain with small head groups		Lamellar phases (vesicles and bilayers)

In general, by changing the size of the hydrophilic domain the type of aggregate morphology for a given hydrophobic moiety can be controlled. With high hydrophobic length compared to volume, linear surfactants will form micelles with smaller hydrophilic head groups. Branched surfactants, where the hydrophobic volume can be substantially more sizeable, require larger hydrophilic blocks to form micelles. The phospholipid DSPE (1,2-distearoyl-*sn*-glycero-3-phosphoethanol-amine, **Figure 1.7**) highlights the relationship between aggregate type and

surfactant architecture. DSPE (CPP = 1.04)⁶² is known to form lamellar structures – bilayers and vesicles – in solution.⁶³ The addition of monomethoxy poly(ethylene glycol), mPEG, to DSPE produces surfactants with the generalized abbreviation MxDSPE (1,2-distearoyl-*sn*-glycero-3-phosphoethanol-amine-*N*-[methoxy(polyethylene glycol)]), where x is the average molecular weight of the mPEG block in kDa. M1DSPE (**Figure 1.7**), with the relatively small mPEG₁₀₀₀ (CPP = 0.47, v and l_c values for DSPE⁶⁴ and a_0 estimated from Duncanson *et al.*⁶⁵) still forms lamellar aggregates in solution.⁶⁶ Upon moving to M2DSPE and M5DSPE (**Figure 1.7**) – with the sterically larger mPEG₂₀₀₀ and mPEG₅₀₀₀, respectively – both predominantly form spherical micelles (CPPs calculated as 0.23 and 0.09, respectively, with v , l_c , and a_0 values from Arleth *et al.*⁶⁴ and Duncanson *et al.*⁶⁵).⁶⁷

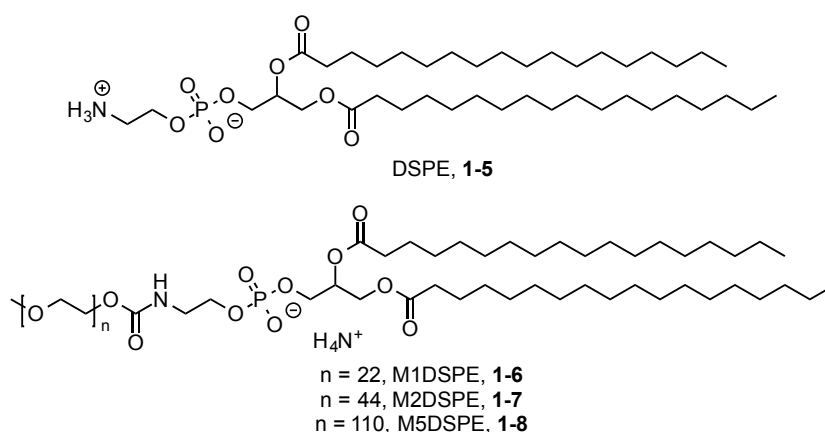


Figure 1.7. Structures of DSPE and MxDSPE.

DSPE, a phospholipid, forms bilayers in solution (CPP = 1.04). MxDSPE is PEGylated DSPE, where M corresponds to monomethoxy poly(ethylene glycol) and x = 1, 2, or 5 corresponds to average molecular weights of 1000, 2000, 5000 g mol⁻¹. In solution M1DSPE (CPP = 0.47) forms lamellar structures while M2DSPE (CPP = 0.23) and M5DSPE (CPP = 0.09) form spherical micelles.

1.2.2 Micelle drug delivery vehicles

Numerous pharmaceuticals and drug candidate leads are poorly water-soluble species. In a recent review, an estimated 40% of currently marketed pharmaceuticals and 70% of those under development are poorly water-soluble.⁶⁸ Poorly water-soluble drugs suffer from reduced and

variable adsorption upon oral administration leading to poor bioavailability.⁶⁹ In addition, the parenteral delivery of low-water solubility drugs is problematic due to the potential for localized precipitation, pain, hemolysis, and toxicity upon injection.⁶⁸ Despite the potentially high therapeutic efficacy for many of these agents, they are not usable in their native form due to low water solubility. The development of water-soluble formulations, therefore, remains a significant challenge to translate these sparingly soluble compounds into clinical applications.

Two different strategies have been developed to overcome the issues associated with poorly water-soluble drugs. The first strategy involves the physical manipulation of drug particles into nanocrystals (crystals of average size below 1 μm). Because of their increased surface area to volume ratio, drug nanocrystals have been shown to exhibit higher solubility and high rates of dissolution in aqueous solutions.⁷⁰ Nanocrystal formulations, however, require high-energy inputs, are not suitable for cytotoxic drugs, lack controlled release, and are not suitable for intravenous (IV) administration.⁷¹ The second strategy solubilizes hydrophobic drugs in colloidal nanoparticles, e.g. micelles, liposomes, or emulsions. Cytotoxic or degradable drugs are protected within the hydrophobic domain while the hydrophilic corona allows for water solubility,⁷² long circulation,^{73,74} and controlled release.⁷⁵ Micelles, liposomes, and emulsions are also suitable for IV administration.⁷¹

Spherical micelles are of specific interest in the delivery of hydrophobic pharmaceuticals because of their small size.⁵⁷ Average diameter is an important factor in determining the circulation time of nanoparticles. Particles less than 5.5 nm in diameter are rapidly cleared by the urinary tract,⁷⁶ while, particles with diameters greater than 200 nm, in contrast, are cleared from circulation by the spleen.⁷⁷

In the field of chemotherapeutics, micelles in the 5.5 – 200 nm range can benefit from the enhanced permeability and retention (EPR) effect, i.e. passive targeting. To grow above 1-2 mm

in diameter, tumor cells create new vasculature that is typically porous and lacking an effective lymphatic system (**Figure 1.8**).^{78,79} Because of this poor vasculature architecture, small nanoparticles can both permeate into (due to large pore sizes) and concentrate in cancerous tissue (due to poor drainage without a lymphatic system). For highly vascularized tumors, e.g. breast cancer, tumor permeation is high for aggregates up to 100 nm in diameter; however, for hypovascular tumors, e.g. pancreatic tumors, only micelles below 30 nm in diameter were found to show effective tumor permeation.⁸⁰ Together, the design of stable micellar aggregates in the 10 – 30 nm size range is of interest because of the combined characteristics of hydrophobic drug solubilization, long-circulation, and high-tumor permeability.

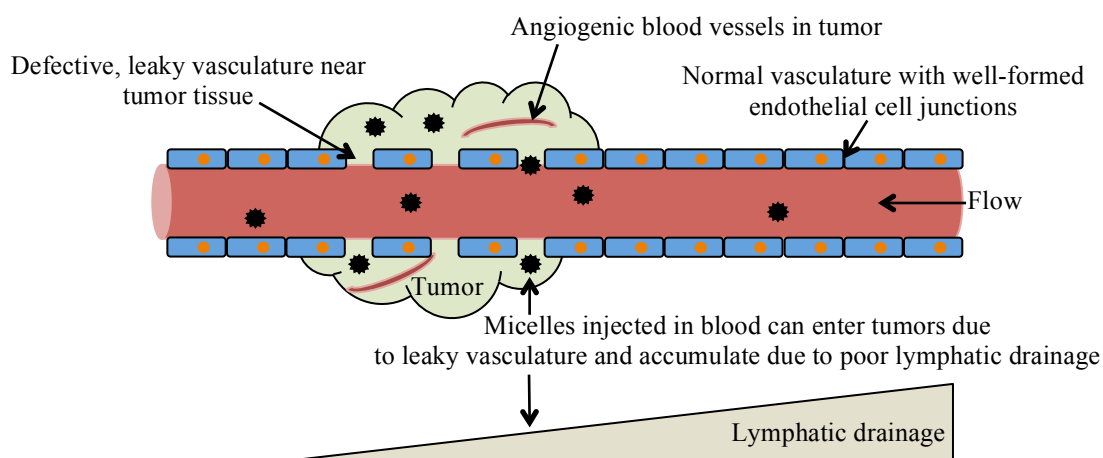


Figure 1.8. Schematic representation of the EPR effect.

Tumor angiogenesis leads to the growth of new, leaky blood vessels that allow for the permeation of nanoparticles that cannot pass the endothelial cell junctions of normal vasculature. The lack of an effective lymphatic system also leads to accumulation of nanoparticles in tumor tissue. Adapted from reference 79.

A number of polymeric surfactant systems have been developed, which can be utilized for drug delivery applications.^{67,71,72} Typically, poly(ethylene glycol) (PEG) is used as the hydrophilic component because of its functionalizability, propensity to increase circulation time, and the ready excretion of disassembled PEGylated surfactants by the kidneys.⁸¹ The hydrophobic components can vary but are typically polymeric esters or amides. Hydrophobic pharmaceuticals, dispersed throughout the hydrophobic core,⁸² can then be incorporated through several different

methods.⁷¹ The two most common laboratory techniques for incorporating drugs into micelles are dialysis and the solvent evaporation method. The solvent evaporation method removes solvent from a surfactant-drug solution under vacuum. The resulting drug-surfactant thin-film is then dispersed with hot, aqueous solvent and sonicated to give drug-loaded micelles. The solvent evaporation method has been found to give more consistent encapsulation results than dialysis.⁸³ Several clinical micellar systems have been developed and are in clinical trials, with Genexol (micellar paclitaxel) approved for use in South Korea (Table 1.3).⁷¹

Table 1.3. Polymeric micelle formulations of water-insoluble drugs approved for clinical use or under clinical trials.

Adapted from reference 71.

Trade Name	Surfactant	Drug	Developer, Status
NK911®	Poly(ethylene glycol)- <i>co</i> -poly(L-aspartic acid)	Doxorubicin	Nippon Kayaku, Phase II
NK105®	Poly(ethylene glycol)- <i>co</i> -poly(L-aspartic acid)	Paclitaxel	Nanocarrier/Nippon Kayaku, Phase II
Genexol-PM	Poly(ethylene glycol)- <i>co</i> -poly(D,L-lactic acid)	Paclitaxel	Samyang, Approved in South Korea, Phase II in U.S.A.

1.2.3 Fluorosurfactants in micellar drug delivery

Fluorosurfactants – hydrophilic-fluorophilic species – are of widespread interest in industrial applications because of their very high surface activity (lower surface tension limits of 15-20 mN/m) compared to analogous hydrocarbon (lower surface tension limits of 30-40 mN/m).⁸⁴ Due to the enhanced hydrophobicity of fluorocarbons, fluorosurfactants also show lower CMCs compared to analogous hydrocarbon-based surfactants.⁵⁵ Despite their excellent surface-active properties and widespread industrial applications, perfluorinated surfactants have found little use in micellar drug delivery. Because of the immiscible nature of fluorosurfactant cores and typical lipophilic drugs, fluorosurfactant micelles are unable to solubilize most pharmaceuticals. While fluorosurfactant micelles were found to work very effectively at the solubilization of the

fluorinated anesthetic sevoflurane (**Figure 1.2**),⁸⁵ the use of purely fluorinated micelles for drug delivery applications is restricted by the limited number of fluorinated pharmaceuticals.

1.2.4 Micelle instability and triphilic surfactants

Spherical micelle drug delivery systems have several benefits, including: small size, passive accumulation via the EPR effect, and solubilization of hydrophobic pharmaceuticals. However, micelles must have sufficient stability *in vivo* in order to take advantage of these benefits. The non-covalent nature of micelles makes shelf and *in-vivo* stability significant challenges.^{40,71,86} Several strategies have been developed to overcome the issue of micellar stability: cross-linking surfactants in micelles to create a covalent structure;⁸⁷⁻⁹⁰ using large, polymeric surfactants that have high kinetic stability;^{86,91,92} and using triphilic surfactants with two mutually immiscible hydrophobic components to increase kinetic stability of micellar aggregates.⁹³⁻⁹⁶

Triphilic surfactants are unique surfactant systems because they incorporate three mutually immiscible components: hydrophilic, lipophilic, and fluorophilic. Upon aggregation, triphilic surfactants possess unique hydrophobic cores wherein hydrocarbon and fluorocarbon components phase segregate.⁹⁷ A number of possible core morphologies are possible depending upon surfactant architecture and block-size ratios.⁹⁸⁻¹⁰⁰ The introduction of a fluorocarbon component does not increase hydrophobic drug encapsulation; rather, the fluorophilic components (and the resulting fluorophilic microphases within the core) increase the stability of the resulting aggregates.¹⁰¹ In a recent review by Amado and Kressler, the application potential of triphilic surfactants is highlighted in contrast with the lack of understanding of such systems in aqueous solution.⁹³ In this thesis, triphilic surfactants will be synthesized and characterized to help elucidate relationships between structure and behavior for these triphilic surfactant systems. This understanding can then be used to better design triphilic micelles for drug delivery systems.

1.3 Nanoemulsion drug delivery

1.3.1 Nanoemulsion - formulation

Nanoemulsions are a colloidal drug delivery system consisting of sub-500 nm particles.¹⁰² In contrast to micelles, nanoemulsions are metastable, non-equilibrium systems. Thermodynamically, a phase-separated state is the lowest energy configuration for an oil-water mixture. To prepare a nanoemulsion, therefore, energy must be input into the system (**Figure 1.9**). Upon emulsification, a dispersed phase (for drug-delivery applications, typically an oil phase) is suspended as nanodroplets in a continuous (aqueous) phase to give an oil-in-water (o/w) emulsion.

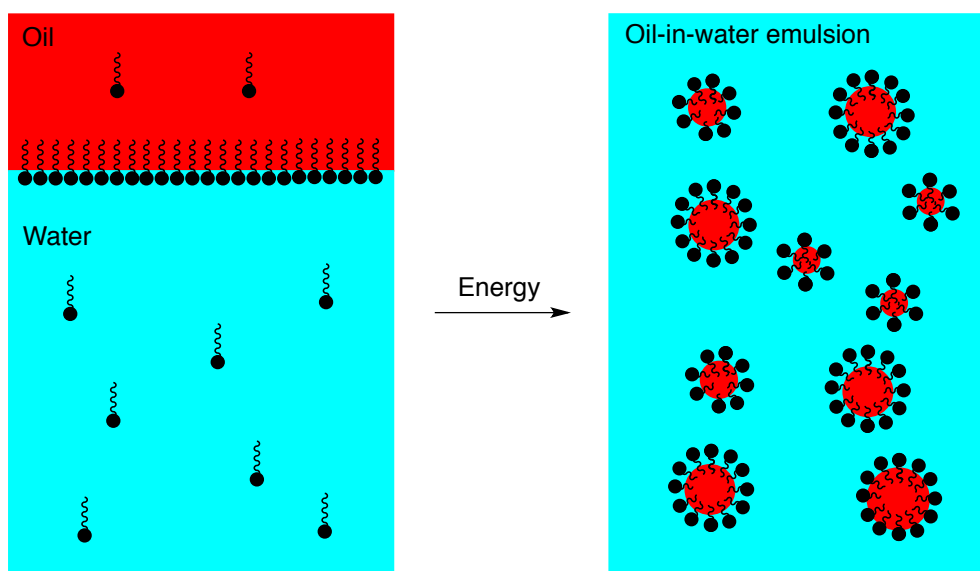


Figure 1.9. Schematic representation of the formation of an emulsion.

An oil-water mixture spontaneously phase-separates. To form an emulsion, energy must be input into the system to disrupt the two phases and the resulting droplets must be stabilized by a surfactant.

The formation of nanodroplets requires deformation and disruption of the oil-phase, which is opposed by Laplace pressure – the pressure between the inside and outside of a curved surface – of up to 0.1 MPa.¹⁰³ There are two different methodologies to achieve nanodroplet formation: low-energy and high-energy emulsification. Low-energy emulsification was first developed in the late 1960's.¹⁰⁴ This newer emulsification technique takes advantage of the change in phase

behavior and interfacial properties with changes in temperature,^{105,106} in component concentration,¹⁰⁷ or in solvent polarity.^{108,109} While the low-energy methods have garnered interest because of their enhanced scalability, low-energy-prepared emulsions tend to suffer from long-term instability.¹¹⁰

Traditionally, emulsions have been prepared by high-energy emulsification methods. High-energy emulsification utilizes mechanical forces – high-shear stirring,¹¹¹ high-pressure homogenization,¹¹² ultrasonic emulsification,¹¹³ or microfluidization¹¹⁴ – to disrupt the oil and water phases and form nanodroplets. The particle sizes and distributions depend heavily upon the conditions utilized to achieve emulsification.^{115,116} Because of the large energy input, 3 MJ m⁻³ is estimated as a lower limit for emulsification,¹⁰³ temperature-sensitive drugs and biologics cannot be emulsified by high-energy means. Mechanical emulsification, however, does allow for greater control of average particle size and for greater variety in the emulsion formulation, e.g. oil-phase and surfactant, than does low-energy emulsification.

The hydrophobic nanodroplets that result from emulsification suffer from high interfacial energy. Without the adsorption of surfactant into the dispersed-phase to stabilize the nanoemulsion, the oil nanodroplets will coalesce and phase-separation will occur.¹¹⁷ For effective adsorption of the droplet to occur, the hydrophobic moiety of the surfactant and the hydrophobicity of the nanodroplet should match. Specifically, it has been found that stable emulsions result when the adsorbed surfactant hydrophobic tails formed strong penetration complexes with the oil phase.^{118,119} In principle, lipophilic nanodroplets will best be stabilized by surfactants bearing hydrocarbon segments able to penetrate the droplet while fluoruous nanodroplets will best be stabilized by fluorosurfactants.

1.3.2 Nanoemulsion - stability

Emulsions are thermodynamically unstable systems; as such, long-term stability is the key issue to solve in formulation. Given the inhomogeneity in particle sizes, emulsion nanodroplets have different velocities and chemical potentials. Flocculation is trapping of smaller particles by larger particles, forming particle aggregates or flocs (**Figure 1.10**).¹²⁰ Due to their higher curvature, smaller droplets have greater chemical potential than do larger droplets. To reduce the chemical potential of the system, average particle size will increase (**Figure 1.10**) through either droplet combination (coalescence) or the diffusion of the oil phase from smaller to larger droplets (Ostwald ripening).¹²¹ Once large enough particles or particle aggregates are formed, creaming (or sedimentation, depending on oil-phase density) will occur (**Figure 1.10**). At the point of creaming, the emulsion will finally minimize system energy through phase separation.¹²⁰

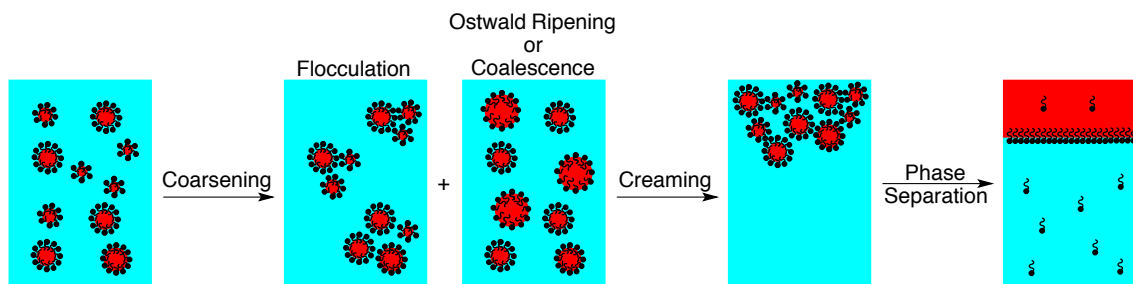


Figure 1.10. Nanoemulsion destabilization process.

Nanoemulsion can grow in particle size as a result of coalescence, flocculation, and Ostwald ripening. Once large enough particles or associations are achieved, particles start to cream (or sediment, based on the density of the oil-phase), which leads to phase separation.

Given nanoemulsions' small average particle size, Brownian motion is able to overcome flocculation and limit creaming for nanoemulsions.¹²² With the appropriate choice of surfactant, coalescence can be prevented through electrostatic (ionic surfactants) or steric repulsion (non-ionic surfactants).¹²³ Therefore, Ostwald ripening – the diffusion of dispersed phase molecules from higher-Laplace-pressure, small droplets to lower-Laplace-pressure, large droplets – is the only method for nanoemulsions to coarsen and decompose.

Two methods have been developed to impede Ostwald ripening and to prepare stable nanoemulsions with long nanoemulsion lifetimes. The first is the two-component or trapped-species method.¹²⁴ The trapped-species method is used when small nanodroplet sizes are readily achievable, but Ostwald ripening is very fast. To slow Ostwald ripening, a second, less soluble additive is added to the oil-phase. With the insoluble additive in the nanodroplet, the diffusion of the more-soluble oil component from smaller to larger droplets (driven by the greater Laplace pressure of smaller droplets) leads to small droplets rich in insoluble oil. The decrease in entropy associated with this demixing of the oil-phase provides a thermodynamic barrier to the diffusion of the more-soluble oil and thus limits Ostwald ripening.

The second method for preparing stable nanoemulsions, with low Ostwald ripening, is the evaporative ripening method.¹¹⁰ The evaporative ripening method is used when the oil-phase is highly viscous. Highly viscous oil-phases can result in less-stable nanoemulsions with large average droplet sizes. To decrease the nanodroplet size in emulsification, a volatile, oil-miscible solvent is added to the oil phase before preparing the emulsion. The oil phase then has a lower viscosity and smaller particle sizes are achievable during high-energy emulsification. After the emulsion has been prepared, the volatile solvent is removed under vacuum. This further reduces the overall size of droplets and what remains is a nanoemulsion with limited Ostwald ripening potential because of the very low solubility and very high viscosity of the emulsified oil-phase.

1.3.3 Fluorinated anesthetic nanoemulsion

Fluorinated anesthetics (**Figure 1.2**) are typically administered by inhalation. The intravenous (IV) delivery of volatile anesthetics is of interest because it leads to more rapid onset of anesthesia.¹²⁵ The use of Intralipid®, a parenteral nutritional fat emulsion, has proven unsuccessful in emulsifying fluorinated anesthetics at clinically useful concentrations.¹²⁶ Previous

work in the Mecozzi laboratory has demonstrated the success in utilizing the dibranched fluorosurfactant M1diH3F8 (**Figure 1.11**), with insoluble perfluorooctyl bromide (PFOB) oil-phase additive, to stably emulsify sevoflurane (20 vol%) for greater than one year.¹²⁷ It was found that a 20 vol% sevoflurane emulsion was effective at inducing anesthesia – from which recovery was fast and rapid – in bolus dosing in rats.¹²⁸

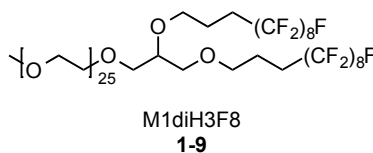


Figure 1.11. Structure of fluorosurfactant M1diH3F8.

M1diH3F8 was able to stably emulsify sevoflurane at 20 vol% for over 1 year. Note on nomenclature: Mx refers to the mPEG hydrophilic block, n is the average molecular weight in thousands; di refers to the dibranched structure; H# and F# refer to the number of hydrogenated and fluorinated carbon atoms, respectively.

In contrast to sevoflurane, the use of surfactants similar to M1diH3F8 (**Figure 1.11**) failed to stably emulsify isoflurane (**Figure 1.2**). Emulsified isoflurane is also of interest for its potential to precondition cardiac tissue before surgery and in transplants.¹²⁹ An isoflurane emulsions containing 15 vol% isoflurane have been prepared using complex mixtures of surfactants and oils.¹³⁰ Despite numerous attempts, 15 vol% isoflurane seems to be the limit for classical hydrocarbon systems; however, work from the Mecozzi group has shown that fluorocarbon surfactants are also ineffective at emulsifying isoflurane. The issue seems to be the mixed fluorophilicity and lipophilicity of isoflurane (the increased lipophilicity coming from isoflurane's chloride substituent, **Figure 1.2**). As such, a triphilic surfactant, with mixed lipophilic and fluorophilic hydrophobic block, has the potential to match the hydrophobicity of isoflurane and provide for a more stable emulsion. In addition, a semifluorinated amphiphile has the potential to simplify the emulsion formulation and to increase the amount of isoflurane that could be emulsified, which would lower dosing.

1.3.4 Hydrophobic-pharmaceutical nanoemulsions

Oil-in-water nanoemulsions are attractive parenteral vehicles for the delivery of hydrophobic pharmaceuticals because of their high drug loading.¹³¹ One of the most widely studied applications for parenteral nanoemulsions is for anticancer formulations, including: photodynamic therapy,¹³² neutron capture,¹³³ and traditional chemotherapy pharmaceuticals.¹³⁴ To be used clinically, the USP stipulates that parenteral emulsions must have an average particle size less than 500 nm¹³⁵ and the FDA recommends a shelf life of 12 months. Nanoemulsions, however, can rapidly phase separate, and shelf life is highly correlated to composition and surfactant design.

There is a relative dearth of information on the application of triphilic surfactants to nanoemulsion formulations. This work investigates whether triphiles have the potential to provide for a stable emulsion formulation. The lipophilic component of triphilic surfactants will penetrate the hydrophobic droplet and solubilize the nanodroplet. In contrast, the fluorophilic domain will not have any impact on droplet solubilization but will reduce Ostwald ripening by inhibiting oil diffusion. Together triphilic surfactants are proposed to increase nanodroplet stability and in turn increase emulsion shelf life.

1.4 Thesis Objectives and Overview

Both micellar and nanoemulsion formulations have contributed to the development of promising drug delivery systems. For both types of systems, nanoparticle stability remains a key challenge in the design and implementation of micelles and nanoemulsions into clinical practice. To address this issue of nanoparticle stability, the scope of this thesis includes the design, synthesis, and study of semifluorinated triphilic – hydrophilic, lipophilic, and fluorophilic – surfactants. Like classical surfactants – hydrophilic and lipophilic surfactants - these triphilic

surfactants will undergo self-assembly due to the hydrophobic effect. Triphilic surfactants, in contrast to classical surfactants, should show increased kinetic and thermodynamic stability. To achieve this goal, two classes of triphilic surfactants, linear and dibranched, have been synthesized. Initial synthetic attempts involved overcoming synthetic challenges of fluorinated alcohol decomposition (Chapter 2). The surfactants synthesized were then characterized and their physicochemical properties investigated in comparison to miktoarm surfactants synthesized by Dr. Aaron McCoy (Chapter 3). Both linear and dibranched surfactants were investigated for their potential to prepare stable isoflurane and propofol nanoemulsions. Stable propofol nanoemulsions were studied in rat models (Chapter 4). Finally, a redesigned triphilic surfactant was synthesized to investigate the potential for preparing solid-drug nanoemulsions (Appendix 1).

1.5 References

- (1) Purser, S.; Moore, P. R.; Swallow, S.; Gouverneur, V. V. Fluorine in Medicinal Chemistry. *Chem. Soc. Rev.* **2008**, 37 (2), 320–330.
- (2) Berger, R.; Resnati, G.; Metrangolo, P.; Weber, E.; Hulliger, J. Organic Fluorine Compounds: A Great Opportunity for Enhanced Materials Properties. *Chem. Soc. Rev.* **2011**, 40 (7), 3496–3508.
- (3) Jeschke, P. The Unique Role of Fluorine in the Design of Active Ingredients for Modern Crop Protection. *ChemBioChem* **2004**, 5 (5), 570–589.
- (4) Champagne, P. A.; Desroches, J.; Hamel, J.-D.; Vandamme, M.; Paquin, J.-F. Monofluorination of Organic Compounds: 10 Years of Innovation. *Chem. Rev.* **2015**, 150409082118002.
- (5) Smart, B. E. Fluorocarbons. In *The chemistry of functional groups, supplement D: The chemistry of halides, pseudo-halides and azides. Part 1*; Patai, S., Rappoport, Z., Eds.; John Wiley & Sons Ltd.: New York, 1983; pp 603–656.
- (6) Blanksby, S. J.; Ellison, G. B. Bond Dissociation Energies of Organic Molecules. *Acc. Chem. Res.* **2003**, 36 (4), 255–263.

- (7) Wiberg, K. B.; Rablen, P. R. Origin of the Stability of Carbon Tetrafluoride : Negative Hyperconjugation Reexamined. *J. Am. Chem. Soc.* **1993**, *115* (2), 614–625.
- (8) Lemal, D. M. Perspective on Fluorocarbon Chemistry. *J. Org. Chem.* **2004**, *69* (1), 1–11.
- (9) Krafft, M. P. Fluorocarbons and Fluorinated Amphiphiles in Drug Delivery and Biomedical Research. *Adv. Drug Deliv. Rev.* **2001**, *47* (2-3), 209–228.
- (10) Bondi, A. Van Der Waals Volumes and Radii. *J. Phys. Chem.* **1964**, *68* (3), 441–451.
- (11) Nagle, J. K. Atomic Polarizability and Electronegativity. *J. Am. Chem. Soc.* **1990**, *112* (12), 4741–4747.
- (12) Miller, T. Atomic and Molecular Polarizabilities. In *Handbook of Chemistry and Physics*; Haynes, W. M., Bruno, T. J., Lide, D. ., Eds.; CRC Press: Boca Raton, FL; pp 10/187–10/196.
- (13) Zhang, G.; Maaloum, M.; Muller, P.; Benoit, N.; Krafft, M. P. Surface Micelles of Semifluorinated Alkanes in Langmuir-Blodgett Monolayers. *Phys. Chem. Chem. Phys.* **2004**, *6* (7), 1566–1569.
- (14) Krafft, M. P. Controlling Phospholipid Self-Assembly and Film Properties Using Highly Fluorinated Components - Fluorinated Monolayers, Vesicles, Emulsions and Microbubbles. *Biochimie* **2012**, *94* (1), 11–25.
- (15) Janjic, J.; Ahrens, E. Fluorine Containing Nanoemulsions for MRI Cell Tracking. *Wiley Interdiscip. Rev. Nanomedicine Nanobiotechnology* **2009**, *1*, 492–501.
- (16) Horvath, I. T. Fluorous Biphasic Chemistry. *Acc. Chem. Res.* **1998**, *31* (10), 641–650.
- (17) Kiss, L. E.; Kövesdi, I.; Rábai, J. An Improved Design of Fluorophilic Molecules: Prediction of the In P Fluorous Partition Coefficient, Fluorophilicity, Using 3D QSAR Descriptors and Neural Networks. *J. Fluor. Chem.* **2001**, *108* (1), 95–109.
- (18) Huque, F. T. T.; Jones, K.; Saunders, R. A.; Platts, J. A. Statistical and Theoretical Studies of Fluorophilicity. *J. Fluor. Chem.* **2002**, *115* (2), 119–128.
- (19) Teng, H. Overview of the Development of the Fluoropolymer Industry. *Applied Sciences*, **2012**, *2*, 496–512.
- (20) Gardiner, J. Fluoropolymers: Origin, Production, and Industrial and Commercial Applications. *Aust. J. Chem.* **2015**, *68* (1), 13.
- (21) Ebnesajjad, S. Introduction to Fluoropolymers. In *Applied Plastics Engineering Handbook - Processing and Materials*; Kutz, M., Ed.; William Andrew: Oxford, UK, 2011; pp 49–60.

- (22) Tervoort, T.; Visjager, J.; Graf, B.; Smith, P. Melt-Processable Poly(tetrafluoroethylene). *Macromolecules* **2000**, *33* (17), 6460–6465.
- (23) Spencer, M. W.; Wetzel, M. D.; Troeltzsch, C.; Paul, D. R. Effects of Acid Neutralization on the Properties of K^+ and Na^+ Poly(ethylene-*co*-Methacrylic Acid) Ionomers. *Polymer (Guildf)*. **2012**, *53* (2), 569–580.
- (24) Heitner-Wirguin, C. Recent Advances in Perfluorinated Ionomer Membranes: Structure, Properties and Applications. *J. Memb. Sci.* **1996**, *120* (1), 1–33.
- (25) Chen, T. Y.; Leddy, J. Ion Exchange Capacity of Nafion and Nafion Composites. *Langmuir* **2000**, *16* (6), 2866–2871.
- (26) Gelbard, G. Organic Synthesis by Catalysis with Ion-Exchange Resins. *Ind. Eng. Chem. Res.* **2005**, *44* (23), 8468–8498.
- (27) Krafft, M. P.; Riess, J. G. Perfluorochemical-Based Oxygen Therapeutics, Contrast Agents, and Beyond. In *Fluorine and Health*; Tressaud, A., Haufe, G., Eds.; Elsevier B.V., 2008; pp 447–486.
- (28) Lanza, G. M.; Winter, P. M.; Caruthers, S. D.; Hughes, M. S.; Hu, G.; Schmieder, A. H.; Wickline, S. A. Theragnostics for Tumor and Plaque Angiogenesis with Perfluorocarbon Nanoemulsions. *Angiogenesis* **2010**, *13* (2), 189–202.
- (29) Menaa, F.; Menaa, B.; Sharts, O. N. Importance of Fluorine and Fluorocarbons in Medicinal Chemistry and Oncology. *J. Mol. Pharm. Org. Process Res.* **2013**, *1* (1), 1–6.
- (30) Freire, M. G.; Gomes, L.; Santos, L. M. N. B. F.; Marrucho, I. M.; Coutinho, J. A. P. Water Solubility in Linear Fluoroalkanes Used in Blood Substitute Formulations. *J. Phys. Chem. B* **2006**, *110* (45), 22923–22929.
- (31) Partlow, K. C.; Chen, J.; Brant, J. A.; Neubauer, A. M.; Meyerrose, T. E.; Creer, M. H.; Nolte, J. A.; Caruthers, S. D.; Lanza, G. M.; Wickline, S. A. ^{19}F Magnetic Resonance Imaging for Stem/progenitor Cell Tracking with Multiple Unique Perfluorocarbon Nanobeacons. *FASEB J.* **2007**, *21* (8), 1647–1654.
- (32) Flogel, U.; Ding, Z.; Hardung, H.; Jander, S.; Reichmann, G.; Jacoby, C.; Schubert, R.; Schrader, J. *In vivo* Monitoring of Inflammation after Cardiac and Cerebral Ischemia by Fluorine Magnetic Resonance Imaging. *Circulation* **2008**, *118* (2), 140–148.
- (33) Yu, J.; Cui, W.; Zhao, D.; Mason, R. P.; Alain, T. Non-Invasive Physiology and Pharmacology Using ^{19}F Magnetic Resonance. In *Fluorine and Health*; Tressaud, A., Haufe, G., Eds.; Elsevier B.V., 2008; pp 197–276.
- (34) Rapoport, N.; Nam, K. H.; Gupta, R.; Gao, Z.; Mohan, P.; Payne, A.; Todd, N.; Liu, X.; Kim, T.; Shea, J.; Scaife, C.; Parker, D. L.; Jeong, E. K.; Kennedy, A. M. Ultrasound-

- Mediated Tumor Imaging and Nanotherapy Using Drug Loaded, Block Copolymer Stabilized Perfluorocarbon Nanoemulsions. *J. Control. Release* **2011**, *153* (1), 4–15.
- (35) Díaz-López, R.; Tsapis, N.; Fattal, E. Liquid Perfluorocarbons as Contrast Agents for Ultrasonography and ^{19}F -MRI. *Pharm. Res.* **2010**, *27* (1), 1–16.
 - (36) Whalen, F. X.; Bacon, D. R.; Smith, H. M. Inhaled Anesthetics: An Historical Overview. *Best Pract. Res. Clin. Anaesthesiol.* **2005**, *19* (3 SPEC. ISS.), 323–330.
 - (37) Behne, M.; Wilke, H.; Harder, S. Clinical Pharmacokinetics of Sevoflurane. *Clin. Pharmacokinet.* **1999**, *36* (1), 13–26.
 - (38) Jakobsson, J. Desflurane: A Clinical Update of a Third-Generation Inhaled Anaesthetic. *Acta Anaesthesiol. Scand.* **2012**, *56* (4), 420–432.
 - (39) Eger, E. I. Isoflurane: A Review. *Anesthesiology* **1981**, *55*, 559–576.
 - (40) Torchilin, V. P. Micellar Nanocarriers: Pharmaceutical Perspectives. *Pharm. Res.* **2007**, *24* (1), 1–16.
 - (41) Mukherjee, I.; Moulik, S. P.; Rakshit, A. K. Tensiometric Determination of Gibbs Surface Excess and Micelle Point: A Critical Revisit. *J. Colloid Interface Sci.* **2013**, *394* (1), 329–336.
 - (42) Letchford, K.; Burt, H. A Review of the Formation and Classification of Amphiphilic Block Copolymer Nanoparticulate Structures: Micelles, Nanospheres, Nanocapsules and Polymersomes. *Eur. J. Pharm. Biopharm.* **2007**, *65* (3), 259–269.
 - (43) Rosen, M. J.; Kunjappu, J. T. *Surfactants and Interfacial Phenomena*, 4th ed.; John Wiley & Sons, Inc.: Hoboken, New Jersey, 2012.
 - (44) Menger, F. M.; Shi, L.; Rizvi, S. A. A. Re-Evaluating the Gibbs Analysis of Surface Tension at the Air/water Interface. *J. Am. Chem. Soc.* **2009**, *131* (30), 10380–10381.
 - (45) Pan, A.; Rakshit, A. K.; Moulik, S. P. Dwelling on the Adsorption of Surfactant at the Air/water Interface in Relation to Its States in the Bulk: A Comprehensive Analysis. *Colloids Surfaces A Physicochem. Eng. Asp.* **2015**, *464*, 8–16.
 - (46) Li, P. X.; Li, Z. X.; Shen, H. H.; Thomas, R. K.; Penfold, J.; Lu, J. R. Application of the Gibbs Equation to the Adsorption of Nonionic Surfactants and Polymers at the Air-Water Interface: Comparison with Surface Excesses Determined Directly Using Neutron Reflectivity. *Langmuir* **2013**, *29* (30), 9324–9334.
 - (47) Israelachvili, J. N. *Intermolecular and Surface Forces*, 3rd ed.; Academic Press: Burlington, MA, 2011.

- (48) Topel, Ö.; Çakır, B. A.; Budama, L.; Hoda, N. Determination of Critical Micelle Concentration of Polybutadiene-*block*-Poly(ethyleneoxide) Diblock Copolymer by Fluorescence Spectroscopy and Dynamic Light Scattering. *J. Mol. Liq.* **2012**, *177*, 40–43.
- (49) Torchilin, V. P.; Levchenko, T. S.; Whiteman, K. R.; Yaroslavov, A. A.; Tsatsakis, A. M.; Rizos, A. K.; Michailova, E. V.; Shtilman, M. I. Amphiphilic Poly-*N*-Vinylpyrrolidones: Synthesis, Properties and Liposome Surface Modification. *Biomaterials* **2001**, *22* (22), 3035–3044.
- (50) Ananthapadmanabhan, K. P.; Kuo, P. L.; Goddard, E. D.; Turro, N. J. Fluorescence Probes for Critical Micelle Concentration. *Langmuir* **1985**, *1* (9), 352–355.
- (51) Carpena, P.; Aguiar, J.; Bernaola-Galván, P.; Carnero Ruiz, C. Problems Associated with the Treatment of Conductivity-Concentration Data in Surfactant Solutions: Simulations and Experiments. *Langmuir* **2002**, *18* (16), 6054–6058.
- (52) Hiemenz, P. C.; Rajagopalan, R. *Principles of Colloid and Surface Chemistry*, 3rd ed.; Marcel Dekker, Inc.: New York, New York, 1997.
- (53) Biedermann, F.; Nau, W. M.; Schneider, H.-J. The Hydrophobic Effect Revisited-Studies with Supramolecular Complexes Imply High-Energy Water as a Noncovalent Driving Force. *Angew. Chem. Int. Ed. Engl.* **2014**, 2–16.
- (54) Meguro, K.; Takasawa, Y.; Kawahashi, N.; Tabata, Y.; Ueno, M. Micellar Properties of a Series of Octaethyleneglycol-*N*-Alkyl Ethers with Homogeneous Ethylene Oxide Chain and Their Temperature Dependence. *J. Colloid Interface Sci.* **1981**, *83* (1), 50–56.
- (55) Kunieda, H.; Shinoda, K. Krafft Points, Critical Micelle Concentrations, Surface Tension, and Solubilizing Power of Aqueous Solutions of Fluorinated Surfactants. *J. Phys. Chem.* **1976**, *80* (22), 2468–2470.
- (56) Yang, C.; Ebrahim Attia, A. B.; Tan, J. P. K.; Ke, X.; Gao, S.; Hedrick, J. L.; Yang, Y. Y. The Role of Non-Covalent Interactions in Anticancer Drug Loading and Kinetic Stability of Polymeric Micelles. *Biomaterials* **2012**, *33* (10), 2971–2979.
- (57) Kwon, G. S.; Okano, T. Polymeric Micelles as New Drug Carriers. *Adv. Drug Deliv. Rev.* **1996**, *21*, 107–116.
- (58) Zana, R. Microviscosity of Aqueous Surfactant Micelles : Effect of Various Parameters. *J. Phys. Chem.* **1999**, *103* (43), 9117–9125.
- (59) Allen, C.; Maysinger, D.; Eisenberg, A. Nano-Engineering Block Copolymer Aggregates for Drug Delivery. *Colloids Surfaces B Biointerfaces* **1999**, *16* (1-4), 3–27.

- (60) Israelachvili, J. N.; Mitchell, D. J.; Ninham, B. W. Theory of Self-Assembly of Hydrocarbon Amphiphiles into Micelles and Bilayers. *J. Chem. Soc. Faraday Trans. 2* **1976**, *72*, 1525.
- (61) Nagarajan, R. Molecular Packing Parameter and Surfactant Self-Assembly: The Neglected Role of the Surfactant Tail. *Langmuir* **2002**, *18* (1), 31–38.
- (62) Garbuzenko, O.; Barenholz, Y.; Prie, A. Effect of Grafted PEG on Liposome Size and on Compressibility and Packing of Lipid Bilayer. *Chem. Phys. Lipids* **2005**, *135* (2), 117–129.
- (63) Ashok, B.; Arleth, L.; Hjelm, R. P.; Rubinstein, I.; Önyüksel, H. *In Vitro* Characterization of PEGylated Phospholipid Micelles for Improved Drug Solubilization: Effects of PEG Chain Length and PC Incorporation. *J. Pharm. Sci.* **2004**, *93* (10), 2476–2487.
- (64) Arleth, L.; Ashok, B.; Onyuksel, H.; Thiyagarajan, P.; Jacob, J.; Hjelm, R. P. Detailed Structure of Hairy Mixed Micelles Formed by Phosphatidylcholine and PEGylated Phospholipids in Aqueous Media. *Langmuir* **2005**, *21* (8), 3279–3290.
- (65) Duncanson, W. J.; Figa, M. a.; Hallock, K.; Zalipsky, S.; Hamilton, J. A.; Wong, J. Y. Targeted Binding of PLA Microparticles with Lipid-PEG-Tethered Ligands. *Biomaterials* **2007**, *28* (33), 4991–4999.
- (66) Kastantin, M.; Ananthanarayanan, B.; Karmali, P.; Ruoslahti, E.; Tirrell, M. Effect of the Lipid Chain Melting Transition on the Stability of DSPE-PEG (2000) Micelles. *Langmuir* **2009**, *25* (13), 7279–7286.
- (67) Gao, Z.; Lukyanov, A. N.; Singhal, A.; Torchilin, V. P. Diacyllipid-Polymer Micelles as Nanocarriers for Poorly Soluble Anticancer Drugs. *Nano Lett.* **2002**, *2* (9), 979–982.
- (68) Williams, H. D.; Trevaskis, N. L.; Charman, S. A.; Shanker, R. M.; Charman, W. N.; Pouton, C. W.; Porter, C. J. H. Strategies to Address Low Drug Solubility in Discovery and Development. *Pharmacol. Rev.* **2013**, *65* (1), 315–499.
- (69) Pouton, C. W. Formulation of Poorly Water-Soluble Drugs for Oral Administration: Physicochemical and Physiological Issues and the Lipid Formulation Classification System. *Eur. J. Pharm. Sci.* **2006**, *29* (3-4 SPEC. ISS.), 278–287.
- (70) Junghanns, J. U. H.; Müller, R. H. Nanocrystal Technology, Drug Delivery and Clinical Applications. *Int. J. Nanomedicine* **2008**, *3* (3), 295–309.
- (71) Chen, H.; Khemtong, C.; Yang, X.; Chang, X.; Gao, J. Nanonization Strategies for Poorly Water-Soluble Drugs. *Drug Discov. Today* **2011**, *16* (7-8), 354–360.
- (72) Kwon, G. S. Polymeric Micelles for Delivery of Poorly Water-Soluble Compounds. *Crit. Rev. Ther. Drug Carrier Syst.* **2003**, *20* (5), 357–403.

- (73) Lukyanov, A. N.; Gao, Z.; Torchilin, V. P. Micelles from Polyethylene Glycol/phosphatidylethanolamine Conjugates for Tumor Drug Delivery. *J. Control. Release* **2003**, *91* (1-2), 97–102.
- (74) Weissig, V.; Whiteman, K. R.; Torchilin, V. P. Accumulation of Protein-Loaded Long-Circulating Micelles and Liposomes in Subcutaneous Lewis Lung Carcinoma in Mice. *Pharm. Res.* **1998**, *15* (10), 1552–1556.
- (75) Aw, M. S.; Kurian, M.; Losic, D. Polymeric Micelles for Multidrug Delivery and Combination Therapy. *Chem. - A Eur. J.* **2013**, *19* (38), 12586–12601.
- (76) Choi, H. S.; Liu, W.; Misra, P.; Tanaka, E.; Zimmer, J. P.; Ipe, B. I.; Bawendi, M. G.; Frangioni, J. V. Renal Clearance of Quantum Dots. *Nat. Biotechnol.* **2007**, *25* (10), 1165–1170.
- (77) Moghimi, S. M.; Hunter, A. C.; Murray, J. C. Long-Circulating and Target-Specific Nanoparticles: Theory to Practice. *Pharmacol. Rev.* **2001**, *53* (2), 283–318.
- (78) Maeda, H.; Greish, K.; Fang, J. The EPR Effect and Polymeric Drugs: A Paradigm Shift for Cancer Chemotherapy in the 21st Century. *Adv. Polym. Sci.* **2006**, *193* (1), 103–121.
- (79) Jhaveri, A. M.; Torchilin, V. P. Multifunctional Polymeric Micelles for Delivery of Drugs and siRNA. *Front. Pharmacol.* **2014**, *5*, 1–26.
- (80) Cabral, H.; Matsumoto, Y.; Mizuno, K.; Chen, Q.; Murakami, M.; Kimura, M.; Terada, Y.; Kano, M. R.; Miyazono, K.; Uesaka, M.; Nishiyama, N.; Kataoka, K. Accumulation of Sub-100 nm Polymeric Micelles in Poorly Permeable Tumours Depends on Size. *Nat. Nanotechnol.* **2011**, *6* (12), 815–823.
- (81) Knop, K.; Hoogenboom, R.; Fischer, D.; Schubert, U. S. Poly(ethylene glycol) in Drug Delivery: Pros and Cons as Well as Potential Alternatives. *Angew. Chemie - Int. Ed.* **2010**, *49* (36), 6288–6308.
- (82) Akiba, I.; Terada, N.; Hashida, S.; Sakurai, K.; Sato, T.; Shiraishi, K.; Yokoyama, M.; Masunaga, H.; Ogawa, H.; Ito, K.; Yagi, N. Encapsulation of a Hydrophobic Drug into a Polymer-Micelle Core Explored with Synchrotron SAXS. *Langmuir* **2010**, *26* (10), 7544–7551.
- (83) Aliabadi, H. M.; Elhasi, S.; Mahmud, A.; Gulamhusein, R.; Mahdipoor, P.; Lavasanifar, A. Encapsulation of Hydrophobic Drugs in Polymeric Micelles through Co-Solvent Evaporation: The Effect of Solvent Composition on Micellar Properties and Drug Loading. *Int. J. Pharm.* **2007**, *329* (1-2), 158–165.
- (84) Schuster, T.; Schellenberger, S.; Friedrich, R.; Klapper, M.; Müllen, K. Branched Fluorinated Amphiphiles Based on Carbohydrates. *J. Fluor. Chem.* **2013**, *154* (2013), 30–36.

- (85) Hoang, K. C.; Mecozzi, S. Aqueous Solubilization of Highly Fluorinated Molecules by Semifluorinated Surfactants. *Langmuir* **2004**, *20* (18), 7347–7350.
- (86) Diezi, T. A.; Bae, Y.; Kwon, G. S. Enhanced Stability of PEG-*block*-poly(*N*-Hexyl Stearate L-Aspartamide) Micelles in the Presence of Serum Proteins. *Mol. Pharm.* **2010**, *7* (4), 1355–1360.
- (87) Li, Y.; Xiao, K.; Luo, J.; Xiao, W.; Lee, J. S.; Gonik, A. M.; Kato, J.; Dong, T. A.; Lam, K. S. Well-Defined, Reversible Disulfide Cross-Linked Micelles for on-Demand Paclitaxel Delivery. *Biomaterials* **2011**, *32* (27), 6633–6645.
- (88) Hu, X.; Li, H.; Luo, S.; Liu, T.; Jiang, Y.; Liu, S. Thiol and pH Dual-Responsive Dynamic Covalent Shell Cross-Linked Micelles for Triggered Release of Chemotherapeutic Drugs. *Polym. Chem.* **2012**, 695–706.
- (89) Wei, R.; Cheng, L.; Zheng, M.; Cheng, R.; Meng, F.; Deng, C.; Zhong, Z. Reduction-Responsive Disassemblable Core-Cross-Linked Micelles Based on Poly(ethylene glycol)-*b*-poly(*N*-2-Hydroxypropyl Methacrylamide)-Lipoic Acid Conjugates for Triggered Intracellular Anticancer Drug Release. *Biomacromolecules* **2012**, *13* (8), 2429–2438.
- (90) Xu, X.; Flores, J. D.; McCormick, C. L. Reversible Imine Shell Cross-Linked Micelles from Aqueous RAFT-Synthesized Thermoresponsive Triblock Copolymers as Potential Nanocarriers for “pH-Triggered” Drug Release. *Macromolecules* **2011**, *44* (6), 1327–1334.
- (91) Glavas, L.; Olsén, P.; Odellius, K.; Albertsson, A. C. Achieving Micelle Control through Core Crystallinity. *Biomacromolecules* **2013**, *14* (11), 4150–4156.
- (92) Pan, P.; Shan, G.; Bao, Y.; Fujita, M.; Maeda, M. Core – Shell Structure, Biodegradation, and Drug Release Behavior of Poly(lactic acid)/Poly(ethylene glycol) Block Copolymer Micelles Tuned by Macromolecular Stereostructure. *Langmuir* **2015**, *31*, 1527–1536.
- (93) Amado, E.; Kressler, J. Triphilic Block Copolymers with Perfluorocarbon Moieties in Aqueous Systems and Their Biochemical Perspectives. *Soft Matter* **2011**, *7* (16), 7144.
- (94) Kyeremateng, S. O.; Busse, K.; Kohlbrecher, J.; Kressler, J. Synthesis and Self-Organization of Poly(propylene oxide)-Based Amphiphilic and Triphilic Block Copolymers. *Macromolecules* **2011**, *44* (3), 583–593.
- (95) Marsat, J. N.; Heydenreich, M.; Kleinpeter, E.; Berlepsch, H. V.; Böttcher, C.; Laschewsky, A. Self-Assembly into Multicompartment Micelles and Selective Solubilization by Hydrophilic-Lipophilic-Fluorophilic Block Copolymers. *Macromolecules* **2011**, *44* (7), 2092–2105.
- (96) Skrabania, K.; Berlepsch, H. V.; Böttcher, C.; Laschewsky, A. Synthesis of Ternary, Hydrophilic-Lipophilic-Fluorophilic Block Copolymers by Consecutive RAFT

Polymerizations and Their Self-Assembly into Multicompartment Micelles. *Macromolecules* **2010**, *43* (1), 271–281.

- (97) Skrabania, K.; Laschewsky, A.; Berlepsch, H. V.; Böttcher, C. Synthesis and Micellar Self-Assembly of Ternary Hydrophilic- Lipophilic-Fluorophilic Block Copolymers with a Linear PEO Chain. *Langmuir* **2009**, *25* (13), 7594–7601.
- (98) Hillmyer, M. A.; Lodge, T. P. Synthesis and Self-Assembly of Fluorinated Block Copolymers. *J. Polym. Sci. Part A Polym. Chem.* **2002**, *40* (1), 1–8.
- (99) Li, Z.; Hillmyer, M. A.; Lodge, T. P. Morphologies of Multicompartment Micelles Formed by ABC Miktoarm Star Terpolymers. *Langmuir* **2006**, *22* (22), 9409–9417.
- (100) Li, Z.; Kesselman, E.; Talmon, Y.; Hillmyer, M. A.; Lodge, T. P. Multicompartment Micelles from ABC Miktoarm Stars in Water. *Science* **2004**, *306* (5693), 98–101.
- (101) Jee, J. P.; McCoy, A.; Mecozzi, S. Encapsulation and Release of Amphotericin B from an ABC Triblock Fluorous Copolymer. *Pharm. Res.* **2012**, *29* (1), 69–82.
- (102) Tucker, W. B.; Mecozzi, S. Nanoemulsions in Medicine. In *Handbook of Nanobiomedical Research, Volume 1*; Torchilin, V. P., Ed.; World Scientific Publishing, 2014; pp 141–167.
- (103) Walstra, P. Principles of Emulsion Formation. *Chem. Eng. Sci.* **1993**, *48* (2), 333–349.
- (104) Shinoda, K.; Saito, H. The Stability of O/W Type Emulsions as Functions of Temperature and the HLB of Emulsifiers: The Emulsification by PIT-Method. *Journal of Colloid and Interface Science*, 1969, *30*, 258–263.
- (105) Fernandez, P.; André, V.; Rieger, J.; Kühnle, A. Nano-Emulsion Formation by Emulsion Phase Inversion. *Colloids Surfaces A Physicochem. Eng. Asp.* **2004**, *251* (1-3), 53–58.
- (106) Izquierdo, P.; Esquena, J.; Tadros, T. F.; Dederen, C.; Garcia, M. J.; Azemar, N.; Solans, C. Formation and Stability of Nano-Emulsions Prepared Using the Phase Inversion Temperature Method. *Langmuir* **2002**, *18* (1), 26–30.
- (107) Gutiérrez, J. M.; González, C.; Maestro, A.; Solè, I.; Pey, C. M.; Nolla, J. Nano-Emulsions: New Applications and Optimization of Their Preparation. *Curr. Opin. Colloid Interface Sci.* **2008**, *13* (4), 245–251.
- (108) Chaix, C.; Pacard, E.; Elaïssari, A.; Hilaire, J. F.; Pichot, C. Surface Functionalization of Oil-in-Water Nanoemulsion with a Reactive Copolymer: Colloidal Characterization and Peptide Immobilization. *Colloids Surfaces B Biointerfaces* **2003**, *29* (1), 39–52.

- (109) Kelmann, R. G.; Kuminek, G.; Teixeira, H. F.; Koester, L. S. Carbamazepine Parenteral Nanoemulsions Prepared by Spontaneous Emulsification Process. *Int. J. Pharm.* **2007**, *342* (1-2), 231–239.
- (110) Fryd, M. M.; Mason, T. G. Advanced Nanoemulsions. *Annu. Rev. Phys. Chem.* **2012**, *63* (1), 493–518.
- (111) Bałdyga, J.; Orciuch, W.; Makowski, Ł.; Malski-Brodzicki, M.; Malik, K. Break up of Nano-Particle Clusters in High-Shear Devices. *Chem. Eng. Process. Process Intensif.* **2007**, *46* (9 SPEC. ISS.), 851–861.
- (112) Schultz, S.; Wagner, G.; Urban, K.; Ulrich, J. High-Pressure Homogenization as a Process for Emulsion Formation. *Chem. Eng. Technol.* **2004**, *27* (4), 361–368.
- (113) Leong, T. S. H.; Wooster, T. J.; Kentish, S. E.; Ashokkumar, M. Minimising Oil Droplet Size Using Ultrasonic Emulsification. *Ultrason. Sonochem.* **2009**, *16* (6), 721–727.
- (114) Okushima, S.; Nisisako, T.; Torii, T.; Higuchi, T. Controlled Production of Monodisperse Double Emulsions by Two-Step Droplet Breakup in Microfluidic Devices. *Langmuir* **2004**, *20* (23), 9905–9908.
- (115) Gramdorf, S.; Hermann, S.; Hentschel, A.; Schrader, K.; Müller, R. H.; Kumpugdee-Vollrath, M.; Kraume, M. Crystallized Miniemulsions: Influence of Operating Parameters during High-Pressure Homogenization on Size and Shape of Particles. *Colloids Surfaces A Physicochem. Eng. Asp.* **2008**, *331* (1-2), 108–113.
- (116) Schulz, M. B.; Daniels, R. Hydroxypropylmethylcellulose (HPMC) as Emulsifier for Submicron Emulsions: Influence of Molecular Weight and Substitution Type on the Droplet Size after High-Pressure Homogenization. *Eur. J. Pharm. Biopharm.* **2000**, *49* (3), 231–236.
- (117) Brösel, S.; Schubert, H. Investigations on the Role of Surfactants in Mechanical Emulsification Using a High-Pressure Homogenizer with an Orifice Valve. *Chem. Eng. Process. Process Intensif.* **1999**, *38* (4-6), 533–540.
- (118) Schulman, J. H.; Stoeckenius, W.; Prince, L. M. Mechanism of Formation and Structure of Micro Emulsions by Electron Microscopy. *J. Phys. Chem.* **1959**, *63* (10), 1677–1680.
- (119) Adamson, A. W.; Gast, A. P. Emulsions, Foams and Aerosols. In *Physical Chemistry of Surfaces*; John Wiley & Sons, Inc.: New York, New York, 1997; pp 500–536.
- (120) Urbina-Villalba, G. An Algorithm for Emulsion Stability Simulations: Account of Flocculation, Coalescence, Surfactant Adsorption and the Process of Ostwald Ripening. *Int. J. Mol. Sci.* **2009**, *10* (3), 761–804.

- (121) Myers, D. Association Colloids: Micelles, Vesicles, and Membranes. In *Surfaces, Interfaces, and Colloids: Principles and Applications*; John Wiley & Sons: New York, New York, 1999; pp 358–396.
- (122) Taylor, P. Ostwald Ripening in Emulsions. *Adv. Colloid Interface Sci.* **1998**, 75 (2), 107–163.
- (123) Tadros, T. F. Application of Surfactants in Emulsion Formation and Stabilisation. In *Applied Surfactants: Principles and Applications*; Wiley-VCH GmbH: Weinheim, Germany, 2005; pp 115–186.
- (124) Kabal'nov, A. S.; Pertzov, A. V.; Shchukin, E. D. Ostwald Ripening in Two-Component Disperse Phase Systems: Application to Emulsion Stability. *Colloid Surface.* **1987**, 24 (1), 19–32.
- (125) Musser, J. B.; Fontana, J. L.; Mongan, P. D. The Anesthetic and Physiologic Effects of an Intravenous Administration of a Halothane Lipid Emulsion (5% vol/vol). *Anesth. Analg.* **1999**, 88 (3), 671–675.
- (126) Zhou, J. X.; Luo, N. F.; Liang, X. M.; Liu, J. The Efficacy and Safety of Intravenous Emulsified Isoflurane in Rats. *Anesth. Analg.* **2006**, 102 (1), 129–134.
- (127) Parlato, M. C.; Jee, J. P.; Teshite, M.; Mecozzi, S. Synthesis, Characterization, and Applications of Hemifluorinated Dibranched Amphiphiles. *J. Org. Chem.* **2011**, 76 (16), 6584–6591.
- (128) Fast, J. P.; Perkins, M. G.; Pearce, R. a; Mecozzi, S. Fluoropolymer-Based Emulsions for the Intravenous Delivery of Sevoflurane. *Anesthesiology* **2008**, 109 (4), 651–656.
- (129) Chiari, P. C.; Pagel, P. S.; Tanaka, K.; Krolikowski, J. G.; Ludwig, L. M.; Trillo, R. A.; Puri, N.; Kersten, J. R.; Warltier, D. C. Intravenous Emulsified Halogenated Anesthetics Produce Acute and Delayed Preconditioning against Myocardial Infarction in Rabbits. *Anesthesiology* **2004**, 101 (5), 1160–1166.
- (130) Krahn, C. L.; Raffin, R. P.; Santos, G. S.; Queiroga, L. B.; Cavalcanti, R. L.; Serpa, P.; Dallegrave, E.; Mayorga, P. E.; Pohlmann, A. R.; Natalini, C. C.; Guterres, S. S.; Limberger, R. P. Isoflurane-Loaded Nanoemulsion Prepared by High-Pressure Homogenization: Investigation of Stability and Dose Reduction in General Anesthesia. *J. Biomed. Nanotechnol.* **2012**, 8 (5), 849–858.
- (131) Shah, P.; Bhalodia, D.; Shelat, P. Nanoemulsion: A Pharmaceutical Review. *Syst. Rev. Pharm.* **2010**, 1 (1), 24.
- (132) Primo, F. L.; Michieletto, L.; Rodrigues, M. A. M.; Macaroff, P. P.; Morais, P. C.; Lacava, Z. G. M.; Bentley, M. V. L. B.; Tedesco, A. C. Magnetic Nanoemulsions as Drug Delivery System for Foscan®: Skin Permeation and Retention in Vitro Assays for Topical

Application in Photodynamic Therapy (PDT) of Skin Cancer. *J. Magn. Magn. Mater.* **2007**, *311* (1 SPEC. ISS.), 354–357.

- (133) Watanabe, T.; Ichikawa, H.; Fukumori, Y. Tumor Accumulation of Gadolinium in Lipid-Nanoparticles Intravenously Injected for Neutron-Capture Therapy of Cancer. *Eur. J. Pharm. Biopharm.* **2002**, *54* (2), 119–124.
- (134) Dias, M. L. N.; Carvalho, J. P.; Rodrigues, D. G.; Graziani, S. R.; Maranhão, R. C. Pharmacokinetics and Tumor Uptake of a Derivatized Form of Paclitaxel Associated to a Cholesterol-Rich Nanoemulsion (LDE) in Patients with Gynecologic Cancers. *Cancer Chemother. Pharmacol.* **2007**, *59* (1), 105–111.
- (135) Globule Size Distribution in Lipid Injectable Emulsions. In *United States Pharmacopeia and National Formulary (USP 36 - NF 31)*; United States Pharmacopeia Convention: Rockville, MD, 2012; pp 321–323.

CHAPTER 2:
Synthetic challenges in fluorinated synthesis – decomposition of
fluorotelomer alcohols

*This chapter is published, in part, under the same title – Reference: Tucker, W.B.; Mecozzi, S.
Base-induced instability of fluorotelomer alcohols. *J. Fluor. Chem.*, **2013**, *156*, 26-29.

Abstract

While the incorporation of perfluoroalkyl substituents has found widespread utility in the fields of fluorous synthesis, extraction and chromatography, fluorotelomer alcohols are remarkably absent from investigations into the use of fluorinated substituents. In addition, fluorotelomer alcohols are also reported in methodological studies to give atypical results.

Work in the Mecozzi group to incorporate fluorotelomer alcohols by Williamson ether syntheses has consistently lead to poor and non-reproducible results. To further understand this anomalous behavior, the stability of fluorotelomer alcohols under basic conditions was studied. HF-elimination across the $\text{CF}_2\text{-CH}_2$ junction has been shown to be facilitated by an intramolecular hydrogen bond. The differences in fluorotelomer alcohol stabilities, those with larger fluorocarbon blocks are more stable than those with smaller fluorinated moieties, were found to be related to the solubility of the alcohols in the solvent. While fluorotelomer alcohols are unstable, they can be rendered kinetically stable if either the alcohol or the base has low solubility in the reaction medium.

2.1 Introduction

Because of their unique hydro- and lipophobicity, the incorporation of fluorocarbons onto otherwise non-fluorous molecules has found widespread application in fluorinated materials,¹ fluorous synthesis^{2,3} and separation.⁴⁻⁷ The application of fluorocarbons in these fields relies upon the unique hydro- and lipophobicity of fluorophilic materials to form a separate fluorous phase. This tendency to only associate with other fluorous groups underlies the unique properties and effective separations achievable with fluorinated compounds. To be broadly applicable, however, the introduction of (semi-)fluorous substituents must be synthetically efficient and reliable. To this end, numerous fluorous synthons and protecting groups have been developed.⁸ Noticeably absent from any such list are fluorotelomer alcohols and their derivatives.

Fluorotelomer alcohols, $F-(CF_2)_x(CH_2)_2-OH$ generally designated FXH₂-OH, are not used in fluorous extraction or synthesis literature. In addition, fluorotelomer alcohols are reported to give abnormal results in methodological and synthetic studies.⁹⁻¹¹ The anomalies associated with fluorotelomer alcohols have been generally attributed to hydrogen-fluoride elimination across the CF_2-CH_2 junction.¹² Yet, the proposed elimination of HF has often been cited as the Achilles' heel of all fluorous ponytails. As such, HF-elimination in fluorotelomer alcohols, a problem already known and expected when utilizing semi-fluorinated materials, raises an understudied question: why do fluorotelomer alcohols decompose more readily than other semifluorinated molecules that also possess a CF_2-CH_2 group?

In the field of biological degradation of fluorotelomer alcohols, the CF_2-CH_2 junction instability has been implicated in their conversion to perfluorinated acids as observed in *in vivo* studies of mice. In this case, HF elimination has been proposed to follow metabolic oxidation of the hydroxyl group.¹³ While the degradation pathway is well understood in biological systems,

the unique chemical instability of fluorotelomer species is both poorly understood and under reported for conditions encountered in synthesis.

In this chapter, a detailed study on the mechanism of fluorotelomer alcohol decomposition in synthetically relevant conditions is presented. First, the unique instability of fluorotelomer alcohols is shown to relate to their structure. Second, the fundamental importance of solubility – the more soluble an alcohol the more rapid its decomposition – is demonstrated. These results provide an explanation for the anomalous behavior of fluorotelomer alcohols. Moreover, these results also explain the peculiar instability of the perfluorohexyl-telomer alcohol, a case well documented in the literature but never completely explained.^{9–11} As such, the mechanism herein reported should be taken into account when devising syntheses for introducing fluorinated substituents into organic molecules.

2.2 Results and Discussion

2.2.1 Anomalous behavior of fluorotelomer alcohols in synthesis

Synthetic issues with fluorotelomer alcohols have presented themselves in the Mecozzi laboratory on numerous occasions and there are several hallmarks of such problems. First, fluorotelomer alcohols yield little to no product when used in Williamson ether syntheses. Second, fluorotelomer alcohols in basic, THF solution typically go from clear to brown-black (**Figure 2.1**). Finally, mesylate electrophiles added to react with fluorotelomer alcohol nucleophiles are typically recovered without having undergone any reaction.

To provide for reproducible and comparable decomposition results, a standard reaction system was developed: to a flask with dry THF were added perfluorotelomer alcohol (enough to achieve a concentration of 12 mM) and 3 equivalents of base after which the reaction was heated to reflux for 24 hours. Sodium hydride and potassium *tert*-butoxide were both utilized in this

study as bases. Stability was then defined as a lack of color change and lack of new signals by ^1H - and ^{19}F -NMR. NMR confirmed the correlation between instability – the appearance of new signals by ^1H - and ^{19}F - NMR – and the empirical observation of color change.



Figure 2.1. Physical appearance of F6H2-OH after being heated in NaH/THF.

2.2.2 Decomposition of fluorotelomer alcohols of different sizes

Alcohols F4H2-OH, F6H2-OH, F8H2-OH and F10H2-OH were all subjected to the standard stability test along with decan-1-ol and 1,1,1,2,2,3,3,4,4,5,5,6,6-tridecafluorooctane pentyl ether (F6H2-O-H5) as controls. Both decan-1-ol and F6H2-O-H5 showed no color change. Decan-1-ol showed no change by NMR. In contrast F6H2-O-H5 did show the appearance of new, low intensity, signals at 5.84, 5.75, 4.22, 3.75, 1.85 and 1.26 ppm (**Figure 2.2**). These new signals correspond to those seen in the decomposition of fluorotelomer alcohols (**Figure 2.3**); however, the extent of decomposition was dramatically less than that seen for any alcohol except F10H2-OH. Note that all NMR spectra not included in this chapter can be found in Appendix 2, Section A.2.

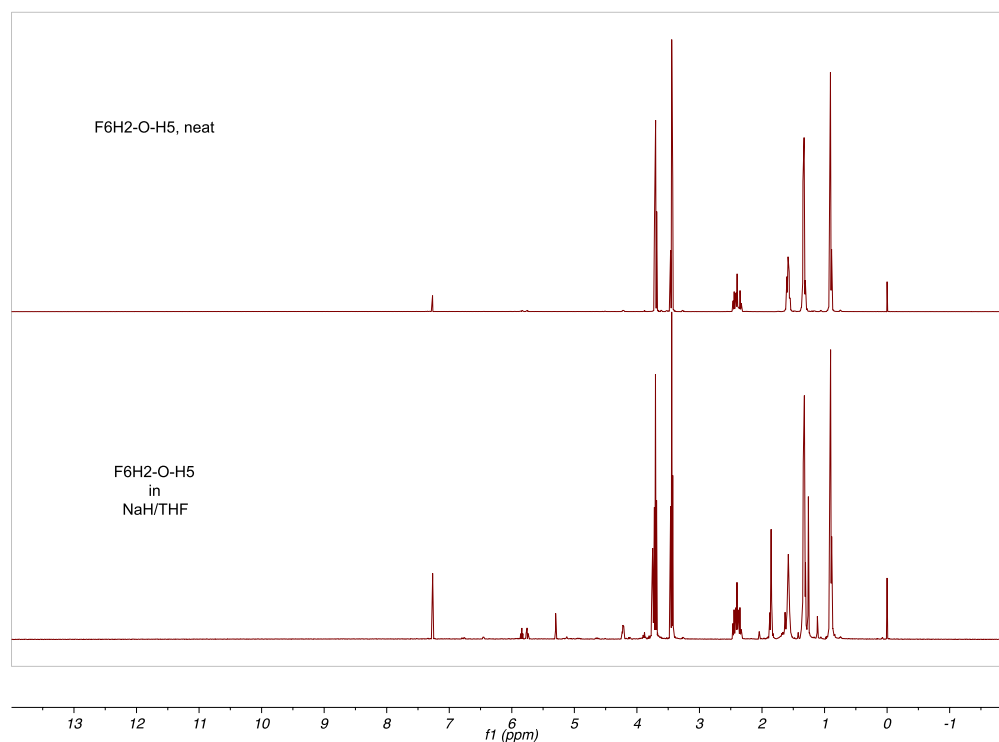


Figure 2.2. ^1H -NMR of F6H2-O-H5 before (top) and after (bottom) refluxing in NaH/THF for 24 h.

In contrast to either control, the fluorotelomer alcohols showed variable rates of decomposition ranging from immediate color change (F4H2-OH) to only mild color change after 24 h (F10H2-OH). In addition to this variable rate of color change, the ^1H -NMR spectra (**Figure 2.3**) for the four, stability-tested alcohols showed different levels of change in appearance. Both F4H2-OH and F6H2-OH show the complete disappearance of starting material signals and the growth of numerous new signals. In addition, F8H2-OH showed numerous new signals by ^1H -NMR but maintained some of the starting material signals. Only F10H2-OH shows minimal sign of decomposition by NMR.

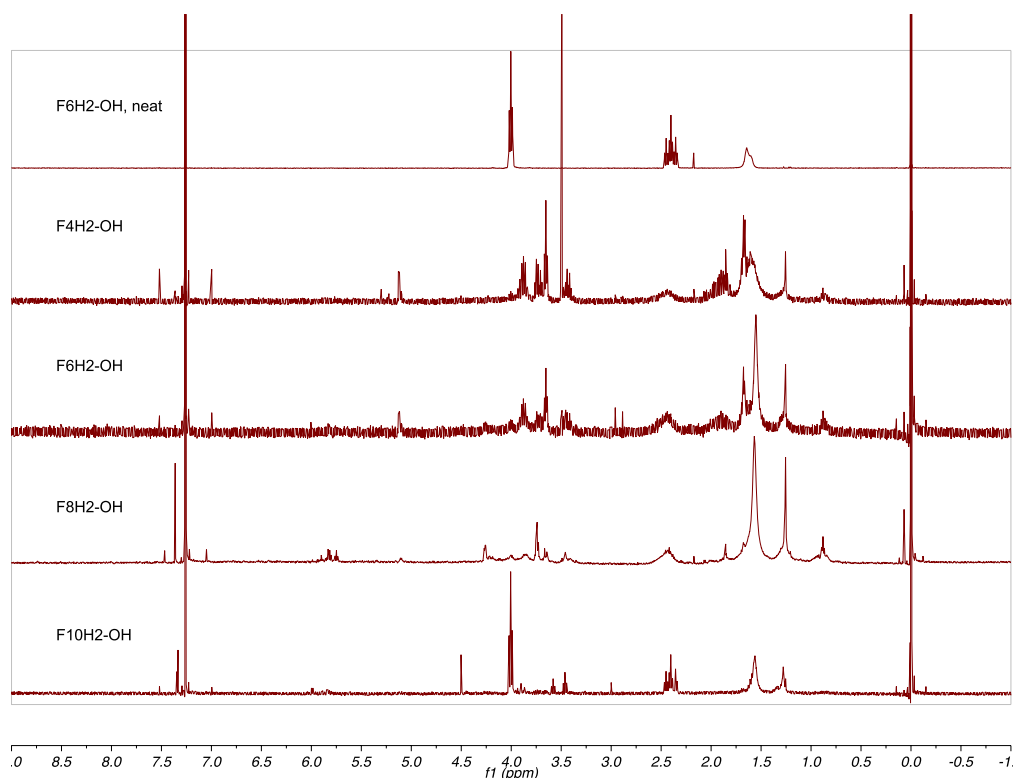


Figure 2.3. ^1H -NMR spectra from top to bottom of neat F6H2-OH (all starting fluorotelomer alcohols ^1H -NMR are identical) and F4H2-OH, F6H2-OH, F8H2-OH and F10H2-OH after stability tests in NaH/THF.

As seen above, F6H2-OH is not uniquely unstable, but rather exists along a continuum of instability, with increased stability coming from larger fluorocarbon-chain lengths. The more interesting results come from the control tests. The lack of decomposition of decan-1-ol confirms that a $\text{CF}_2\text{--CH}_2$ junction is necessary for the type of decomposition that is being observed to occur. Furthermore, as expected F6H2-O-H5 does show decomposition – it has a $\text{CF}_2\text{--CH}_2$ junction that can eliminate HF – though much less than its analogous alcohol (F6H2-OH). This suggests that the hydroxyl group plays a role in enhancing the decomposition of fluorotelomer alcohols over other species that have a $\text{CF}_2\text{--CH}_2$ junction. Ellis *et al.* has suggested that the unique chemical ionization fragmentations observed by mass spectrometry for fluorotelomer alcohols was the result of the intramolecular hydrogen bond shown in **Figure 2.4**.¹⁴

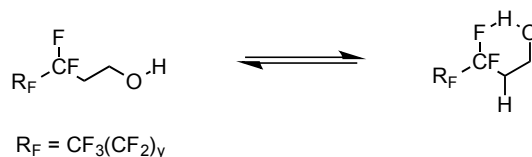


Figure 2.4. Intramolecular hydrogen-bond structure proposed by Ellis *et al.*

2.2.3 Fluorotelomer alcohol decomposition – mechanistic investigations

Our hypothesis is that an intramolecular hydrogen bond (**Figure 2.4**) catalyzes the elimination of HF, starting the chain of events that leads to further decomposition of the fluorinated alcohols. Other heteroatoms usually outcompete aliphatic fluorine as hydrogen-bond acceptors, but aliphatic fluorines have been demonstrated to form hydrogen bonds.¹⁵ To further test this hydrogen-bond-enhanced-decomposition hypothesis, fluorinated alcohols with a single methylene spacer, F3H1-OH, F6H1-OH and F8H1-OH, were tested under the same conditions. These single-methylene alcohols showed no decomposition. The lack of decomposition for F3H1-OH, F6H1-OH and F8H1-OH can be explained by considering that alcohols with a single methylene between the first CF₂ and the hydroxyl group are unable to form the intramolecular hydrogen bond that catalyzes HF elimination. This is supported by a recent theoretical study by Cormanich *et al.*, where calculations at the B3LYP/aug-cc-pVDZ level of theory and basis set showed that an intramolecular H-bond cannot form between fluorine and hydroxyl groups when involved in five-membered rings.¹⁶ Together, hydroxyl group-catalyzed HF elimination appears to be the best explanation for the uniquely enhanced instability of fluorotelomer alcohols.

The mechanism of HF elimination and subsequent alcohol decomposition – through reaction of the intermediate alkene – was investigated via timed stability tests of F6H2-OH. The reaction was quenched after 15 min, 30 min, 1 h, 2 h and 24 h. All reactions were worked up by simple aqueous extraction using D₂O. Free fluoride was observed by ¹⁹F-NMR in the aqueous washings from all stability tests, while no starting alcohol was observed in the D₂O washings. An overlay

of the ^1H -NMR spectra for each time point between 5.0 and 7.0 ppm is shown in **Figure 2.5**. A double of triplets at 5.9 ppm with coupling constants of 33 and 6.5 Hz is seen to increase in intensity up to 1 h and then decrease to a low, steady-state level between 2 and 24 h. The NMR chemical shifts and coupling constants are comparable to those observed from the literature for semi-fluorinated alkenes.^{17,18} Together, these results suggest that the semi-fluorinated alkene is indeed an intermediate in the decomposition pathway. It should be noted that the results do not rule out the possibility of a second elimination to form a highly polarized alkyne, but there is currently no evidence to support such a pathway.

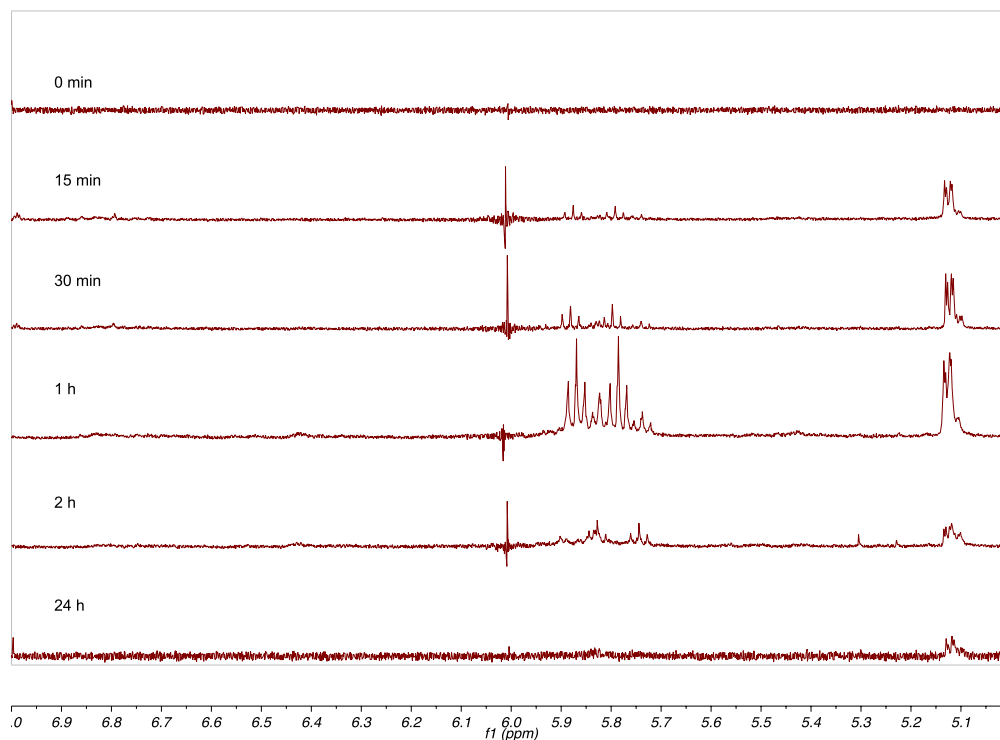


Figure 2.5. Appearance and disappearance of vinyl proton signals during timed stability test of F6H2-OH, times from top to bottom: 0 min, 15 min, 30 min, 1 h, 2 h, 24 h.

By Bent's rule,¹⁹ the semi-fluorinated alkene produced by HF elimination is expected to be unstable. In addition, the semi-fluorinated alkene is highly polarized and susceptible to nucleophilic attack and oligomerization via an anionic mechanism (**Figure 2.6**). This

oligomerization process explains the myriad of new signals observed in the ‘product’ $^1\text{H-NMR}$ (**Figure 2.3**). The resulting product mixture proved intractable to purification, possessed a very low R_f by TLC, and was un-analyzable by mass spectrometry. The hydrogen-bond-facilitated elimination mechanism can explain the unique instability of fluorotelomer alcohols but not the differences in the rate and extent of decomposition observed among the alcohols.

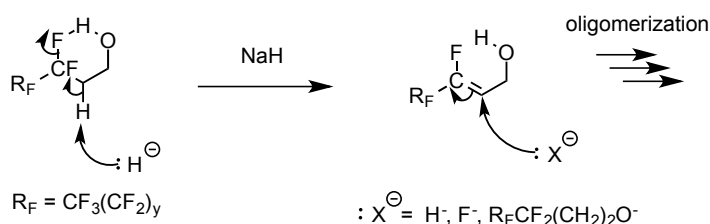


Figure 2.6. Proposed decomposition pathway of fluorotelomer alcohols using sodium hydride as the base.

2.2.4 Alcohol and base – solubility and stability

The change from a non-hydrogen-bonded conformer to a hydrogen-bonded conformer (**Figure 2.4**) necessarily involves a change in the dipole moment of the fluorotelomer alcohols and this offered potential insight into the role that polarity might play in stability. Using Gaussian 09²⁰ through geometry optimization at B3LYP/6-31G** level of theory and basis set, the dipole moments of each conformer for the alcohols were calculated. The non-hydrogen-bond conformers have an average dipole moment of 2.14 ± 0.16 Debye. The hydrogen-bond conformers have an average dipole moment of 1.04 ± 0.03 Debye. Given the large change in dipole moment upon forming the intramolecular hydrogen bond, solvent polarity was investigated as a potential factor in favoring the hydrogen-bond (more-reactive) conformer over the linear (less reactive) conformer. Polar solvents were expected to favor the non-hydrogen-bond conformer and hence increase stability.

To test the effect of solvent polarity on alcohol stability, F6H2-OH was concomitantly tested in hexanes, THF and DMF using NaH as the base. The time it took each reaction to turn brown was 24 h in hexanes, 50 min in THF and 12 min in DMF. The trend is the exact opposite of that expected: polar solvents decrease stability instead of increasing it. This unexpected trend can be attributed to two factors. First, HF elimination proceeds through a very polar transition state (formation of a carbanion and subsequent elimination of fluoride). A polar solvent is better able to stabilize the developing charges, thus lowering the barrier to decomposition. Second, the different solvents affect the solubility of the base. The more poorly soluble the base, the more selective that base becomes for the more acidic hydroxyl proton over the less acidic methylene proton.

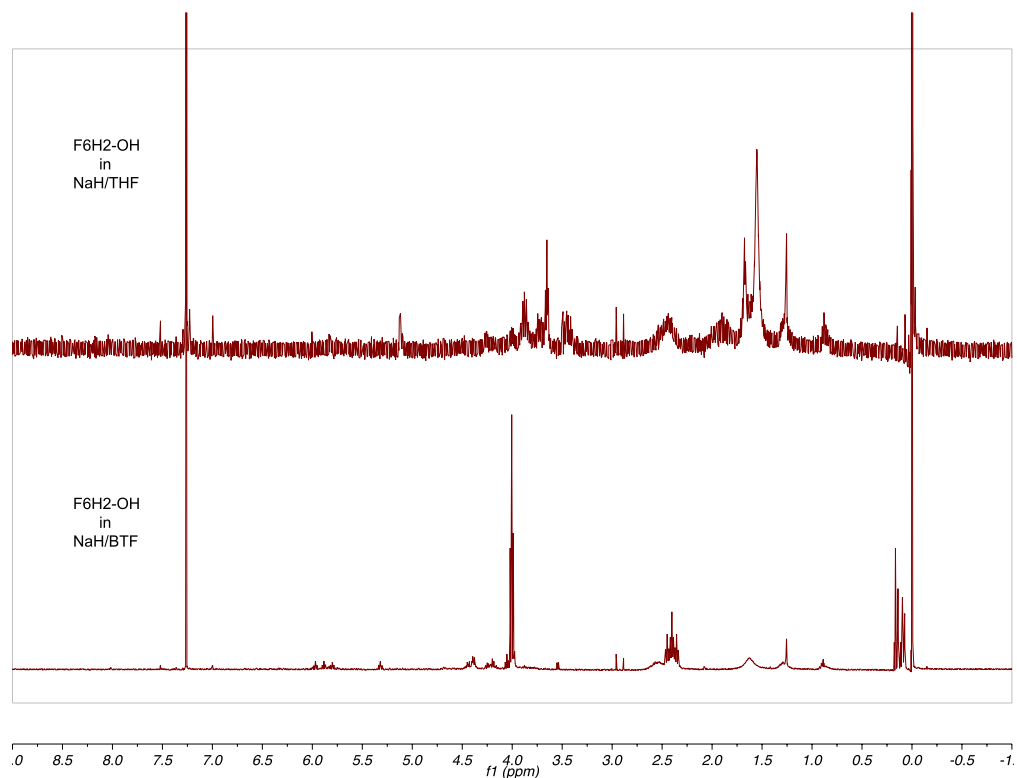


Figure 2.7. Comparison of F6H2-OH decomposition under standard stability conditions (NaH/THF, Top) and less-soluble base conditions (NaH/BTF, Bottom).

Potassium *tert*-butoxide was chosen as a more soluble base to investigate the role of base solubility in alcohol decomposition. The overall trend remains the same as that observed with NaH, though the rate of decomposition is dramatically accelerated: 16 min to brown color in hexanes, 12 min in THF and 7 min in DMF. Thus, as the solubility of the base increased, the stability of the alcohol diminished. The most dramatic example of this base solubility was obtained when F6H2-OH was tested in BTF (α,α,α -trifluorotoluene) with NaH. Sodium hydride is completely insoluble in BTF and F6H2-OH showed as little decomposition as F10H2-OH in THF with NaH, the least amount of decomposition for any FxH2-OH system tested (**Figure 2.7**). Overall, solvent polarity affects the rate of decomposition by two means: increased polarity lowers the activation barrier to HF elimination and increases the base solubility thus allowing the base to abstract the less acidic methylene proton.

By analogy to the effect of base solubility on alcohol stability, fluorotelomer alcohol solubility was investigated as a means of explaining stability differences among alcohols. The solubility of all fluorotelomer alcohols in THF was determined by addition of 100 mg of each alcohol to 5 mL of THF, vortexing the solution and then letting it sit for 10 min. If there was no phase separation or precipitation of the alcohol, 100 mg more was added and the process repeated. The results of the solubility tests indicate that F4H2-OH and F6H2-OH are both fully miscible in THF. However, F8H2-OH and F10H2-OH were soluble up to 1.1 M and 9.0 mM, respectively. F10H2-OH, which showed the least decomposition, also has the lowest solubility in THF. This suggests a correlation between the solvation of the alcohol, vis-à-vis solubility, and stability of the alcohol under basic conditions.

Given the vastly different miscibility of F6H2-OH and F10H2-OH in THF, both were retested in DMF, as a more solubilizing solvent. F6H2-OH turned brown in 12 min, while F10H2-OH did the same in 14 min. In addition, the resulting ^1H -NMR (**Figure 2.8**) of the

F10H2-OH stability tested in DMF showed almost no remaining starting material signals. These results show very similar times for color changes to occur between alcohols that possessed dramatic differences in THF. This suggests that the solvation of the alcohol, in terms of solubility, is also important to the degradation of fluorotelomer alcohols under basic conditions. When the alcohol is not very soluble the $\text{CF}_2\text{-CH}_2$ junction is less accessible to the base. Hence, base-catalyzed HF elimination is afforded kinetic protection. The result is increased stability in THF for the less soluble F8H2-OH and F10H2-OH.

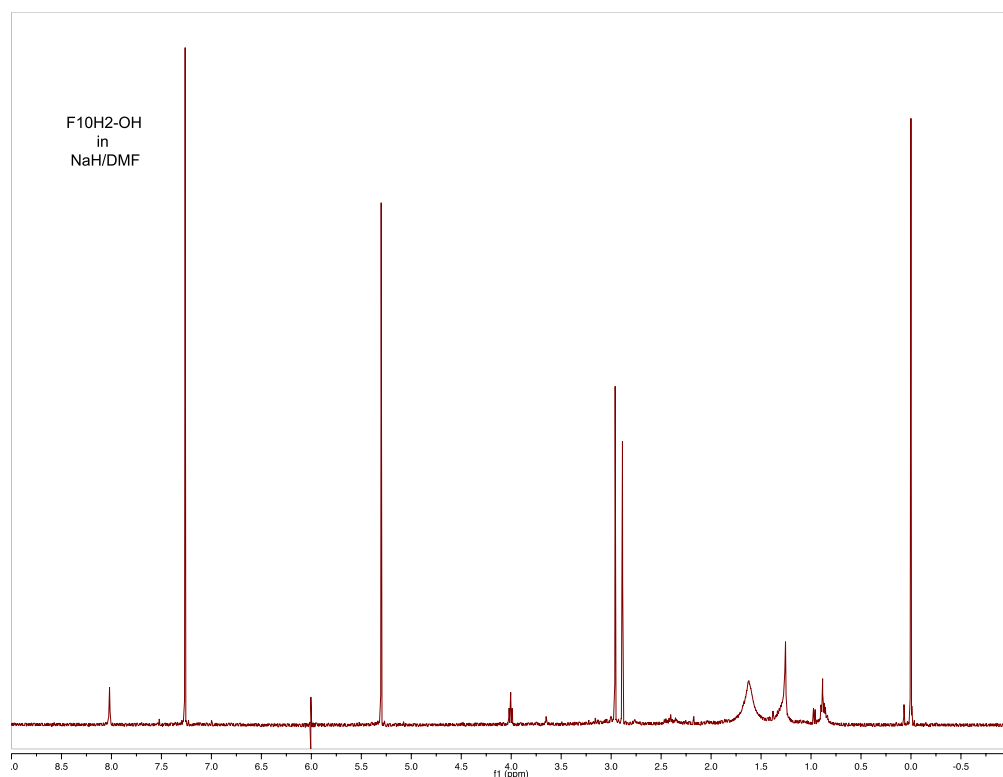


Figure 2.8. Resulting ^1H -NMR of F10H2-OH stability tested in NaH/DMF.

The possibility that the slow rate of decomposition observed with the larger alcohols could be due to the spontaneous formation of supramolecular fluorous aggregates, which would prevent the intramolecular elimination of HF, was also considered. To probe the viability of aggregation by fluorotelomer alcohols, solutions of 12 mM fluorotelomer alcohol in THF were prepared and

analyzed by dynamic light scattering (DLS). No aggregates were observed for any alcohol at the concentrations used to monitor decomposition behavior.

A study of aggregation behavior of F8H2-OH in THF was carried out by ^{19}F -NMR experiments of solutions ranging from 1 mM to 1 M. Using 0.1 mM BTF as an internal reference, ^{19}F -NMR spectra were collected and the change in chemical shift, in Hz, of the trifluoromethyl groups was plotted against the log of concentration (**Figure 2.9**). By NMR, F8H2-OH was only observed to aggregate at concentrations at or above 1 M, concentrations that approach the solubility limit of F8H2-OH. Therefore, while possible, aggregation seems unlikely as an explanatory factor for alcohol stability. Aggregation can further be ruled out for two reasons. First, F4H2-OH and F6H2-OH are both fully soluble in THF and show no signs of aggregation by DLS, yet F6H2-OH decomposes more slowly than F4H2-OH. Second, F8H2-OH is more stable still and yet shows no signs of aggregating at the concentrations used – either by DLS or by NMR.

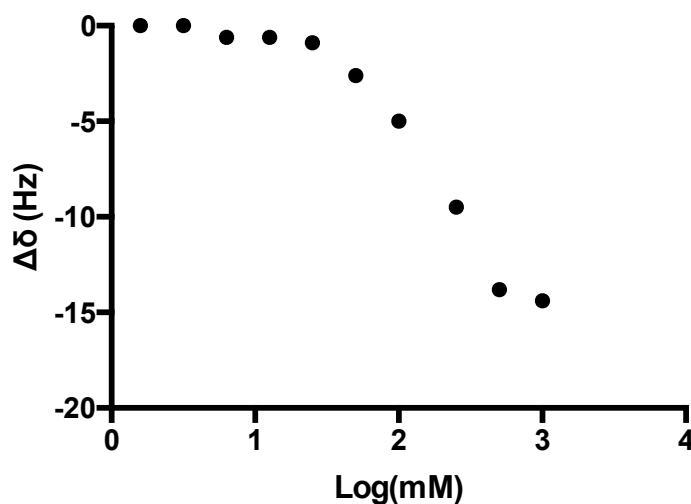


Figure 2.9. Change in CF_3 chemical shift against concentration for F8H2-OH.

2.3 Conclusions

The ready decomposition of fluorotelomer alcohols was investigated. Fluorotelomer alcohols are uniquely unstable due to the formation of an intramolecular hydrogen bond, which facilitates HF elimination. It has been demonstrated, spectroscopically, that HF elimination is indeed the mechanism by which decomposition initiates. The resulting, unstable alkene is then proposed to oligomerize to give an intractable mixture of unidentifiable products. Solvation is the best mechanism to explain the differences in the decomposition with changes in solvent, base and fluorous-segment length. In contrast to the mechanism elucidated in *in vivo* degradation, these results demonstrate an HF-elimination pathway that does not first depend on oxidation of the alcohol. The data also suggest a means of circumventing the instability problem for synthetic ends: the use of solvents in which either the base or alcohol is not very soluble. The effectiveness of this type of methodology has been used in a recent publication by Zaggia *et al.* to yield semi-fluorinated ethers from fluorotelomer alcohols and bromoalkanes in aqueous KOH in good to excellent yields (**Figure 2.10**).²¹

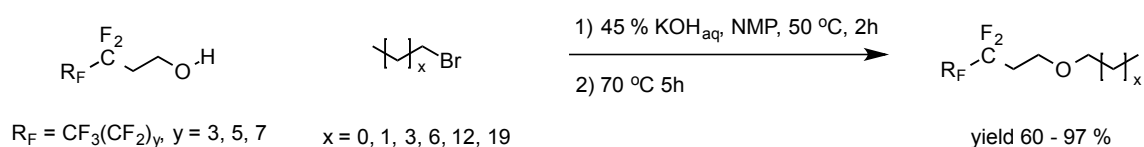


Figure 2.10. Synthetic methodology for synthesis of semifluorinated ethers utilizing fluorotelomer alcohols devised by Zaggia *et al.*

2.4 Experimental

2.4.1 Materials

Fluorous chemicals were purchased from SynQuest Laboratories Inc. (Alachua, FL). All solvents were of ACS grade or higher and were purchased from Sigma-Aldrich (St. Louis, MO). All other reagents were purchased from Sigma-Aldrich (St. Louis, MO) and were used as

received unless otherwise specified. ^1H - and ^{19}F -NMR spectra were obtained on Varian Unity-Inova 400 and Unity-Inova 500 spectrometers using CDCl_3 as solvent with TMS as an internal reference. BTF was added as an internal reference as needed. Particle sizes were determined by dynamic light scattering (DLS) using a NICOMP 380ZLS, Particle Sizing System (Santa Barbara, CA).

2.4.2 Methods

To a dry 25 mL round bottom flask on ice, under argon were added 10 mL of dry solvent (THF, BTF, hexane or DMF) and 0.36 mmol of base (NaH or potassium tert-butoxide). To this were added 0.12 mmol of $\text{F}_x\text{H}_2\text{OH}$. The reaction was then slowly warmed from 0 °C to reflux and allowed to react for 24 h. The reaction was then cooled, diluted with 50 mL DCM and washed with 50 mL water. The organic layer was then dried over magnesium sulfate and condensed under reduced pressure.

Full-sized NMR spectra for each alcohol before and after the stability tests and all NMR spectra not included within this chapter can be found in Appendix 2, Section A.2.

2.5 References

- (1) Berger, R.; Resnati, G.; Metrangolo, P.; Weber, E.; Hulliger, J. Organic Fluorine Compounds: A Great Opportunity for Enhanced Materials Properties. *Chem. Soc. Rev.* **2011**, 40 (7), 3496–3508.
- (2) Curran, D. P. Strategy-Level Separations in Organic Synthesis: From Planning to Practice. *Angew. Chemie - Int. Ed.* **1998**, 37 (9), 1174–1196.
- (3) Zhang, W. Fluorous Linker-Facilitated Chemical Synthesis. *Chem. Rev.* **2009**, 109 (2), 749–795.

- (4) Yoshida, J. I.; Itami, K. Tag Strategy for Separation and Recovery. *Chem. Rev.* **2002**, *102* (10), 3693–3716.
- (5) Curran, D. P.; Sinha, M. K.; Zhang, K.; Sabatini, J. J.; Cho, D.-H. Binary Fluorous Tagging Enables the Synthesis and Separation of a 16-Stereoisomer Library of Macrospheptides. *Nat. Chem.* **2012**, *4* (3), 235–235.
- (6) Tzschucke, C. C.; Markert, C.; Bannwarth, W.; Roller, S.; Hebel, A.; Haag, R. Modern Separation Techniques for the Efficient Workup in Organic Synthesis. *Angew. Chemie - Int. Ed.* **2002**, *41* (21), 3964–4000.
- (7) Zhang, W.; Curran, D. P. Synthetic Applications of Fluorous Solid-Phase Extraction (F-SPE). *Tetrahedron* **2006**, *62* (51), 11837–11865.
- (8) Rábai, J. Getting Started in Synthesis: A Tabular Guide to Selected Monofunctional Fluorous Compounds. In *Handbook of Fluorous Chemistry*; Gladysz, J. A., Curran, D. P., Horvath, I. ., Eds.; Wiley-VCH GmbH: Weinheim, Germany, 2005; pp 156–174.
- (9) Xu, W.; Osei-Prempeh, G.; Lema, C.; Davis Oldham, E.; Aguilera, R. J.; Parkin, S.; Rankin, S. E.; Knutson, B. L.; Lehmler, H. J. Synthesis, Thermal Properties, and Cytotoxicity Evaluation of Hydrocarbon and Fluorocarbon Alkyl β -D-Xylopyranoside Surfactants. *Carbohydr. Res.* **2012**, *349*, 12–23.
- (10) Meinert, H.; Geister, U. Semifluorinated Symmetrical Diethers. *J. Fluor. Chem.* **1994**, *68* (2), 221–226.
- (11) Harada, N. A.; Nishikata, T.; Nagashima, H. Vinyl Polymerization versus [1,3] O to C Rearrangement in the Ruthenium-Catalyzed Reactions of Vinyl Ethers with Hydrosilanes. *Tetrahedron* **2012**, *68* (15), 3243–3252.
- (12) Rocaboy, C.; Rutherford, D.; Bennett, B. L.; Gladysz, J. A. Strategy and Design in Fluorous Phase Immobilization: A Systematic Study of the Effect of “Pony Tails” $(\text{CH}_2)_3(\text{CF}_2)_{n-1}\text{CF}_3$ on the Partition Coefficients of Benzenoid Compounds. *J. Phys. Org. Chem.* **2000**, *13* (10), 596–603.
- (13) Zhang, X. J.; Lai, T. B.; Kong, R. Y. C. Biology of Fluoro-Organic Compounds. *Top. Curr. Chem.* **2012**, *308*, 365–404.
- (14) Ellis, D. A.; Mabury, S. A. Chemical Ionization Pathways of Polyfluorinated Chemicals - A Connection to Environmental Atmospheric Processes. *J. Am. Soc. Mass Spectrom.* **2003**, *14* (10), 1177–1191.
- (15) Caminati, W.; Melandri, S.; Maris, A.; Ottaviani, P. Relative Strengths of the O-H---Cl and O-H---F Hydrogen Bonds. *Angew. Chemie - Int. Ed.* **2006**, *45* (15), 2438–2442.

- (16) Cormanich, R.; Freitas, M. P.; Tormena, C. F.; Rittner, R. The F^{•••}HO Intramolecular Hydrogen Bond Forming Five-Membered Rings Hardly Appear in Monocyclic Organofluorine Compounds. *RSC Adv.* **2012**, 2 (10), 4169.
- (17) Petrov, V. A. New Electrophilic Reaction of Perfluoroalkylethylenes. Synthesis and Some Reactions of 1-Halo-1,1,2-Trihydroperfluoroalkenes. *J. Org. Chem.* **1995**, 60 (11), 3423–3426.
- (18) Banks, R. E.; Barlow, M. G.; Nickkho-Amiry, M. Preparation of 2,3,3,3-Tetrafluoropropene from Trifluoroacetylacetone and Sulphur Tetrafluoride. *J. Fluor. Chem.* **1997**, 82 (2), 171–174.
- (19) Lemal, D. M. Perspective on Fluorocarbon Chemistry. *J. Org. Chem.* **2004**, 69 (1), 1–11.
- (20) Frisch, M. J. T.; Trucks, G. W.; Schlegel, H. B.; Scuseria, G. E.; Robb, M. A.; Cheeseman, J. R.; Scalmani, G.; Barone, V.; Mennucci, B.; Petersson, G. A.; Nakatsuji, H.; Caricato, M.; Li, X.; Hratchian, H. .; Izaylov, A. F.; Bloino, J.; Zheng, G.; Sonnenberg, J. L.; Hada, M.; Ehara, M.; Toyota, K.; Fukuda, R.; Hasegawa, J.; Ishida, M.; Nakajima, N.; Honda, Y.; Kitao, O.; Nakai, H.; Vreven, T.; Montgomery Jr., J. A.; Peralata, J. E.; Ogliaro, F.; Bearpark, M.; Heyd, J. J.; Brothers, E.; Kudin, K. N.; Staroverov, V. N.; Kobayashi, R.; Normand, J.; Raghavachari, K.; Rendell, A.; Burant, J. C.; Iyengar, S. S.; Tomasi, J.; Cossi, M.; Rega, N.; Millam, N. J.; Klene, M.; Knox, J. E.; Corss, J. B.; Bakken, V.; Adamo, C.; Jaramillo, J.; Gomperts, R.; Stratmann, R. E.; Yazyev, O.; Austin, A. J.; Cammi, R.; Pomelli, C.; Ochterski, J. W.; Martin, R. L.; Morokuma, K.; Zakrzewski, V. G.; Voth, G. A.; Salvador, P.; Dannenberg, J. J.; Dapprich, S.; Daniels, A. D.; Farkas, O.; Foresman, J. B.; Ortiz, J. V.; Cioslowski, J.; Fox, D. J. Gaussian 09, B. 1 Revision, Gaussian, Inc. Wallingford, CT. 2009.
- (21) Zaggia, A.; Conte, L.; Padoan, G.; Ceretta, F. Synthesis and Characterization of Partially Fluorinated Ethers. *J. Fluor. Chem.* **2010**, 131 (8), 844–851.

CHAPTER 3:

Relationship between structure and behavior of semifluorinated triphilic surfactants

Contribution: Dr. Aaron McCoy, with Matthew Murphy and Melissa Stagg, synthesized the miktoarm surfactants. Samantha Fix assisted William Tucker in the synthesis of the linear surfactants. William Tucker completed all other work and studies presented in this chapter.

*This chapter is published, in part, under the same title – Reference: Tucker, W.B.; McCoy, A.M.; Fix, S.M.; Stagg, M.F.; Murphy, M.M.; Mecozi, S. Synthesis, physicochemical characterization, and self-assembly of linear, dibranched, and miktoarm semifluorinated triphilic polymers. *J. Polym. Sci. A., Polym. Chem.* **2014**, 52, 3324-3336.

Abstract

In this chapter is described the synthesis and characterization of linear and dibranched triphiles containing hydrophilic, lipophilic and fluorophilic moieties in an attempt to elucidate the relationship between semi-fluorinated surfactant structure and aggregate behavior in aqueous solution. The addition of fluorocarbon substituents and increasing their length led to an exponential decrease in critical micelle concentration (CMC) and a logarithmic increase in core microviscosity. In addition, triphilic micelles showed greater kinetic stability, dissociating more slowly in the presence of human serum, than did diphilic micelles. Finally, encapsulation studies with the hydrophobic drug paclitaxel (PTX) showed that the ability to solubilize and retain PTX increased with the presence of and with the increasing size of the fluorocarbon moiety. In comparison, miktoarm triphiles (synthesized by Dr. Aaron McCoy, Matthew Murphy, and Melissa Stagg) did not show a dramatic increase in thermodynamic stability, kinetic stability, or PTX solubilization/retention. This suggests that placement of fluorocarbons – rather than just the addition of fluorocarbons – in a triphilic structure is important in maximizing the ability of fluorous substituents to improve micelle behavior for possible drug-delivery applications.

3.1 Introduction

Polymeric micelles have found applications in fields ranging from catalysis^{1,2} to antimicrobials³ to drug delivery.^{4,5} In each application there are specific characteristics that are important to consider when designing a micellar surfactant: particle size, critical micelle concentration (CMC), microviscosity, surface morphology, and aggregate stability. Given the relative ease of surfactant synthesis and modulation, drug delivery has become a chief area of focus for micelles.

Torchilin *et al.* have demonstrated the effectiveness of utilizing poly(ethylene glycol)ated (PEGylated) phospholipids for use as micelle-based drug delivery systems.⁶ PEGylated phospholipids exhibit very low CMCs and small average particle sizes, two important properties in micellar drug delivery. Specifically, micelles based on 1,2-distearoyl-*sn*-glycero-3-phosphoethanolamine-*N*-[methoxy(polyethylene glycol)] (MxDSPE, **Figure 3.1**) have been shown to not only efficiently solubilize hydrophobic drugs but also to be effective in their delivery.⁷

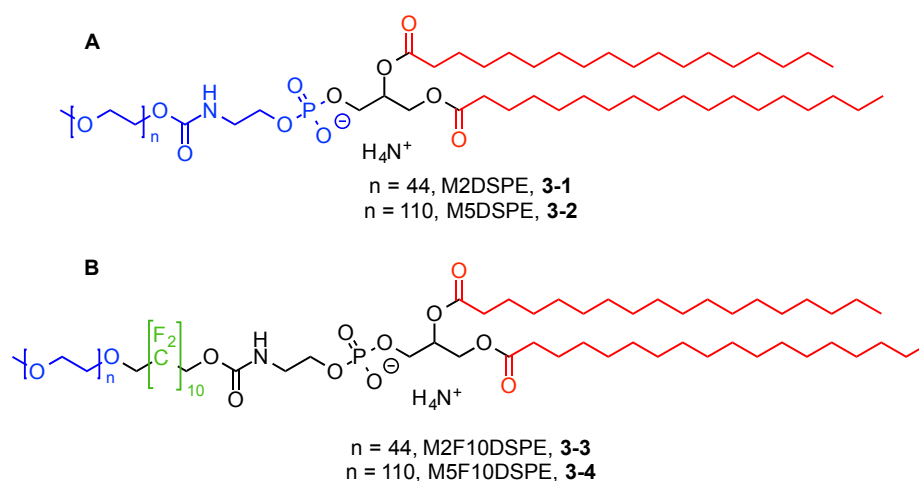


Figure 3.1. A – Structure of MxDSPE, surfactants studied extensively by Torchilin *et al.*, and B – MxF10DSPE, triphilic surfactants studied previously in the Mecozi laboratory.

MxDSPE, $x = 2$ or 5 , are classical amphiphiles (blue = hydrophilic, red = lipophilic) known to form micelles in solution. MxF10DSPE, $x = 2$ or 5 , are triphilic surfactants (blue = hydrophilic, green = fluorophilic, red = lipophilic).

Early work in the Mecozzi group led to the development of diblock, fluorosurfactants for the solubilization⁸ and emulsification⁹ of volatile, fluoruous anesthetics. This work on diphilic fluorosurfactants evolved into the synthesis and study of semi-fluorinated MxF10DSPE triphilic surfactants (**Figure 3.1**). Compared to their non-fluorinated analogues the MxF10DSPE surfactants displayed enhanced kinetic and thermodynamic stability and exhibited improved drug-release profiles for amphotericin B.¹⁰ The study of MxF10DSPEs was limited to comparing triphilic surfactants to their diphilic (hydrophilic-lipophilic) analogues.

This chapter presents work that sought to expand on previous work with MxF10DSPE surfactants. Bates *et al.* have shown that multiblock amphiphiles can exhibit a wide variety of structures and behaviors, with the potential to offer unique materials for a wide variety of purposes.¹¹ A number of studies have looked at the aggregation of semi-fluorinated RAFT polymers in water.^{12–15} The relationship between structure and aqueous aggregation behavior remains an important step in fully understanding the behavior of triphilic species.¹⁶ Together, a systematic study was undertaken to evaluate the relationship between structure and function, in water, of semi-fluorinated triphilic surfactants.

Two polymeric architectures were chosen (linear and dibranched, **Figure 3.2**) for this study. Fluorocarbon moieties of varying size were then introduced to evaluate the effect of increasing the fluorocarbon size on the physicochemical properties of the resulting triphiles. The effect upon kinetic stability and encapsulation ability for the resulting micelles was also studied. These results were compared to those for the structurally divergent miktoarm surfactants (synthesized by Dr. Aaron McCoy, **Figure 3.2**). These results highlight the fact that changes in triphilic architecture and block composition can be used to modulate the physicochemical properties of a micelle, including its stability in physiological conditions and the ability to encapsulate hydrophobic molecules. Moreover, the variance in block configuration (linear/dibranched or miktoarm)

indicates that the placement of and not just the presence of fluorocarbons is an important design criterion for effectively improving micelle stability and drug solubilization and retention.

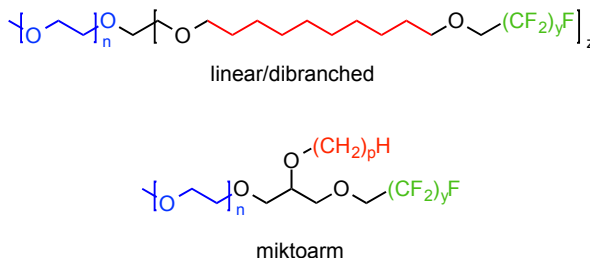


Figure 3.2. Generalized structure of triphilic surfactants synthesized.

The triphilic surfactants presented all contain a hydrophilic moiety (blue), lipophilic moiety (red), and fluorophilic moiety (green). Note on nomenclature: linear surfactants ($z = 1$) are designated $M_xH\#F\#$, where M_x refers to the mPEG hydrophilic block of x molecular weight in kDa, $H\#$ and $F\#$ refer to the number of hydrogenated and fluorinated carbon atoms respectively; dibranched surfactants ($z = 2$) are designated $M_xdiH\#F\#$, where di indicates the dibranched structure; miktoarm surfactants are designated $M_x\mu H\#F\#$, where μ indicates the miktoarm structure. Linear and dibranched surfactants designated $H\#-O-F\#$ possess an ether linkage between blocks (as shown above).

3.2 Results and Discussion

3.2.1 Design of triphilic surfactants

In designing the triphilic surfactants to form exclusively micellar aggregates, the critical packing parameter (CPP) was considered.¹⁷ Values for fluorinated and semi-fluorinated hydrophobic blocks are not readily available for CPP calculations; as such, CPP analysis was approached holistically. For linear surfactants, a smaller hydrophilic block such as mPEG₁₀₀₀ has been proven – by previous work in the Mecozzi laboratory – to favor micelle formation for a number of linear fluorophilic (up to 15 fluorocarbons in length) and lipophilic (up to 19 hydrocarbons in length) groups. Therefore mPEG₁₀₀₀ was chosen as the hydrophilic group for the linear triphiles. For the dibranched surfactants, such as M1DSPE¹⁸ and previously synthesized fluorosurfactants,⁹ it has been found that mPEG₁₀₀₀ is too small to give rise to micellar aggregation. Given the larger hydrophobic volume of fluorocarbons compared to hydrocarbons¹⁹ and the relatively high CPP (0.23) for M2DSPE, mPEG₅₀₀₀ was chosen over mPEG₂₀₀₀ to ensure

that all the dibranched surfactants would form micellar aggregates. Finally, the Mecozzi group had yet to investigate miktoarm surfactants, thus mPEG₁₀₀₀ and mPEG₂₀₀₀ were both investigated for their potential to give micellar aggregates from miktoarm surfactants.

3.2.2 Synthesis of triphilic surfactants

Synthesis of the linear surfactants, and by extension the dibranched surfactants, started with 9-decen-1-ol. The first attempted syntheses utilized an atom transfer radical addition (**Figure 3.3**), employing methodology developed by Brace.²⁰ A perfluoroalkyl iodide (either perfluorohexyl iodide or perfluorooctyl iodide) is added to 9-decen-1-ol with sodium dithionite or AIBN as a radical initiator. Subsequent reduction by zinc in acetic acid then removed the iodide to give HO-H10F6 and HO-H10F8 in moderate yield. While HO-H10F8 worked well in subsequent Williamson ether syntheses, the smaller HO-H10F6 was found to readily decompose under the basic reaction conditions. HO-H10F6 suffered from HF elimination across the CF₂-CH₂ junction, a potential pitfall when using semi-fluorinated molecules under basic conditions.²¹

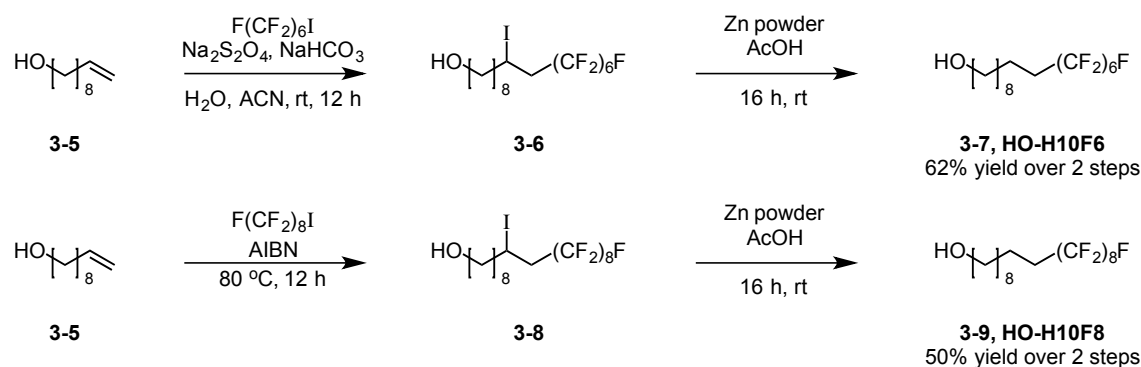


Figure 3.3. Radical synthesis of HO-H10F6 and HO-H10F8.

Given the basic-instability of semi-fluorinated alcohols smaller than HO-H10F8, an anionic synthesis was developed that produced more stable alcohols for further reactions (**Figure 3.4**). A semi-fluorinated alkene ether is prepared by Williamson ether synthesis using 9-decen-1-yl

methane sulfonate and 1H,1H-perfluorobutan-1-ol (F3H1-OH) or 1H,1H-perfluoro-heptan-1-ol (F6H1-OH). Only 1H,1H-perfluoro-alcohols were found to proceed in high yields, as 1H,1H,2H,2H-perfluoroalcohols suffered from complete HF elimination in lieu of any S_N2 reaction.²² Hydroboration oxidation of the semi-fluorinated alkene gave the linear semi-fluorinated alcohols in good overall yield. Stability tests of HO-H10-O-F3 and HO-H10-O-F6 showed no decomposition.

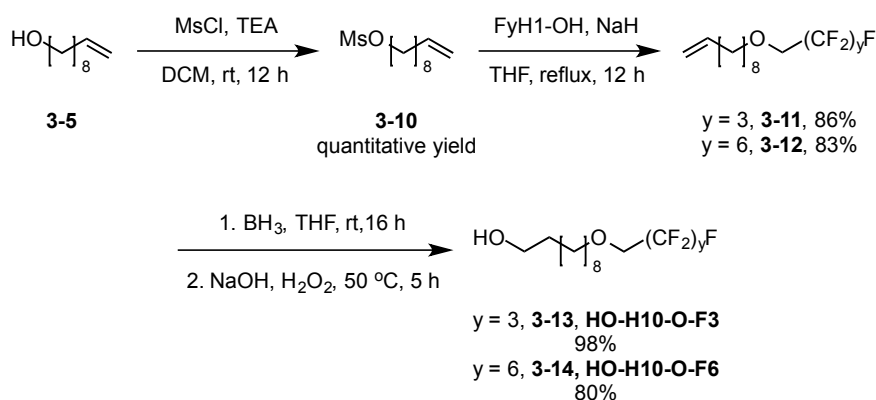


Figure 3.4. Anionic synthesis of HO-H10-O-F3 and HO-H10-O-F6.

The linear surfactants M1H10 (starting from decan-1-ol), M1H10-O-F3, M1H10-O-F6, and M1H10F8 were synthesized by PEGylation (**Figure 3.5**) of their respective alcohols. PEGylation proceeded by Williamson ether synthesis using mPEG₁₀₀₀ methane sulfonate, prepared from commercially available mPEG₁₀₀₀. Sodium hydride and benzotrifluoride (BTF) were found to be the best base and solvent for this reaction.

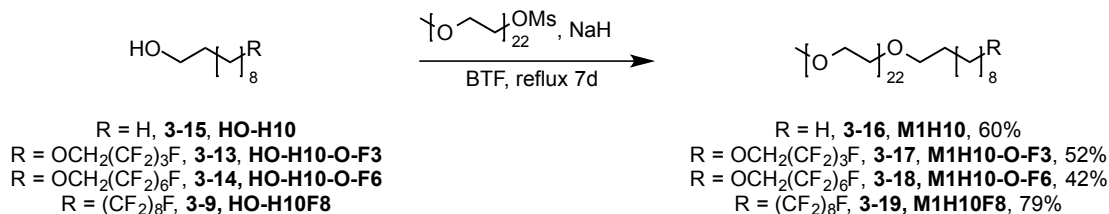


Figure 3.5. Synthesis of linear surfactants M1H10, M1H10-O-F3, M1H10-O-F6, and M1H10F8.

The linear alcohols were used to synthesize dibranched alcohols by a concomitant S_N2 reaction and ring opening of epichlorohydrin (**Figure 3.6**). The reaction proceeds with neat alcohol as both solvent and reactant. The low yields are in part a result of poor chromatographic separation of the linear and dibranched species. PEGylation of the dibranched alcohol with mPEG₅₀₀₀ methane sulfonate proceeded well under the same reaction conditions as those devised for the linear alcohols (**Figure 3.6**).

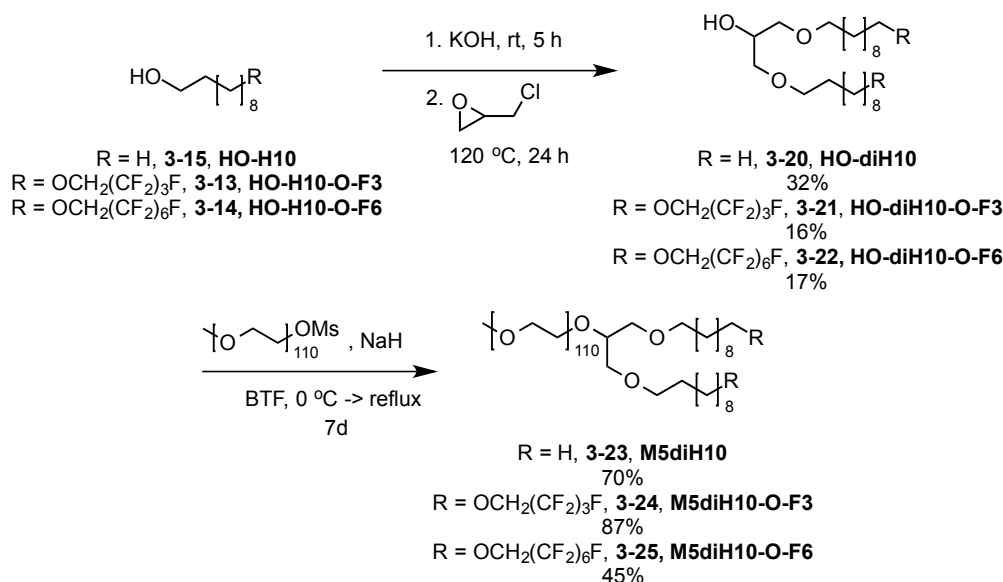


Figure 3.6. Synthesis of dibranched surfactants M5diH10, M5diH10-O-F3, and M5diH10-O-F6.

The miktoarm alcohols were prepared starting from glycerol (**Figure 3.7**). Acetal protection of the two primary alcohols proceeds in low yield due to the mixture of 1,2- and 1,3-protection products.²³ Subsequent alkylation of the secondary alcohol was then found to proceed best using alkyl methane sulfonates in a mixture of KOH and refluxing toluene. Reductive ring opening with DIBALH afforded the 3-benzyloxy-2-alkoxy-1-propanol intermediates. Mesylation and Williamson ether synthesis with semi-fluorinated alcohol 1H,1H-perfluoronon-1-ol (HO-H1F8) followed by aluminum chloride deprotection gave the miktoarm alcohols. HOμH10F8 was PEGylated with mPEG₁₀₀₀ methane sulfonate to provide a surfactant to directly compare to

M1H10F8. The larger HO μ H18F8 was PEGylated with the more voluminous mPEG₂₀₀₀ to ensure micelle formation.

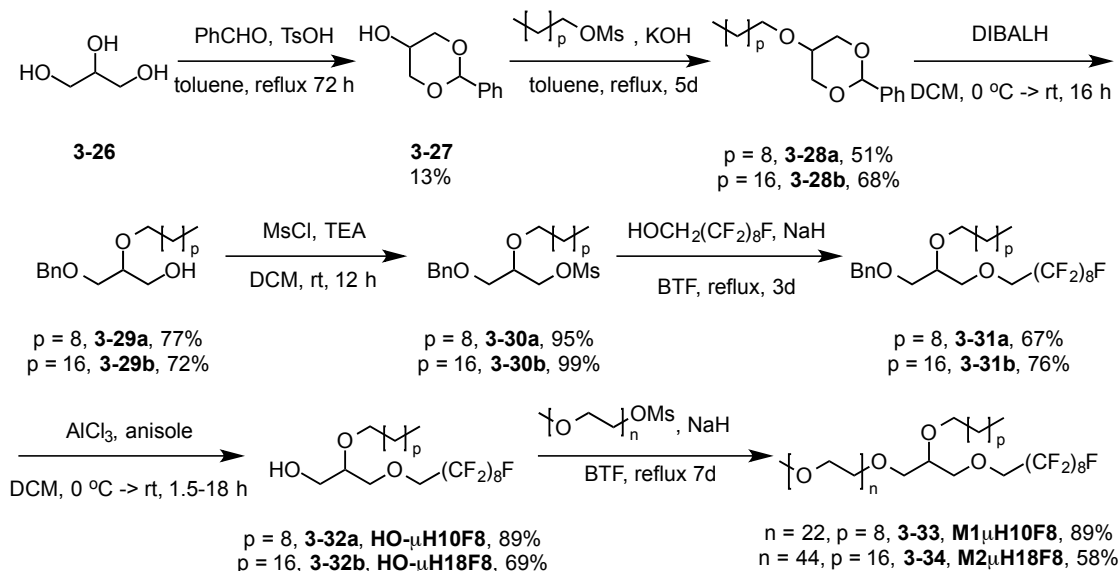


Figure 3.7. Synthesis of miktoarm surfactants M1 μ H10F8 and M2 μ H18F8

3.2.3 Characterization of surfactants - MW, microviscosity, CMC

Each amphiphile was analyzed by MALDI mass spectrometry to determine average molecular weight (Table 3.1). To determine the critical micelle concentration (CMC), the concentration above which aggregates begin to form, surface tension analysis was used. Surfactant solutions were prepared in deionized water at concentrations from 1 mM to 1 nM. The CMC was then determined as the cross over of two lines and the error was determined by weighted, least-squares analysis (Table 3.1). M5diH10-O-F6 produced inconclusive results by surface tension measurements and was thus analyzed by pyrene encapsulation fluorescence.²⁴ Solutions above the CMC were analyzed by dynamic light scattering (DLS) to establish average particle size (Table 3.1). Most of the surfactants showed small (<20 nm), narrow size-distributions consistent with spherical micelles. Note that cryogenic transmission electron microscopy (cryo-TEM) is typically used to verify the morphology of the aggregates formed. For

the amphiphiles presented here, cryo-TEM failed due to the highly solvated nature of the PEG (rendering it indistinguishable from the surrounding vitrified water),²⁵ and the relatively small size of the hydrophobic blocks. Core microviscosity for each amphiphile was determined by encapsulation and fluorescence analysis of 1,3-bis-(1-pyrenyl)propane (P3P). The microviscosity is presented as the ratio of the monomer fluorescence (I_M) over the excimer fluorescence (I_E), with higher I_M/I_E ratios corresponding to greater microviscosities (**Table 3.1**).²⁶

Table 3.1. Physicochemical data of comparison, linear, miktoarm, and dibranched surfactants

Amphiphile	Mol. Wt. (g mol ⁻¹)	pCMC (-log(M) \pm SD)	Ave Size (nm)	Microviscosity (I_M/I_E)
M2DSPE	2,805.5	4.90 \pm 0.17	13.9 \pm 1.6	5.60 \pm 0.22
M5DSPE	5,801.1	5.38 \pm 0.10	18.6 \pm 2.8	5.23 \pm 0.03
M1F13	1,726.5	6.08 \pm 0.13	11.9 \pm 1.3	3.40 \pm 0.18
M1H10	1,232.2	3.01 \pm 0.25	149.7 \pm 36.0	2.75 \pm 0.11
M1H10-O-F3	1,558.6	3.82 \pm 0.08	9.5 \pm 1.3	5.99 \pm 0.32
M1H10-O-F6	1,577.2	4.53 \pm 0.12	10.6 \pm 1.0	6.26 \pm 0.19
M1H10F8	1,647.8	5.85 \pm 0.06	10.7 \pm 1.2	6.81 \pm 0.11
M1 μ H10F8	1,692.0	5.51 \pm 0.05	10.8 \pm 1.0	5.08 \pm 0.06
M2 μ H18F8	2,563.5	4.61 \pm 0.07	11.5 \pm 1.5	5.38 \pm 0.08
M5diH10	5,097.8	3.92 \pm 0.14	16.1 \pm 1.6	3.64 \pm 0.23
M5diH10-O-F3	5,672.7	4.44 \pm 0.18	21.6 \pm 5.9	6.76 \pm 0.13
M5diH10-O-F6	6,150.0	5.07 \pm 0.03	20.3 \pm 6.5	6.83 \pm 0.17

The first trend to notice is the effect of the fluorinated moieties on the average particle size (**Table 3.1**). For the linear amphiphiles, the addition of the fluororous block was essential for micelle formation, with M1H10 showing the formation of random aggregates by DLS and M1H10-O-F3 showing a DLS consistent with small, spherical micelles. Further changes in the length of the fluorocarbon block do not show significant changes in average particle size going from M1H10-O-F3 to M1H10F8. Both miktoarm surfactants are of similar size to the linear, triphilic surfactants. This suggests that the introduction of a fluorocarbon group to a terminal position (linear) or a pendant, intermediary position (miktoarm) leads to no significant difference in terms of aggregate size.

In contrast to the linear surfactants, M5diH10 (the non-fluorinated analogue) does form aggregates consistent with micelles (**Table 3.1**). Upon introduction of the terminal fluorocarbon substituent, both M5diH10-O-F3 and M5diH10-O-F6 show a larger distribution of sizes, but no significant differences in average size. The introduction of and placement of fluorocarbon substituents onto a micellar surfactant, therefore, seems to have little effect upon average size of the micellar aggregate. If a surfactant does not form micelles, however, the introduction of fluorocarbons may perturb the type of aggregate formed.

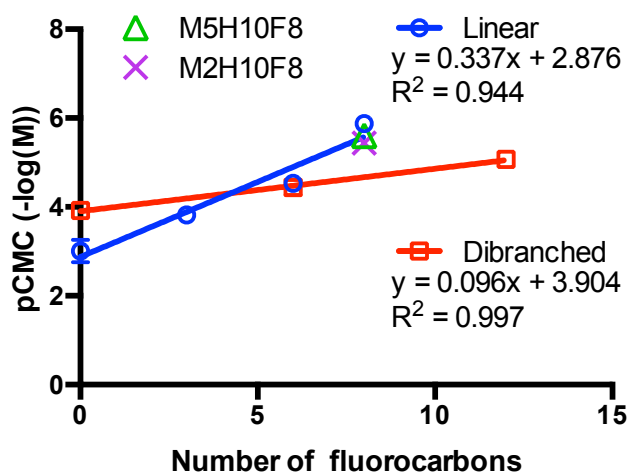


Figure 3.8. Relationship between number of fluorocarbons and pCMC ($-\log(M) \pm SD$, $n = 4$) for the linear and dibranch amphiphiles.

A linear relationship can be seen to exist between the number of fluorocarbons and the pCMC for the linear and the dibranch amphiphiles. The difference in slope is attributed to differences in hydrophobic architecture rather than differences in mPEG block size (M1 v. M5) due to the relative lack of change seen for the linear series M1H10F8 (blue circle), M2H10F8 (purple x), and M5H10F8 (green triangle).

Upon analysis of **Table 3.1** trends between CMC and the number of fluorocarbons can be observed. As shown in Figure 3.7, there is a linear relationship between pCMC ($-\log(M)$) and the number of fluorinated carbon atoms. Linear relationships between CMC ($\log(M)$) and the number of $-\text{CH}_2$ ²⁷ or $-\text{CF}_2$ ²⁸ has been reported previously. Here, the interesting result is the difference in slope between the linear and dibranch surfactants (**Figure 3.8**). There are two differences between the two classes of amphiphiles that could account for this. The first is the difference in

PEG block size (M1-linear surfactants compared to M5-dibranched surfactants). To evaluate the effect of PEG size, two other surfactants M2H10F8 and M5H10F8 were synthesized and their pCMC determined. It was found that M2H10F8 and M5H10F8 had pCMCs of 5.44 and 5.60, respectively (purple x and green triangle, respectively, in **Figure 3.8**). The lack of significant change in CMC with change in mPEG size has been seen previously in the Mecozzi laboratory by Dr. Elham Nejati for MxF13 surfactants, which have pCMCs of: 6.08 ($x = 1$), 6.16 ($x = 2$), and 6.09 ($x = 5$). As such, it seems that the difference in PEG size is not the determining factor.

The second difference that can explain the variation in CMC trends between linear and dibranched surfactants is that of hydrophobic architecture itself. The linear polymers have a much smaller base hydrophobic block (H10) than the dibranched polymers (diH10). Thus the addition of each fluorocarbon to the linear architecture has a larger effect, whereas the addition of fluorocarbons to the larger dibranched hydrophobic block has a diminished effect. This difference in the effectiveness of each fluorocarbon on the CMC thus explains the difference in slope for **Figure 3.8**, a result of the size of the hydrocarbon block size relative to the fluorocarbon block size.

In comparison to the linear surfactants, the miktoarm surfactant architecture does not lower the CMC as significantly (**Table 3.1**). Comparison of M1H10F8 (pCMC = 5.85 ± 0.06) and its miktoarm analogue M1 μ H10F8 (pCMC = 5.51 ± 0.05) show that the linear arrangement leads to a significantly ($P < 0.0001$) lower CMC than does the miktoarm arrangement. While the result is not as great, the introduction of fluorocarbons in a miktoarm architecture for M1 μ H10F8 does lead to a decrease in the CMC over its non-fluorinated analogue M1H10 (pCMC = 3.01 ± 0.25). In general, therefore, the introduction of fluorocarbons does increase the thermodynamic stability of micelles (lower the CMC), but the placement of fluorocarbons determines the extent of stability increase.

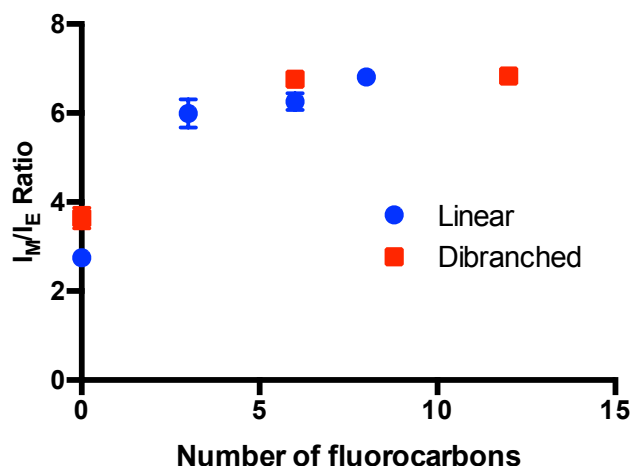


Figure 3.9. Relationship between microviscosity (I_M/I_E ratio \pm SD, $n = 3$) and the number of fluorocarbons for linear and dibranched amphiphiles.

Microviscosity measurements of the triblock surfactants show dramatically different behavior than either the hydrocarbon M1H10/M5diH10 or fluorocarbon M1F13 diblock amphiphiles (Table 3.1). The diblock surfactants show similar I_M/I_E ratios, while the smallest triblock amphiphiles – M1H10-O-F3 and M5diH10-O-F3 – show a sharp increase in microviscosity. In **Figure 3.9**, the microviscosities for all hydrocarbon-diblock and triblock amphiphiles are plotted against the number of fluorocarbons in each amphiphile. This plot shows a logarithmic increase in microviscosity with the number of fluorocarbons. Hence the initial addition of a small number of fluorocarbons causes the most dramatic increase in microviscosity compared to the diphilic analogues. Typically, increases in microviscosity are associated with more crystalline micelles resulting from either chain entanglement or tighter packing of unimers.⁴ The triblock amphiphiles are believed to show higher microviscosities, compared to the diblock surfactants, due to hydrophobic phase segregation of the fluorocarbon and hydrocarbon blocks (into core and shell domains, **Figure 3.10**), which results in tighter unimer packing within the micelles.

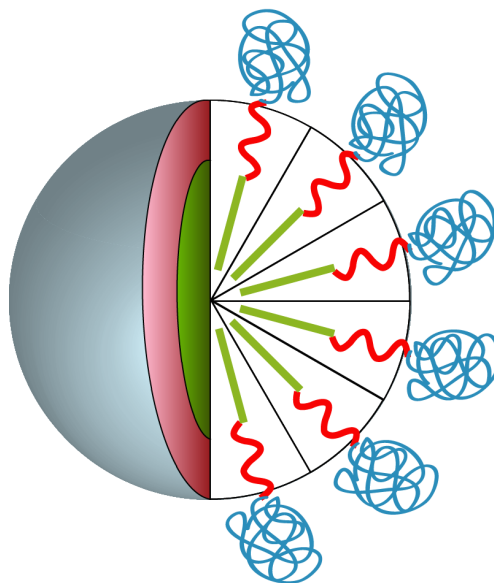


Figure 3.10. Proposed core-shell-corona structure of linear and dibranched triphilic amphiphiles.

Phase segregation of the triphilic micelles will occur to minimize the negative interactions between immiscible phases (green = fluorophilic core, red = lipophilic shell, blue = hydrophilic corona). Credit to Dr. Joseph Moore for his Adobe Illustrator work.

The miktoarm surfactants show their most divergent physicochemical difference in terms of microviscosity (**Table 3.1**). The miktoarm surfactants show similar microviscosity measurements compared to each other (I_M/I_E values of 5.08 ± 0.06 and 5.38 ± 0.08 for M1 μ H10F8 and M2 μ H18F8, respectively), but both show significantly lower microviscosity measurements than any of the linear or dibranched triphilic surfactants. The parallel arrangement of fluorocarbon and hydrocarbon chain does not allow for the formation of a core-shell structure within the core. Miktoarm surfactants form a variety of compartmental, multi-domain core-segregated structures. The switch from core-shell segregation (linear and dibranched surfactants) to multi-domain segregation of the fluorocarbon and hydrocarbon blocks in miktoarm-derived micelles leads to a less rigid micelle with lower microviscosity.²⁹

3.2.4 Characterization of triphilic micelles – kinetic stability

The use of fluorocarbon segments was investigated not only for their potential effects on CMC, micelle formation, or microviscosity of aggregates, but also for the potential to improve kinetic stability *in vivo*. Micelles spontaneously form and as such do not have a kinetic stability in pure water above the CMC. Upon the addition of dissociative media (like hydrophobic blood proteins) micelles will show different rates of dissociation.³⁰ This rate of dissociation is the kinetic stability of a micelle.

Micelles have found widespread use in the development of drug delivery and of central importance is the lifetime of micelles *in vivo*.³¹ For this application, better results have been observed with long circulating particles.⁷ Using methodology developed by Chen *et al.* the dissociation of micelles in human serum was monitored through Förster Resonance Energy Transfer (FRET) (**Figure 3.11**).³² The 95% confidence interval for each was calculated by fitting a one-phase exponential decay using GraphPad PRISM 6 (**Table 3.2**). It was found that non-fluorinated micelles (M5diH10, M2DSPE, and M5DSPE) rapidly dissociated *in vitro* when exposed to human serum (observed by a decrease in FRET ratio). For the semi-fluorinated micelles, both the architecture and block composition are important.

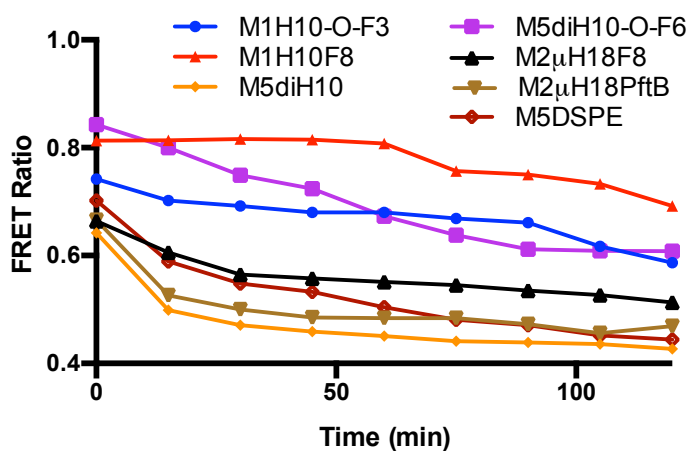


Figure 3.11. FRET stability profiles of representative micelles.

The linear surfactants showed a dramatic increase in stability with only the addition of an F3 block. For all three linear, semi-fluorinated surfactants the trend line was quite flat and an attempt to fit the data by one-phase exponential decay gave ambiguous results. For the dibranched triblock amphiphiles, in contrast, M5diH10-O-F3 did not show significant increase in stability over the non-fluorinated M5diH10. Only M5diH10-O-F6 showed significant increase in stability compared to M5diH10. This is likely due to the less efficient packing of the dibranched hydrophobic amphiphiles – compared to the linear amphiphiles. The less efficient packing leads to a smaller effect of each fluorocarbon, in the dibranched amphiphiles, on the kinetic stability.

Table 3.2. *In vitro* half-lives of comparison, linear, miktoarm, and dibranched surfactants

Half-life 95% confidence intervals were determined by fitting the FRET plots to a one-phase exponential decay using GraphPad PRISM 6.

Amphiphile	Half-life 95% CI (min)	Goodness of fit (R^2)
M2DSPE	17 – 35	0.98
M5DSPE	18 – 46	0.98
M1F13	<i>Not measured - fluorosurfactant</i>	
M1H10	<i>Not measured – non-micellar surfactant</i>	
M1H10-O-F3	<i>Ambiguous*</i>	0.90
M1H10-O-F6	<i>Ambiguous*</i>	0.94
M1H10F8	<i>Ambiguous*</i>	0.83
M1 μ H10F8	8.2 – 18	0.98
M2 μ H18F8	15 – 39	0.97
M5diH10	7.5 – 14	0.98
M5diH10-O-F3	13 – 16	0.99
M5diH10-O-F6	34 – 148	0.98

*The one-phase exponential decay fits failed to give meaningful rate constants for the linear surfactants because they are too flat.

Kinetic stability is a measure of how quickly micelles disassociate in dissociative media. The linear surfactants all show a dramatic increase in stability over non-fluorinated (MxDSPE and M5diH10) surfactants, M5diH10-O-F3, and the miktoarm surfactants. The moderate increase in stability among the dibranched surfactants and the lack of stability increase in the miktoarm surfactant suggests an underlying explanation for kinetic stability: microviscosity. The miktoarm surfactants and the non-fluorinated surfactants all possess very similar microviscosities and all show very similar FRET stabilities. Only the linear and larger dibranched surfactants show a

great enough increase in microviscosity – core crystallinity – to lead to an increase in kinetic stability. The more crystalline the micellar aggregates, the slower the unimer exchange, which in turn leads to a slower rate of dissociation as micelles equilibrate towards a unimer-dominated regime.

3.2.5 Characterization of triphilic micelles – hydrophobic-drug encapsulation

Given the possible structure of the linear/dibranched (fluorocarbon core-hydrophobic intermediate shell-hydrophilic corona)^{16,33} and miktoarm (compartmental structure) triphiles,²⁹ encapsulation of paclitaxel (PTX, **Figure 3.12**), a model hydrophobic species, was investigated. It is known that hydrophobic molecules can be encapsulated in classical hydrocarbon-based micelles by sequestration within the hydrophobic core.³⁴ Here PTX encapsulation was investigated to probe the effect of an inner-fluorous core (linear/dibranched amphiphiles) compared to a mixed hydrocarbon/fluorocarbon core (miktoarm amphiphiles) on the solubilization of hydrophobic species.

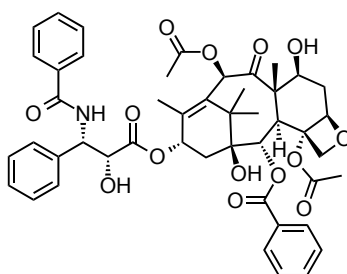


Figure 3.12. Structure of model hydrophobic drug paclitaxel.

Paclitaxel was chosen as the model hydrophobic drug because it is not solubilized to any extent in a purely fluorophilic micelle (**Figure 3.13**). This allows for the direct interrogation of how PTX is encapsulated into a hydrophobic shell, in the case of the linear and dibranched amphiphiles, or a mixed core, in the case of the miktoarm amphiphiles. PTX loaded micelles were prepared by the solvent evaporation method (SEM), which we found to give more reproducible

results and to give higher drug loading.³⁵ All encapsulation data are presented as the average percent weight of the encapsulated PTX in linear and miktoarm amphiphiles (**Figure 3.13**) and dibranched amphiphiles (**Figure 3.14**). Equimolar amounts of surfactants were used in all encapsulation studies to allow for direct comparisons. Note that M1H10 was not studied for its encapsulation ability because it forms random aggregates

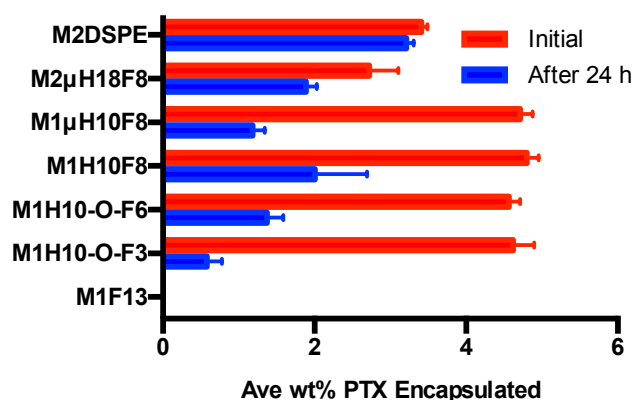


Figure 3.13. Percent weight encapsulation (mean \pm SD, $n = 3$) of paclitaxel (PTX) by linear and miktoarm surfactants.

Each of the linear amphiphiles and M1μH10F8 were able to initially encapsulate the same amount of PTX on a percent weight basis (**Figure 3.13**), despite varying fluorocarbon lengths. M2DSPE and M2μH18F8 were also within error of each other initially ($P = 0.08$). However, after 24 hours – when poorly encapsulated PTX is lost^{36,37} – an increase in the PTX remaining encapsulated in the linear-surfactant micelles can be seen with increasing size of the fluorocarbon moiety. The increase in average wt% PTX remaining after 24 hours trends with the increase in microviscosity. This suggests that more PTX is retained for a longer period of time in M1H10F8 due to its less dynamic, more crystalline aggregates. At the point of 8 fluorocarbons (M1H10F8), the retention of PTX for linear surfactants is not significantly different than M2DSPE ($P = 0.09$). Therefore, despite the smaller number of hydrocarbons in which to solubilize PTX, a significant increase in microviscosity can lead to an increase in PTX solubilization ability.

In the case of the miktoarm amphiphiles (**Figure 3.13**), trends that relate the amount of PTX encapsulated to the microviscosity can be observed. The less viscous micelle M1 μ H10F8 retains less PTX than the more viscous M2 μ H18F8 ($P = 0.005$). In addition to differences in microviscosity, M1 μ H10F8 has 55% the number of hydrocarbons of M2 μ H18F8 and the wt% PTX retained in M1 μ H10F8 is roughly 60% that of M2 μ H18F8 (1.182 wt% and 1.887 wt%, respectively). In turn, M2 μ H18F8 has half the number of hydrocarbons in the core compared to M2DSPE and the percent weight encapsulation of PTX after 24 hours for M2 μ H18F8 (1.89 wt%) is slightly more than half of that for M2DSPE (3.21 wt%). This suggests that for miktoarm surfactants, where microviscosity is not significantly increased, the number of hydrocarbons plays a role in determining the amount of drug that can be solubilized.

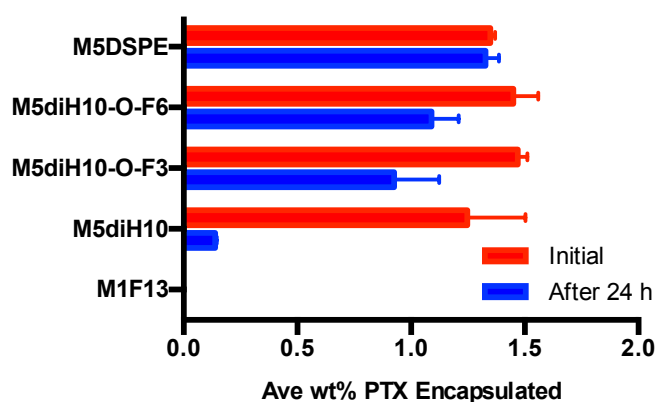


Figure 3.14. Percent weight encapsulation (mean \pm SD, $n = 3$) of paclitaxel (PTX) by dibranched surfactants.

Dibranched amphiphiles show a similar trend to the linear amphiphiles. The higher microviscosity of M5diH10-O-F3 and M5diH10-O-F6 is directly related to the higher encapsulation of and retention of PTX after 24 hours (**Figure 3.14**) compared to M5diH10. Like the linear surfactants, the increase in microviscosity of the triphilic dibranched surfactants can overcome the smaller hydrocarbon component of these surfactants, compared to M5DSPE, to increase PTX retention. Both M5diH10-O-F3 and M5diH10-O-F6 have 55% the number of

hydrocarbons as does M5DSPE, but the retention of PTX for both surfactants is within error ($P = 0.06$ for both) of M5DSPE.

Together, the linear and dibranched amphiphile encapsulation data show that an inner hydrophobic core is not necessary for stable encapsulation of hydrophobic species such as PTX. Moreover, as the fluororous inner-core increases in size, the micelles show enhanced retention ability as a result of the more tightly packed micellar structure, vis-à-vis microviscosity. The linear arrangement of hydrocarbon and fluorocarbon segments shows both enhanced kinetic stability and enhanced ability to retain hydrophobic species over time

Ultimately, when one directly compares the linear (M1H10F8) and miktoarm (M1 μ H10F8) architectures several points stand out. Both M1H10F8 and M1 μ H10F8 have very similar CMC's and particle sizes. Their point of divergence is microviscosity. M1H10F8 has a microviscosity (6.81, **Table 3.1**) significantly greater than that of M1 μ H10F8 (5.01, **Table 3.1**). This results in higher average wt% retention of PTX by M1H10F8 than M1 μ H10F8. Given the poor encapsulation of the FRET dyes by M1 μ H10F8, the FRET data can be considered uncertain. It can be inferred from the performance of M2 μ H18F8 (which has a higher microviscosity) that M1 μ H10F8 would dissociate far more rapidly than M1H10F8, which suggests that the difference in microviscosity has an important impact on kinetic stability.

3.3 Conclusions

The peculiar properties of fluorocarbons offer a means of not only improving micellar kinetic and thermodynamic stability, but also a way of improving and probing encapsulation behavior. Herein the syntheses for the preparation of linear and dibranched semi-fluorinated amphiphiles have been presented. Both surfactant architectures were studied in an attempt to establish relationships between the ternary amphiphile structure and the resulting physicochemical

behavior of the aggregates. These results were then compared to miktoarm surfactants synthesized by Dr. Aaron McCoy. For linear and dibranched amphiphiles, the introduction of fluorocarbon moieties significantly increases their thermodynamic stability and microviscosity. Both of these factors seemingly arise from the formation of a core-shell (fluorocarbon-hydrocarbon) structure within the hydrophobic core. In comparison, the fluorocarbons in miktoarm surfactants cannot all sequester into a unique phase and so enhancements in thermodynamic stability and microviscosity are less pronounced. For only the linear surfactants, with any sized fluorocarbon blocks and for dibranched surfactants (with a large enough fluorocarbon block) was their kinetic stability significantly greater, which was correlated with higher microviscosity.

All amphiphiles that formed small, narrow size distributions in water that were consistent with micelles were studied for their ability to encapsulate PTX. The semi-fluorinated linear surfactants typically retained less of the PTX initially encapsulated compared to the phospholipid-based M2DSPE polymers. The triphilic dibranched surfactants encapsulated and retained PTX within error of M5DSPE. Taken together, the results for the linear and dibranched semi-fluorinated triphiles show that changes in architecture and composition of the amphiphiles blocks can be rationally used to modulate the physicochemical properties of a micelle, including stability in physiological conditions and encapsulation of hydrophobic molecules.

3.4 Experimental

3.4.1 Materials

All fluorinated compounds were obtained from SynQuest Laboratories, Inc. (Alachua, FL, USA). 1,2-distearoyl-*sn*-glycero-3-phosphoethanolamine-*N*-[methoxy(polyethylene glycol)-2000] (M2DSPE) and 1,2-distearoyl-*sn*-glycero-3-phosphoethanolamine-*N*-[methoxy(polyethylene

glycol)-5000] (M5DSPE) were purchased from Avanti Polar Lipids Inc. (Alabaster, AL, USA). Paclitaxel was purchased from LC Laboratories (Woburn, MA, USA). 1,3-Bis-(1-pyrenyl)propane (P3P) was purchased from Life Technologies (Carlsbad, CA, USA). Pooled normal human serum was purchased from Innovative Research (Novi, MI, USA). All solvents were of ACS grade or higher and were purchased from Sigma-Aldrich (St. Louis, MO, USA). All other reagents were purchased from Sigma-Aldrich (St. Louis, MO, USA) and were used as received, unless otherwise specified. Chromatographic separations were performed using Silicycle 60 Å SiO₂. Surfactants were purified by automated flash chromatography using a CombiFlash® Rf 4x system (Teledyne Isco, Lincoln, NE, USA) equipped with ELSD for compound visualization and a REDI-Sep Rf Gold C-18 silica high performance aqueous reverse phase cartridge. Products were eluted with a 10% to 100% MeOH in water (0.1% formic acid) gradient. ¹H- and ¹⁹F-NMR spectra were obtained on Varian Unity-Inova 400 and Unity-Inova 500 spectrometers using deuteriochloroform (CDCl₃) as the solvent with TMS as an internal reference.

3.4.2 mPEG mesylate (Mx-OMs) synthesis

To a dry 100 mL roundbottom flask charged with argon were added 50 mL DCM and 5 g monomethyl poly(ethylene glycol) alcohol (4.9 mmol M1-OH/2.5 mmol M2OH/1.03 mmol M5OH). The mixture was cooled to 0 °C before adding TEA (2 mL, 14.7 mmol mPEG₁₀₀₀-OH/1.04 mL, 7.5 mmol mPEG₂₀₀₀-OH/0.43 mL, 3.06 mmol mPEG₅₀₀₀-OH), which was allowed to stir for 30 minutes before methanesulfonyl chloride was added (1 mL, 12.2 mmol mPEG₁₀₀₀-OH/0.48 mL, 6.25 mmol mPEG₂₀₀₀-OH/0.2 mL, 2.55 mmol mPEG₅₀₀₀-OH). The reaction was allowed to stir overnight as it warmed to room temperature. The reaction was then diluted with 100 mL DCM and washed with 3, 50 mL aliquots saturated ammonium chloride solution, dried

over magnesium sulfate and then reduced to a minimum volume under reduced pressure. The mPEG-OMs was then precipitated with cold ether, vacuum filtered, and freeze dried from 50/50 DCM/benzene to give a white, crystalline product in 67% (**M1-OMs**), 86% (**M2-OMs**) and 93% (**M5-OMs**) yields. **M1-OMs** MALDI: Distribution centered on $[M+Na^+] = 1063.4$, PDI of starting mPEG 1.27. NMR: 1H -NMR (400 MHz, $CDCl_3$): δ 4.38 (m, 2H), 3.82 (m, 1H), 3.77 (m, 2H), 3.64 (m, 89H), 3.55 (m, 2H), 3.47 (m, 1H), 3.38 (s, 3H), 3.09 (s, 3H); **M2-OMs** MALDI: Distribution centered on $[M+Na^+] = 1938.4$, PDI of starting mPEG 1.10. NMR: 1H -NMR (400 MHz, $CDCl_3$): δ 4.38 (m, 2H), 3.79 (m, 2H), 3.77 (m, 2H), 3.64 (m, 165H), 3.56 (m, 2H), 3.38 (s, 3H), 3.09 (s, 3H); **M5-OMs** MALDI: Distribution centered on $[M+Na^+] = 5161.5$, PDI of starting mPEG 1.05. NMR: 1H -NMR (400 MHz, $CDCl_3$): δ 3.84 – 3.44 (m, 490H), 3.38 (s, 3 H), 3.08 (s, 3H).

3.4.3 Linear and dibranched alcohol syntheses

HO-H10F6 (3-7)

To a dry 50 mL roundbottom flask were added 1.00 mL (5.04 mmol) 9-decen-1-ol (**3-5**), 2.67 g (6.0 mmol) perfluorooctyl iodide, 1.03 g (5.04 mmol) 85% sodium dithionite, 431 mg (5.04 mmol) sodium bicarbonate, and 15 mL ACN with 5 mL DI water. The reaction was allowed to stir overnight at room temperature. The reaction was then diluted with 100 mL DCM, washed with 50 mL each $Na_2S_2O_3$ and brine. The organic layers were dried over $MgSO_4$ and condensed under reduced pressure to give an off-white solid **3-6**. This was then dissolved in 10 mL acetic acid and stirred with 0.98 g zinc powder for 24 hours open to the air. The reaction was then quenched with 200 mL saturated $NaHCO_3$ solution and extracted with 300 mL DCM. The organic layers were then washed with 100 mL each saturated $NaHCO_3$ solution and brine and then dried over $MgSO_4$ and concentrated under reduced pressures to give a white solid. The solid

was recrystallized twice from hot toluene to give pure **HO-H10F6** in 62% overall yield. NMR: ^1H NMR (400 MHz, CDCl_3): δ 3.62 (t, J = 6.9 Hz, 2H), 2.14 (ttt, J = 20, 9, 2 Hz, 2H), 1.65 – 1.52 (m, 4H), 1.4 – 1.23 (m, 12H). ^{19}F NMR (376 MHz, CDCl_3): δ -81.22 (3F), -114.77 (2F), -122.39 (2F), -123.39 (2F), -124.01 (2F), -126.63 (2F).

HO-H10F8 (3-9)

To a dry 10 mL roundbottom flask were added 1.02 mL (5.75 mmol) 9-decen-1-ol (**3-5**) and 1.34 mL (5.0 mmol) perfluorooctyl iodide. The mixture was degassed at room temperature with argon for 45 minutes before 8.2 mg (0.05 mmol) AIBN were added and the mixture slowly heated to 80 °C while being very rapidly stirred with a small stir bar. This reaction was allowed to run overnight. The reaction was then cooled to room temperature, diluted with 100 mL DCM, washed with 50 mL each $\text{Na}_2\text{S}_2\text{O}_3$ and brine. The organic layers were dried over MgSO_4 and condensed under reduced pressure to give an off-white solid **3-8**. This was then dissolved in 10 mL acetic acid and stirred with 0.98 g zinc powder for 24 hours open to the air. The reaction was then quenched with 200 mL saturated NaHCO_3 solution and extracted with 300 mL DCM. The organic layers were then washed with 100 mL each saturated NaHCO_3 solution and brine and then dried over MgSO_4 and concentrated under reduced pressures to give a white solid. The solid was recrystallized twice from hot toluene to give pure **HO-H10F8** in 50% overall yield. NMR: ^1H NMR (400 MHz, CDCl_3): δ 3.65 (t, J = 6.9 Hz, 2H), 2.05 (ttt, J = 18, 9.5, 2 Hz, 2H), 1.65 – 1.52 (m, 4H), 1.4 – 1.23 (m, 12H). ^{19}F NMR (376 MHz, CDCl_3): δ -81.15 (3F), -114.77 (2F), -122.32 (6F), -123.11 (2F), -123.92 (2F), -126.49 (2F).

3-10: To a dry roundbottom, at 0 °C argon, were added 25 mL dry DCM, 9-decen-1-ol (2.5 mL, 13 mmol) and TEA (4.3 mL, 31 mmol). This stirred for 30 minutes before methanesulfonyl

chloride (1.3 mL, 16 mmol) was added dropwise. After running overnight, the reaction was diluted with 50 mL DCM and then washed with 3, 50 mL aliquots of saturated ammonium chloride solution. The organic layers were dried over MgSO_4 and condensed under reduced pressure to give 3.21 g (quantitative yield) of yellow oil. NMR: ^1H NMR (400 MHz, CDCl_3): δ 5.81 (ddt, $J = 16.5, 10, 6.5$ Hz, 1H), 4.99 (ddt, $J = 16.5, 2, 1$ Hz, 1H), 4.93 (ddt, $J = 10, 2, 1$ Hz, 1H), 4.22 (t, $J = 7$ Hz, 2H), 3.00 (s, 3H), 2.04 (qt, $J = 6.5, 1$ Hz, 2H), 1.60 (q, $J = 7$ Hz, 2H), 1.41 – 1.29 (m, 10H).

3-11 and **3-12**: To a 100 mL oven-dried roundbottom, under argon, were added 35 mL of THF and 761 mg (31 mmol) of NaH. The suspension was cooled to 0 °C over before 28 mmol of semi-fluorinated alcohol were added (3.25 mL 1H,1H-perfluorobutan-1-ol (F3H1-OH)/ 5.8 mL 1H,1H-perfluoroheptan-1-ol (F6H1-OH)) dropwise over the course of 1 hour. Then 3.20 g (13 mmol) of 9-decen-1-yl methane sulfonate were added (as a solution in 10 mL of anhydrous THF). This was then warmed slowly to reflux and allowed to react for 24 hours. The reaction was then allowed to cool and diluted with 100 mL of DCM. This was washed with 3, 50 mL aliquots of saturated NH_4Cl solution and dried over MgSO_4 and condensed under reduced pressure to give an opaque, yellow liquid. The product was then purified by column chromatography (4% ethyl acetate in hexanes) to give 3.83 g (86% yield **3-11**) and 5.28 g (83% yield **3-12**) of product as a clear liquid. 10-(1H,1H-perfluorobutoxy)dec-1-ene (**3-11**) NMR: ^1H NMR (400 MHz, CDCl_3): δ 5.81 (ddt, $J = 16.5, 10, 6.5$ Hz, 1H), 4.99 (ddt, $J = 16.5, 2, 1$ Hz, 1H), 4.93 (ddt, $J = 10, 2, 1$ Hz, 1H), 3.90 (tt, $J = 14, 2$ Hz, 2H), 3.58 (t, $J = 7$ Hz, 2H), 2.04 (qt, $J = 6.5, 1$ Hz, 2H), 1.60 (q, $J = 7$ Hz, 2H), 1.41 – 1.29 (m, 10H). ^{19}F NMR (376 MHz, CDCl_3): δ -81.51 (3F), -121.09 (2F), -128.28 (2F). 10-(1H,1H-perfluoroheptoxy)dec-1-ene (**3-12**) NMR: ^1H NMR (400 MHz, CDCl_3): δ 5.81 (ddt, $J = 16.5, 10, 6.5$ Hz, 1H), 4.99 (ddt, $J = 16.5, 2, 1$ Hz, 1H), 4.93 (ddt, $J = 10, 2, 1$ Hz, 1H), 3.91 (tt, $J =$

14, 2 Hz, 2H), 3.59 (t, $J = 7$ Hz, 2H), 2.04 (qt, $J = 6.5$, 1 Hz, 2H), 1.59 (q, $J = 7$ Hz, 2H), 1.39 – 1.29 (m, 10H). ^{19}F NMR (376 MHz, CDCl_3): δ -81.26 (3F), -120.03 (2F), -122.69 (2F), -123.29 (2F), -123.91 (2F), -126.59 (2F).

HO-H10-O-F3 (3-13) and HO-H10-O-F6 (3-14): To an oven-dried round-bottom flask was added BH_3 -THF (1.0 M, 16.5 mmol). The solution was diluted with 10 mL of dry THF and then cooled to 0 °C. The semi-fluorinated alkene ether (10-(1H,1H-perfluorobutoxy)dec-1-ene **3-11** (3.83 g, 11.2 mmol)/10-(1H,1H-perfluoroheptoxy)dec-1-ene **3-12** (5.28 g, 10.8 mmol)) was added dropwise and the reaction was allowed to stir at room temperature for 16 h. The reaction was cooled to 10 °C followed by addition of NaOH solution (3 M, 20 mL). Hydrogen peroxide (30 wt% in water, 6 mL) was added at 10 °C. The reaction mixture was stirred at 50 °C for 2 h and then cooled to room temperature. Ether (20 mL) was added and the organic phase was washed with water (20 mL), brine (20 mL), and dried over MgSO_4 and condensed under reduced pressure to give 3.9 g (98% yield **HO-H10-O-F3, 3-13**), 4.5 g (80% yield **HO-H10-O-F6, 3-14**) of clear oil. **HO-H10-O-F3 (3-13)** NMR: ^1H NMR (400 MHz, CDCl_3): δ 3.90 (tt, $J = 14$, 2 Hz, 2H), 3.64 (t, $J = 7$ Hz, 2H), 3.58 (t, $J = 7$ Hz, 2H), 1.60 (septet, $J = 7$ Hz, 4H), 1.41 – 1.29 (m, 12H). ^{19}F NMR (376 MHz, CDCl_3): δ -81.51 (3F), -121.08 (2F), -128.28 (2F). **HO-H10-O-F6 (3-14)** NMR: ^1H NMR (400 MHz, CDCl_3): δ 3.92 (tt, $J = 14$, 2 Hz, 2H), 3.64 (t, $J = 7$ Hz, 2H), 3.59 (t, $J = 7$ Hz, 2H), 1.58 (septet, $J = 7$ Hz, 4H), 1.36 – 1.29 (m, 12H). ^{19}F NMR (376 MHz, CDCl_3): δ -81.29 (3F), -120.07 (2F), -122.71 (2F), -123.32 (2F), -123.93 (2F), -126.66 (2F).

HO-diH10 (3-20), HO-diH10-O-F3 (3-21) and HO-diH10-O-F6 (3-22): To an oven dried 25 mL round-bottom flask were added 22.7 mmol alcohol (3.59 g HO-H10 (**3-15**), 8.1 g HO-H10-O-F3 (**3-13**), 11.5 g HO-H10-O-F6 (**3-14**)) and 0.51 g (9.08 mmol) of crushed KOH. This was

allowed to stir at room temperature until all of the KOH dissolved. Epichlorohydrin (0.42 g, 4.54 mmol) was then added and the reaction was heated to 120 °C and allowed to react overnight, stirring vigorously. The reaction was then allowed to cool and diluted with 100 mL brine and extracted with 3, 100 mL aliquots DCM. The organic layers were then dried over MgSO₄ and concentrated under reduced pressure. The resulting oil was then distilled under reduced pressure (20 mmHg at 200 °C) to remove excess starting alcohol. The remaining oil was then purified by flash chromatography (twice, once with 17% EtOAc in hexanes and then again in 10% hexanes in DCM) to give semi-solid product (2.7 g 32% yield **HO-diH10 (3-20)**/0.550 g, 16% yield **HO-diH10-O-F3 (3-21)**/1.852 g, 43% yield **HO-diH10-O-F6 (3-22)**). **HO-diH10 (3-20)** NMR: ¹H NMR (400 MHz, CDCl₃): δ 3.94 (p, *J* = 6.4 Hz, 1H), 3.47 (A of ABX, *J*_{AB} = 9.9 Hz, *J*_{AX} = 4.2 Hz, 2H), 3.45 (t, *J* = 6.7 Hz, 4H), 3.45 (B of ABX, *J*_{AB} = 9.9 Hz, *J*_{BX} = 6.4 Hz, 2H), 2.66 (broad s, 1H), 1.55 – 1.50 (m, 4H), 1.23 (broad s, 28H), 0.84 (t, *J* = 7 Hz, 6H). **HO-diH10-O-F3 (3-21)** NMR: ¹H NMR (400 MHz, CDCl₃): δ 3.93 (pentet, *J* = 5 Hz, 1H), 3.90 (tt, *J* = 14, 2 Hz, 5H), 3.58 (t, *J* = 7 Hz, 4H), 3.47 (t, *J* = 7 Hz, 4H), AB of an ABX with signals at 3.45 and 3.47 (*J*_{AB} = 10 Hz, *J*_{AX} = *J*_{BX} = 5 Hz, 4 H), 2.49 (broad singlet, 1H), 1.58 (sextet, *J* = 7 Hz, 8H), 1.41 – 1.29 (m, 24H). ¹⁹F NMR (376 MHz, CDCl₃): δ -81.51 (3F), -121.08 (2F), -128.28 (2F). **HO-diH10-O-F6 (3-22)** NMR: ¹H NMR (400 MHz, CDCl₃): 3.91 (2 signals, 1 the obscured x of an ABX and 1 tt, *J* = 14, 2 Hz, 5H), 3.59 (t, *J* = 6.6 Hz, 4H), 3.46 (t, *J* = 6.7 Hz, 4H), AB of an ABX with signals at 3.48 and 3.43 (*J*_{AB} = 10 Hz, *J*_{AX} = 11 Hz, *J*_{BX} = 9 Hz, 4H), 1.58 (sextet, *J* = 7 Hz, 8H), 1.39 – 1.24 (m, 24H). ¹⁹F NMR (376 MHz, CDCl₃): δ -81.37 (6F), -120.11 (4F), -122.76 (4F), -123.36 (4F), -123.37 (4F), -126.69 (4F).

3.4.4 Miktoarm alcohol syntheses

Decan-1-OMs and Octadecan-1-OMs: Alcohol (decanol 5.012 g, 31.66 mmol/octadecanol 1.609 g, 5.95 mmol) was dissolved in anhydrous DCM (50.0 mL) and flask flushed with Ar. TEA (decanol (8.80 mL, 63.1 mmol)/octadecanol (1.3 mL, 9.33 mmol)) was added to solution and flask cooled in ice bath. MsCl (decanol (3.70 mL, 47.6 mmol)/octadecanol (0.6 mL, 7.72 mmol)) was then added via syringe, dropwise, and reaction stirred under Ar overnight, allowing the ice bath to warm to room temperature. Reaction was then stopped and washed with 4, 100 mL aliquots of aqueous NH_4Cl , dried over MgSO_4 and condensed under reduced pressure. Yield: 7.413 g decyl methane sulfonate (99%), 1.973 g octadecyl methane sulfonate (95%). Decyl methane sulfonate: ^1H NMR (400 MHz, CDCl_3): δ 4.22 (t, $J = 6.6$ Hz, 2H), 3.00 (s, 3H), 1.75 (p, $J = 6.7$ Hz, 2H), 1.42 (t, $J = 7.5$ Hz, 2H), 1.26 (m, 12H), 0.88 (t, $J = 6.8$ Hz, 3H). Octadecyl methane sulfonate: ^1H NMR (400 MHz, CDCl_3): δ 4.16 (t, $J = 6.4$ Hz, 2H), 2.95 (s, 3H), 1.69 (p, $J = 6.8$ Hz, 2H), 1.37-1.12 (m, 30H), 0.83 (t, $J = 6.8$ Hz, 3H).

2-phenyl-1,3-dioxan-5-ol (3-27): glycerol (**3-26**) (24.31 g, 264.0 mmol) and benzaldehyde (28.03 g, 264.1 mmol) were dissolved in anhydrous toluene (70 mL) and flask flushed with argon. *P*-toluenesulfonic acid monohydrate (115.1 mg, 0.61 mmol) was added and flask fitted with Dean-Stark trap and heated to reflux. After 72 hours, reaction was cooled to room temperature and washed with sodium bicarbonate (100 mL), brine (100 mL), dried over MgSO_4 , and remaining toluene was placed in freezer overnight to crystallize out product. White crystals were then collected by filtration and dried under vacuum to yield 4.487 g (24.90 mmol, 9% yield). **3-27** NMR: ^1H NMR (400 MHz, CDCl_3): δ 7.48 (m, 2H), 7.36 (m, 3H), 5.50 (s, 1H), 4.12 (dd, $J = 12.0, 1.4$ Hz, 2H), 4.02 (dd, $J = 12.0, 1.3$ Hz, 2H), 3.54 (dt, $J = 10.6, 1.5$ Hz, 1H), 3.36 (d, $J = 10.5$ Hz, 1H).

5-(decyloxy)-2-phenyl-1,3-dioxane (3-28a) and **5-(octadecyloxy)-2-phenyl-1,3-dioxane (3-28b)**: 2-phenyl-1,3-dioxan-5-ol (**3-27**) (**3-28a** 3.686 g, 20.46 mmol/**3-28b** 4.860 g, 26.97 mmol) was dissolved in anhydrous toluene (**3-28a** 80 mL/**3-28b** 130 mL) and crushed KOH (5a 2.30 g, 41.0 mmol/5b 3.08 g, 54.9 mmol) added. Reaction fitted with Dean-Stark trap and heated to reflux for 6 hours. Reaction then cooled, and alkyl methane sulfonate (decyl methane sulfonate 7.413 g, 31.36 mmol/octadecyl methane sulfonate 5.218 g, 14.97 mmol) added as solution in toluene (20 mL). Reaction fitted with condenser and heated to reflux for 5 days. Reaction was then cooled to room temperature, diluted with 100 mL water, extracted with 3, 100 mL aliquots of ether, dried over MgSO₄ and condensed under reduced pressure. Crude oil purified by flash column (5% ethyl acetate in hexanes) to obtain 3.309 g 5-(decyloxy)-2-phenyl-1,3-dioxane (10.33 mmol, 51%)(**3-28a**), 8.060 g 5-(octadecyloxy)-2-phenyl-1,3-dioxane (**3-28b**) (18.63 mmol, 70%). **3-28a**: ¹H NMR (400 MHz, CDCl₃): δ 7.50 (m, 2H), 7.33 (m, 3H), 5.54 (s, 1H), 4.31 (dd, *J* = 12.4, 1.2 Hz, 2H), 4.02 (dd, *J* = 12.4, 1.6 Hz, 2H), 3.53 (t, *J* = 6.8 Hz, 2H), 3.24 (t, *J* = 2.0 Hz, 1H), 1.65 (p, *J* = 6.8 Hz, 2H), 1.28 (m, 14H), 0.88 (t, *J* = 6.8 Hz, 3H). **3-28b**: ¹H NMR (400 MHz, CDCl₃): δ 7.51 (m, 2H), 7.33 (m, 3H), 5.54 (s, 1H), 4.32 (dd, *J* = 12.5, 1.4 Hz, 2H), 4.03 (dd, *J* = 12.5, 1.8 Hz, 2H), 3.54 (t, *J* = 6.7 Hz, 2H), 3.25 (p, *J* = 1.8 Hz, 1H), 1.65 (p, *J* = 7.6 Hz, 2H), 1.25 (m, 30H), 0.88 (t, *J* = 6.9 Hz, 3H).

3-(benzyloxy)-2-(decyloxy)propan-1-ol (3-29a) and **3-(benzyloxy)-2-(octadecyloxy)propan-1-ol (3-29b)**: **3-28a** (7.745 g, 24.17 mmol) **3-28b** (903.1 mg, 2.087 mmol) was dissolved in anhydrous DCM to achieve 400 mmol L⁻¹ concentration and the flask flushed with argon. Reaction cooled in ice bath, and 1 M DIBAL (**3-29a** 48.3 mL/**3-29b** 4.2 mL) was added dropwise over 20 minutes and reaction stirred overnight, allowing reaction to warm to room temperature. Reaction was quenched dropwise with 0.5 M NaOH (**3-29a** 30 mL/**3-29b** 3 mL), then diluted

with 0.5 M NaOH (10 mL) and extracted with 2, 50 mL aliquots DCM. Combined organics were washed with 2, 100 mL aliquots Rochelle's salt, 100 mL brine, dried over MgSO₄ and condensed under reduced pressure. The crude oil was purified by column chromatography (0-5% methanol in DCM) to yield 6.01 g 3-(benzyloxy)-2-(decyloxy)propan-1-ol (**3-29a**) (18.6 mmol, 77%), 650 mg 3-(benzyloxy)-2-(octadecyloxy)propan-1-ol (**3-29b**) (1.50 mmol, 72%). **3-29a** ¹H NMR (400 MHz, CDCl₃): δ 7.36-7.26 (m, 5H), 4.54 (AB quartet, 2H), 3.74 (m, 1H), 3.66-3.48 (m, 6H), 2.10 (dd, *J* = 5.7, 6.9 Hz, 1H), 1.57 (p, *J* = 7.0 Hz, 2H), 1.26 (m, 14H), 0.88 (t, *J* = 6.8 Hz, 3H). **3-29b** ¹H NMR (400 MHz, CDCl₃): δ 7.35-7.24 (m, 5H), 4.53 (AB quartet, 2H), 3.72 (m, 1H), 3.64-3.48 (m, 6H), 2.27 (t, *J* = 5.0 Hz, 1H), 1.57 (p, *J* = 7.0 Hz, 2H), 1.26 (m, 32H), 0.88 (t, *J* = 6.8 Hz, 3H).

3-(benzyloxy)-2-(decyloxy)propyl methanesulfonate (3-30a) and **3-(benzyloxy)-2-(octadecyloxy)propyl methanesulfonate (3-30b)**: **3-29** (**3-29a** 6.01 g, 18.6 mmol/**3-29b** 215.4 mg, 0.495 mmol) was dissolved in anhydrous DCM to achieve a 50 mmol L⁻¹ concentration and the flask was flushed with Ar. TEA (**3-30a** 5.20 mL/**3-30b** 0.14 mL) was added and reaction cooled in ice bath. MsCl (**3-30a** 2.20 mL/**3-30b** 0.06 mL) was added dropwise and reaction was stirred under Ar overnight, allowing ice bath to warm to room temperature. Reaction was then diluted with DCM (50 mL) and washed with 3 aliquots saturated NH₄Cl solution, dried over MgSO₄ and condensed under reduced pressure to give pale yellow oil. (**3-30a** 7.102 g, 95% yield/**3-30b** 0.253 g, quantitative yield). **3-30a** ¹H NMR (400 MHz, CDCl₃): δ 7.33 (m, 5H), 4.54 (dd, *J* = 12.1, 2.3 Hz, 2H), 4.39 (dd, *J* = 10.9, 3.8 Hz, 1H), 4.27 (dd, *J* = 10.8, 5.7 Hz, 1H), 3.70 (p, *J* = 4.7 Hz, 1H), 3.55 (m, 4H), 3.00 (s, 3H), 1.56 (p, *J* = 6.8 Hz, 2H), 1.28 (m, 14H), 0.88 (t, *J* = 6.8 Hz, 3H). **3-30b** ¹H NMR (500 MHz, CDCl₃): δ 7.41-7.33 (m, 5H), 4.60 (dd, *J* = 14.8, 12.1

Hz, 2H), 4.44 (dd, $J = 10.9, 3.8$ Hz, 1H), 4.33 (dd, $J = 10.9, 5.6$ Hz, 1H), 3.76 (m, 1H), 3.62 (m, 4H), 3.04 (s, 3H), 1.62 (p, $J = 6.8$ Hz, 2H), 1.32 (m, 32H), 0.95 (t, $J = 7.0$ Hz, 3H).

((2-(decyloxy)-3-(1H,1H-perfluorononyloxy)propoxy) methyl)benzene (3-31a) and ((2-(octadecyloxy)-3-(1H,1H-perfluorononyloxy)propoxy)methyl)benzene (3-31b): **3-30 (3-30a**

3.160 g, 7.9 mmol/**3-30b** 1.79 g, 3.49 mmol) was dissolved in anhydrous benzotrifluoride, F8H1-OH (**3-31a** 5.21 g, 11.57 mmol/**3-31b** 3.14 g, 6.98 mmol) added, and flask flushed with Ar. NaH slowly added (**3-31a** 667 mg, 28 mmol/**3-31b** 335 mg, 14 mmol), and reaction heated to reflux for 3 days. Reaction was quenched dropwise with H₂O and further diluted with water and DCM and layers separated. Organics dried over MgSO₄ and condensed under vacuum. Purified by column chromatography (5% ethyl acetate in hexanes) to obtain pure product (**3-31a** 3.985 g, 67% yield/**3-31b** 2.29 g, 76% yield). **3-31a** ¹H NMR (400 MHz, CDCl₃): δ 7.33 (m, 5H), 4.54 (s, 2H), 4.00 (t, $J = 13.9$ Hz, 2H), 3.76 (dd, $J = 10.4, 4.0$ Hz, 1H), 3.68 (dd, $J = 10.4, 5.6$ Hz, 1H), 3.61 (p, $J = 4.7$ Hz, 1H), 3.54 (m, 4H), 1.56 (p, $J = 6.8$ Hz, 2H), 1.28 (m, 14H), 0.88 (t, $J = 6.8$ Hz, 3H). ¹⁹F NMR (376 MHz, CDCl₃): δ -81.19 (3F), -120.22 (2F), -122.38 (6F), -123.12 (2F), -123.80 (m, 2F), -126.52 (2F). **3-31b** ¹H NMR (400 MHz, CDCl₃): δ 7.33 (m, 5H), 4.54 (s, 2H), 3.99 (t, $J = 14.4$ Hz, 2H), 3.77 (dd, $J = 10.4, 4.2$ Hz, 1H), 3.69 (dd, $J = 10.4, 5.5$ Hz, 1H), 3.61 (p, $J = 4.9$ Hz, 1H), 3.54 (m, 4H), 1.55 (p, $J = 7.0$ Hz, 2H), 1.28 (m, 32H), 0.88 (t, $J = 6.8$ Hz, 3H). ¹⁹F NMR (376 MHz, CDCl₃): δ -81.31 (3F), -120.28 (2F), -122.44 (6F), -123.19 (2F), -123.85 (2F), -126.60 (2F).

HO- μ H10F8 (3-32a) and HO- μ H18F8 (3-32b): **3-31 (3-31a** 3.679 g, 4.8 mmol/**3-31b** 2.265 g, 2.6 mmol) was dissolved in anhydrous DCM to achieve 20 mmol L⁻¹ concentration and anisole (HO- μ H10F8 2.10 mL, 19.8 mmol/HO- μ H18F8 1.14 mL, 10.45 mmol) was added. Flask was

flushed with Ar and cooled in ice bath. AlCl_3 (HO- μH10F8 1.951 g, 14.63 mmol/ HO- μH18F8 1.045 g, 7.84 mmol) was added and reaction was stirred under Ar. After (HO- μH10F8 18 hours/HO- μH18F8 1.5 hours) reaction was quenched dropwise with 0.5 M HCl, and further diluted with 0.5 M HCl and layers separated. Organic layer was washed with H_2O , brine, dried over MgSO_4 and condensed under reduced pressure. Crude oil was purified by column chromatography, ((HO- μH10F8 10-40%/HO- μH18F8 10%) ethyl acetate in hexanes) to give pure product (HO- μH10F8 2.875 g, 89% yield/HO- μH18F8 1.400 g, 69% yield). **HO- μH10F8** ^1H NMR (400 MHz, CDCl_3): δ 4.00 (t, $J = 13.7$ Hz, 2H), 3.73 (m, 3H), 3.57 (m, 4H), 2.00 (t, $J = 6.1$ Hz, 1H), 1.57 (p, $J = 7.1$ Hz, 2H), 1.26 (m, 14H), 0.88 (t, $J = 6.8$ Hz, 3H). ^{19}F NMR (376 MHz, CDCl_3): δ -81.25 (3F), -120.16 (2F), -122.42 (6F), -123.16 (2F), -123.82 (2F), -126.57 (2F). **HO- μH18F8** ^1H NMR (400 MHz, CDCl_3): δ 3.99 (t, $J = 13.8$ Hz, 2H), 3.73 (m, 3H), 3.52 (m, 4H), 2.11 (t, $J = 5.9$ Hz, 1H), 1.57 (p, $J = 7.2$ Hz, 2H), 1.26 (m, 32H), 0.88 (t, $J = 6.8$ Hz, 3H). ^{19}F NMR (376 MHz, CDCl_3): δ -81.18 (3F), -120.12 (2F), -122.39 (6F), -123.13 (2F), -123.79 (2F), -126.53 (2F).

3.4.5 Linear and dibranched triphile syntheses

To a dry 100 mL flask charged with argon were added 50 mL benzotrifluoride (BTF) and 4.0 mmol alcohol. The mixture was cooled on ice and 5.0 mmol NaH were added. This was allowed to stir for 30 minutes before adding 2.0 mmol mPEG-OMs. The reaction was then heated to reflux and allowed to react for 7 days. The reaction was cooled, diluted with 100 mL DCM and washed with 150 mL NH_4Cl solution, 50 mL brine and dried over MgSO_4 . The organics were then concentrated to a minimum volume under reduced pressure and the surfactants precipitated upon addition of 500 mL cold ether. The solid was collected by vacuum filtration and then

purified by reverse-phase chromatography. The product was then freeze dried from 50/50 DCM/Benzene to give a powdery solid.

M1H10 (3-16): 60% Yield, MALDI: Distribution centered on $[M+Na^+]=1255.2$, 1H NMR (400 MHz, $CDCl_3$): δ 3.85 – 3.81 (m, 1H), 3.68 – 3.61 (m, 91H), 3.58-3.54 (m, 5H), 3.44 (t, $J = 7$ Hz, 2H), 3.38 (s, 3H), 1.57 (pentet, $J = 7.3$ Hz, 2H), 1.33 – 1.16 (m, 14H), 0.878 (t, $J = 6.9$ Hz, 3H).

M1F13: 58% Yield, MALDI: Distribution centered on $[M+Na^+]=1749.5$, 1H NMR (400 MHz, $CDCl_3$): δ 4.04 (t, $J = 14$ Hz, 2H), 3.46 – 3.46 (m, 106H), 3.38 (s, 3H). ^{19}F NMR (376 MHz, $CDCl_3$): δ -81.10 (3F), -120.13 (2F), -122.01 (16F), -123.01 (2F), -123.79 (2F), -126.45 (2F).

M1H10-O-F3 (3-17): 52% Yield, MALDI: Distribution centered on $[M+Na^+] = 1581.6$, 1H NMR (400 MHz, $CDCl_3$): δ 3.90 (tt, $J = 13.7, 1.7$ Hz, 2H), 3.84 – 3.81 (m, 1H), 3.75 – 3.71 (m, 1H), 3.68 – 3.61 (m, 95H), 3.60 – 3.54 (m, 6H), 3.44 (t, $J = 6.9$ Hz, 2H), 3.38 (s, 3H), 1.58 (sextet, $J = 7.1$ Hz, 4H), 1.35 – 1.22 (m 12H). ^{19}F NMR (376 MHz, $CDCl_3$): δ -81.39 (3F), -121.12 (2F), -128.20 (2F).

M1H10-O-F6 (3-18): 42% Yield, MALDI: Distribution centered on $[M+Na^+] = 1600.2$, 1H NMR (400 MHz, $CDCl_3$): δ 3.92 (tt, $J = 13.3, 2.2$ Hz, 2H), 3.70 - 3.62 (m, 95H), 3.61 – 3.54 (m, 9H), 3.44 (t, $J = 6.6$ Hz, 2H), 3.38 (s, 3H), 1.63-1.52 (m, 4H), 1.33 – 1.23 (m, 12H). ^{19}F NMR (376 MHz, $CDCl_3$): δ -81.28 (3F), -120.07 (2F), -122.73 (2F), -123.34 (2F), -123.95 (2F), -126.64 (2F).

M1H10F8 (3-19): 79% Yield, MALDI: Distribution centered on $[M+Na^+] = 1670.8$, 1H NMR (400 MHz, $CDCl_3$): δ 3.86-3.80 (m, 1H), 3.76 – 3.54 (m, 98H), 3.45 (t, $J = 6.7$ Hz, 2H), 3.38 (s, 3H), 2.05 (ttt, $J = 19, 8.2, 2$ Hz, 2H), 1.57 (septet, $J = 6.7$ Hz, 2H), 1.42 – 1.20 (m, 10H). ^{19}F NMR (376 MHz, $CDCl_3$): δ -81.19 (3F), -114.74 (2F), -122.36 (6F), -123.16 (2F), -123.96 (2F), -126.57 (2F).

M5diH10 (3-23): 70% Yield, MALDI: Distribution centered on $[M+Na^+] = 5120.8$, 1H NMR (400 MHz, $CDCl_3$): δ 3.82 (dd, $J = 6.4, 4.6$ Hz, 2H), 3.76 (dd, $J = 6.5, 4.7$ Hz, 2H), 3.70 – 3.59 (m, 530H), 3.56-3.53 (m, 3H), 3.50 – 3.45 (m, 6H), 3.42 (t, $J = 6.8$ Hz, 4H), 3.38 (s, 3H), 1.55 (pentet, $J = 7.8$ Hz, 4H), 1.34 – 1.21 (m, 28H), 0.88 (t, $J = 6.3$ Hz, 6H).

M5diH10-O-F3 (3-24): 87% Yield, MALDI: Distribution centered on $[M+Na^+] = 5695.7$, 1H NMR (400 MHz, $CDCl_3$): δ 3.90 (tt, $J = 13.8, 1.7$ Hz, 4H), 3.82 (dd, $J = 5.8, 4.6$ Hz, 2H), 3.71 (dd, $J = 6.3, 4.9$ Hz, 2H), 3.71 – 3.53 (m, 453H), 3.50 – 3.41 (m, 12H), 3.38 (s, 3H), 1.63 – 1.51 (m, 8H), 1.39 – 1.23 (m 28H). ^{19}F NMR (376 MHz, $CDCl_3$): δ -81.39 (6F), -121.096 (4F), -128.200 (4F).

M5diH10-O-F6 (3-25): 45% Yield, MALDI: Distribution centered on $[M+Na^+] = 6173.0$, 1H NMR (400 MHz, $CDCl_3$): δ 3.917 (tt, $J = 13.2, 2.8$ Hz, 4H), 3.75 – 3.79 (m, 6H), 3.68 – 3.45 (m, 480H), 3.42 (t, $J = 7$ Hz, 4H), 3.38 (s, 3H), 1.61 – 1.53 (m, 8H), 1.33 – 1.27 (m, 26H); ^{19}F NMR (376 MHz, $CDCl_3$): δ -81.13 (6F), -119.94 (4F), -122.66 (4F), -123.21 (4F), -123.82 (4F), -126.50 (4F).

All amphiphiles are, at most, as polydisperse as the mPEG-OH from which they are synthesized.

3.4.6 Miktoarm triphile syntheses

Alcohol and Mx-OMs were dissolved in 20-75 mL BTF to achieve 20 mM concentrations. Flask flushed with Ar, NaH added (to achieve 40 mM concentration), and flask heated to reflux. After 5 days reaction was cooled to room temperature and quenched dropwise with H₂O. The organics were dried over MgSO₄. Solvents evaporated under reduced pressure, and crude polymer purified by reverse phase chromatography. Solid was lyophilized to give white, fluffy product.

M1 μ H10F8 (3-33): 89% Yield, MALDI: Distribution centered on $[M+Na^+] = 1715.0$, ¹H NMR (400 MHz, CDCl₃): δ 4.02 (t, $J = 14$ Hz, 2H), 3.81 (m, 1H), 3.75 (dd, $J = 10.4, 3.6$ Hz, 2H), 3.67-3.62 (m, 80H), 3.59-3.51 (m, 7H), 3.46 (m, 1H), 3.38 (s, 3H), 1.57 (p, $J = 7.2$ Hz, 2H), 1.26 (m, 16H), 0.88 (t, $J = 6.8$ Hz, 3H). ¹⁹F NMR (400 MHz, CDCl₃): δ -81.14 (3F), -120.18 (2F), -122.36 (6F), -123.09 (2F), -123.77 (2F), -126.48 (2F).

M2 μ H18F8 (3-34): 58% Yield, MALDI: Distribution centered on $[M+Na^+] = 2586.5$, ¹H NMR (400 MHz, CDCl₃): δ 4.03 (t, $J = 13.9$ Hz, 2H), 3.82 (m, 2H), 2.76 (dd, $J = 10.5, 3.6$ Hz, 1H), 3.60-3.50 (m, 144H), 3.55 (m, 6H), 3.47 (m, 2H), 3.38 (s, 3H), 1.55 (p, $J = 6.8$ Hz, 2H), 1.26 (m, 26H), 0.88 (t, $J = 7.0$ Hz, 3H). ¹⁹F NMR (400 MHz, CDCl₃): δ -81.27 (3F), -120.28 (2F), -122.49 (6F), -123.22 (2F), -123.89 (2F), -126.65 (2F).

All amphiphiles are, at most, as polydisperse as the mPEG-OH from which they are synthesized.

3.4.7 Physicochemical characterization

Micelle preparation – solvent evaporation method (SEM). Polymer is dissolved in MeOH or ACN to a desired concentration. 1 mL of polymer solution and additive (e.g. PTX in ACN) are added to a 25 mL roundbottom flask and rotated for 5 minutes at 60 °C on a rotary evaporator, no

vacuum, and then the solvent was removed in vacuo with rotation for 15 minutes. The film was then dispersed with Millipore water heated to 60 °C and filtered with a 0.45- μ m nylon filter.

Particle size determination by dynamic light scattering (DLS). Micelles were prepared by solvent evaporation, polymer solution concentration 1 mg mL⁻¹ in MeOH. Particle sizes of polymeric aggregates were analyzed by dynamic light scattering (Malvern Zetasizer Nano ZS, Malvern Instruments Ltd., Westborough, MA). The surfactant solution was measured directly without dilution and analyzed. Each particle size analysis was run at room temperature and repeated in triplicate with the number of scans of each run determined automatically by the instrument according to the concentration of the solution. The data was analyzed using NICOMP analysis and reported as volume weighted average diameters.

Critical micelle concentration (CMC) determination – Surface Tensiometry. Surfactant was dissolved in Millipore water to a concentration of 1 mM and concentrations down to 1 nM were prepared by serial dilution and transferred to 20 mL disposable scintillation vials. After solutions were made, the samples were heated in a water bath at 40 °C with sonication for 2-3 hours and allowed to equilibrate for 24 hours. Surface tensions were measured on a KSV sigma 701 tensiometer (KSV Instruments, Helsinki, Finland) equipped with a Julabo F12-MC circulator for constant temperature control. Custom round rod made of platinum with a diameter of 1.034 mm with wetted length of 3.248 mm was used. The rod was submerged in absolute alcohol and flame dried with a Bunsen burner for 4 seconds. This was repeated after 4 minutes. The rod was then hung on the instrument and allowed to cool to room temperature without touching any surface. Before running the experimental samples, the surface tension of millipore water was measured as a control to confirm the rod was fully cleaned and surface tension was within 1 mN/m of 78.2

mN/m. The surface tension measurements began with the least concentrated solution and proceeded to successively more concentrated solutions. The surface tension at each concentration was measured in quadruplet and average recorded. The critical micelle concentration value was determined from the crossover point of two lines: the baseline of minimal surface tension and the slope where surface tension showed linear decline; error determined by weighted least squares analysis.

Critical aggregation concentration (CMC) determination – Pyrene Fluorescence. Based on the methodology developed by Torchilin *et al.*²⁴ Micelles were prepared by the solvent evaporation method. 200 μL micelle solutions in MeOH ranging in concentration from $10^{-4.0}$ to $10^{-8.0}$ M were delivered to 25 mL roundbottom flasks with 100 μL 10 mg mL^{-1} pyrene solution. The thin films were dispersed with 2 mL 60 °C PBS and filtered with a 0.45- μm nylon filter. The fluorescence analysis was carried out on an AMINCO-Bowman Series 2 spectrometer with excitation at 339 nm, emission at 390 nm and a spectral window of 370 – 400 nm. The analysis was carried out in triplicate and the average CMC and standard deviation are reported.

Microviscosity measurement. Surfactant solutions of 0.2 mmol L^{-1} in MeOH and a 2.7 ng mL^{-1} 1,3-bis-(1-pyrenyl)propane (P3P) in chloroform were prepared. Micelle solutions were then prepared via the solvent evaporation method with 67 μL of the P3P solution added and solutions stored in amber vials. The fluorescence analysis was carried out on an AMINCO-Bowman Series 2 spectrometer with excitation at 333 nm, emission at 378 nm and a spectral window of 350 – 500 nm.

Föster resonance energy transfer (FRET) stability. Surfactant solutions of 1 mg mL⁻¹ in methanol and 0.1 mg mL⁻¹ of 1,1'-dioctadecyl-3,3,3',3'-tetramethylindocarbocyanine perchlorate (DiI) and 3,3'-dioctadecyloxacarbocyanine perchlorate (DiO) in methanol were prepared. Micellar solutions were then prepared by the solvent evaporation method. For blank micelles only polymer solution is used; for FRET loaded micelles, 46 µL DiI and 44 µL of DiI are added.

Three analytic samples were then prepared (the two components were mixed just before analysis: 50 µL of FRET dye loaded micelles and 950 µL PBS (used to set sensitivity), 50 µL empty micelles and 950 µL human serum (used to correct for baseline), 150 µL FRET dye loaded micelles and 2.85 mL human serum (mixed gently before first measurement and vigorously before each measurement, every 15 minutes, thereafter. The fluorescence analysis was carried out on an AMINCO-Bowman Series 2 spectrometer with excitation at 484 nm and emission at 565 nm. The FRET ratio calculated was the ratio of $I_{565}/(I_{501}+I_{565})$.

Paclitaxel (PTX) encapsulation measurements. Micelles solutions were prepared in triplicate using the solvent evaporation method. PTX stock solution was generated by dissolving PTX in ACN, aided by sonication, at a concentration of 1 mg mL⁻¹. Surfactant was dissolved in ACN to give a final concentration of 2.4×10^{-3} mol L⁻¹. One mL of surfactant solution was then mixed with 230 µL PTX solution. The sample was then centrifuged at 12,000 rpm for 5 minutes and filtered through 0.45-µm nylon syringe filter to remove any insoluble precipitate. A 100-µL aliquot of micelle solution was mixed with 900 µL of ACN and the remaining micelle solution was allowed to sit for 24 hours. The sample was then re-centrifuged at 12,000 rpm for 5 minutes and filtered through 0.45-µm nylon syringe filter to remove any insoluble precipitate. A 100-µL aliquot of micelle solution was mixed with 900 µL of ACN. The paclitaxel loaded in the micelle was

quantified by reverse phase HPLC. The HPLC system used was a Shimadzu prominence HPLC system (Shimadzu, Japan), consisting of a LC-20AT pump, SIL-20 AC HT autosampler, CTO-20 AC column oven and an SPD-M20A diode array detector. 20 μL of the mixture was injected into a C18 column (Agilent XDB-C8, 4.6 \AA x 150 mm), eluting with an isocratic mixture of 25% water in acetonitrile. The run time was 7 min, the flow rate was 1.0 mL min^{-1} and the detection was set at 227 nm.

3.5 References

- (1) Lipshutz, B. H.; Isley, N. A.; Fennewald, J. C.; Slack, E. D. On the Way towards Greener Transition-Metal-Catalyzed Processes as Quantified by E Factors. *Angew. Chemie - Int. Ed.* **2013**, 52 (42), 10952–10958.
- (2) Isley, N. A.; Gallou, F.; Lipshutz, B. H. Transforming Suzuki-Miyaura Cross-Couplings of MIDA Boronates into a Green Technology: No Organic Solvents. *J. Am. Chem. Soc.* **2013**, 135 (47), 17707–17710.
- (3) Caillier, L.; de Givenchy, E. T.; Levy, R.; Vandenberghe, Y.; Geribaldi, S.; Guittard, F. Polymerizable Semi-Fluorinated Gemini Surfactants Designed for Antimicrobial Materials. *J. Colloid Interface Sci.* **2009**, 332 (1), 201–207.
- (4) Allen, C.; Maysinger, D.; Eisenberg, A. Nano-Engineering Block Copolymer Aggregates for Drug Delivery. *Colloids Surfaces B Biointerfaces* **1999**, 16 (1-4), 3–27.
- (5) Torchilin, V. P. Multifunctional, Stimuli-Sensitive Nanoparticulate Systems for Drug Delivery. *Nat. Rev. Drug Discov.* **2014**, 13 (11), 813–827.
- (6) Trubetskoy, V. S.; Torchilin, V. P. Use of Polyoxyethylene-Lipid Conjugates as Long-Circulating Carriers for Delivery of Therapeutic and Diagnostic Agents. *Adv. Drug Deliv. Rev.* **1995**, 16 (2-3), 311–320.
- (7) Weissig, V.; Whiteman, K. R.; Torchilin, V. P. Accumulation of Protein-Loaded Long-Circulating Micelles and Liposomes in Subcutaneous Lewis Lung Carcinoma in Mice. *Pharm. Res.* **1998**, 15 (10), 1552–1556.
- (8) Hoang, K. C.; Mecozzi, S. Aqueous Solubilization of Highly Fluorinated Molecules by Semifluorinated Surfactants. *Langmuir* **2004**, 20 (18), 7347–7350.

- (9) Parlato, M. C.; Jee, J. P.; Teshite, M.; Mecozzi, S. Synthesis, Characterization, and Applications of Hemifluorinated Dibranching Amphiphiles. *J. Org. Chem.* **2011**, *76* (16), 6584–6591.
- (10) Jee, J. P.; McCoy, A.; Mecozzi, S. Encapsulation and Release of Amphotericin B from an ABC Triblock Fluorous Copolymer. *Pharm. Res.* **2012**, *29* (1), 69–82.
- (11) Bates, F. S.; Hillmyer, M. A.; Lodge, T. P.; Bates, C. M.; Delaney, K. T.; Fredrickson, G. H. Multiblock Polymers: Panacea or Pandora's Box? *Science*. **2012**, *336* (6080), 434–440.
- (12) Chen, J.; Li, J. J.; Luo, Z. H. Synthesis, Surface Property, Micellization and pH Responsivity of Fluorinated Gradient Copolymers. *J. Polym. Sci. Part A Polym. Chem.* **2013**, *51* (5), 1107–1117.
- (13) Chen, Y.; Zhang, Y.; Wang, Y.; Sun, C.; Zhang, C. Synthesis, Characterization, and Self-Assembly of Amphiphilic Fluorinated Gradient Copolymer. *J. Appl. Polym. Sci.* **2013**, *127* (3), 1485–1492.
- (14) Zhou, Y.; Luo, Z.; Chen, J. Theoretical Modeling Coupled with Experimental Study on the Preparation and Characterization Comparison of Fluorinated Copolymers : Effect of Chain Structure on Copolymer Properties. *AIChE J.* **2013**, *59* (8), 3019–3033.
- (15) Alaimo, D.; Beigbeder, A.; Dubois, P.; Broze, G.; Jérôme, C.; Grignard, B. Block, Random and Palm-Tree Amphiphilic Fluorinated Copolymers: Controlled Synthesis, Surface Activity and Use as Dispersion Polymerization Stabilizers. *Polym. Chem.* **2014**, *5* (18), 5273–5282.
- (16) Amado, E.; Kressler, J. Triphilic Block Copolymers with Perfluorocarbon Moieties in Aqueous Systems and Their Biochemical Perspectives. *Soft Matter* **2011**, *7* (16), 7144.
- (17) Israelachvili, J. N.; Mitchell, D. J.; Ninham, B. W. Theory of Self-Assembly of Hydrocarbon Amphiphiles into Micelles and Bilayers. *J. Chem. Soc. Faraday Trans. 2* **1976**, *72*, 1525.
- (18) Ashok, B.; Arleth, L.; Hjelm, R. P.; Rubinstein, I.; Önyüksel, H. *In Vitro* Characterization of PEGylated Phospholipid Micelles for Improved Drug Solubilization: Effects of PEG Chain Length and PC Incorporation. *J. Pharm. Sci.* **2004**, *93* (10), 2476–2487.
- (19) Rolland, J. P.; Santaella, C.; Vierling, P. Molecular Packing of Highly Fluorinated Phosphatidylcholines in Monolayers. *Chem. Phys. Lipids* **1996**, *79* (1), 71–77.
- (20) Brace, N. O. Syntheses with Perfluoroalkyl Radicals from Perfluoroalkyl Iodides. A Rapid Survey of Synthetic Possibilities with Emphasis on Practical Applications. Part One: Alkenes, Alkynes and Allylic Compounds. *J. Fluor. Chem.* **1999**, *93* (1), 1–25.

- (21) Rocaboy, C.; Rutherford, D.; Bennett, B. L.; Gladysz, J. A. Strategy and Design in Fluorous Phase Immobilization: A Systematic Study of the Effect of “Pony Tails” $(\text{CH}_2)_3(\text{CF}_2)_{n-1}\text{CF}_3$ on the Partition Coefficients of Benzenoid Compounds. *J. Phys. Org. Chem.* **2000**, *13* (10), 596–603.
- (22) Tucker, W. B.; Mecozzi, S. Base-Induced Instability of Fluorotelomer Alcohols. *J. Fluor. Chem.* **2013**, *156*, 26–29.
- (23) Juaristi, E.; Antúnez, S. Conformational Analysis of 5-Substituted 1,3-Dioxanes. 6. Study of the Attractive Gauche Effect in O-C-C-O Segments. *Tetrahedron* **1992**, *48* (29), 5941–5950.
- (24) Torchilin, V. P.; Levchenko, T. S.; Whiteman, K. R.; Yaroslavov, A. A.; Tsatsakis, A. M.; Rizos, A. K.; Michailova, E. V.; Shtilman, M. I. Amphiphilic Poly-*N*-vinylpyrrolidones: Synthesis, Properties and Liposome Surface Modification. *Biomaterials* **2001**, *22* (22), 3035–3044.
- (25) Johansson, E.; Lundquist, A.; Zuo, S.; Edwards, K. Nanosized Bilayer Disks: Attractive Model Membranes for Drug Partition Studies. *Biochim. Biophys. Acta - Biomembr.* **2007**, *1768* (6), 1518–1525.
- (26) Zana, R. Microviscosity of Aqueous Surfactant Micelles : Effect of Various Parameters. *J. Phys. Chem.* **1999**, *103* (43), 9117–9125.
- (27) Meguro, K.; Takasawa, Y.; Kawahashi, N.; Tabata, Y.; Ueno, M. Micellar Properties of a Series of Octaethyleneglycol-*N*-Alkyl Ethers with Homogeneous Ethylene Oxide Chain and Their Temperature Dependence. *J. Colloid Interface Sci.* **1981**, *83* (1), 50–56.
- (28) Kunieda, H.; Shinoda, K. Krafft Points, Critical Micelle Concentrations, Surface Tension, and Solubilizing Power of Aqueous Solutions of Fluorinated Surfactants. *J. Phys. Chem.* **1976**, *80* (22), 2468–2470.
- (29) Li, Z.; Hillmyer, M. A.; Lodge, T. P. Morphologies of Multicompartment Micelles Formed by ABC Miktoarm Star Terpolymers. *Langmuir* **2006**, *22* (22), 9409–9417.
- (30) Yang, C.; Ebrahim Attia, A. B.; Tan, J. P. K.; Ke, X.; Gao, S.; Hedrick, J. L.; Yang, Y. Y. The Role of Non-Covalent Interactions in Anticancer Drug Loading and Kinetic Stability of Polymeric Micelles. *Biomaterials* **2012**, *33* (10), 2971–2979.
- (31) Torchilin, V. P. Structure and Design of Polymeric Surfactant-Based Drug Delivery Systems. *J. Control. Release* **2001**, *73* (2-3), 137–172.
- (32) Chen, H.; Kim, S.; He, W.; Wang, H.; Low, P. S.; Park, K.; Cheng, J. X. Fast Release of Lipophilic Agents from Circulating PEG-PDLLA Micelles Revealed by in Vivo Förster Resonance Energy Transfer Imaging. *Langmuir* **2008**, *24* (10), 5213–5217.

- (33) Moughton, A. O.; Hillmyer, M. A.; Lodge, T. P. Multicompartment Block Polymer Micelles. *Macromolecules* **2012**, *45* (1), 2–19.
- (34) Akiba, I.; Terada, N.; Hashida, S.; Sakurai, K.; Sato, T.; Shiraishi, K.; Yokoyama, M.; Masunaga, H.; Ogawa, H.; Ito, K.; Yagi, N. Encapsulation of a Hydrophobic Drug into a Polymer-Micelle Core Explored with Synchrotron SAXS. *Langmuir* **2010**, *26* (10), 7544–7551.
- (35) Aliabadi, H. M.; Elhasi, S.; Mahmud, A.; Gulamhusein, R.; Mahdipoor, P.; Lavasanifar, A. Encapsulation of Hydrophobic Drugs in Polymeric Micelles through Co-Solvent Evaporation: The Effect of Solvent Composition on Micellar Properties and Drug Loading. *Int. J. Pharm.* **2007**, *329* (1-2), 158–165.
- (36) Vakil, R.; Kwon, G. S. Poly(ethylene glycol)-*b*-Poly(ϵ -Caprolactone) and PEG-Phospholipid Form Stable Mixed Micelles in Aqueous Media. *Langmuir* **2006**, *22* (23), 9723–9729.
- (37) Li, L. B.; Tan, Y. B. Preparation and Properties of Mixed Micelles Made of Pluronic Polymer and PEG-PE. *J. Colloid Interface Sci.* **2008**, *317* (1), 326–331.

CHAPTER 4:

Triphilic surfactant-based anesthetic nanoemulsions

Contribution: Dr. Aaron McCoy, Ph.D. helped prepare and monitor the particle size for the miktoarm-surfactant-based emulsions. Dr. Colby Parks, M.D. carried out the *in vivo* animal studies with assistance from William Tucker. Dr. Christopher Warren, Ph.D. carried out the advanced statistical analysis for the *in vivo* studies. William Tucker completed all other work and studies presented in this chapter.

*This chapter has been, in part, prepared as a manuscript to be submitted to *Anesthesiology*: Parks. C.; Tucker, W.; Amlong, C.; Mecozzi, S.; Pearce, R. Lipid-Free Fluoropolymer Based Propofol Emulsions in Lipid Reversal of Propofol Anesthesia in Rats.

Abstract

Anesthetics delivered by intravenous (IV) injection exhibit more rapid onset compared to inhaled delivery; however, the IV delivery of neat anesthetics is complicated by their hydrophobicity, which can lead to patient death upon IV injection. The preparation of anesthetic nanoemulsions is of interest as a means of improving upon anesthetic delivery while avoiding the complications associated with injection. The formulation of isoflurane and reformulation of propofol are investigated here. No prior formulation of isoflurane could achieve concentrations \geq 20 vol%, thus limiting its clinical applicability. Propofol is widely used to induce anesthesia as the commercially available, soybean-oil based nanoemulsion Diprivan®; however, Diprivan suffers from issues with microbial growth and hyperlipidemia. Triphilic surfactants synthesized previously for micellar applications were found effective at stably emulsifying isoflurane at up to 30-vol% (a clinically useful concentration) and propofol at 1 wt% (the same concentration as Diprivan®). Attempts to improve upon the successful isoflurane formulation to create emulsions with greater stability proved ineffective and work is ongoing. The successful propofol formulations were investigated in rat models and were shown to exhibit efficacy similar to Diprivan® with the potential for lipid reversal.

4.1 Introduction

Nanoemulsions are colloidal systems consisting of sub-500 nm droplets of one immiscible liquid dispersed within a larger volume of another liquid.¹ The distribution of immiscible, dispersed-phase (typically oil) droplets in a continuous phase (typically water) is thermodynamically unstable. Adding surfactant molecules to a nanoemulsion, which adsorb onto the nanodroplets, is required to render the colloidal system kinetically stable.² The development of ideal surfactants/surfactant mixtures that can stabilize the nanodroplets through the formation of strong penetration complexes lies at the heart of developing stable nanoemulsions.^{3,4}

Given their small size, oil-in-water nanoemulsions have garnered interest as parenteral drug delivery vehicles. The hydrophobic droplet acts as a reservoir for the sparingly water-soluble pharmaceutical agent and the surfactants solubilize the droplet. This sequestration inside a nanodroplet thus increases the amount of drug that can be dissolved in water and protects the solubilized species. Together, nanoemulsions offer the potential for new routes of administration, particularly for compounds that need large doses not attainable in micellar formulations.⁵

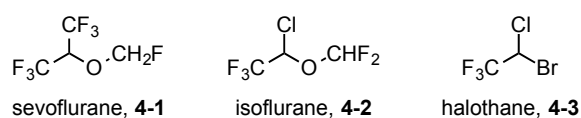


Figure 4.1 Structure of the volatile anesthetics sevoflurane, isoflurane, and halothane.

The IV-delivery of volatile anesthetics (rather than delivery by inhalation) has been of interest for a number of decades because it allows for more rapid onset of anesthesia.⁶ In addition, previous studies with halothane (**Figure 4.1**) nanoemulsions have shown that the depth of anesthesia can be controlled by the rate of infusion and that the rate of recovery was faster than recovery from inhalation delivery.⁷ To date, however, the emulsification of more modern, volatile anesthetics like sevoflurane and isoflurane (**Figure 4.1**) has been hampered by their fluorophilicity (low lipophilicity). For example, attempts to emulsify sevoflurane with Intralipid

(a traditional, soybean-oil based emulsion) yielded a maximum 3.5 vol% formulation.⁸ This concentration would require too large of a dose to be clinically useful. In contrast, the Mecozzi laboratory has demonstrated that fluoropolymers can effectively solubilize sevoflurane at 25 vol% for up to one year and are effective at inducing anesthesia in rats.^{6,9} This increase in sevoflurane concentration is due to a better match between the fluorophilicity of the fluoropolymer tail and sevoflurane.

Despite previous success with sevoflurane, isoflurane could not be stabilized at similarly high concentrations with purely fluorophilic surfactants. Isoflurane is soluble up to 8.2 vol% in Intralipid (still too low to be clinically useful).⁸ It should be noted that isoflurane exhibits a solubilization in Intralipid greater than double that of sevoflurane (3.5 vol%). The enhanced solubility of isoflurane, compared to sevoflurane, is due to the substitution of a chloride for a CF₃ (**Figure 4.1**), which makes isoflurane more lipophilic.

Recent development of isoflurane emulsions has lead to the creation of a 15 vol% formulation, but 15 vol% seems to be the maximum concentration achievable using classical surfactants.¹⁰ Triphilic surfactants, with mixed lipophilicity and fluorophilicity, were hypothesized to be more ideal for emulsifying isoflurane (a molecule with mixed lipophilicity and fluorophilicity) than either classical surfactants (lipophilic-hydrophilic) or fluorosurfactants (fluorophilic-hydrophilic). Several triphilic surfactants, perfluorooctyl bromide (PFOB, potential additive), and phosphatidylcholine (potential co-surfactant) were investigated. To date, 20 vol% (which is stable for 77 days), 25 vol% (stable for 14 days), and 30 vol% (stable for 7 days) isoflurane emulsions have been prepared. While the triphilic surfactants have produced the best results to date, attempts to improve the emulsion shelf life have thus far proven unsuccessful. Work is ongoing in the Mecozzi group to create stable, high-concentration, isoflurane emulsions.

In comparison to the fluorinated anesthetics sevoflurane and isoflurane, propofol and etomidate (**Figure 4.2**) are readily emulsified in Intralipid at clinically effective concentrations. While etomidate is not widely used due to its deleterious side effects,¹¹ propofol is commonly used for induction and maintenance of general anesthesia, as well as for sedation in the operating room and intensive care unit. The current, clinically used formulation of soybean-oil-based emulsion of propofol is Diprivan® (AstraZeneca, London, United Kingdom).¹² This formulation is clinically effective but does have several drawbacks. First, Diprivan, as with all nanoemulsions, suffers from issues with instability.^{13,14} Second, Diprivan has several issues related to its formulation (specifically its soybean oil content): microbial growth^{15–17} and the occurrence of hyperlipidemia (elevated triglycerides and propofol infusion syndrome).^{18–21} Finally, Diprivan is a very painful injection (due to free propofol or the rapid release of propofol upon injection).^{22–25}

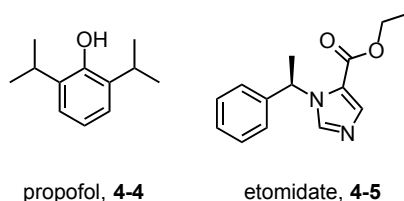
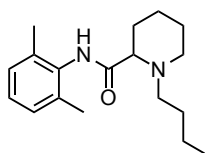


Figure 4.2. Structure of propofol and etomidate, non-volatile anesthetics commonly used to induce anesthesia.

There have been many attempts to reformulate Diprivan to address its enumerated issues. Preservatives and anti-microbial agents such as EDTA and sodium metabisulfite have been added.¹² The oil and lecithin content has been varied.²⁶ Different sizes of triglycerides and new solvents have been tested.^{27,28} Alternative emulsions have been developed to minimize the free concentration of propofol.^{29,30} A recent example is Aquafol (Daewon Pharmaceutical Co., Ltd., Seoul, Korea), a 1% propofol emulsion with 10% purified poloxamer 188 and 0.7% poly-ethylene glycol 660 hydroxystearate (using no lipid), which has become clinically available in Korea.^{31–33}

Triphilic surfactants were investigated in a propofol emulsion reformulation due to their unique architecture (lipophilic and fluorophilic blocks). Our hypothesis was that a semi-fluorinated surfactant could lead to shelf-stable formulations – without added soybean oil – that would show comparable pharmacokinetics to Diprivan. Three of the successful triphilic surfactant formulations and an oil-free, egg-lecithin-based formulation were evaluated in rats, and their anesthetic effects compared favorably to the clinically used formulation of Diprivan.

In addition to testing these emulsions for stability and efficacy, the removal of soybean oil from the propofol formulation offered the potential to investigate whether a post-induction injection of lipid would accelerate recovery from the anesthetic effects of propofol. This “lipid-rescue” method is effective at eliminating the toxic effects of several other lipid-soluble drugs including bupivacaine (**Figure 4.3**).³⁴ The octanol:water partition coefficient (log P) of propofol is 3.79,³⁵ which makes it even more lipid soluble than bupivacaine (log P 3.41).³⁶ If the lipid solubility of propofol causes a decreased effect site concentration with a post-induction lipid infusion then the duration of anesthesia caused by propofol may be reduced with a lipid infusion, similar to bupivacaine. One oil-free, triphilic formulation was tested for lipid rescue and showed potentially positive results.



bupivacaine, **4-6**

Figure 4.3. Structure of bupivacaine, a local anesthetic for which lipid rescue has been demonstrated.

4.2 Results and Discussion

4.2.1 Isoflurane nanoemulsion formulation

Triphilic surfactants, with both lipophilic and fluorophilic moieties, were hypothesized to be superior surfactants for the emulsification of isoflurane (a molecule with mixed lipophilicity and fluorophilicity). Both linear and dibranched surfactants were considered as potential surfactants for an isoflurane emulsion. M5H10F8, **Figure 4.4**, was the first triphilic surfactant synthesized and the first investigated for its ability to emulsify isoflurane.

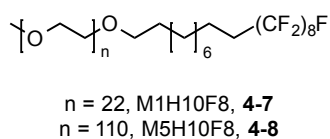


Figure 4.4. Structure of M_xH10F8 ($x = 1, 5$) triphilic surfactants used in isoflurane emulsions.

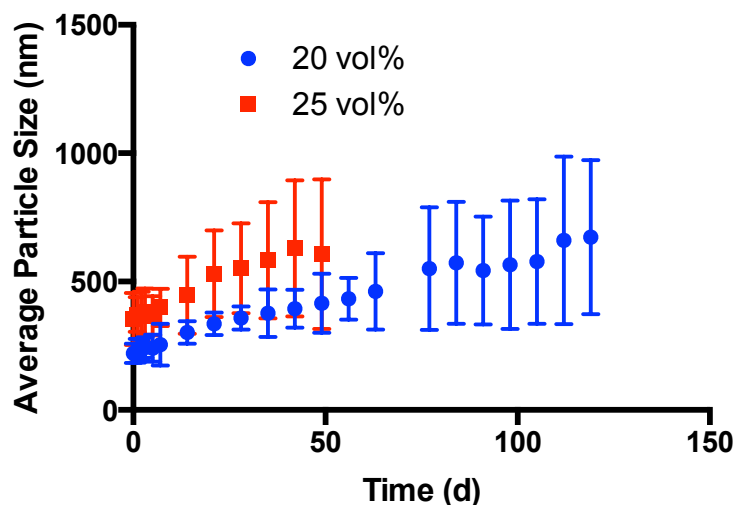


Figure 4.5. Average particle size over time with SD given by error bars ($n = 3$) for 20 and 25 vol% isoflurane emulsions with M5H10F8 as the surfactant.

To test the ability of M5H10F8 to emulsify isoflurane, a 20 vol% isoflurane emulsion with 10 vol% perfluorooctyl bromide (PFOB, a less water-soluble stabilizing additive) was prepared by high-energy emulsification. This emulsion remained below 500 nm (the USP cutoff for IV-injectable emulsions) and was stable for 119 days before phase separation (**Figure 4.5**). Given

the success of this initial emulsion, a 25 vol% formulation with 10 vol% PFOB was prepared. The 25 vol% emulsion remained below 500 nm for 14 days and was stable for 49 before phase separation. These results seemed promising for the use of triphilic surfactants to emulsify isoflurane.

Previous work on sevoflurane had shown that M1F13 produced more stable emulsions than M5F13. The smaller mPEG hydrophilic block allows for closer packing of surfactants around the droplet, which limits Ostwald ripening (diffusion of oil-phase from smaller droplets to larger droplets) and thus increases emulsion stability. By extension, it was reasoned that M1H10F8 should produce a more stable isoflurane emulsion than did M5H10F8. Inexplicably, all attempts to emulsify isoflurane with M1H10F8 (at any concentration of isoflurane, with or without PFOB) failed to produce a stable emulsion.

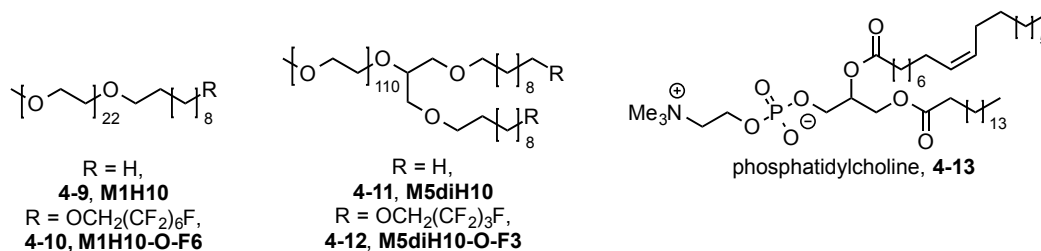


Figure 4.6. Structure of other surfactants investigated for isoflurane emulsions.

In light of the failure of M1H10F8 to stably emulsify isoflurane, both the less fluorophilic M1H10-O-F6 and the dibranched surfactant M5diH10-O-F3 (**Figure 4.6**) were studied. Dibranched surfactants have been shown to be better surfactants to stabilize emulsions due to, again, tighter surfactant packing. Yet, for isoflurane neither M1H10-O-F6 nor M5diH10-O-F3 were not able to give a stable emulsion. With the failure of M1H10F8 (with or without PFOB), M1H10-O-F6, and M5diH10-O-F3 to emulsify isoflurane at any concentration, the choice of surfactants and additives was reevaluated. First, the assumption that a semi-fluorinated surfactant was needed was evaluated by testing M1H10 with and without Lipoid E80 (an egg lecithin

derivative that is 80% phosphatidylcholine), M5diH10 with Lipoid E80, and Lipoid E80 alone (**Figure 4.6**). These classical surfactants and surfactant mixtures were not able to make a stable emulsion or one that was stable for more than 24 hours (**Figure 4.7**).

Lipoid E80 does, however, give a 30 vol% isoflurane emulsion that is stable for 24 hours. This transiently successful emulsification at 30 vol% represents a first for isoflurane. In an effort to improve on this formulation, an equimolar amount of M1H10F8 was added (**Figure 4.7**). While this initial formulation was worse than Lipoid E80 alone, it was more stable than any emulsion with M1H10F8 to date. Thus an emulsion with double the surfactant concentration (of both surfactants) was prepared. This emulsion was stable for two weeks before phase separation occurred. This formulation is the best, high-concentration isoflurane emulsion attempted to date.

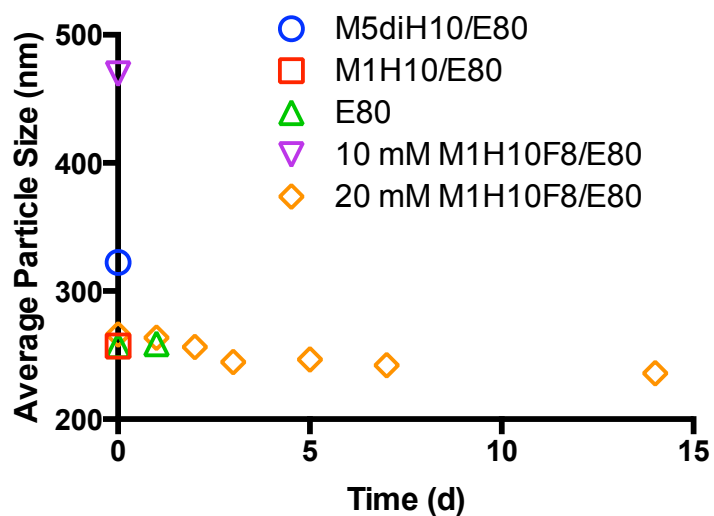


Figure 4.7. Average particle size over time (error bars omitted for clarity) for 30 vol% isoflurane emulsions with Lipoid E80 as surfactant or co-surfactant.

With the existence of a 15 vol% isoflurane emulsion already in the literature, it has been decided that any new formulation must be substantially better (≥ 25 vol%). No formulation has yet proven to be stable at or above 25 vol% for more than two weeks. Moreover, the formulation of stable isoflurane emulsions remains doggedly empirical in nature, with first principles attempts

over the M1H10-O-F6 formulation given its smaller average size and distribution and was given the abbreviation L3 for the *in vivo* tests.

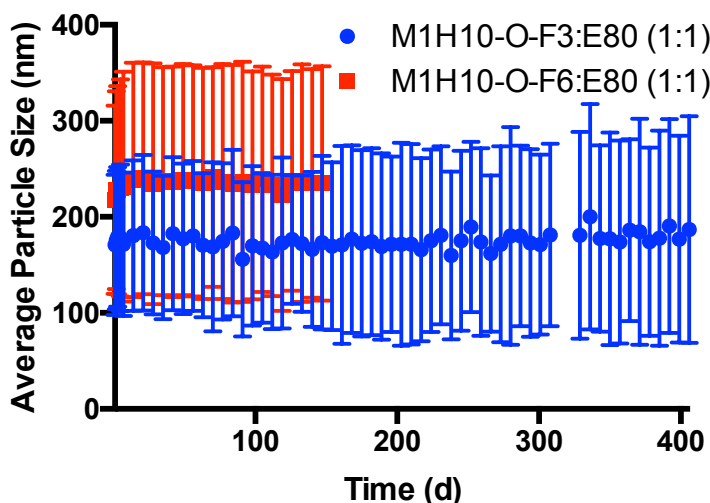


Figure 4.9. Average particle size over time with SD given by error bars ($n = 3$) for the linear M1H10-O-Fx ($x = 3, 6$), Lipoid E80, propofol emulsions

For the linear surfactants (M1H10, M1H10-O-F3, and M1H10-O-F6), the fluorophilic substituent was found to be necessary for stable emulsion formulation. While Lipoid E80 was also found to be necessary, the amount of Lipoid E80 added was varied to find an optimum concentration. Even cutting the concentration in half (2:1 M1H10-O-F3:Lipoid E80) gave significantly higher initial diameter (**Figure 4.10.A**), initial standard deviation (**Figure 4.10.B**), and initial average particle size growth (**Figure 4.10.C**). While reducing the Lipoid E80 content had detrimental effects, the opposite extreme (removing the triphilic surfactant) demonstrated that stable emulsions could be made with only Lipoid E80 (**Figure 4.11**) if the solution were made isotonic with blood using glycerol (formulation L80). If sodium chloride were used for isotonicity, the resulting emulsion was not stable and phase separated within several hours because the added salt reduced the effective charge-charge repulsion between polar headgroups on the zwitterionic phosphatidylcholine.

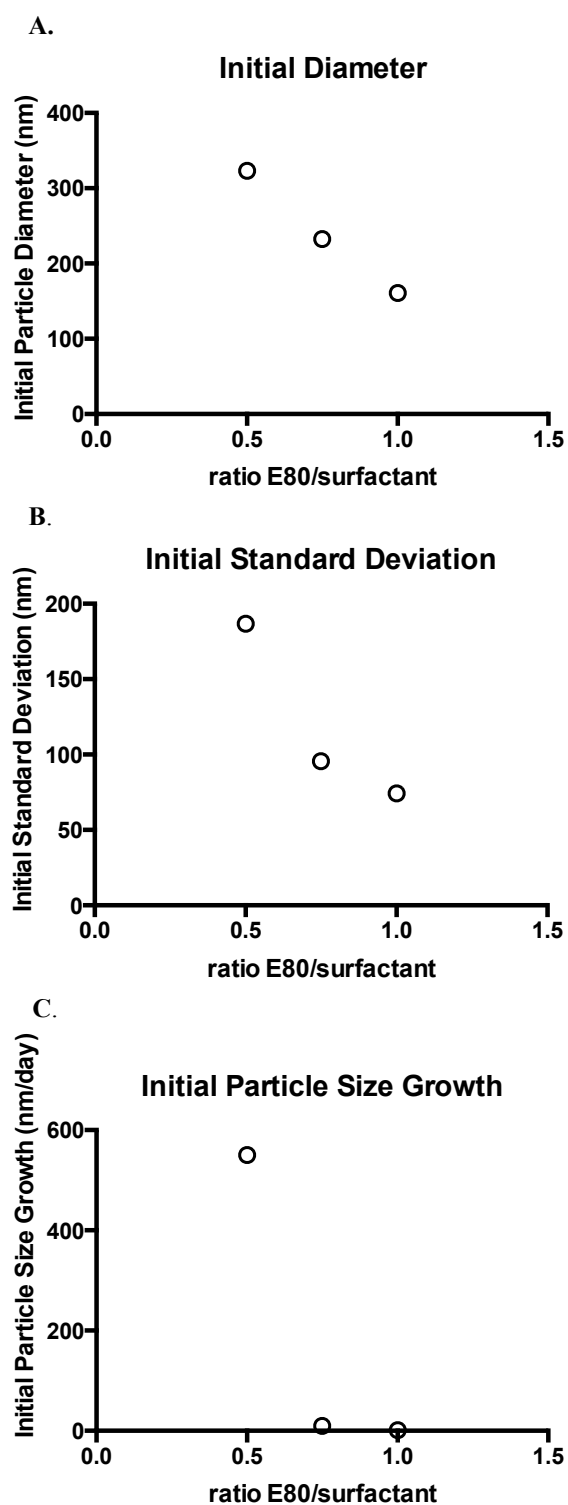


Figure 4.10. Effect of added Lipoid E80 co-surfactant on M1H10-O-F3/propofol emulsion A. initial diameter, B. initial particle size standard deviation, and C. initial particle size growth.

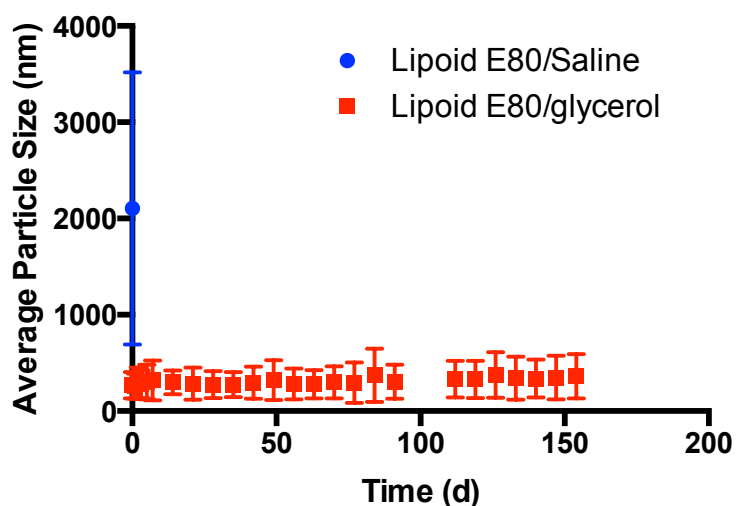


Figure 4.11. Average particle size over time with SD given by error bars ($n = 3$) for Lipoid E80 emulsions.

Concomitantly with the development of the linear/Lipoid E80 formulations, work was carried out with Dr. Aaron McCoy to investigate the potential for using the miktoarm surfactants for emulsifying propofol. It was found that a formulation containing only M1 μ H10F8 surfactant and propofol dispersed in normal saline formed a stable emulsion (B8 formulation, **Figure 4.12**). The surfactant M2 μ H18F8, with a larger lipophilic component, was found to form a more stable emulsion (**Figure 4.12**). Originally, there was concern that the M2 μ H18F8 and M1H10-O-F3/Lipoid E80 formulations were so stable that they might not be effective due to slow propofol release. Therefore, the less-stable M1 μ H10F8-based emulsion was selected for *in vivo* study.

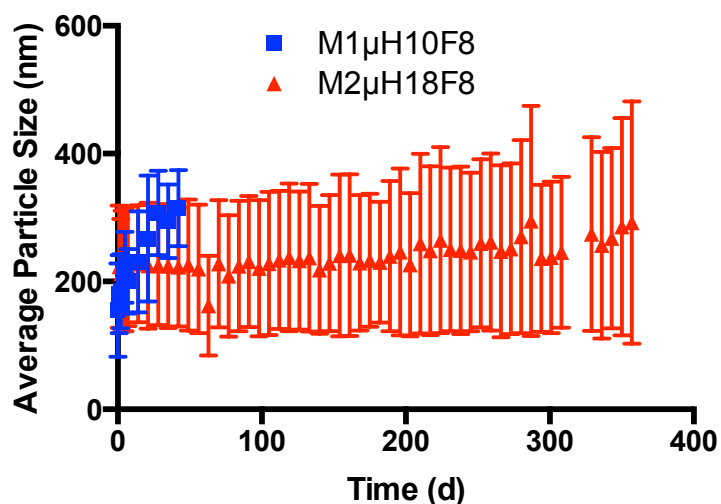


Figure 4.12. Average particle size over time with SD given by error bars ($n = 3$) for miktoarm surfactants M1 μ H10F8 (B8) and M2 μ H18F8.

A third formulation type was devised after testing *in vivo* had already begun. The initial results for L3 and B8 did not show the expected shorter duration of action compared to Diprivan. This third design centered on the unique ability of triphilic surfactants to dissolve both fluorinated and lipophilic agents. M1H10F8 (**Figure 4.4**) was selected as a surfactant and perfluorooctyl bromide (PFOB) included as a stabilizing additive. Conceptually, PFOB would form a fluorinated droplet around which M1H10F8 would absorb. Propofol would then be dissolved in the lipophilic shell surrounding the fluorophilic droplet. The working hypothesis was that propofol would be released quickly because it would exist in a readily accessible shell. Three different amounts of PFOB (5, 10, and 20 vol%) were investigated, **Figure 4.13**. While there was no significant difference in average size, the 20 vol% PFOB formulation had the longest shelf life and was selected for *in vivo* testing and its formulation given the abbreviation F8. In total, four formulations were selected to test against Diprivan, they contain: M1 μ H10F8 (B8), M1H10-O-F3 with Lipoid E80 co-surfactant (L3), M1H10F8 with PFOB (F8), and Lipoid E80 (L80) (**Figure 4.14**).

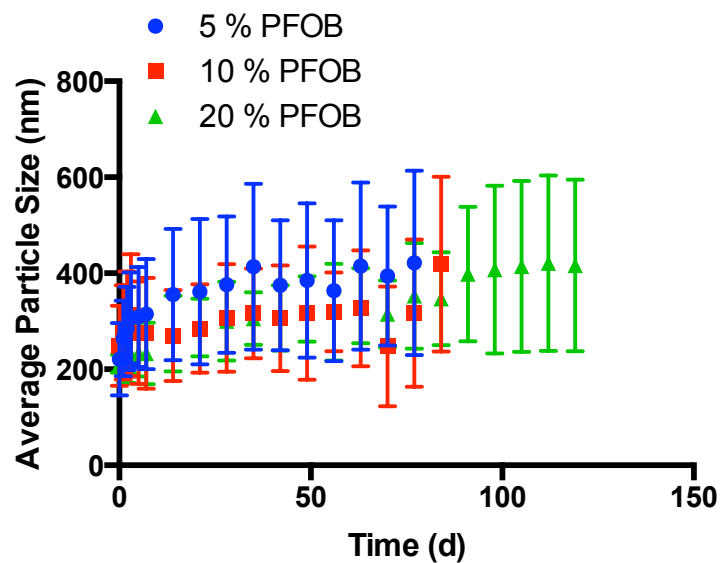


Figure 4.13. Average particle size over time with SD given by error bars ($n = 3$) for the M1H10F8-based propofol emulsions with various concentrations of added perfluorooctyl bromide (PFOB).

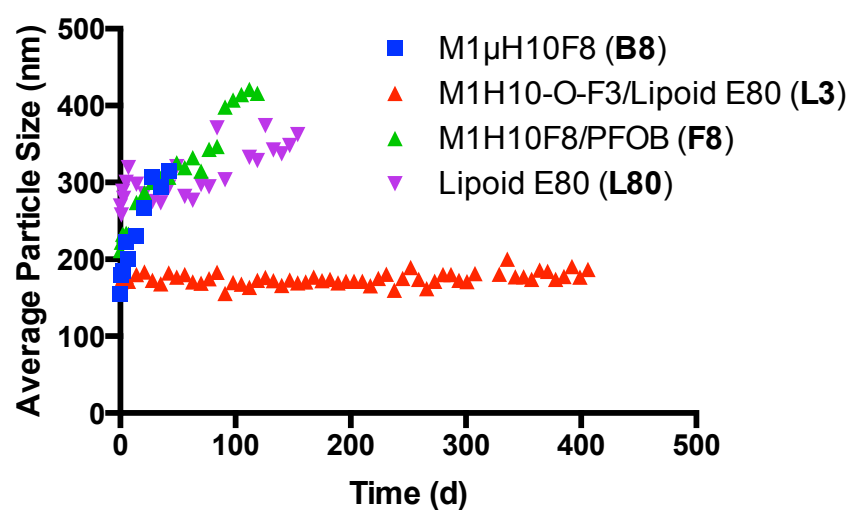


Figure 4.14. Average particle size over time (error bars omitted for clarity) for the four emulsions (B8, L3, F8, L80) tested against Diprivan.

4.2.3 Propofol *in vivo* testing

For all emulsions, five bolus doses were tested: 5, 6.25, 7.5, 10 and 15 mg kg⁻¹. The most startling result from *in vivo* tests was the L80 formulation – containing only propofol and Lipoid

E80 – which did not cause a loss in righting reflex (LORR, a surrogate for unconsciousness) at even the highest dose (15 mg kg^{-1}). The rats did become visibly agitated and attempted to jump out of the observation cage. These results suggest that propofol had very slow release and blood concentration remained just below anesthesia inducing levels.

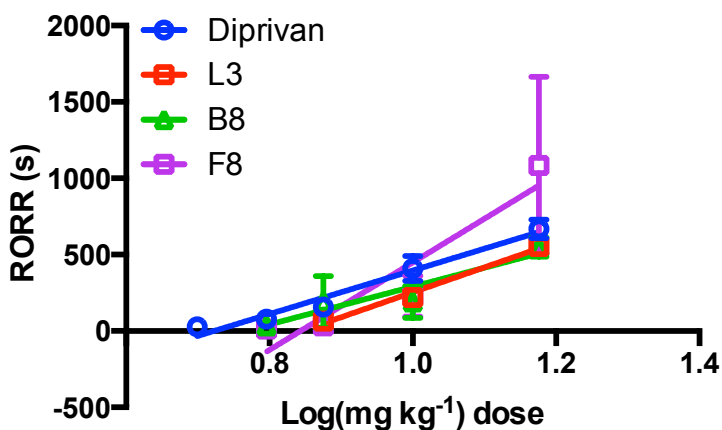


Figure 4.15. Time to recovery of righting reflex (RORR) as a function of drug dose.

Assuming first order kinetics, the drug dose is expressed on a $\log(\text{mg kg}^{-1})$ basis for the propofol content of the emulsions (Diprivan, L3, B8, and F8). The x-axis intersection of the linear regression line is the calculated threshold dose for inducing loss of righting reflex (LORR) as a surrogate for unconsciousness.³⁷

Diprivan, L3, B8, and F8 proved effective in causing LORR. The time until recovery of righting reflex (RORR, a surrogate for resumption of consciousness) was then plotted against the $\log(\text{mg kg}^{-1})$ of the four doses tested (**Figure 4.15**). The threshold doses (x-intercepts) for causing LORR are shown in **Figure 4.15** and listed in **Table 4.1**.

Table 4.1. Threshold dose \pm SEM for each of the three emulsions L3, B8 and F8 and for Diprivan. Dose in mg kg^{-1} is transformed from the x-intercept $\log(\text{mg kg}^{-1})$.

Formulation	Threshold Dose ($\text{mg kg}^{-1} \pm \text{SEM}$)
Diprivan	5.84 ± 1.03
L3	7.17 ± 1.02
B8	6.63 ± 1.06
F8	8.56 ± 1.08

After a Benjamini-Hochberg multiple comparison correction, there was no significant difference between threshold doses of Diprivan and B8, and L3 was not different from B8 or F8.

The other three pairs (Diprivan/L3, Diprivan/F8, B8/F8) were significantly different (P -value < 0.05). These variations may be of little clinical relevance. Notably, F8 proved effective at inducing anesthesia but with prolonged duration at the highest 15 mg kg^{-1} dose. The rats that received 15 mg kg^{-1} of F8 also showed very long recovery to normal behavior after RORR.

Significant differences in the trend-line slopes represent changes in clearance with a lower slope indicating more rapid clearance or decreased bioavailability at the effect site, i.e. a faster recovery of righting reflex for a given dose. Comparisons of the trend-line slopes showed no significant differences. The trend line for F8 was the most different, but it is not significantly different compared to the other three emulsions.

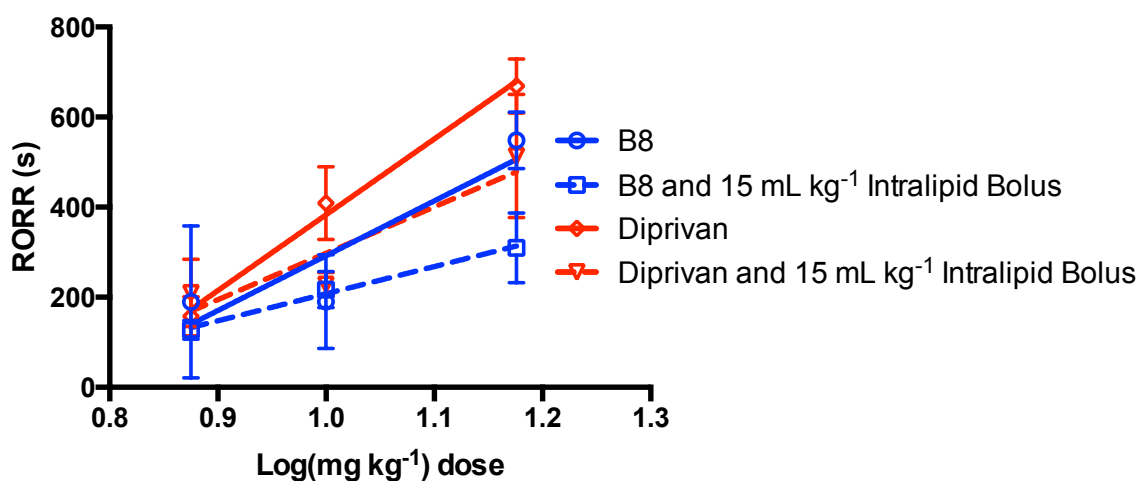


Figure 4.16. Data for Diprivan and B8 with and without lipid bolus.

Data are plotted as a time to recovery of righting reflex (RORR) as a function of drug dose, expressed on a $\log(\text{mg kg}^{-1})$ basis for the propofol component of Diprivan and B8.

Three bolus doses of 7.5, 10, and 15 mg kg^{-1} for Diprivan and B8 were tested for potential lipid reversal. Again, the slope of the trend line was used to represent clearance (**Figure 4.16** and **Table 4.2**). The reduction in slope seen with both Diprivan and B8 after lipid bolus was found significant after a Benjamini-Hochberg multiple comparison correction. As the dose increases, the magnitude of the reduction in duration of anesthesia increases. Little if any reduction was

seen with 7.5 mg kg⁻¹ dose for either formulation. At the 10 mg kg⁻¹ dose no difference was seen for B8 after lipid bolus.

Table 4.2. Slope ± SEM of linear regression lines for Diprivan and B8 emulsion with and without lipid bolus injection.

Formulation	Slope ± SEM	Slope – Lipid ± SEM	P-value	Significant Difference
Diprivan	1602 ± 84	1030 ± 202	0.013	Yes
B8	1250 ± 178	602 ± 94	0.003	Yes

For large doses (15 mg kg⁻¹) of B8 and Diprivan administered in combination with decreasing doses of lipid (15, 7.5, and 3.75 mL kg⁻¹), little if any reduction was seen with the smaller lipid doses compared to 15 mg kg⁻¹ doses without the addition of lipid (**Figure 4.17**).

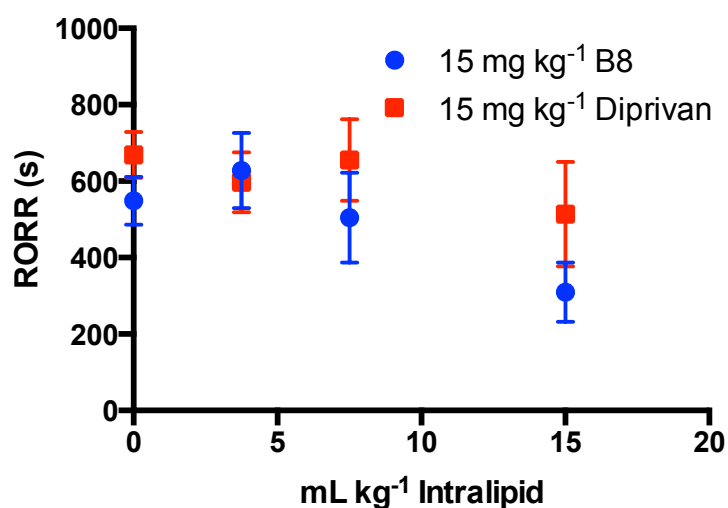


Figure 4.17. Time to return of righting reflex (RORR) v. lipid dose for Diprivan and B8.

The 15 mL kg⁻¹ lipid dose caused a significant reduction in duration of anesthesia for B8 ($p < 0.001$), and approached significance for Diprivan ($P = 0.063$).

These triphile-based emulsions of propofol (L3, B8, and F8) were able to reliably induce anesthesia in rats. There were no ill effects either acutely or after more than 10 administrations over a 2-3 week period. In addition, the threshold doses for the lipid-free emulsions were similar to Diprivan. Although there were some statistically significant differences, these may not be of significance clinically.

Clearance of propofol from its effect site can be accelerated with lipid bolus after an induction dose. This effect was observed even with the lipid-based formulation (Diprivan) but was stronger for the lipid-free formulation B8. The effect was most significant when a high dose of drug (15 mg kg^{-1}) was followed by a high volume of lipid (15 mL kg^{-1}).

Several mechanisms have been proposed for lipid rescue in treating toxicity from bupivacaine (4-5) as well as other drugs. The most commonly cited mechanism proceeds by partitioning: the lipid acts as an intravascular sink, causing decreased concentrations of drug at the effect site. A second proposed mechanism is the accelerated shunting of the drug to its site of metabolism, which is typically the liver for lipid-soluble drugs.^{34,37,38} In either case, there is increased clearance of the drug from the effect site, which in the case of propofol are GABA_A receptors in the central nervous system. We see this in the decreased slope of the linear regression lines when propofol administration is followed by a bolus dose of lipid. Partitioning has been proposed as a mechanism for several lipid soluble drugs (local anesthetics, calcium channel blockers, beta blockers, etc.) whose toxicity has been treated with lipid infusion.^{39,40} Given that propofol is more lipid soluble, log P (octanol:water partition coefficient) 3.79,³⁵ than bupivacaine, log P of 3.41,³⁶ partitioning could be the mechanism that explains the results observed.

It would follow then that a high lipid dose would shorten the duration of anesthesia more than a lower dose, but we saw a lack of effect with the 7.5 and 3.75 mL kg^{-1} doses of lipid. There is some evidence that for bupivacaine toxicity, the lipid bolus works to reverse inhibition of fatty acid metabolism in cardiac muscle.³⁷ It may be possible that the added lipid interferes with propofol binding to the GABA_A receptor, and that there is a threshold concentration required to see this effect, which the 7.5 and 3.75 mL kg^{-1} doses are not large enough to reach.

The 15 mL kg^{-1} dose of lipid that was found to be effective in this study is quite large, and 15 mL kg^{-1} would not be clinically useful in humans if this volume were required to accelerate

recovery from propofol. However, it is possible that lower volumes would be effective in a human as compared to a rat. Induction of anesthesia with propofol in humans typically requires 1-2 mg kg⁻¹, but in rats that dose is 5-10 times greater. A similar reduction in lipid dose to 1.5 - 3 mL kg⁻¹ may be useful clinically.

A limitation in this study is that the observer determining loss and recovery of righting reflex was not blinded to the specific emulsion being tested. The observer was blinded to dose, but due to the differences in visual appearance of the emulsions, it was impractical to be blind to the emulsion. Secondly, the exact time of loss or recovery of righting reflex is inherently difficult to determine. The method used to determine RORR involved the rat spontaneously turning itself from the supine to the prone position. In an attempt to confirm recovery and maintain consistency, the animal was placed on its back and had to right itself two additional times before the time was recorded. This process was slower for some animals when compared to others receiving the same emulsion. Allowing them to spontaneously right themselves also provided opportunity for noises or movement within the experimental area to seemingly startle them awake. A method of regularly stimulating the animal, by toe pinch for example, could have helped to improve consistency of this procedure.

4.3 Conclusions

Linear triphilic surfactants with the proper additives were shown to be effective at stabilizing isoflurane and propofol nanoemulsions. Miktoarm surfactants were also shown to be effective at stabilizing propofol nanoemulsions. While the formulation of isoflurane emulsions remains empirical in nature, two trends have presented themselves as important design criterion for further research: the use of triphilic surfactants is important for the development of stable formulations

and the use of both fluorophilic and lipophilic additives have shown potential to improve emulsion stability.

The use of semi-fluorinated triphilic surfactants for the emulsification of propofol – a lipophilic molecule – represents a novel application. Triphilic surfactants have demonstrated the potential to apply disparate design criteria into one surfactant system for stable nanoemulsion formulation: lipophilic components for solubilization of the lipophilic pharmaceutical and fluorophilic components for stabilization of the colloidal system. To date, propofol has been the only lipophilic drug investigated in such a system but the potential exists for the development of an array of lipophilic-pharmaceutical nanoemulsions.

The three lipid-free, triphilic-surfactant-based formulations of propofol all showed similar efficacy and potency (in producing and maintaining anesthesia with bolus dosing), which was comparable to Diprivan. Additionally, clearance of propofol from its effect site was accelerated with lipid after an induction dose using either lipid-based Diprivan or lipid-free fluoropolymer-based emulsions but more substantially for the lipid-free emulsion. These lipid free formulations have the potential to avoid complications related to microbial growth and hyperlipidemia that are seen with the currently available formulation of propofol, and their effects may to a certain extent be reversible with a lipid infusion.

4.4 Experimental

4.4.1 Materials

Surfactants were all prepared as described previously.⁴¹ Lipoid E80 was purchased from Lipoid GmbH (Ludwigshafen, Germany). Perfluorooctyl bromide (PFOB) was purchased from SynQuest Laboratories Inc. (Alachua, FL). Isoflurane was purchased from Abbott Labs (N. Chicago, IL). Propofol (2,6-diisopropylphenol), glycerol, ethanol, and methanol were purchased

from Sigma Aldrich Co. (Milwaukee, WI). Sterile saline solution was purchased from CareFusion (Yorba Linda, CA). Intralipid was purchased from Baxter Healthcare Corp. (Deerfield, IL).

4.4.2 Surfactant synthesis

To a dry 100 mL flask charged with argon were added 50 mL benzotrifluoride (BTF) and 4.0 mmol HO-H10F8 (synthesized as described in Chapter 3). The mixture was cooled on ice and 5.0 mmol NaH were added. This was allowed to stir for 30 minutes before adding 2.0 mmol mPEG₅₀₀₀-OMs (synthesized as described in Chapter 3). The reaction was then heated to reflux and allowed to react for 7 days. The reaction was cooled, diluted with 100 mL DCM and washed with 150 mL NH₄Cl solution, 50 mL brine and dried over MgSO₄. The organics were then concentrated to a minimum volume under reduced pressure and the surfactants precipitated upon addition of 500 mL cold ether. The solid was collected by vacuum filtration and then purified by reverse-phase chromatography. The product was then freeze dried from 50/50 DCM/Benzene to give a powdery solid. **M5H10F8 (4-8)**: 78% Yield, MALDI: Distribution centered on $[M+Na^+] = 5545.7$, ¹H NMR (400 MHz, CDCl₃): δ 3.83-3.81 (m, 3H), 3.71 – 3.54 (m, 503H), 3.48-3.45 (m, 4H), 3.38 (s, 3H), 2.05 (ttt, $J = 18, 8, 1$ Hz, 2H), 1.63-1.53 (m, 4H), 1.40 – 1.23 (m, 12H). ¹⁹F NMR (376 MHz, CDCl₃): δ -81.14 (3F), -114.77 (2F), -122.24 (6F), -123.12 (2F), -123.92 (2F), -126.51 (2F).

All other surfactants were synthesized as described previously (c.f. Chapter 3).⁴¹

4.4.3 Emulsion preparation

All emulsions were prepared by combining the surfactant and any water-soluble additives (Lipoid E80) in water (with salt or glycerol for isotonicity). The solutions were sonicated until

completely dissolved. Anesthetic (isoflurane or propofol) and any water-insoluble additives (PFOB) were added to the polymer solutions for a total volume of 17 mL. The high-speed homogenizer (Power Gen 500) from Fisher Scientific (Hampton, NH) and the microfluidizer (model 110 S) from Microfluidics Corp. (Newton, MA) were first cleaned with 70% and 100% ethanol, followed by 70% and 100% methanol, and finally with three rinses of Millipore water. Once prepared, each emulsion mixture was then homogenized with the high-speed homogenizer for 1 minute at 21000 rpm at room temperature. The crude emulsion was then microfluidized for 1 minute at 5000 psi with the cooling bath kept at 10 °C. The final emulsion was then filtered with a 30 mm diameter, 0.45 µm nylon filter and stored in 50 mL plastic centrifuge tubes from Corning Inc. (Corning, NY) at 4 °C. After preparation and filtration of the emulsions, the emulsion droplet sizes were measured by dynamic light scattering (NICOMP 380ZLS) from Particle Sizing Systems (Santa Barbara, CA). An aliquot of the emulsion, approximately 150 µL, was diluted in 3 mL of Millipore water to achieve an intensity factor range of 300–350. Each measurement was run for 5 minutes at room temperature and repeated in triplicate. The data were analyzed by Gaussian analysis and reported as a volume-weighted average diameter. The emulsion errors for all polymers were taken as an average of the standard deviations of each individual measurement.

4.4.4 Animal Testing

All animal studies were approved by the University of Wisconsin Animal Care and Use Committee, Madison, Wisconsin, and were performed in accordance with the guidelines laid out in the Guide for the Care and Use of Laboratory Animals published by the National Research Council.

Phase 1 and 2 experiments were carried out in six male Sprague-Dawley rats (Harlan Sprague-Dawley, Inc., Indianapolis, IN) weighing approximately 280 g. The rats were received from the supplier with a surgically implanted jugular catheter. In all cases, the rats received only one dose of anesthetic per day.

In phase 1, experiments to measure loss (LORR) and recovery (RORR) of righting reflex were conducted using five different propofol formulations: 1) Diprivan; 2) L3; 3) B8; 4) F8; 5) L80. Observers were blinded to dose but not the emulsion being tested. For each of the first three formulations, five different doses ($5\text{--}15\text{ mg kg}^{-1}$) were administered five times each. For F8, each of the five doses was administered three times each. For L80, the highest dose (15 mg kg^{-1}) was tested five times. Since this dose did not lead to LORR, a limited number of lower doses were studied, and none led to LORR. Dosing was based on previously published data for propofol in rats.^{42–44}

After weighing the rat and restraining it with a towel the propofol emulsions were administered. The plug placed at the end of the catheter was removed and replaced with a 23-gauge blunt tip needle connected to an insulin-type syringe. To remove the heparin-based fill solution and check that no blockage was obstructing the catheter, the syringe plunger was slowly withdrawn until blood filled the catheter. The 23-gauge blunt tip needle was then removed and the catheter was connected using a 23-gauge connector tip to the tubing and syringe containing the propofol emulsion to be tested. The rat was placed in a transparent cage for observation. The catheter was primed with 40 μL of the emulsion, corresponding to the volume of the catheter, and then the administration of the emulsion was started. The emulsion injection rate was controlled through an infusion pump (11 plus; Harvard Apparatus, Holliston, MA). A bolus dose was delivered over 20 s regardless of the dose. LORR was evaluated by rolling the rat onto its back and observing whether the animal was able to right itself. The times to achieve and to recover

from LORR were recorded. When the rat completely recovered from LORR, the catheter was flushed with 40 μL of 0.9% saline solution to remove the residual emulsion and then refilled with 40 μL of a heparin-based fill solution. The end of the catheter was sealed with a sterile plug.

In phase 2, experiments to measure the effect of a lipid bolus on the anesthetic effects of Diprivan and B8 were conducted. For both, three different doses (7.5, 10, and 15 mg kg^{-1}) were administered five times each. The three doses chosen reliably caused LORR with both emulsions as determined in phase 1. In the same fashion as in phase 1, the rats were restrained and connected to the tubing and syringe containing the propofol emulsion. Procedures for bolus dose administration and determination of loss and recovery of righting reflex were carried out as in phase 1. Sixty seconds after starting the bolus propofol dose, the animals' catheters were connected to tubing and a syringe containing Intralipid (20 wt% lipid emulsion). A bolus of lipid was then administered over 60 seconds. For the highest propofol dose administered, three different lipid bolus doses were administered five times each (3.75, 7.5, and 15 mL kg^{-1}). For the two decreased doses of propofol only the highest dose of lipid was administered. Dosing was based on previously published data utilizing lipid for treatment of drug toxicity in rats.^{34,39,40,45,46}

4.4.5 Statistical Analysis

The x-intercept of the linear regression line for each emulsion was used to represent the threshold dose for causing LORR.⁴⁷ To compare x-intercepts for each emulsion, linear regression lines were fit to the aggregate data sets for the four emulsions. The equation of these linear regression lines was used to calculate x-intercept. Using the standard errors calculated from the coefficient and intercept, statistical significance of the difference in threshold doses was determined using the *t*-test. For all analyses, differences were considered significant at an uncorrected *P*-value of 0.05. Multiple comparison correction was performed using the Benjamini-

Hochberg method. Doses for which the majority of administrations did not cause LORR were excluded from linear regression analysis.

The slope of the linear regression line for each emulsion was used to represent clearance. To compare slopes for each emulsion, a similar method was used with linear regression lines fit to the aggregate data sets for the four emulsions. Using these linear equations, the *t*-test for slope difference with a Benjamini-Hochberg multiple comparison correction was used to compare slopes and determine significant differences in clearance. This method was also used to compare effects of lipid bolus on Diprivan and B8. To evaluate the effect of changing the volume of lipid bolus on duration of anesthesia, a standard *t*-test was used.

4.5 References

- (1) Tucker, W. B.; Mecozzi, S. Nanoemulsions in Medicine. In *Handbook of Nanobiomedical Research, Volume 1*; Torchilin, V. P., Ed.; World Scientific Publishing, 2014; pp 141–167.
- (2) Brösel, S.; Schubert, H. Investigations on the Role of Surfactants in Mechanical Emulsification Using a High-Pressure Homogenizer with an Orifice Valve. *Chem. Eng. Process. Process Intensif.* **1999**, 38 (4-6), 533–540.
- (3) Schulman, J. H.; Stoeckenius, W.; Prince, L. M. Mechanism of Formation and Structure of Microemulsions by Electron Microscopy. *J. Phys. Chem.* **1959**, 63 (10), 1677–1680.
- (4) Adamson, A. W.; Gast, A. P. Emulsions, Foams and Aerosols. In *Physical Chemistry of Surfaces*; John Wiley & Sons, Inc.: New York, New York, 1997; pp 500–536.
- (5) Shah, P.; Bhalodia, D.; Shelat, P. Nanoemulsion: A Pharmaceutical Review. *Syst. Rev. Pharm.* **2010**, 1 (1), 24.
- (6) Fast, J. P.; Perkins, M. G.; Pearce, R. A; Mecozzi, S. Fluoropolymer-Based Emulsions for the Intravenous Delivery of Sevoflurane. *Anesthesiology* **2008**, 109 (4), 651–656.
- (7) Johannesson, G.; Alm, P.; Biber, B.; Lennander, O.; Werner, O. Halothane Dissolved in Fat as an Intravenous Anaesthetic to Rats. *Acta Anaesthesiol. Scand.* **1984**, 28 (4), 381–384.

- (8) Zhou, J. X.; Luo, N. F.; Liang, X. M.; Liu, J. The Efficacy and Safety of Intravenous Emulsified Isoflurane in Rats. *Anesth. Analg.* **2006**, *102* (1), 129–134.
- (9) Parlato, M. C.; Jee, J. P.; Teshite, M.; Mecozzi, S. Synthesis, Characterization, and Applications of Hemifluorinated Dibranching Amphiphiles. *J. Org. Chem.* **2011**, *76* (16), 6584–6591.
- (10) Krahn, C. L.; Raffin, R. P.; Santos, G. S.; Queiroga, L. B.; Cavalcanti, R. L.; Serpa, P.; Dallegrave, E.; Mayorga, P. E.; Pohlmann, A. R.; Natalini, C. C.; Guterres, S. S.; Limberger, R. P. Isoflurane-Loaded Nanoemulsion Prepared by High-Pressure Homogenization: Investigation of Stability and Dose Reduction in General Anesthesia. *J. Biomed. Nanotechnol.* **2012**, *8* (5), 849–858.
- (11) Erdoes, G.; Basciani, R. M.; Eberle, B. Etomidate -- A Review of Robust Evidence for Its Use in Various Clinical Scenarios. *Acta Anaesthesiol. Scand.* **2014**, *58* (4), 380–389.
- (12) Baker, M. T.; Naguib, M. Propofol: The Challenges of Formulation. *Anesthesiology* **2005**, *103* (4), 860–876.
- (13) Park, J. W.; Park, E.-S.; Chi, S.-C.; Kil, H. Y.; Lee, K.-H. The Effect of Lidocaine on the Globule Size Distribution of Propofol Emulsions. *Anesth. Analg.* **2003**, *97* (3), 769–771.
- (14) Han, J.; Davis, S. S.; Washington, C. Physical Properties and Stability of Two Emulsion Formulations of Propofol. *Int. J. Pharm.* **2001**, *215* (1-2), 207–220.
- (15) Bennett, S. N.; McNeil, M. M.; Bland, L. A.; Arduino, M. J.; Villarino, M. E.; Perrotta, D. M.; Burwen, D. R.; Welbel, S. F.; Pegues, D. A.; Stroud, L. Postoperative Infections Traced to Contamination of an Intravenous Anesthetic, Propofol. *N. Engl. J. Med.* **1995**, *333* (3), 147–154.
- (16) Wachowski, I.; Jolly, D. T.; Hrazdil, J.; Galbraith, J. C.; Greacen, M.; Clanachan, A. S. The Growth of Microorganisms in Propofol and Mixtures of Propofol and Lidocaine. *Anesth. Analg.* **1999**, *88* (1), 209–212.
- (17) Langevin, P. B.; Gravenstein, N.; Doyle, T. J.; Roberts, S. A.; Skinner, S.; Langevin, S. O.; Gulig, P. A. Growth of *Staphylococcus aureus* in Diprivan and Intralipid: Implications on the Pathogenesis of Infections. *Anesthesiology* **1999**, *91* (5), 1394–1400.
- (18) Wolf, A.; Weir, P.; Segar, P.; Stone, J. Impaired Fatty Acid Oxidation in Propofol Infusion Syndrome Relation between Occurrence of Type 1 Diabetes and Asthma. *Lancet* **2001**, *357*, 606–607.
- (19) Wong, J. M. Propofol Infusion Syndrome. *Am. J. Ther.* **2010**, *17* (5), 487–491.

- (20) Mayette, M.; Gonda, J.; Hsu, J. L.; Mihm, F. G. Propofol Infusion Syndrome Resuscitation with Extracorporeal Life Support: A Case Report and Review of the Literature. *Ann. Intensive Care* **2013**, *3* (1), 32.
- (21) Rosen, D. J.; Nicoara, A.; Koshy, N.; Wedderburn, R. V. Too Much of a Good Thing? Tracing the History of the Propofol Infusion Syndrome. *J. Trauma-Injury Infect. Crit. Care* **2007**, *63* (2), 443–447.
- (22) Tan, C. H.; Onsiong, M. K. Pain on Injection of Propofol. *Anaesthesia* **1998**, *53* (5), 468–476.
- (23) Damitz, R.; Chauhan, A. Rapid Dissolution of Propofol Emulsions under Sink Conditions. *Int. J. Pharm.* **2015**, *481* (1-2), 47–55.
- (24) Dubey, P. K.; Kumar, A. Pain on Injection of Lipid-Free Propofol and Propofol Emulsion Containing Medium-Chain Triglyceride: A Comparative Study. *Anesth. Analg.* **2005**, *101* (4), 1060–1062.
- (25) Ohmizo, H.; Obara, S.; Iwama, H. Mechanism of Injection Pain with Long and Long-Medium Chain Triglyceride Emulsive Propofol. *Can. J. Anaesth.* **2005**, *52* (6), 595–599.
- (26) Song, D.; Hamza, M.; White, P. F.; Klein, K.; Recart, A.; Khodaparast, O. The Pharmacodynamic Effects of a Lower-Lipid Emulsion of Propofol: A Comparison with the Standard Propofol Emulsion. *Anesth. Analg.* **2004**, *98* (3), 687–691, table of contents.
- (27) Rau, J.; Roizen, M. F.; Doenicke, A. W.; O'Connor, M. F.; Strohschneider, U. Propofol in an Emulsion of Long- and Medium-Chain Triglycerides: The Effect on Pain. *Anesth. Analg.* **2001**, *93* (2), 382–384, 3rd contents page.
- (28) Egan, T. D.; Kern, S. E.; Johnson, K. B.; Pace, N. L. The Pharmacokinetics and Pharmacodynamics of Propofol in a Modified Cyclodextrin Formulation (Captisol) versus Propofol in a Lipid Formulation (Diprivan): An Electroencephalographic and Hemodynamic Study in a Porcine Model. *Anesth. Analg.* **2003**, *97* (1), 72–79, table of contents.
- (29) Cai, W.; Deng, W.; Yang, H.; Chen, X.; Jin, F. A Propofol Microemulsion with Low Free Propofol in the Aqueous Phase: Formulation, Physicochemical Characterization, Stability and Pharmacokinetics. *Int. J. Pharm.* **2012**, *436* (1-2), 536–544.
- (30) Damitz, R.; Chauhan, A. Kinetically Stable Propofol Emulsions with Reduced Free Drug Concentration for Intravenous Delivery. *Int. J. Pharm.* **2015**, *486* (1-2), 232–241.
- (31) Jung, J. A.; Choi, B. M.; Cho, S. H.; Choe, S. M.; Ghim, J. L.; Lee, H. M.; Roh, Y. J.; Noh, G. J. Effectiveness, Safety, and Pharmacokinetic and Pharmacodynamic Characteristics of Microemulsion Propofol in Patients Undergoing Elective Surgery under Total Intravenous Anaesthesia. *Br. J. Anaesth.* **2010**, *104* (5), 563–576.

- (32) Sim, J. Y.; Lee, S. H.; Park, D. Y.; Jung, J. A.; Ki, K. H.; Lee, D. H.; Noh, G. J. Pain on Injection with Microemulsion Propofol. *Br. J. Clin. Pharmacol.* **2009**, *67* (3), 316–325.
- (33) Lee, E.-H.; Lee, S.-H.; Park, D.-Y.; Ki, K.-H.; Lee, E.-K.; Lee, D.-H.; Noh, G.-J. Physicochemical Properties, Pharmacokinetics, and Pharmacodynamics of a Reformulated Microemulsion Propofol in Rats. *Anesthesiology* **2008**, *109* (3), 436–447.
- (34) Weinberg, G. L.; VadeBoncouer, T.; Ramaraju, G. A.; Garcia-Amaro, M. F.; Cwik, M. J. Pretreatment or Resuscitation with a Lipid Infusion Shifts the Dose-Response to Bupivacaine-Induced Asystole in Rats. *Anesthesiology* **1998**, *88* (4), 1071–1075.
- (35) Babu, M. K. M.; Godiwala, T. N. Toward the Development of an Injectable Dosage Form of Propofol: Preparation and Evaluation of Propofol-Sulfobutyl Ether 7- β -Cyclodextrin Complex. *Pharm. Dev. Technol.* **2004**, *9* (3), 265–275.
- (36) Hansch, C.; Albert, L.; Hoekman, D. H. *Exploring QSAR: Hydrophobic, Electronic, and Steric Constants*; American Chemical Society: Washington, DC, 1995.
- (37) Weinberg, G. L. Lipid Emulsion Infusion. *Anesthesiology* **2012**, *117* (1), 180–187.
- (38) Weinberg, G.; Ripper, R.; Feinstein, D. L.; Hoffman, W. Lipid Emulsion Infusion Rescues Dogs from Bupivacaine-Induced Cardiac Toxicity. *Reg. Anesth. Pain Med.* **2003**, *28* (3), 198–202.
- (39) Jamaty, C.; Bailey, B.; Larocque, A.; Notebaert, E.; Sanogo, K.; Chauny, J.-M. Lipid Emulsions in the Treatment of Acute Poisoning: A Systematic Review of Human and Animal Studies. *Clin. Toxicol.* **2010**, *48* (1), 1–27.
- (40) Perez, E.; Bania, T. C.; Medlej, K.; Chu, J. Determining the Optimal Dose of Intravenous Fat Emulsion for the Treatment of Severe Verapamil Toxicity in a Rodent Model. *Acad. Emerg. Med.* **2008**, *15* (12), 1284–1289.
- (41) Tucker, W. B.; McCoy, A. M.; Fix, S. M.; Stagg, M. F.; Murphy, M. M.; Mecozzi, S. Synthesis, Physicochemical Characterization, and Self-Assembly of Linear, Dibranched, and Miktoarm Semifluorinated Triphilic Polymers. *J. Polym. Sci. Part A Polym. Chem.* **2014**, *52* (23), 3324–3336.
- (42) Adam, H. K.; Glen, J. B.; Hoyle, P. A. Pharmacokinetics in Laboratory Animals of ICI 35 868, A New I.V. Anaesthetic Agent. *Br. J. Anaesth.* **1980**, *52* (8), 743–746.
- (43) Glen, J. B.; Hunter, S. C. Pharmacology of an Emulsion Formulation of ICI 35 868. *Br. J. Anaesth.* **1984**, *56* (6), 617–626.
- (44) Brammer, a; West, C. D.; Allen, S. L. A Comparison of Propofol with Other Injectable Anaesthetics in a Rat Model for Measuring Cardiovascular Parameters. *Lab. Anim.* **1993**, *27* (3), 250–257.

- (45) Hiller, D. B.; Di Gregorio, G.; Kelly, K.; Ripper, R.; Edelman, L.; Boumendjel, R.; Drasner, K.; Weinberg, G. L. Safety of High Volume Lipid Emulsion Infusion: A First Approximation of LD₅₀ in Rats. *Reg. Anesth. Pain Med.* **35** (2), 140–144.
- (46) Di Gregorio, G.; Schwartz, D.; Ripper, R.; Kelly, K.; Feinstein, D. L.; Minshall, R. D.; Massad, M.; Ori, C.; Weinberg, G. L. Lipid Emulsion Is Superior to Vasopressin in a Rodent Model of Resuscitation from Toxin-Induced Cardiac Arrest. *Crit. Care Med.* **2009**, *37* (3), 993–999.
- (47) Liao, M.; Sonner, J. M.; Husain, S. S.; Miller, K. W.; Jurd, R.; Rudolph, U.; Eger, E. I. R (+) Etomidate and the Photoactivable R (+) Azetomidate Have Comparable Anesthetic Activity in Wild-Type Mice and Comparably Decreased Activity in Mice with a N265M Point Mutation in the Gamma-Aminobutyric Acid Receptor $\beta 3$ Subunit. *Anesth. Analg.* **2005**, *101* (1), 131–135.

Appendix 1:

**Redesigned triphilic surfactants for hydrophobic pharmaceutical
nanoemulsions**

Abstract

The use of nanoemulsions for lipophilic pharmaceuticals has been of interest for their very high drug loading, compared even to other colloidal delivery systems like micelles. Triphilic surfactants with an overall hydrophilic-lipophilic-fluorophilic design were found to be effective at emulsifying propofol, a lipophilic anesthetic, for intravenous (IV) delivery. This design was found effective for propofol, where the desired outcome was the fast release of propofol for rapid induction of anesthesia. For the delivery of other hydrophobic drugs, however, a slow and sustained release is desired. As such, a redesign of the triphilic surfactant to a hydrophilic-fluorophilic-lipophilic architecture was devised. The lipophilic tail would stabilize the oily nanodroplet while the fluorophilic shell would provide a barrier to release of the pharmaceutical drug, thus decreasing the release rate of the drug. A successful synthetic methodology was devised for this revised triphilic surfactant, and a test 5.8 mg mL⁻¹ paclitaxel emulsions was prepared, which was found to be stable for two weeks. Ongoing research is dedicated to optimizing the surfactant design to improve shelf stability of this formulation.

A1.1 Introduction

An estimated 40% of currently marketed pharmaceuticals, and 70% of those under development, are poorly water-soluble species.¹ Nanoemulsions, in contrast to micelles, offer the potential to solubilize very high concentrations of drug in aqueous media.² This potential has sparked numerous investigations into preparing oil-in-water nanoemulsion for the solubilization and delivery of hydrophobic pharmaceuticals.³

Nanoemulsions are small enough that Brownian motion inhibits creaming/sedimentation and flocculation.⁴ Coalescence of droplets can be inhibited through design of the surfactant(s) used.⁵ This leaves Ostwald ripening (the diffusion of the oil phase from smaller droplets to larger droplets) as the main mechanism by which nanoemulsions are destabilized. Triphilic surfactants have already been demonstrated to very effectively stabilize anesthetic nanoemulsions for prolonged shelf life (Chapter 4). Triphilic surfactants have here been considered for their potential to stably emulsify chemotherapeutics for IV drug delivery, with a redesign from work presented in Chapter 4.

Previous studies on anesthetic emulsions in the Mecozzi laboratory have focused on the formulation of shelf-stable nanoemulsion formulations. Once an anesthetic nanoemulsion is injected, its rapid release of encapsulated cargo is required to ensure a rapid loss of consciousness/induction of anesthesia. For a non-anesthetic, hydrophobic pharmaceutical emulsion, however, rapid release is not only undesired, but bolus release of drug could also be very detrimental to the patient.¹ To try and optimize the triphilic surfactant system for IV delivery of chemotherapeutics, the structure chosen for investigation inverts those studied to date (hydrophilic-lipophilic-fluorophilic) to a hydrophilic-fluorophilic-lipophilic structure.

Our hypothesis is that a hydrophilic-fluorophilic-lipophilic design will form a unique emulsion structure (**Figure A1.1**). First, the lipophilic tail will penetrate and stabilize the

emulsion droplet. The intermediate fluorophilic moiety is then set up to form a fluorophilic shell, which will inhibit diffusion out of the droplet (given the immiscibility of lipophilic and fluorophilic species). Finally the hydrophilic head group will solubilize the droplet and prevent coalescence.

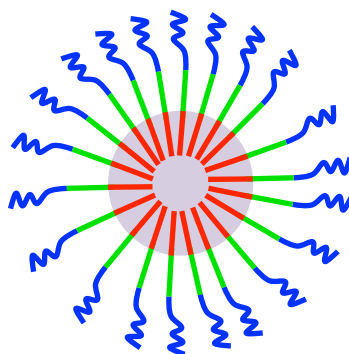


Figure A1.1. Hypothesized structure of redesigned triphilic surfactant emulsion.

The oil droplet (grey circle) will be stabilized by penetration of the lipophilic (red) tails of the surfactant. The intermediate fluorocarbon (green) linker will then form a fluorophilic shell that will prevent diffusion out of the droplet and the entire complex will be made water-soluble by the hydrophilic (blue) head group.

The synthesis of a hydrophilic-lipophilic-fluorophilic surfactant was designed and the surfactant M2F8-O-H18 synthesized and characterized. A paclitaxel emulsion has been prepared utilizing this surfactant, which was stable for 14 days. Ongoing work is looking into optimizing the surfactant design, finding appropriate additives to stabilize the droplet, and devising an appropriate *in vitro* system to quantify emulsion stability and the drug-release rate.

A1.2 Results and Discussion

A1.2.1 Redesigned triphilic synthesis and characterization

The synthesis of M2F8-O-H18 (**Figure A1.2**) was based on previous work to synthesize MxF10DSPE, $x = 2, 5$,⁶ and other triphilic surfactants.⁷ First, 1H,1H,10H,10H-decan-1,10-diol was mono-protected with benzyl bromide in a KOH/DMF solution. The resulting mono-benzylated product (**A1-2**) was alkylated by Williamson ether synthesis with octadecan-1-OMs.

Hydrogenation removed the benzyl-protecting group and the resulting HO-F8-O-H18 alcohol was coupled to mPEG₂₀₀₀-OMs. The HO-F8-O-H18 tail is significantly longer than other linear surfactants studied; as such the larger mPEG₂₀₀₀ was chosen (instead of the smaller mPEG₁₀₀₀ used in other linear triphiles) to ensure high water solubility. In addition, this would allow for comparison of physicochemical properties to the previously synthesized M2 μ H18F8 miktoarm surfactant.

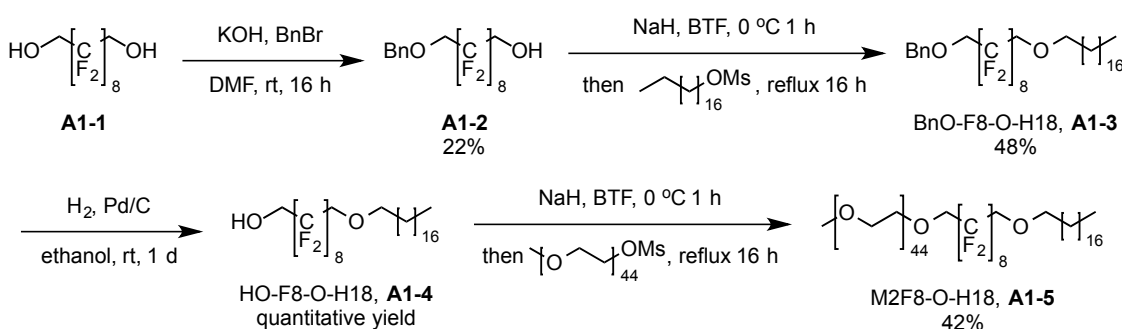


Figure A1.2. Synthesis of M2F8-O-H18.

When dissolved in water, M2F8-O-H18 surfactant was found to form micelles with a mean diameter of 16.3 ± 4.1 nm, which is not significantly different than M2 μ H18F8 (11.5 ± 1.5 nm). The critical micelle concentration CMC for M2F8-O-H18 was found to be 5.31 ± 0.09 (-log(M)), which is significantly lower ($P = 0.0006$) than that for M2 μ H18F8. Together, these data reinforce what was observed in Chapter 3: the relative lack of difference that changes in fluorocarbon placement can have on aggregate size, but the substantial difference the placement of fluorocarbons can have on pCMC.

A1.2.2 Paclitaxel emulsion formulation

Paclitaxel (**Figure A1.3**) was selected as the lipophilic chemotherapeutic to investigate the potential of M2F8-O-H18 to form a stable emulsion. To form an emulsion the lipophilic

component must be a liquid, but paclitaxel is a solid. Soybean oil was chosen as the first oil additive because of its ubiquitous use in nanoemulsion formulations. Paclitaxel was found not to be soluble in soybean oil (at room or elevated temperatures) at any useful concentration. A literature search of other nanoemulsion formulations found that 2-octyldodecan-1-ol (**Figure A1.3**) has been used as an oil additive in previous nanoemulsion formulations.^{8,9} While paclitaxel was also found to be poorly soluble in 2-octyldodecan-1-ol at room temperature, paclitaxel readily dissolved at useful concentrations at high temperatures.

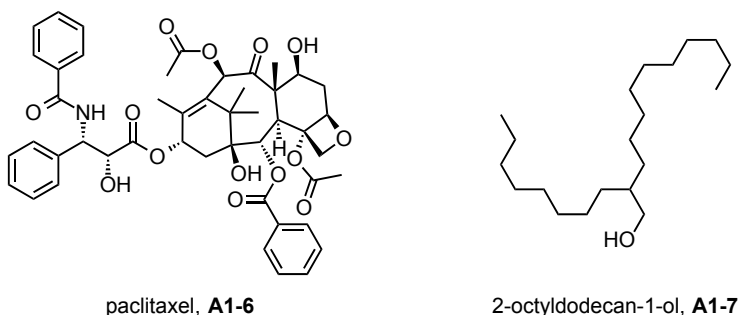


Figure A1.3. Structure of paclitaxel (PTX) and 2-octyldodecan-1-ol.

To prepare a paclitaxel emulsion, 100 mg of paclitaxel were dissolved in 3 mL of hot 2-octyldodecan-1-ol. The resulting solution was diluted with 10 mL of room temperature ether. The resulting mixture remained homogenous even at room temperature. Ether was chosen because it could be removed *in vacuo* after emulsification. The removal of ether under vacuum should also help to reduce the average particle size and increase the stability of the emulsion – a process known as the evaporative ripening method.¹⁰ The paclitaxel mixture was then added to the M2F8-O-H18 in saline solution and the emulsion prepared by high-speed homogenization followed by microfluidization. Ether was then removed under vacuum and the emulsion filtered with a 0.45 mm nylon filter.

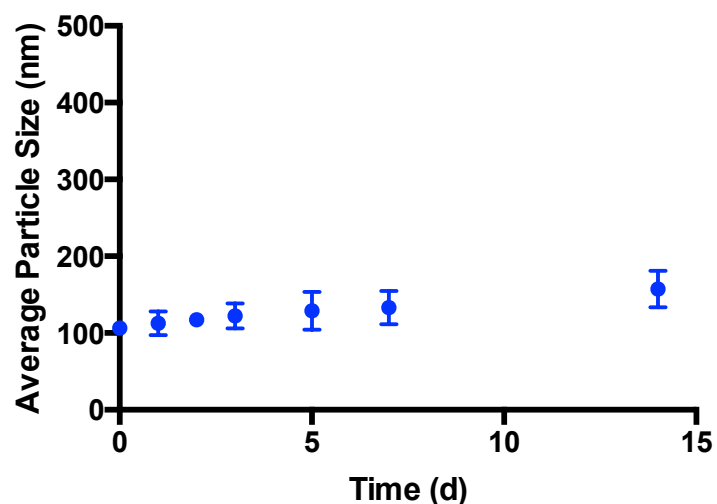


Figure A1.4. Average particle size over time with SD given by error bars ($n = 3$) for 100 mg PTX emulsion with M2F8-O-H18 as the surfactant and 2-octyl-dodecan-1-ol additive.

Particle size measurements of the emulsion over time (**Figure A1.4**) showed an emulsion with small average particle size and very small standard deviations, a possible result of the evaporative ripening method preparation. Over the course of two weeks, little change in particle size was observed and the emulsion seemed stable. Before measuring the particle size on day 21, however, small crystalline precipitate was observed on the bottom of the container, which demonstrated a loss of emulsion integrity. Nonetheless, these data are good for a first attempt and suggest that this revised triphilic emulsion design will work as hypothesized.

A1.3 Conclusions

A synthesis for the preparation of hydrophilic-fluorophilic-lipophilic-type triphilic surfactants has been devised. The methodology is modular and so allows for the variation of hydrophilic, fluorophilic and lipophilic sizes. Furthermore, these surfactants represent a new class of surfactants for the Mecozzi group, which are worth studying further to elucidate relationships between structure and function.

The redesigned triphilic surfactant M2F8-O-H18 was designed for its potential to emulsify lipophilic pharmaceuticals for IV drug delivery. To emulsify chemotherapeutics, however, there is an additional hurdle to overcome: most chemotherapy drugs are solids. Thus to emulsify a drug like paclitaxel, an appropriate oil additive had to be chosen, in which to dissolve paclitaxel. Here 2-octyldodecan-1-ol (**A1-7**) was chosen. While a stable emulsion could be prepared, part of its long-term instability might have arisen from the relatively low solubility of paclitaxel in 2-octyldodecan-1-ol. Therefore, a more appropriate oil additive (a number of nut and seed oils have been used in the literature)¹¹ should be investigated to find one in which paclitaxel is more soluble.

Emulsion stability for this type of triphilic surfactant design might also be improved by two other methods. The first would be to use perfluorooctyl bromide (PFOB) as a co-additive for the emulsion. PFOB would absorb in the fluorophilic shell and potentially help to further impede diffusion out of the lipophilic droplet. The second method would be to further modify the surfactant structure (**Figure A1.5**). To help ensure that a fluorophilic shell is indeed formed over the surface of the oil droplet, a second fluorophilic substituent could be added off from the main surfactant chain using established methodologies for preparing miktoarm-type surfactants.^{7,12} This additional arm could serve to increase the impenetrability of the fluorophilic shell to slow drug diffusion/release and increase shelf life.

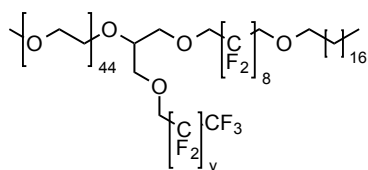


Figure A1.5. Structure of modified M2F8-O-H18 with pendent fluorophilic substituent (y = 2-5).

A1.4 Experimental

A1.4.1 Materials

All fluorinated compounds were obtained from SynQuest Laboratories, Inc. (Alachua, FL, USA). Paclitaxel was purchased from LC Laboratories (Woburn, MA, USA). All solvents were of ACS grade or higher and were purchased from Sigma-Aldrich (St. Louis, MO, USA). All other reagents were purchased from Sigma-Aldrich (St. Louis, MO, USA) and were used as received, unless otherwise specified. Chromatographic separations were performed using Silicycle 60 Å SiO₂. M2F8-O-H18 was purified by automated flash chromatography using a CombiFlash® Rf 4x system (Teledyne Isco, Lincoln, NE, USA) equipped with ELSD for compound visualization and a REDI-Sep Rf Gold C-18 silica high performance aqueous reverse phase cartridge. Products were eluted with a 10% to 100% MeOH in water (0.1% formic acid) gradient. ¹H- and ¹⁹F-NMR spectra were obtained on Varian Unity-Inova 400 and Unity-Inova 500 spectrometers using deuteriochloroform (CDCl₃) as the solvent with TMS as an internal reference.

A1.4.2 M2F8-O-H18 synthesis

Octadecan-1-OMs: Octadecanol 2.0 g (7 mmol) was dissolved in anhydrous DCM (25 ml) and flask flushed with Ar. TEA (2.3 mL, 17 mmol) was added to solution and flask cooled in ice bath before adding 0.7 mL dropwise by syringe. The reaction then stirred under Ar overnight, allowing the ice bath to warm to room temperature. Reaction was then stopped and washed with 3, 50 mL aliquots of aqueous NH₄Cl, dried over MgSO₄ and condensed under reduced pressure to give 2.6 g octadecyl methane sulfonate (quantitative). Octadecyl methane sulfonate: ¹H NMR (400 MHz, CDCl₃): δ 4.16 (t, *J* = 6.4 Hz, 2H), 2.95 (s, 3H), 1.69 (p, *J* = 6.8 Hz, 2H), 1.37-1.12 (m, 30H), 0.83 (t, *J* = 6.8 Hz, 3H).

A1-2: To a 100 mL roundbottom flask were added 50 mL DMF, 5 g (11 mmol) 1H,1H,10H,10H-perfluorodecan-1,10-diol, and 607 mg (11 mmol) crushed KOH. This was allowed to stir for 30 minutes before 0.43 mL (3.6 mmol) benzyl bromide was added and the reaction left to run overnight. The mixture was then diluted with 100 mL ether and washed with 100 mL 10% sulfuric acid solution. The organics were then dried over MgSO₄ and concentrated *in vacuo* to give a white semi-solid. The product was purified by column chromatography (20% ethyl acetate in hexanes) to give 1.35 g (22% yield) of white solid product. **A1-2:** ¹H NMR (400 MHz, CDCl₃): δ 7.40 – 7.26 (m, 5H), 4.68 (s, 2H), 4.10 (td, *J* = 14, 7.6 Hz, 2H), 3.94 (t, *J* = 14 Hz, 2H), 2.01 (t, *J* = 7.6 Hz, 1H). ¹⁹F NMR (376 MHz, CDCl₃): δ -119.75 (2F), -122.34 (8F), -122.81 (2F), -123.65 (2F), -123.97 (2F).

BnOF8-O-H18 (A1-3): To a 100 mL oven-dried roundbottom, under argon, were added 50 mL of BTF and 90 mg (3.6 mmol) of NaH. The suspension was cooled to 0 °C and 1.35 g (2.4 mmol) of **A1-2** were added. This was allowed to stir for 1 hour before adding 1.7 g (4.8 mmol) of octadecan-1-OMs (as a solution in 5 mL of anhydrous BTF). This was then warmed slowly to reflux and allowed to react for 24 hours. The reaction was then allowed to cool and diluted with 100 mL of DCM. This was washed with 3, 50 mL aliquots of saturated NH₄Cl solution and dried over MgSO₄ and condensed under reduced pressure to give a yellow solid. The product was then purified by column chromatography (12% ethyl acetate in hexanes) to give 923 mg (48% yield) of product as a white solid. **BnOF8-O-H18 (A1-3):** ¹H NMR (400 MHz, CDCl₃): δ 7.38 – 7.26 (m, 5H), 4.68 (s, 2H), 3.92 (q, *J* = 12.3 Hz, 4H), 3.59 (t, *J* = 6.6 Hz, 2H), 1.60 (pseudo-pentet, *J* = 1.5 Hz, 2H), 1.38 – 1.18 (m, 34H), 0.88 (t, *J* = 6.3 Hz). ¹⁹F NMR (376 MHz, CDCl₃): δ -119.76 (2F), -120.04 (2F), -122.35 (8F), -123.71 (2F), -123.88 (2F).

HOF8-O-H18 (A1-4): To a 250 mL oven-dried roundbottom were added 50 mL ethanol and 923 mg (1.1 mmol) **A1-3**. The flask was flushed with argon for 40 minutes before adding 75 mg, 10 wt% Pd/C and then flushed with argon for 40 minutes longer. The flask was then flushed with hydrogen and left under a hydrogen atmosphere for 24 hours. The flask was then flushed with argon for 1 hour before being opened to the air, diluted with 100 mL DCM, and filtered through celite. The solvent was then removed *in vacuo* to give a white solid (pure by NMR). **HOF8-O-H18 (A1-4):** ^1H NMR (400 MHz, CDCl_3): δ 4.10 (td, $J = 14, 7.6$ Hz, 2H), 3.59 (t, $J = 14$ Hz, 2H), 1.99 (t, $J = 7.6$ Hz, 1H), 1.60 (pseudo-pentet, $J = 1.5$ Hz, 2H), 1.38 – 1.18 (m, 34H), 0.88 (t, $J = 6.3$ Hz). ^{19}F NMR (376 MHz, CDCl_3): δ -120.04 (2F), -122.37 (8F), -122.84 (2F), -123.95 (4F).

M2F8-O-H18 (A1-5): To a dry 100 mL flask charged with argon were added 40 mL benzonitrile (BTF) and 784 mg (1.1 mmol) HO-F8-O-H18. The mixture was cooled on ice and 60 mg (2.2 mmol) NaH were added. This was allowed to stir for 30 minutes before adding 1.3 g (0.6 mmol) mPEG-OMs. The reaction was then heated to reflux and allowed to react for 5 days. The reaction was cooled, diluted with 200 mL DCM and washed with 100 mL NH_4Cl solution, 50 mL brine and dried over MgSO_4 . The organics were then concentrated to a minimum volume under reduced pressure and the surfactants precipitated upon addition of 500 mL cold ether. The solid was collected by centrifugation and vacuum filtration and then purified by reverse-phase chromatography. The product was then freeze dried from 50/50 DCM/Benzene to give a powdery solid. **M2F8-O-H18 (A1-5):** 42% Yield, MALDI: Distribution centered on $[\text{M}+\text{Na}^+] = 2468.7$, ^1H NMR (400 MHz, CDCl_3): δ 4.04 (t, $J = 13.9$, 2H), 3.92 (t, $J = 13.9$, 2H), 3.82 - 3.47 (m, 156H), 3.61 – 3.54 (m, 9H), 3.38 (s, 3H), 1.60 (pseudo-pentet, 2H), 1.38 – 1.18

(m, 32H), 0.88 (t, $J = 6.3$ Hz). ^{19}F NMR (376 MHz, CDCl_3): δ -120.05 (2F), -120.21 (2F), -122.38 (8F), -123.88 (4F).

A1.4.3 M2F8-O-H18 characterization

Particle size determination by dynamic light scattering (DLS). Micelles were prepared by solvent evaporation, polymer solution concentration 1 mg mL^{-1} in MeOH. Particle sizes of polymeric aggregates were analyzed by dynamic light scattering (Malvern Zetasizer Nano ZS, Malvern Instruments Ltd., Westborough, MA). The surfactant solution was measured directly without dilution and analyzed. Each particle size analysis was run at room temperature and repeated in triplicate with the number of scans of each run determined automatically by the instrument according to the concentration of the solution. The data was analyzed using NICOMP analysis and reported as volume weighted average diameters.

Critical micelle concentration (CMC) determination – Surface Tensiometry. Surfactant was dissolved in Millipore water to a concentration of 1 mM and concentrations down to 1 nM were prepared by serial dilution and transferred to 20 mL disposable scintillation vials. After solutions were made, the samples were heated in a water bath at 40°C with sonication for 2-3 hours and allowed to equilibrate for 24 hours. Surface tensions were measured on a KSV sigma 701 tensiometer (KSV Instruments, Helsinki, Finland) equipped with a Julabo F12-MC circulator for constant temperature control. Custom round rod made of platinum with a diameter of 1.034 mm with wetted length of 3.248 mm was used. The rod was submerged in absolute alcohol and flame dried with a Bunsen burner for 4 seconds. This was repeated after 4 minutes. The rod was then hung on the instrument and allowed to cool to room temperature without touching any surface. Before running the experimental samples, the surface tension of millipore water was measured as

a control to confirm the rod was fully cleaned and surface tension was within 1 mN/m of 78.2 mN/m. The surface tension measurements began with the least concentrated solution and proceeded to successively more concentrated solutions. The surface tension at each concentration was measured in quadruplet and average recorded. The critical micelle concentration value was determined from the crossover point of two lines: the baseline of minimal surface tension and the slope where surface tension showed linear decline; error determined by weighted least squares analysis.

A1.4.4 Emulsion preparation

401 mg of M2F8-O-H18 were added to 14 mL normal saline and thoroughly dissolved by sonication. 100 mg paclitaxel (**A1-6**) were dissolved in 3 mL hot 2-octyldodecan-1-ol (**A1-7**) and diluted with 10 mL ether to make a stable suspension. The oil and aqueous phases were mixed together by high-speed homogenization and microfluidization. The high-speed homogenizer (Power Gen 500) from Fisher Scientific (Hampton, NH) and the microfluidizer (model 110 S) from Microfluidics Corp. (Newton, MA) were first cleaned with 70% and 100% ethanol, followed by 70% and 100% methanol, and finally with three rinses of Millipore water. Once prepared, each emulsion mixture was then homogenized with the high-speed homogenizer for 1 min at 21000 rpm at room temperature. The crude emulsion was then microfluidized for 1 min at 5000 psi with the cooling bath kept at 10 °C. The ether was then removed *in vacuo*. The final emulsion was then filtered with a 30 mm dia., 0.45 µm nylon filter and stored in 45 mL plastic centrifuge tubes from Corning Inc. (Corning, NY) at 4 °C. After preparation and filtration of the emulsion, the emulsion droplet size was measured by dynamic light scattering (NICOMP 380ZLS) from Particle Sizing Systems (Santa Barbara, CA). An aliquot of the emulsion, approximately 150 µL, was diluted in 3 mL of Millipore water to achieve an intensity factor

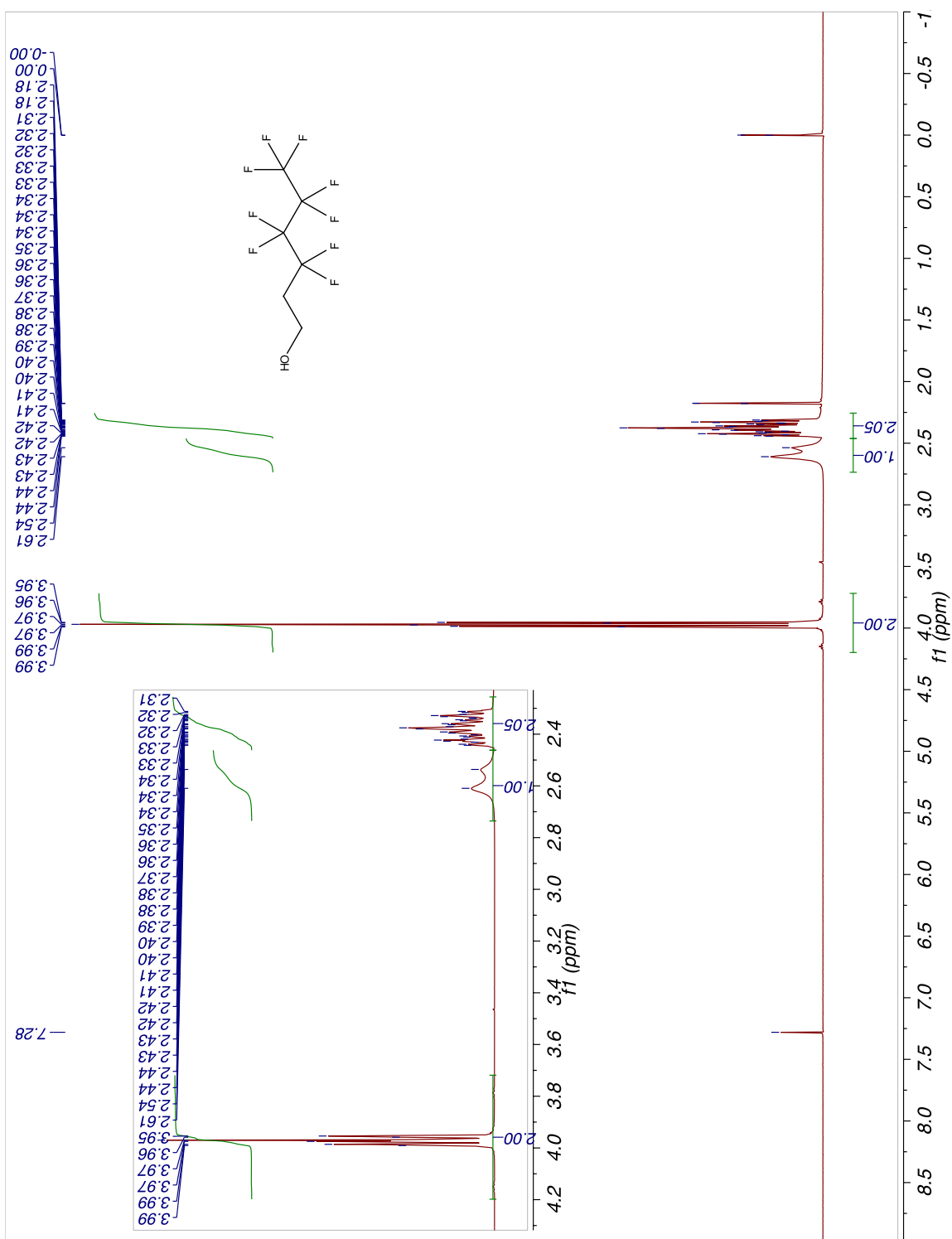
range of 300–350. Each measurement was run for 5 minutes at room temperature and repeated in triplicate. The data were analyzed by Gaussian analysis and reported as a volume-weighted average diameter. The emulsion errors for all polymers were taken as an average of the standard deviations of each individual measurement.

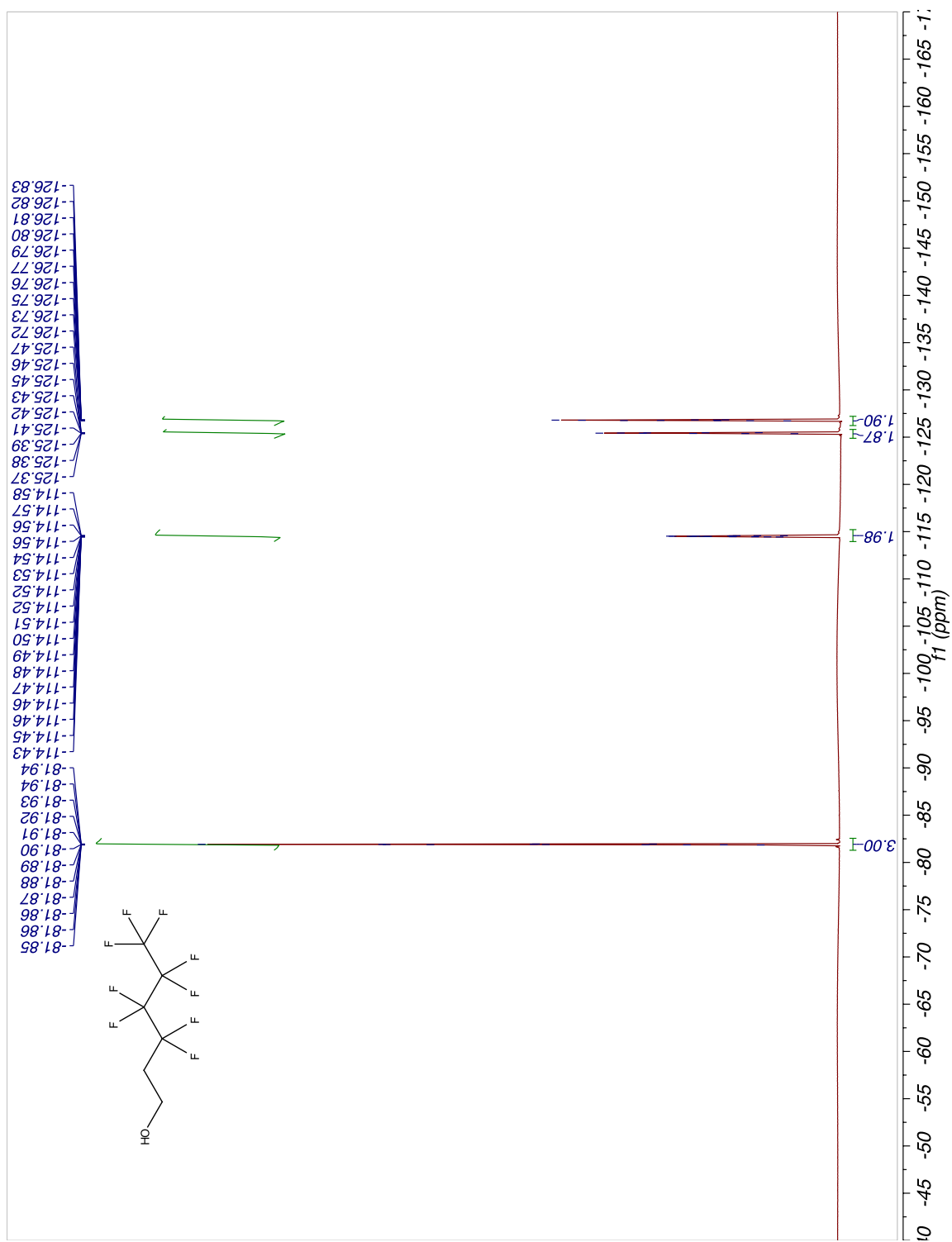
A1.5 References

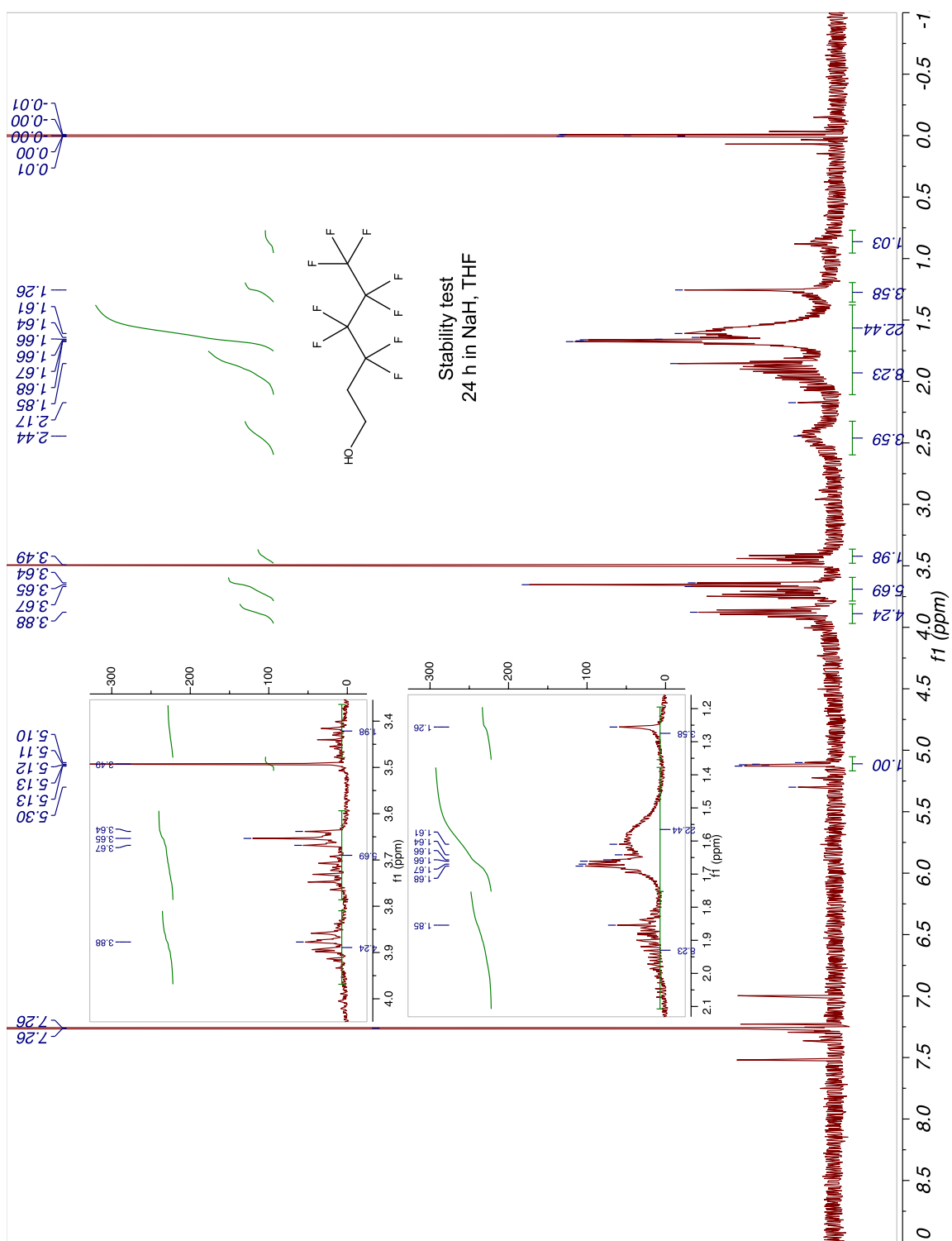
- (1) Williams, H. D.; Trevaskis, N. L.; Charman, S. A.; Shanker, R. M.; Charman, W. N.; Pouton, C. W.; Porter, C. J. H. Strategies to Address Low Drug Solubility in Discovery and Development. *Pharmacol. Rev.* **2013**, *65* (1), 315–499.
- (2) Chen, H.; Khemtong, C.; Yang, X.; Chang, X.; Gao, J. Nanonization Strategies for Poorly Water-Soluble Drugs. *Drug Discov. Today* **2011**, *16* (7-8), 354–360.
- (3) Tucker, W. B.; Mecozzi, S. Nanoemulsions in Medicine. In *Handbook of Nanobiomedical Research, Volume 1*; Torchilin, V. P., Ed.; World Scientific Publishing, 2014; pp 141–167.
- (4) Taylor, P. Ostwald Ripening in Emulsions. *Adv. Colloid Interface Sci.* **1998**, *75* (2), 107–163.
- (5) Tadros, T. F. Application of Surfactants in Emulsion Formation and Stabilisation. In *Applied Surfactants: Principles and Applications*; Wiley-VCH GmbH: Weinheim, Germany, 2005; pp 115–186.
- (6) Jee, J. P.; McCoy, A.; Mecozzi, S. Encapsulation and Release of Amphotericin B from an ABC Triblock Fluorous Copolymer. *Pharm. Res.* **2012**, *29* (1), 69–82.
- (7) Tucker, W. B.; McCoy, A. M.; Fix, S. M.; Stagg, M. F.; Murphy, M. M.; Mecozzi, S. Synthesis, Physicochemical Characterization, and Self-Assembly of Linear, Dibranched, and Miktoarm Semifluorinated Triphilic Polymers. *J. Polym. Sci. Part A Polym. Chem.* **2014**, *52* (23), 3324–3336.
- (8) Yilmaz, E.; Borchert, H. H. Effect of Lipid-Containing, Positively Charged Nanoemulsions on Skin Hydration, Elasticity and Erythema - An *in vivo* Study. *Int. J. Pharm.* **2006**, *307* (2), 232–238.
- (9) Yilmaz, E.; Borchert, H. H. Design of a Phytosphingosine-Containing, Positively-Charged Nanoemulsion as a Colloidal Carrier System for Dermal Application of Ceramides. *Eur. J. Pharm. Biopharm.* **2005**, *60* (1), 91–98.

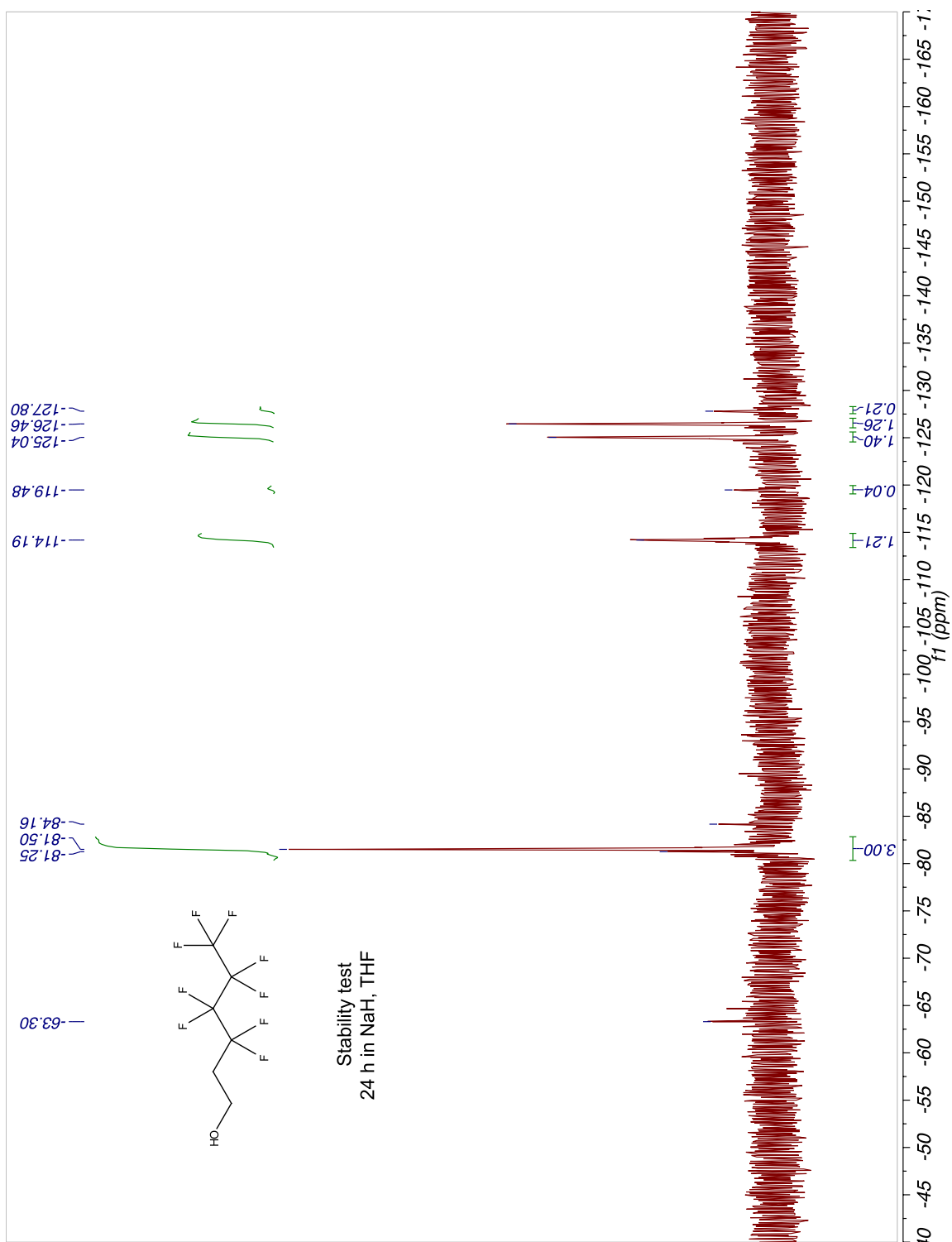
- (10) Fryd, M. M.; Mason, T. G. Advanced Nanoemulsions. *Annu. Rev. Phys. Chem.* **2012**, *63* (1), 493–518.
- (11) Tirnaksiz, F.; Akkus, S.; Celebi, N. Nanoemulsions as Drug Delivery Systems. In *Surfactant Science Series*; Fanun, M., Ed.; CRC Press: Boca Raton, FL, 2010; Vol. 150, pp 221–244.
- (12) Huang, W.; Jin, C.; Derzon, D. K.; Huber, T. A.; Last, J. A.; Provencio, P. P.; Gopalan, A. S.; Dugger, M.; Sasaki, D. Y. Synthesis of Ether-Linked Fluorocarbon Surfactants and Their Aggregational Properties in Organic Solvents. *J. Colloid Interface Sci.* **2004**, *272* (2), 457–464.

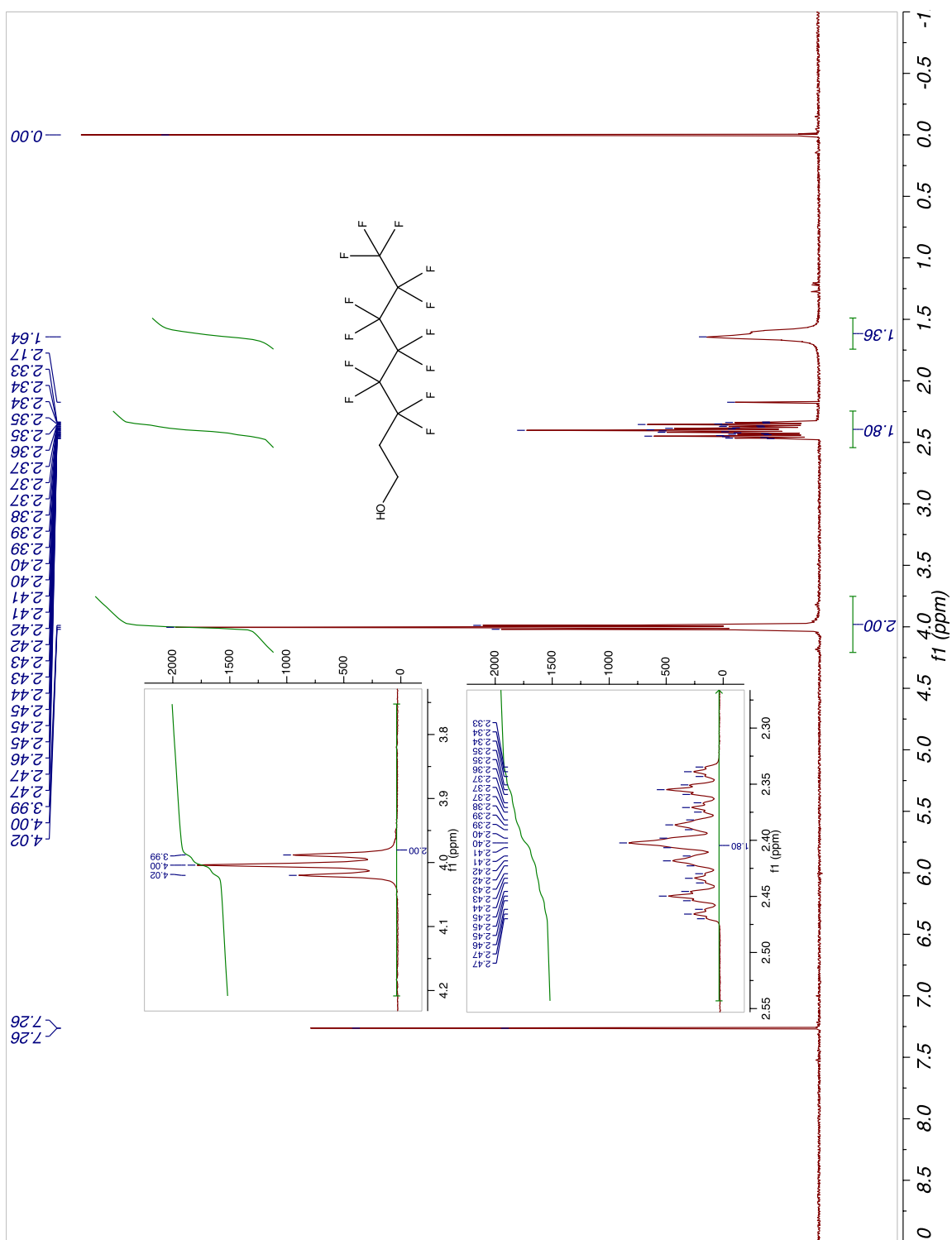
Appendix 2:
Supplementary Data

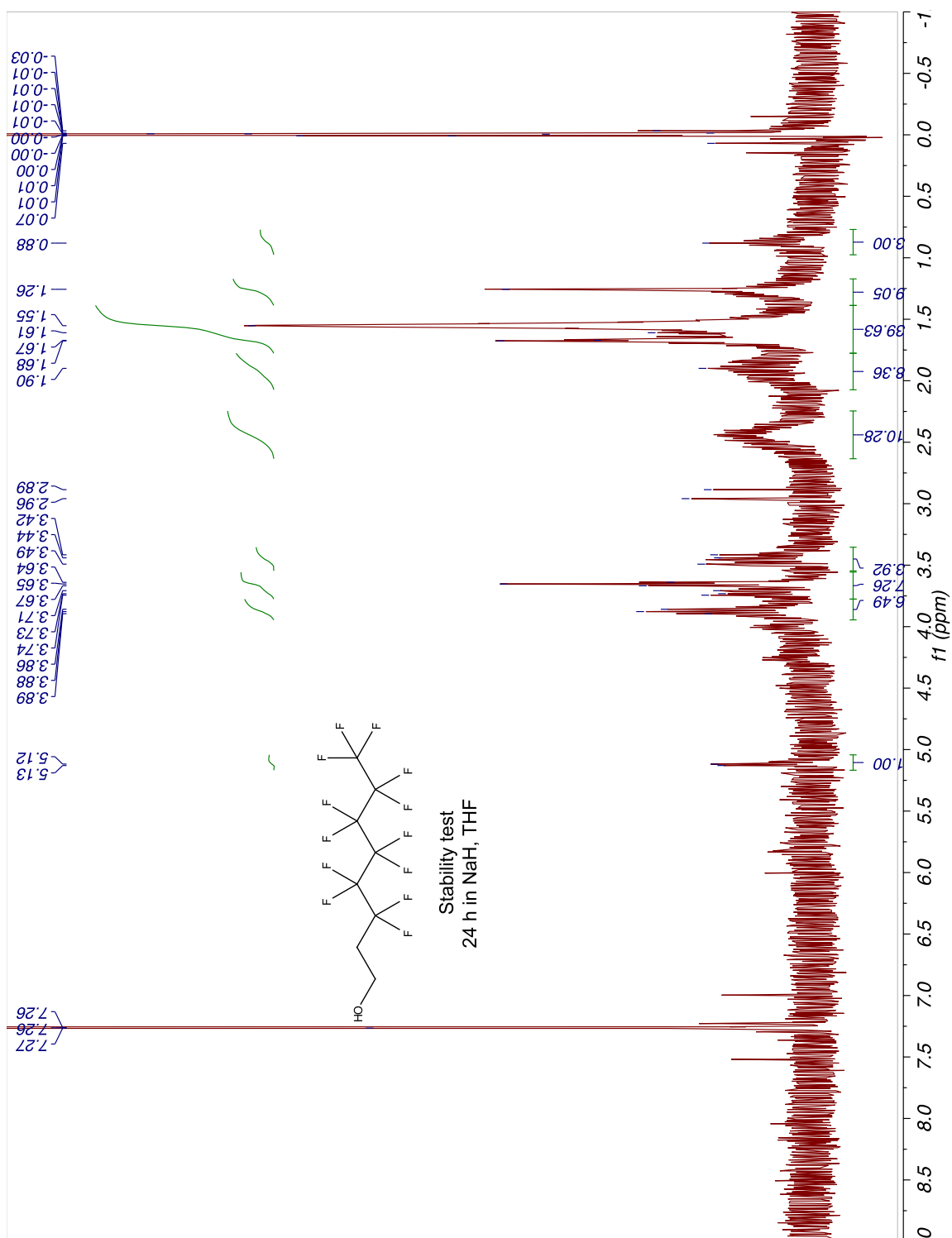


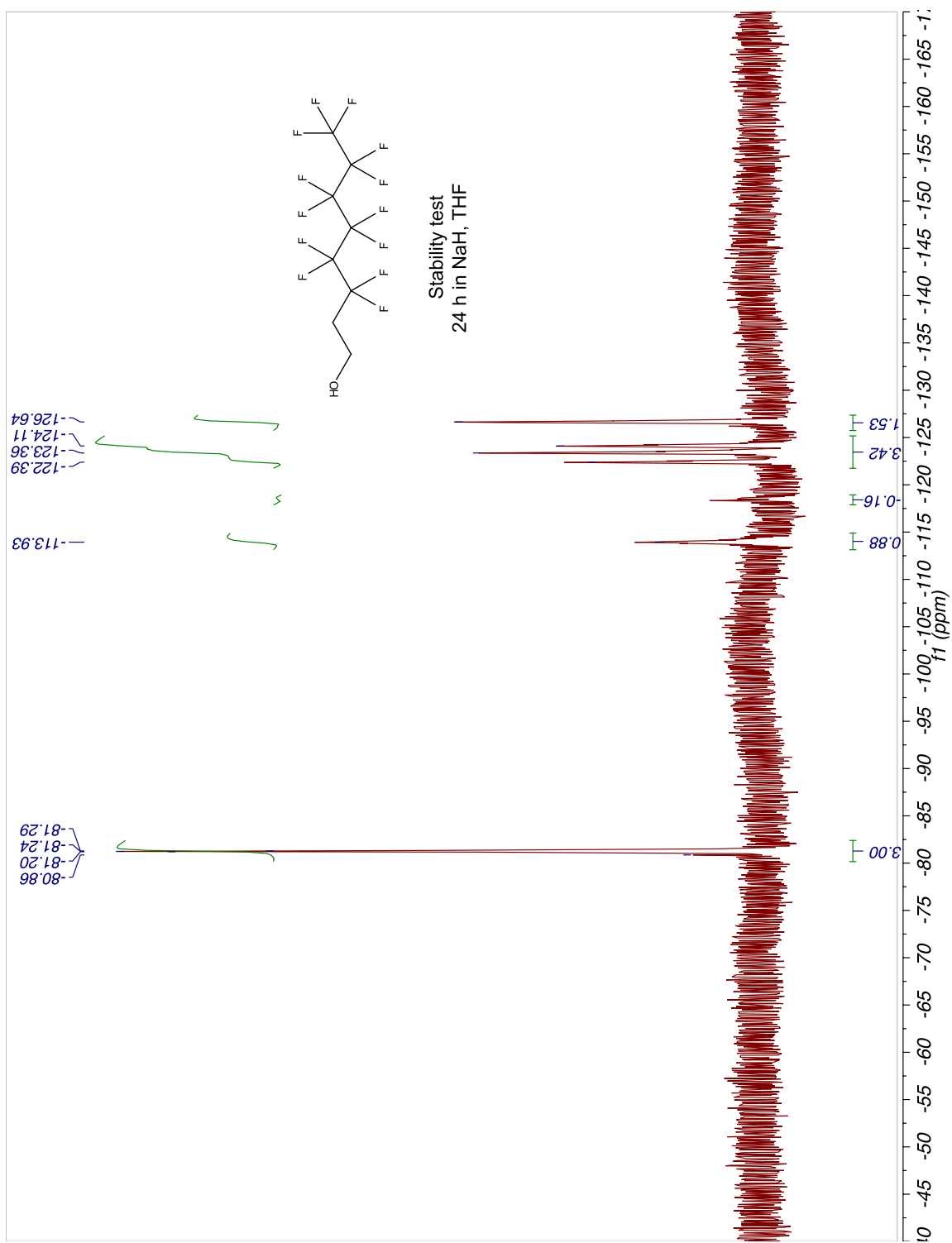


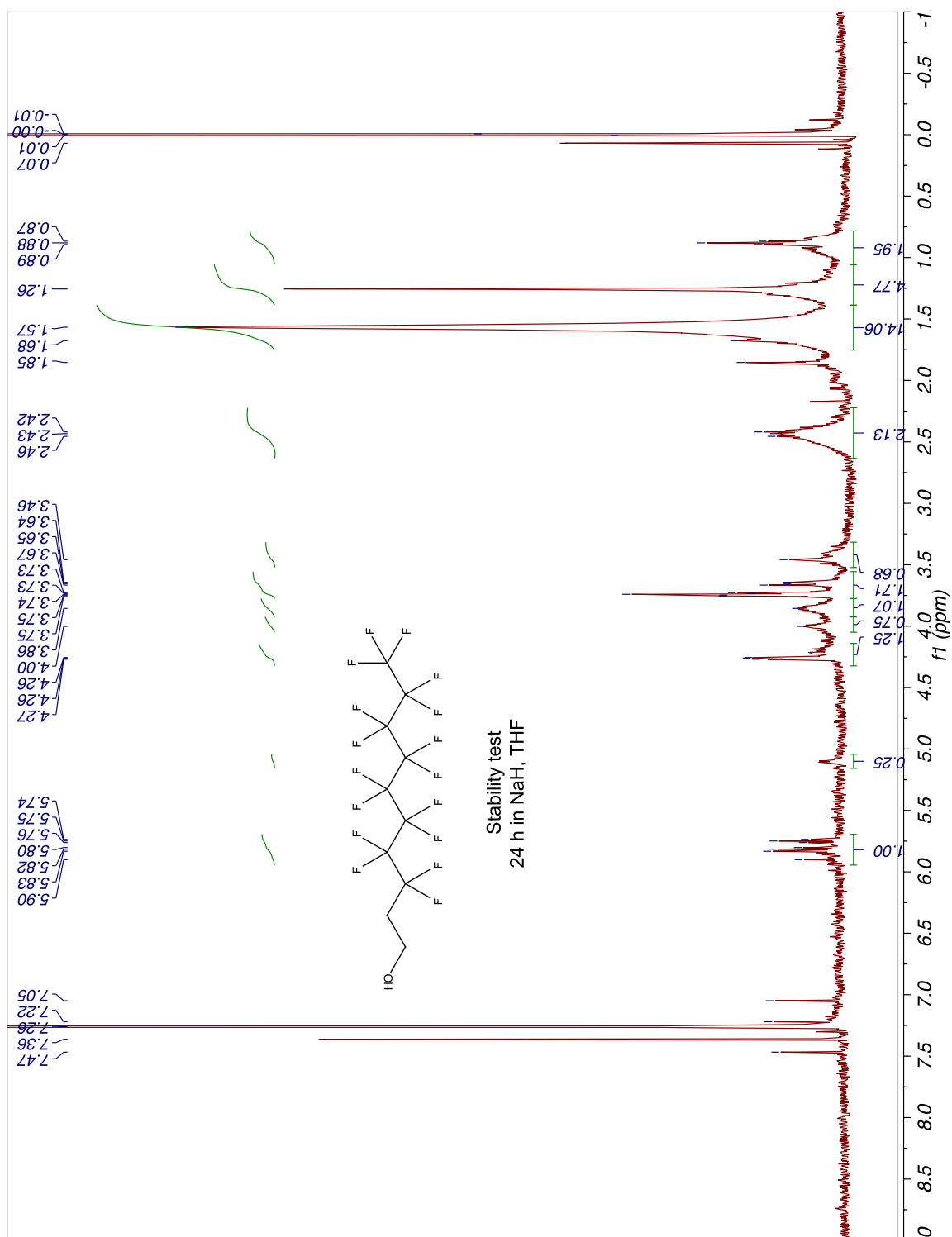


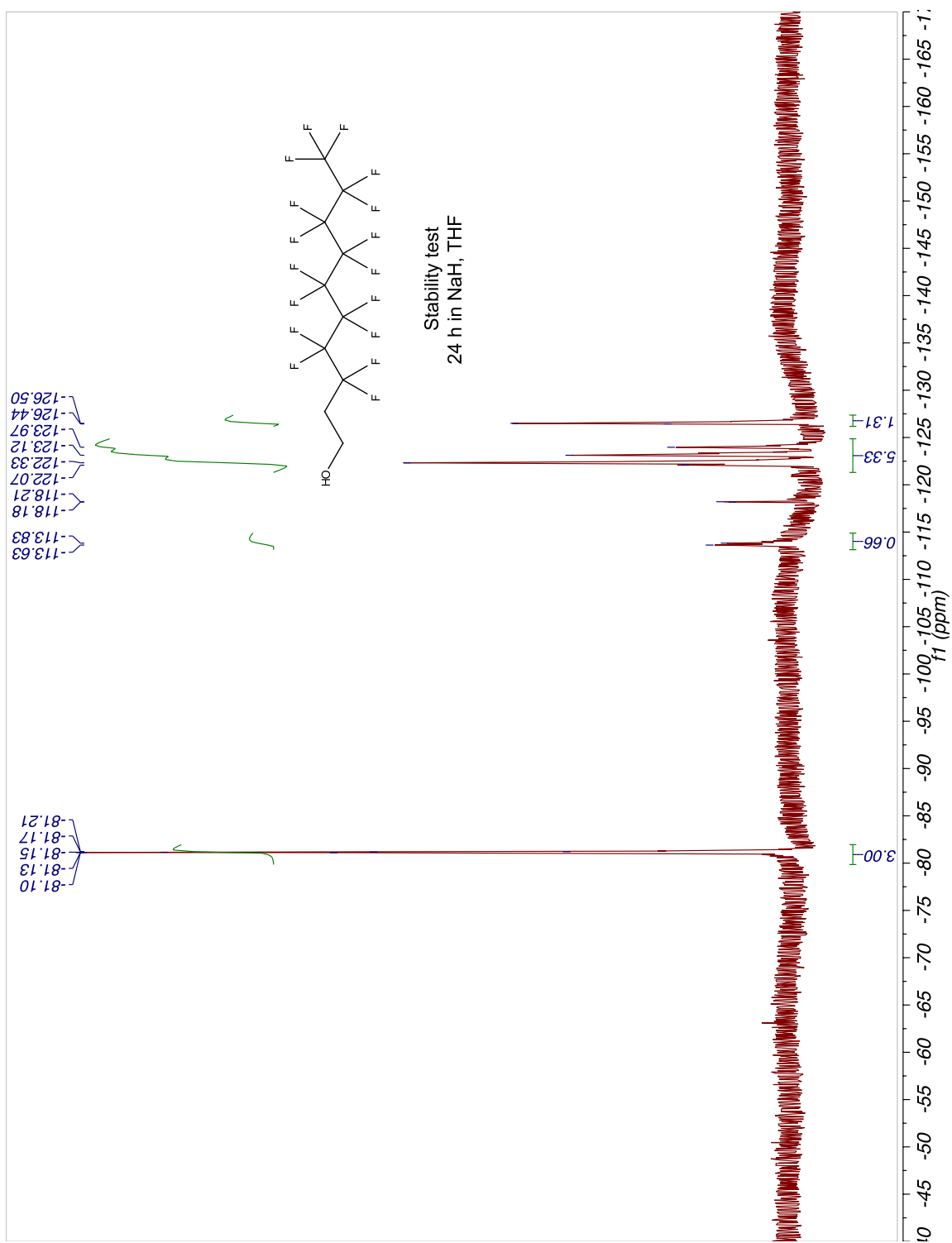


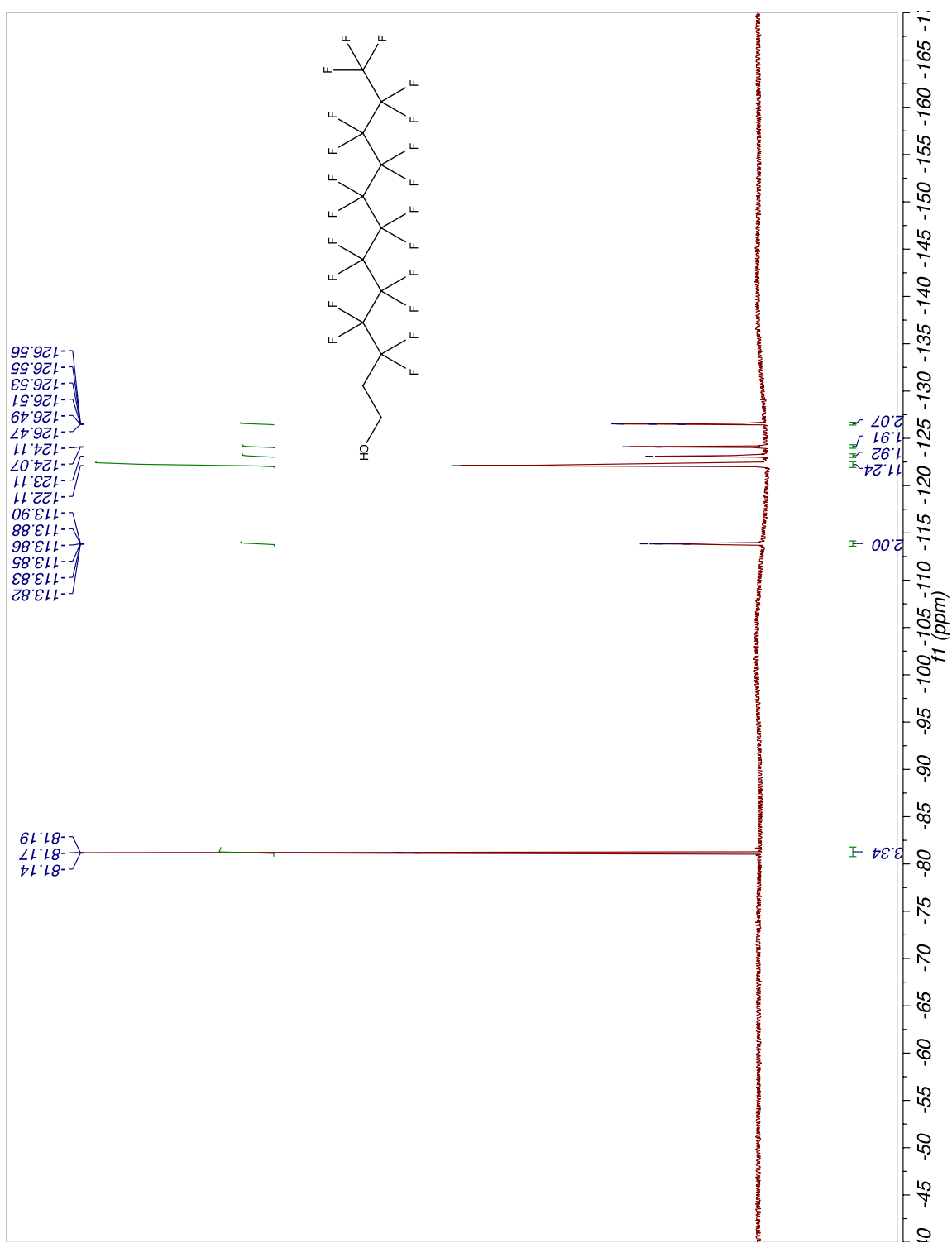


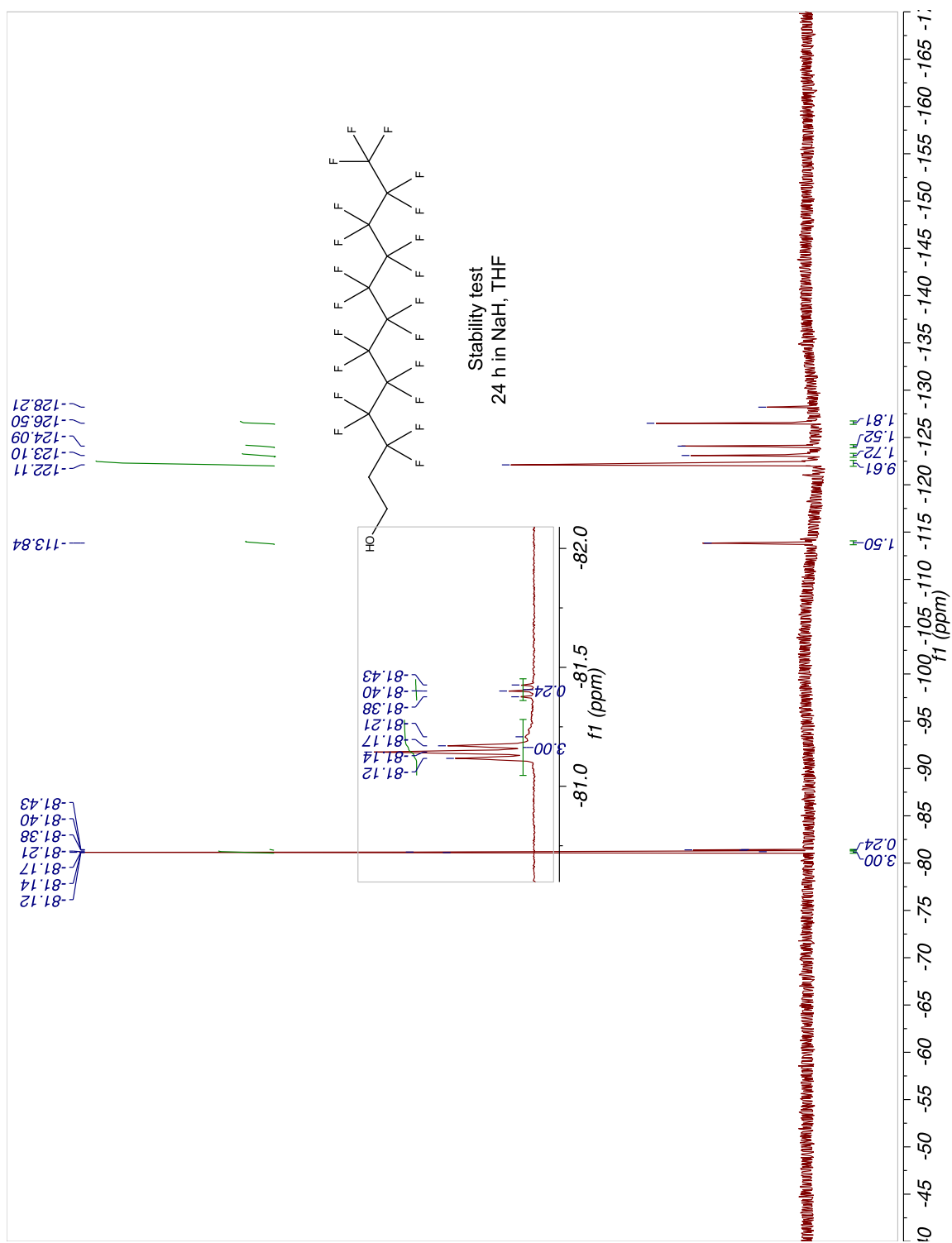


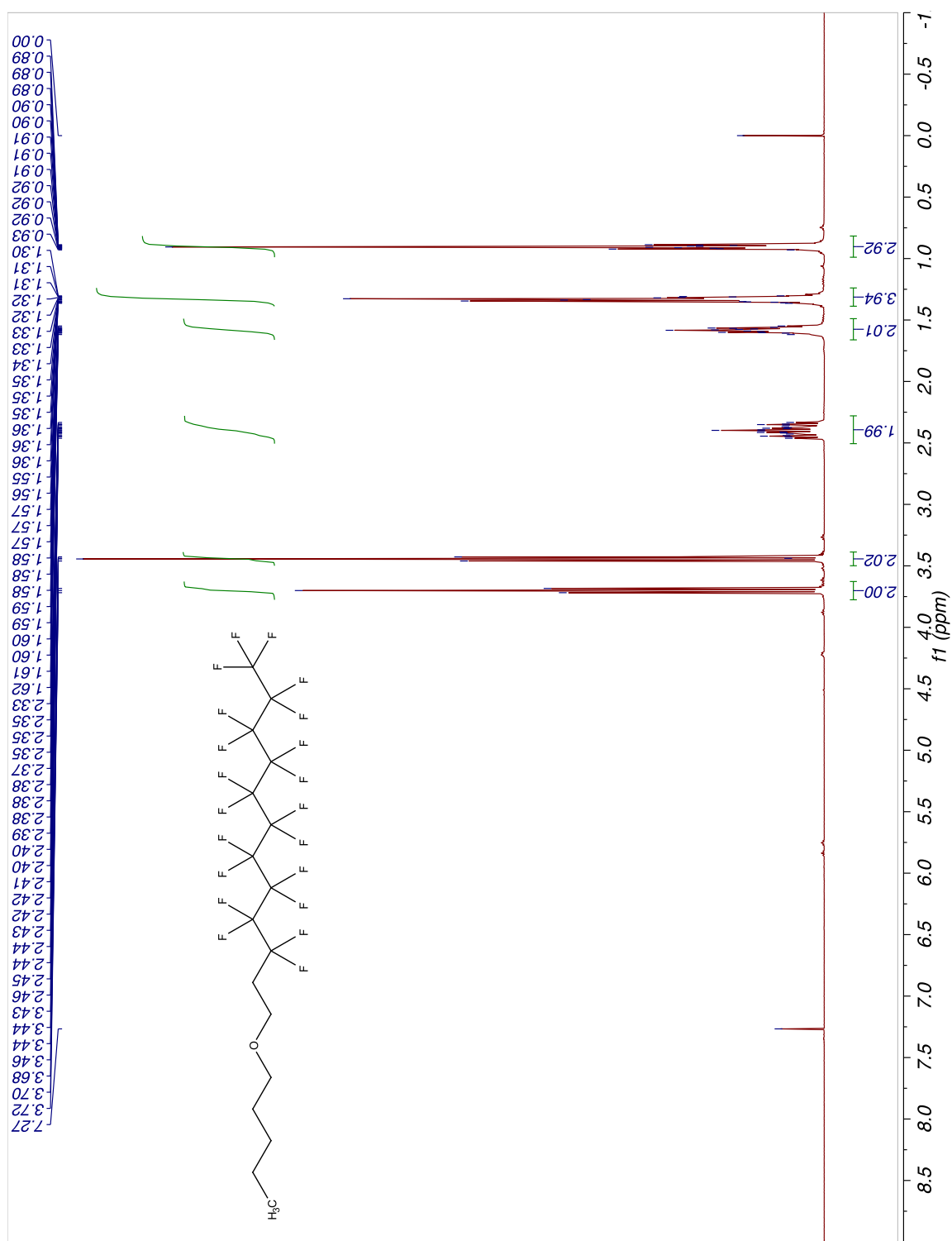


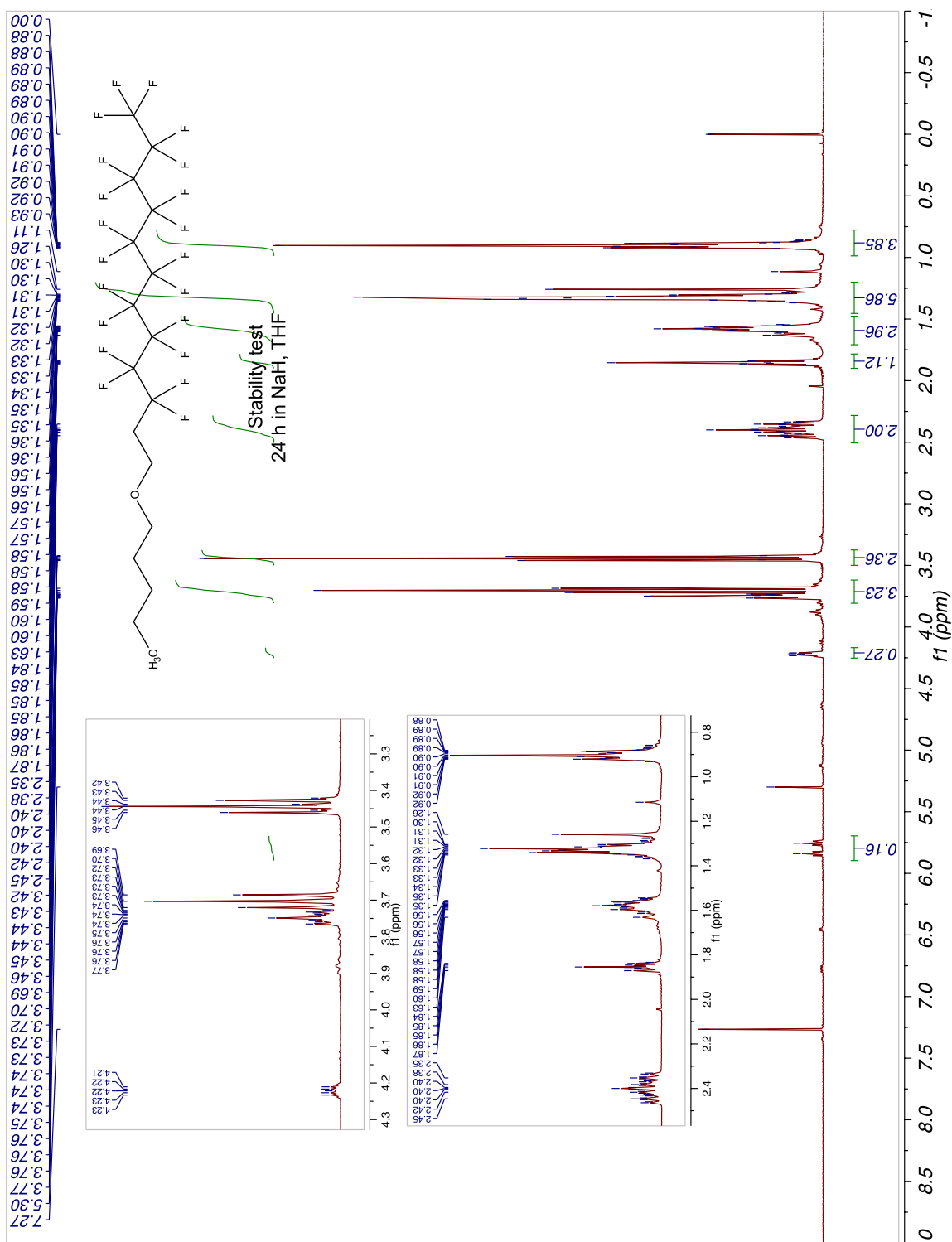


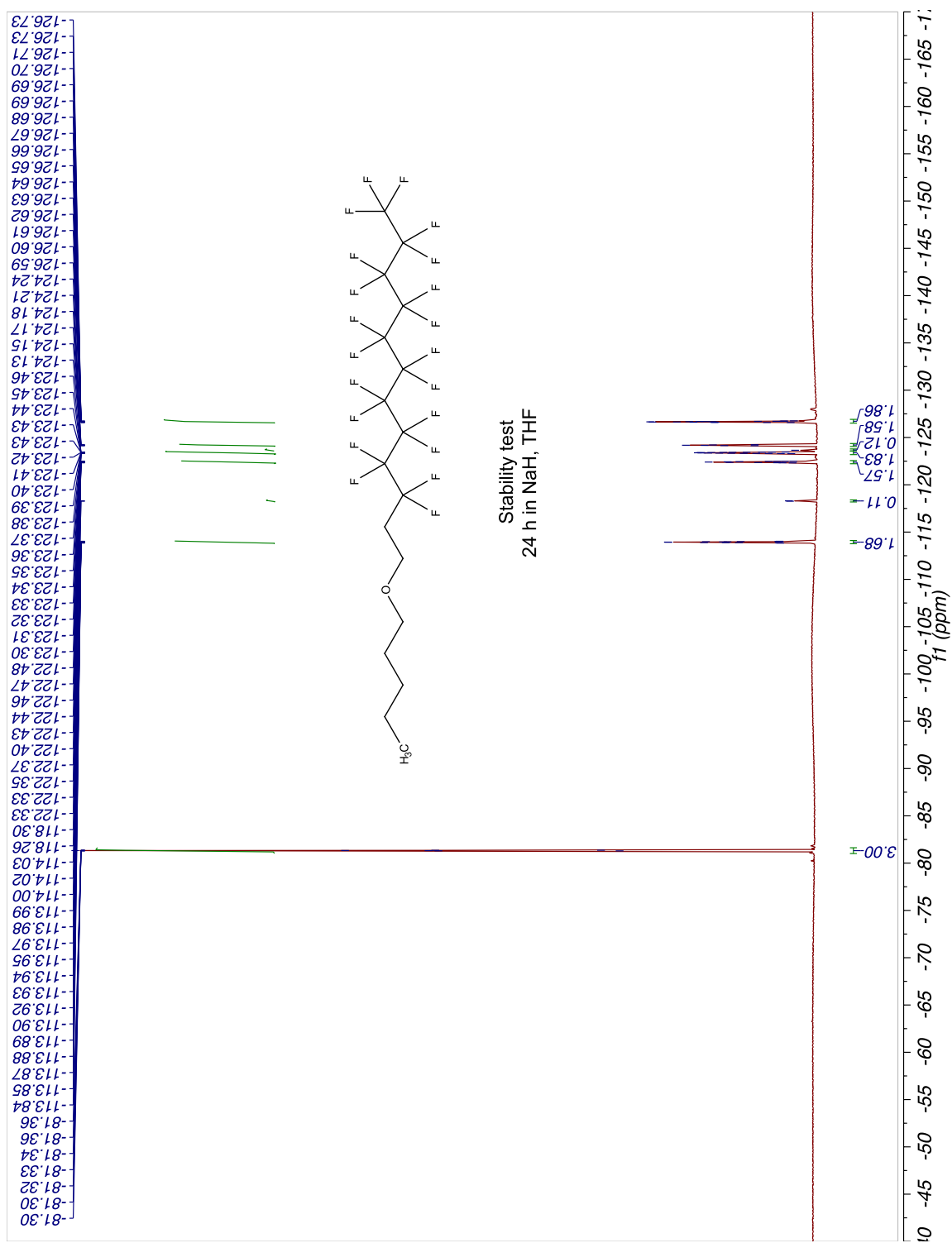


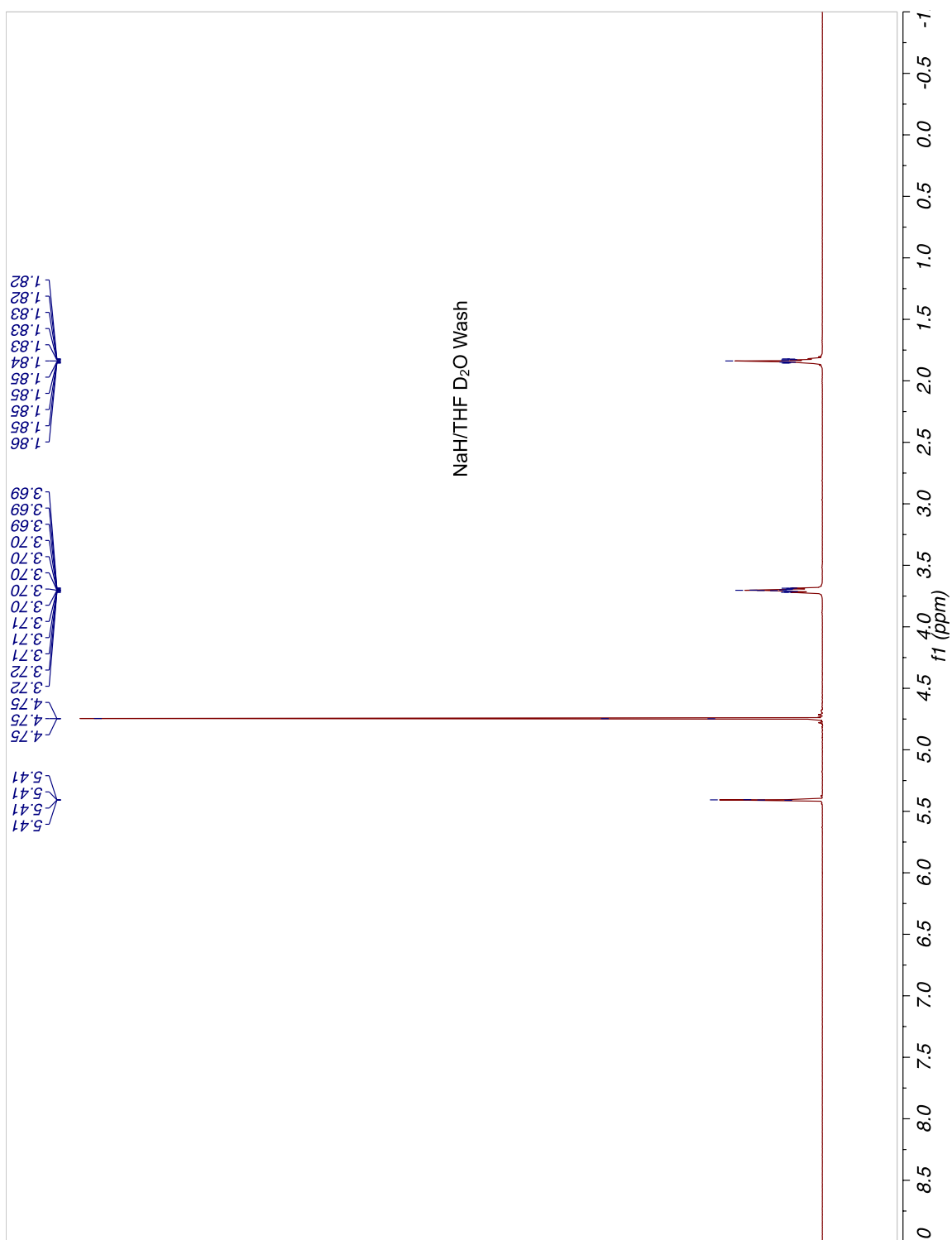


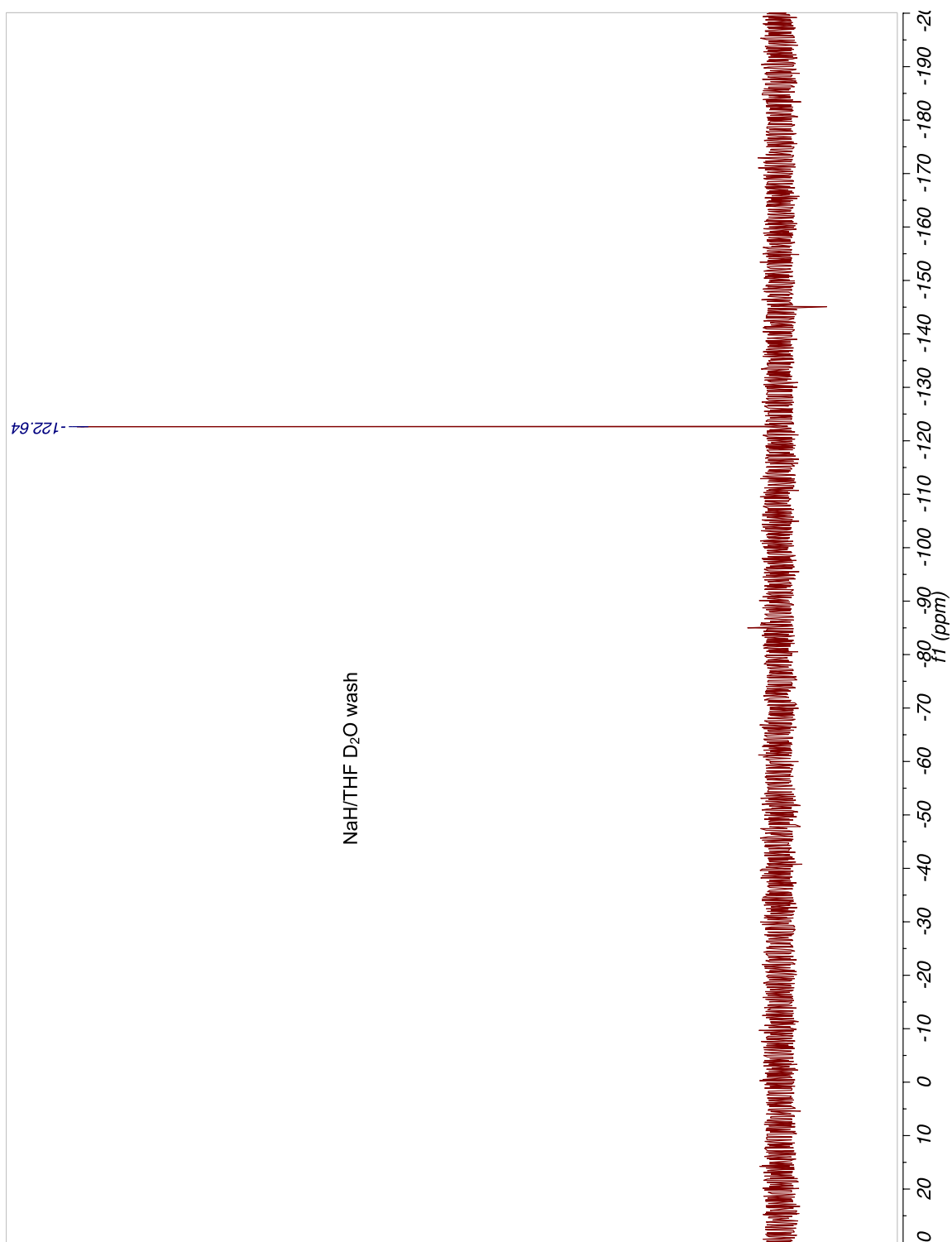






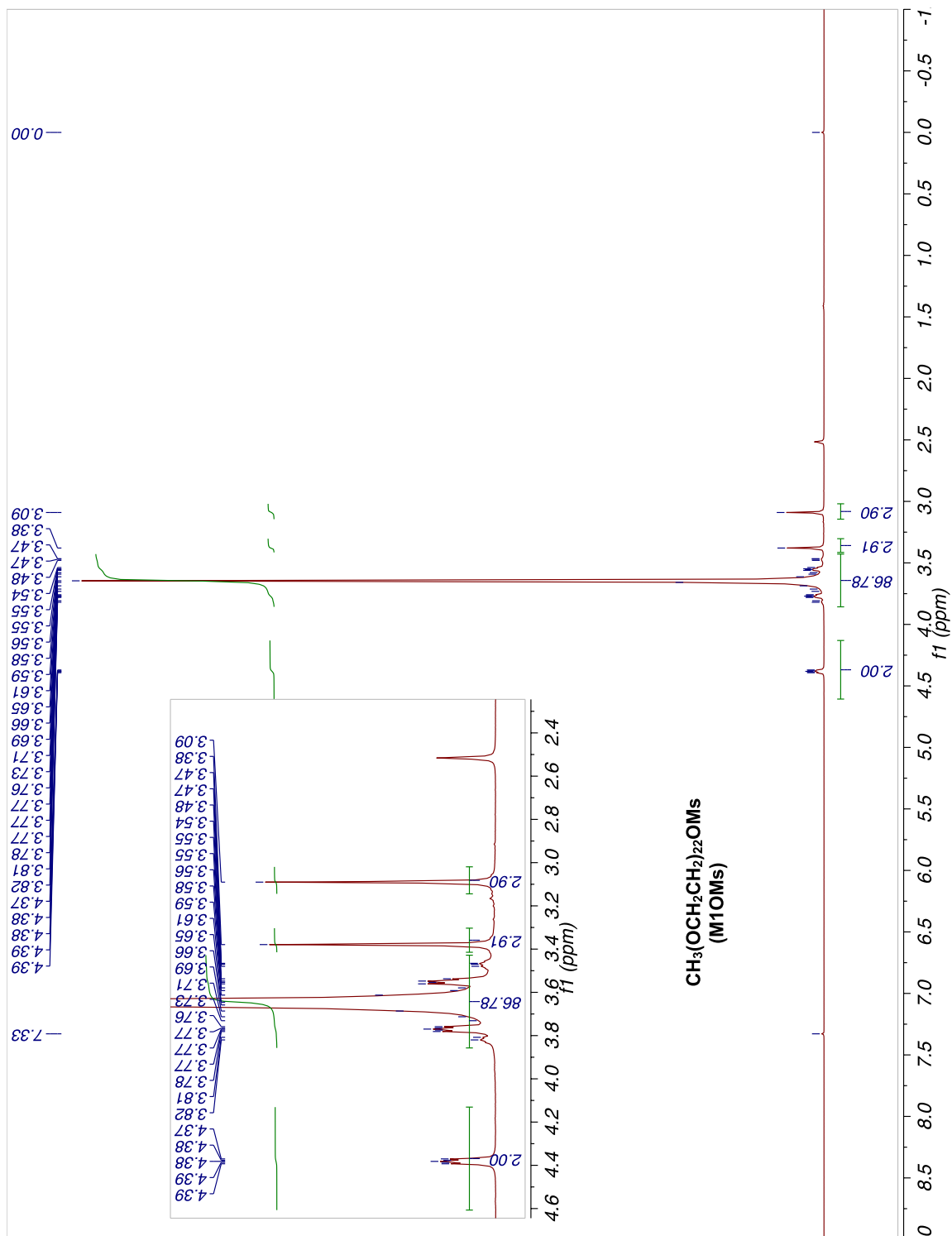


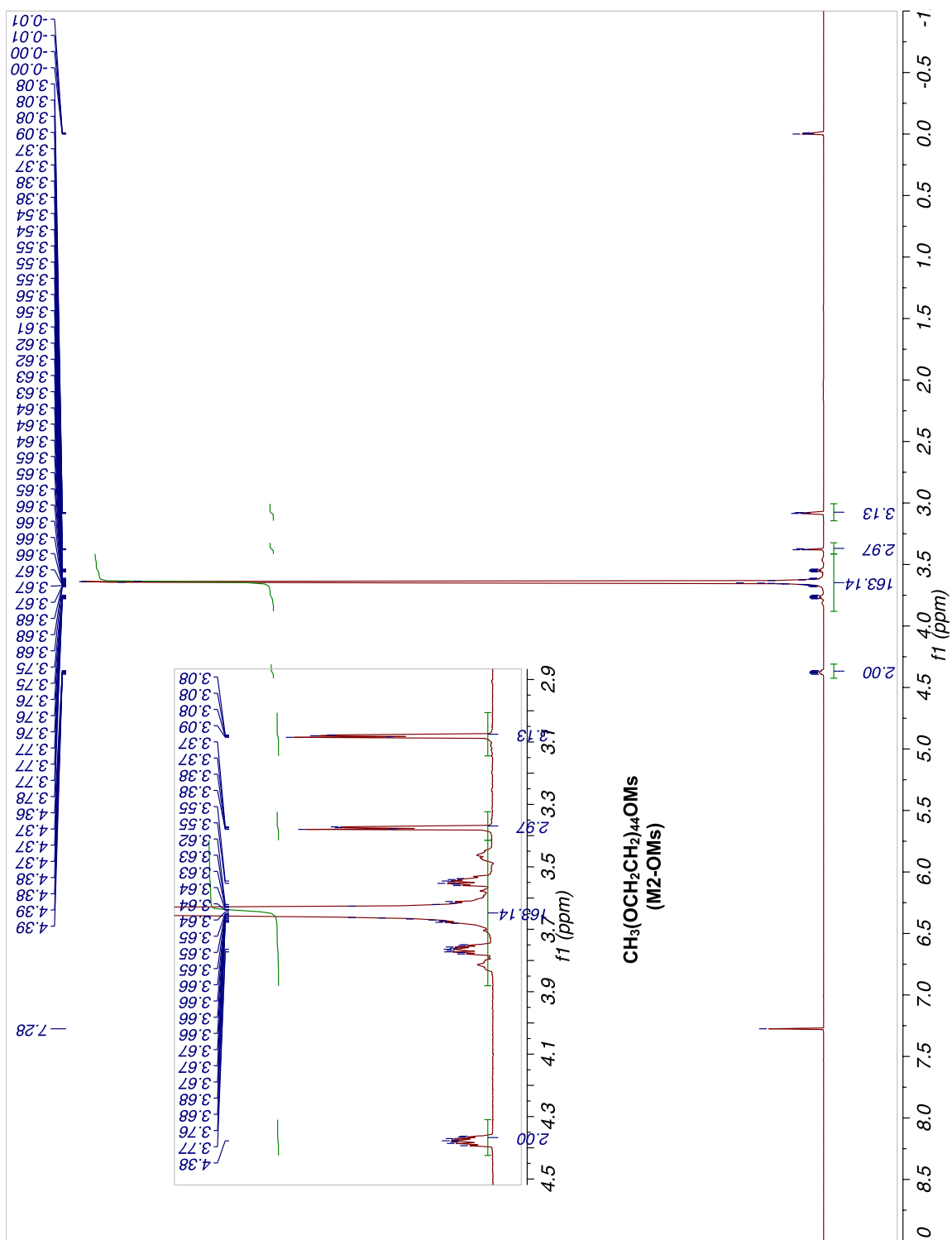


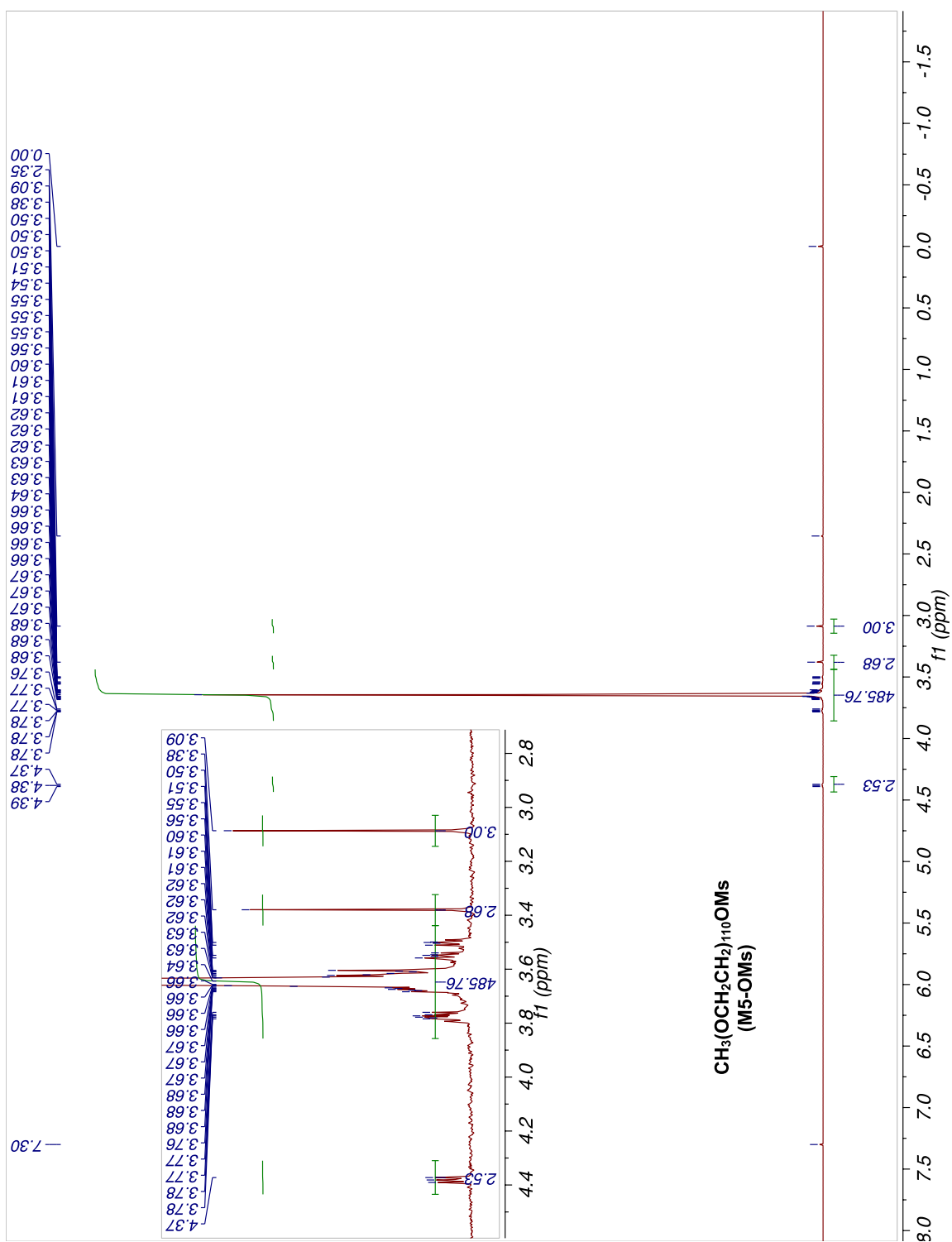


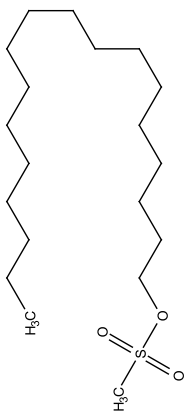
A2.2 Triphilic surfactant data

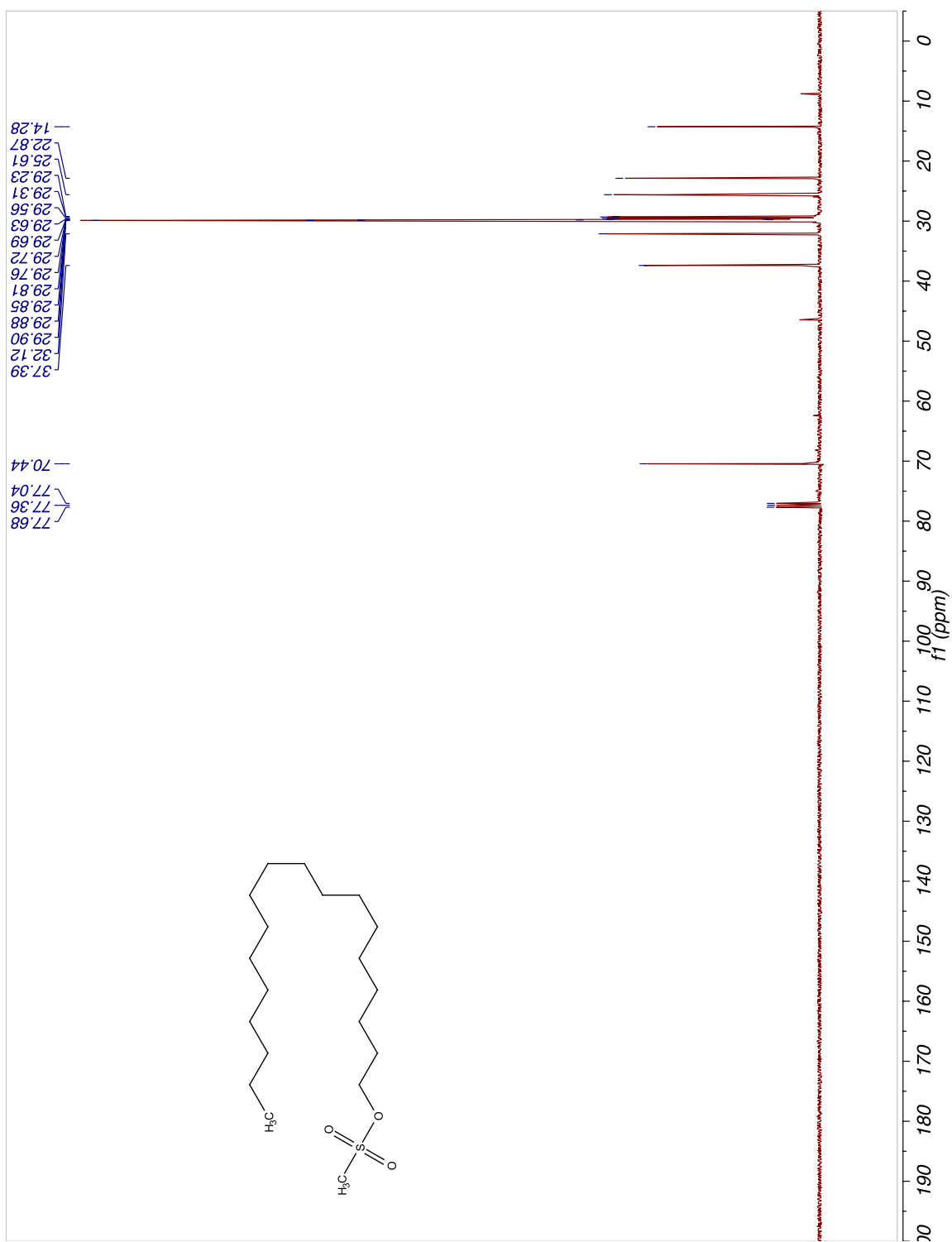
A2.2.1. NMR spectra

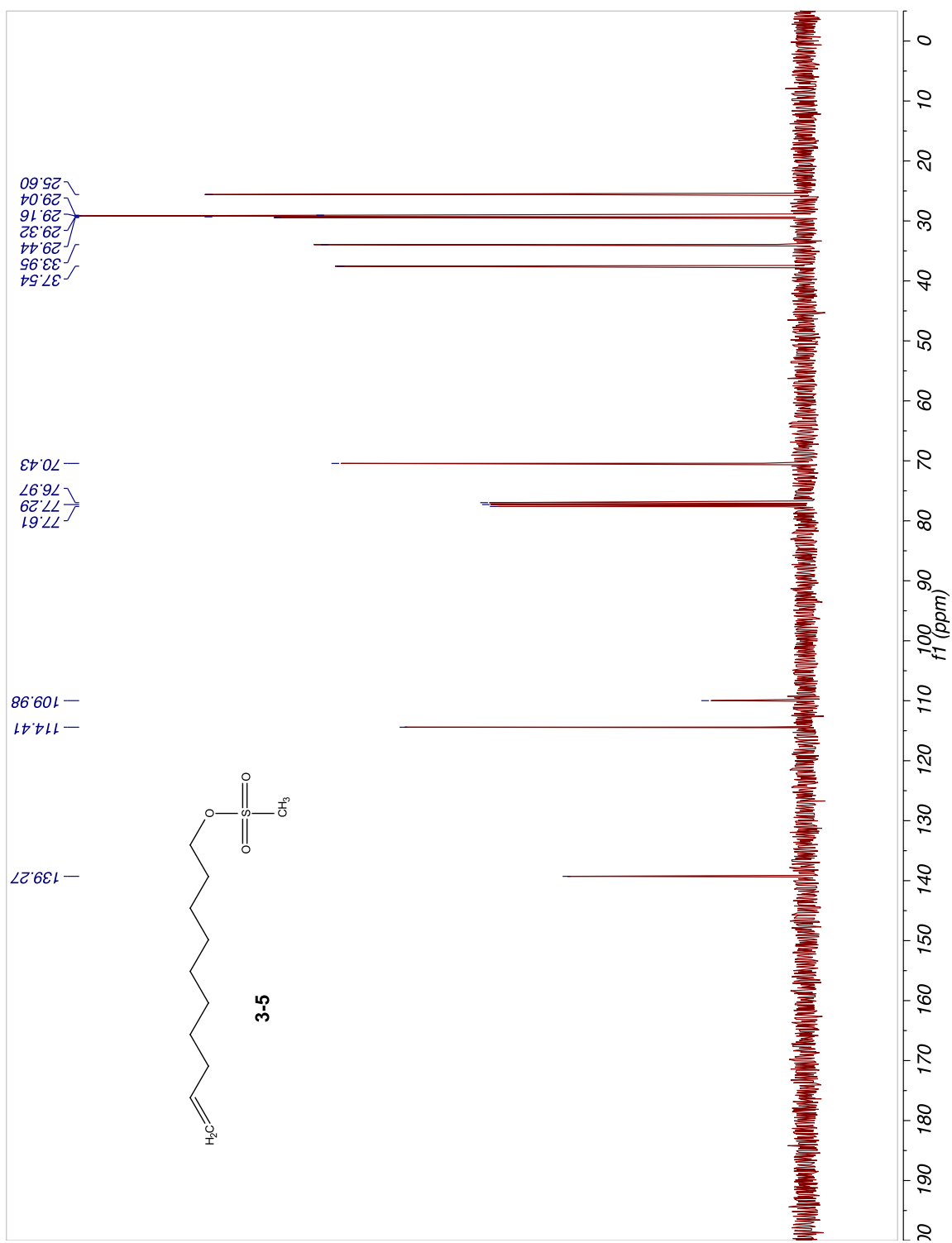


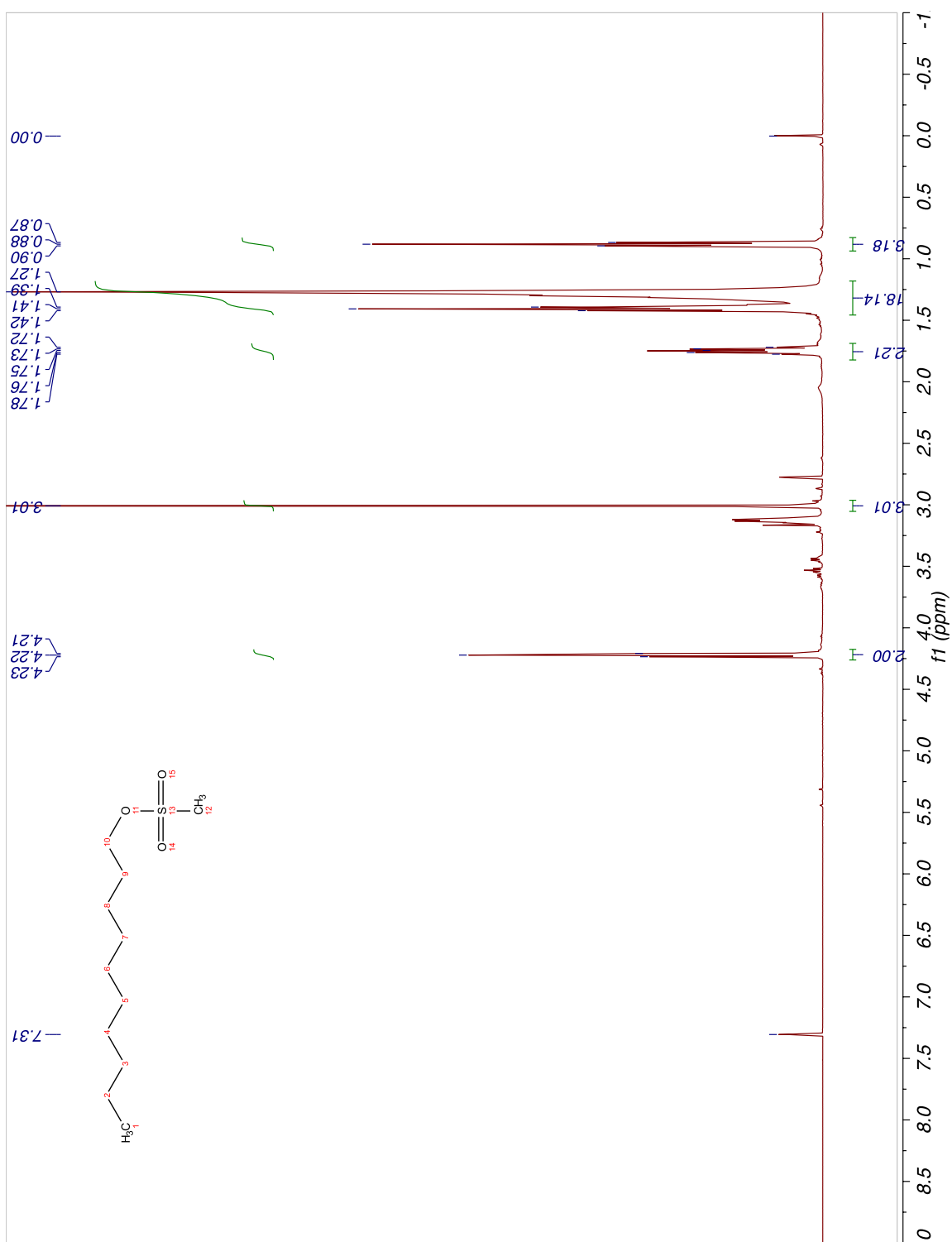


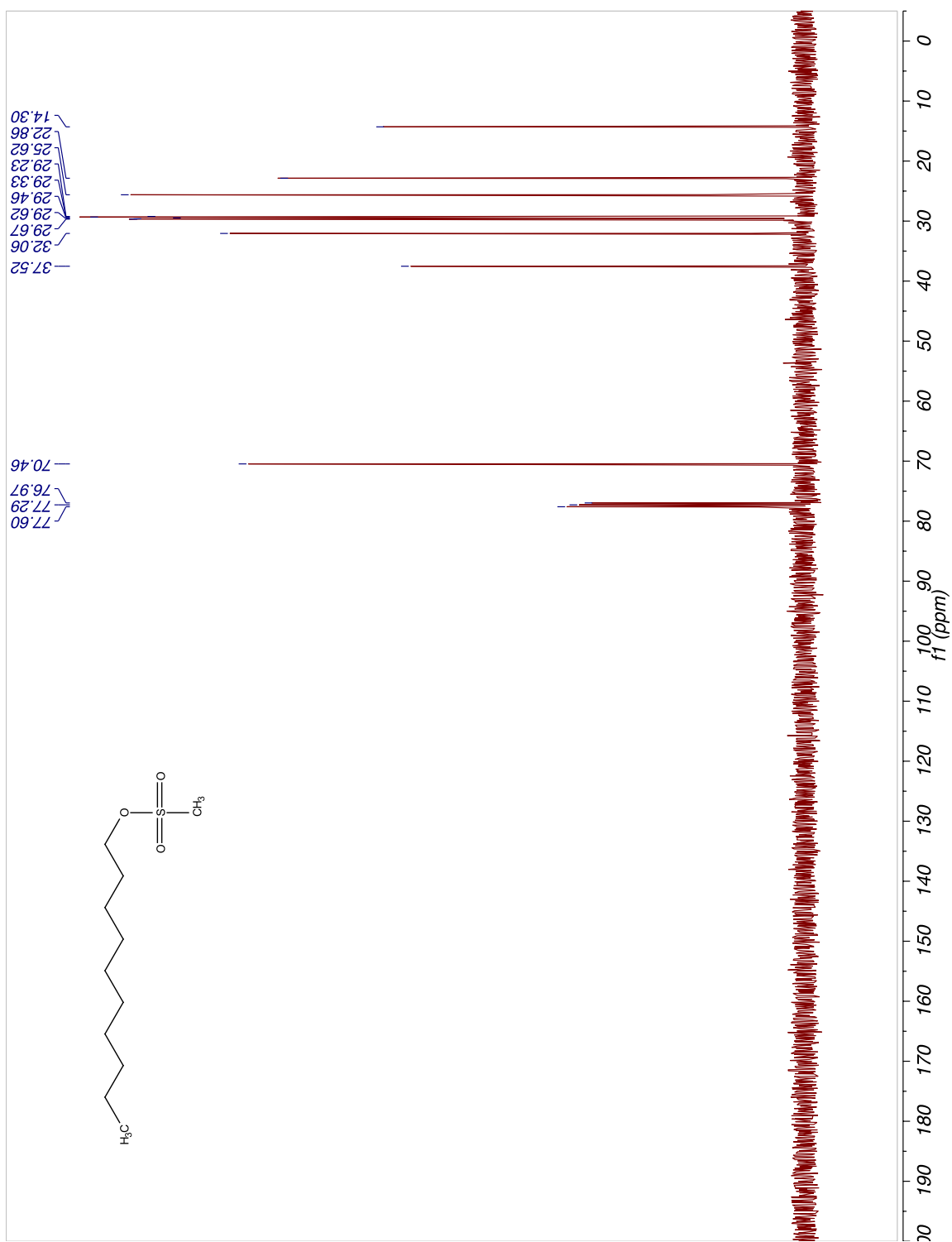


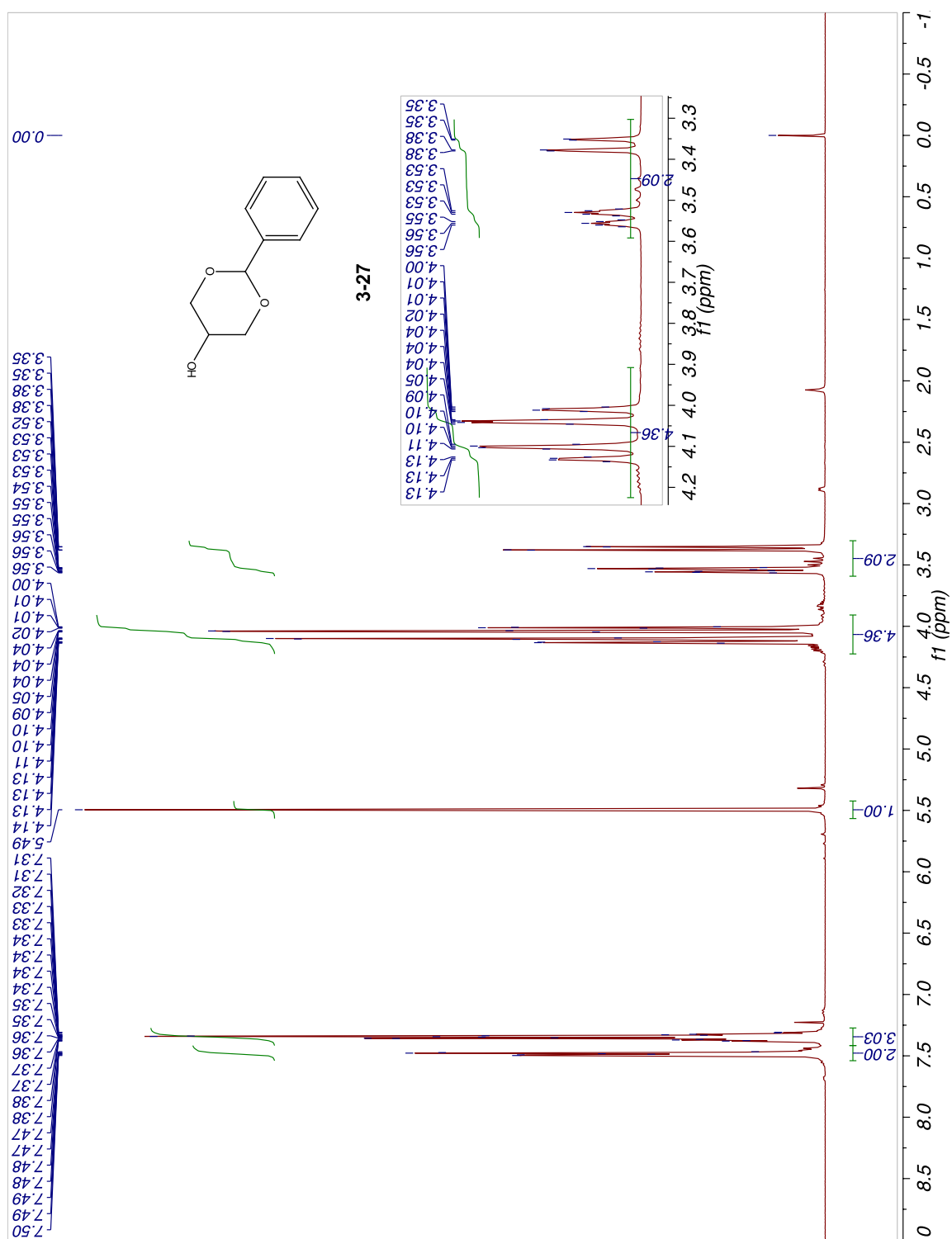


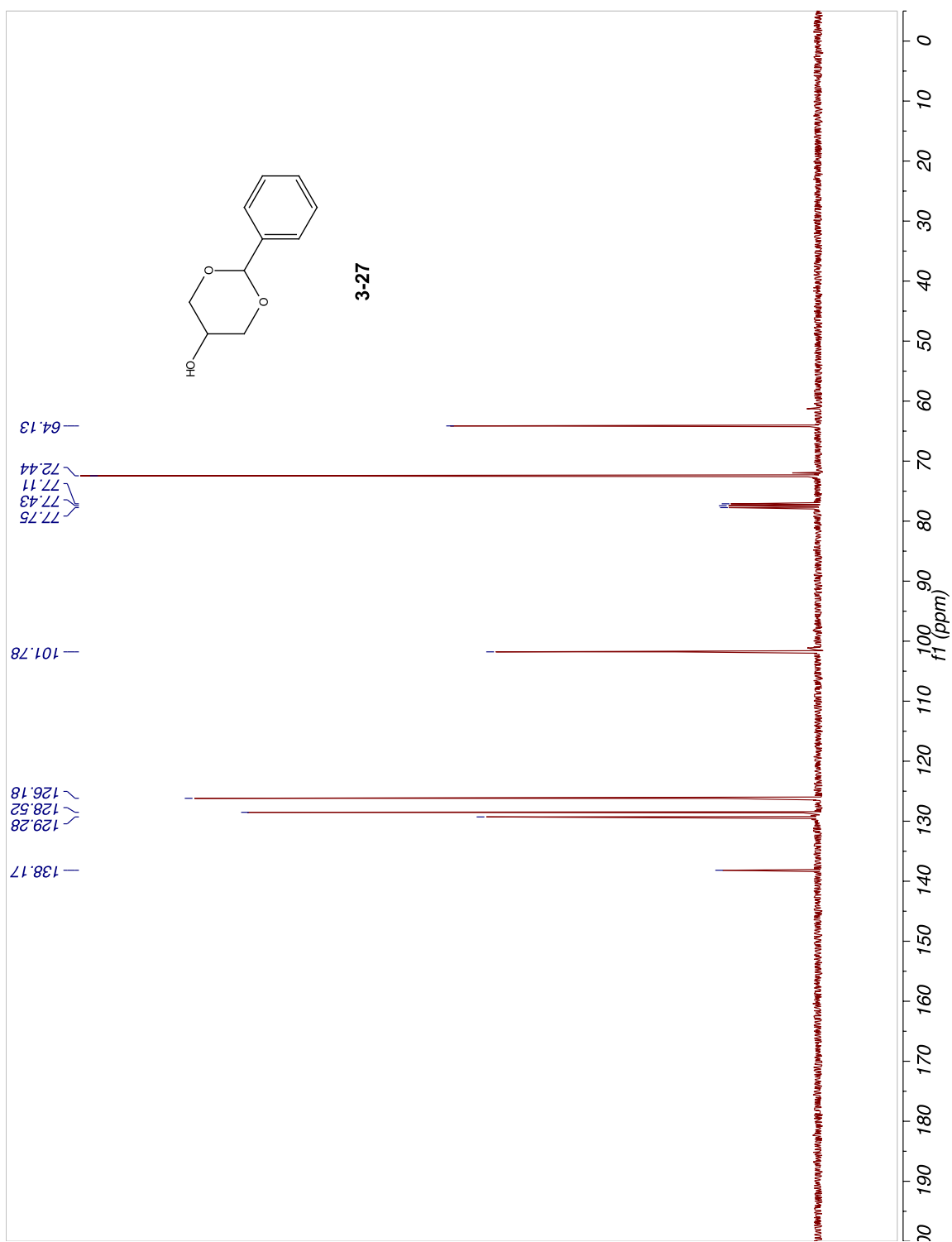


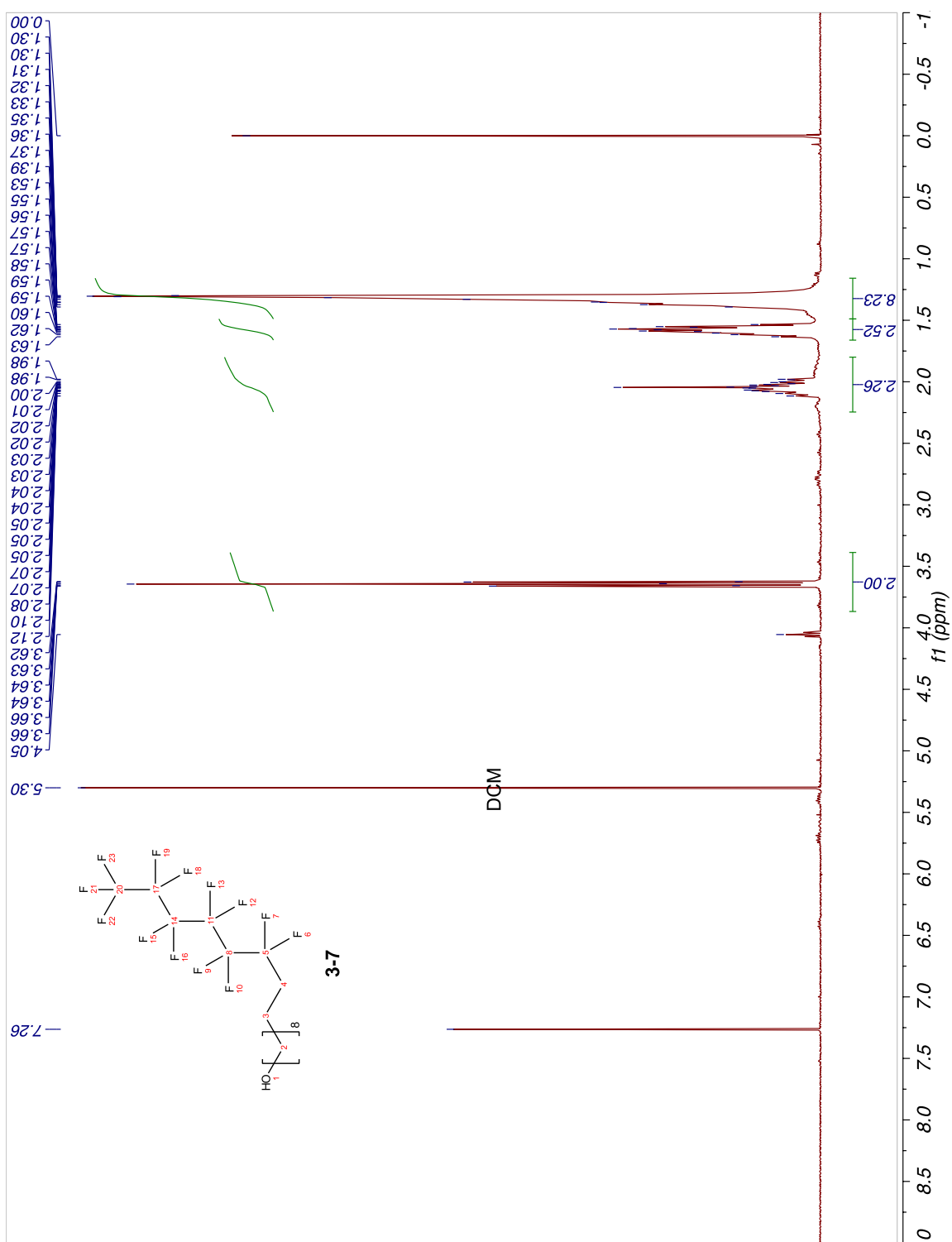


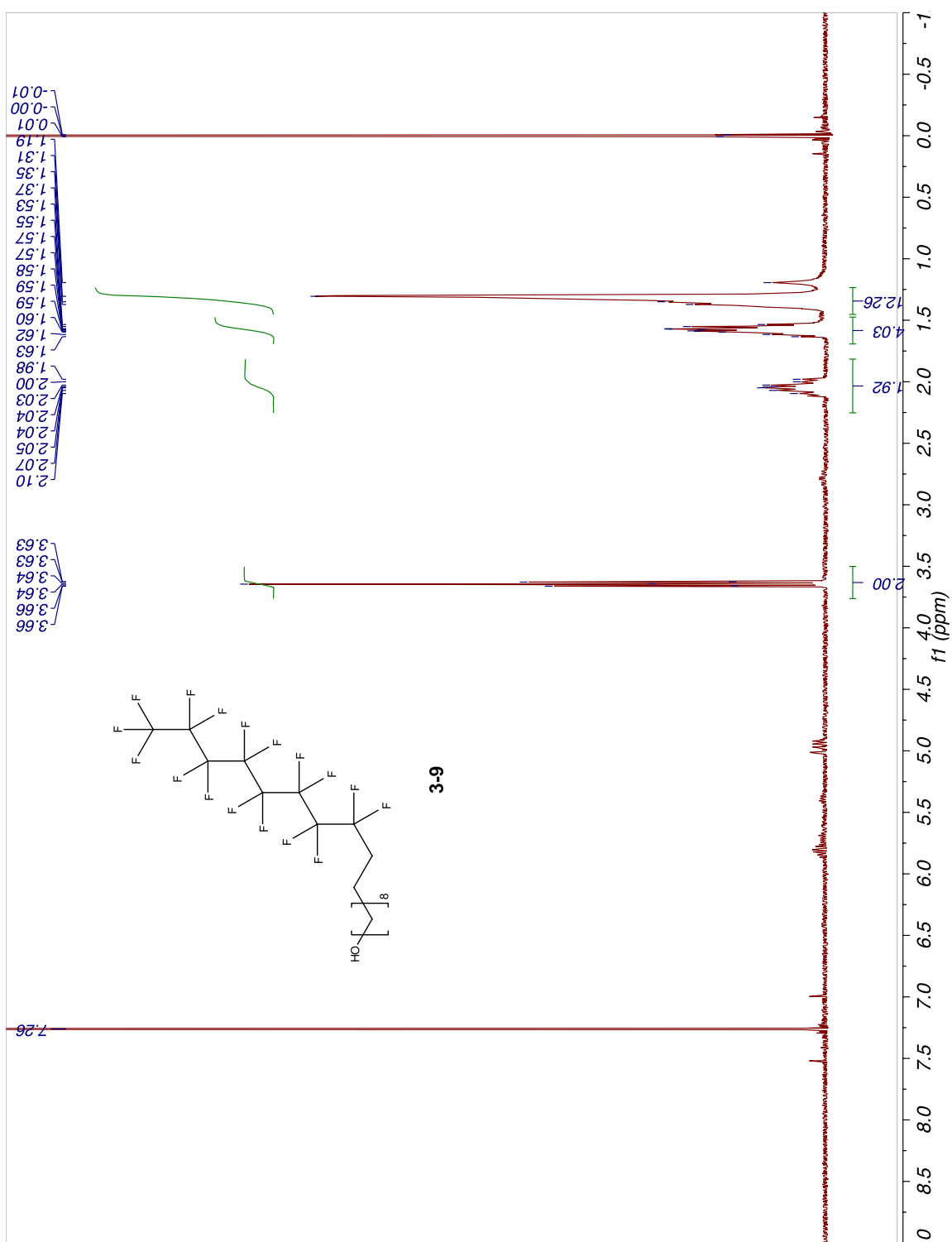


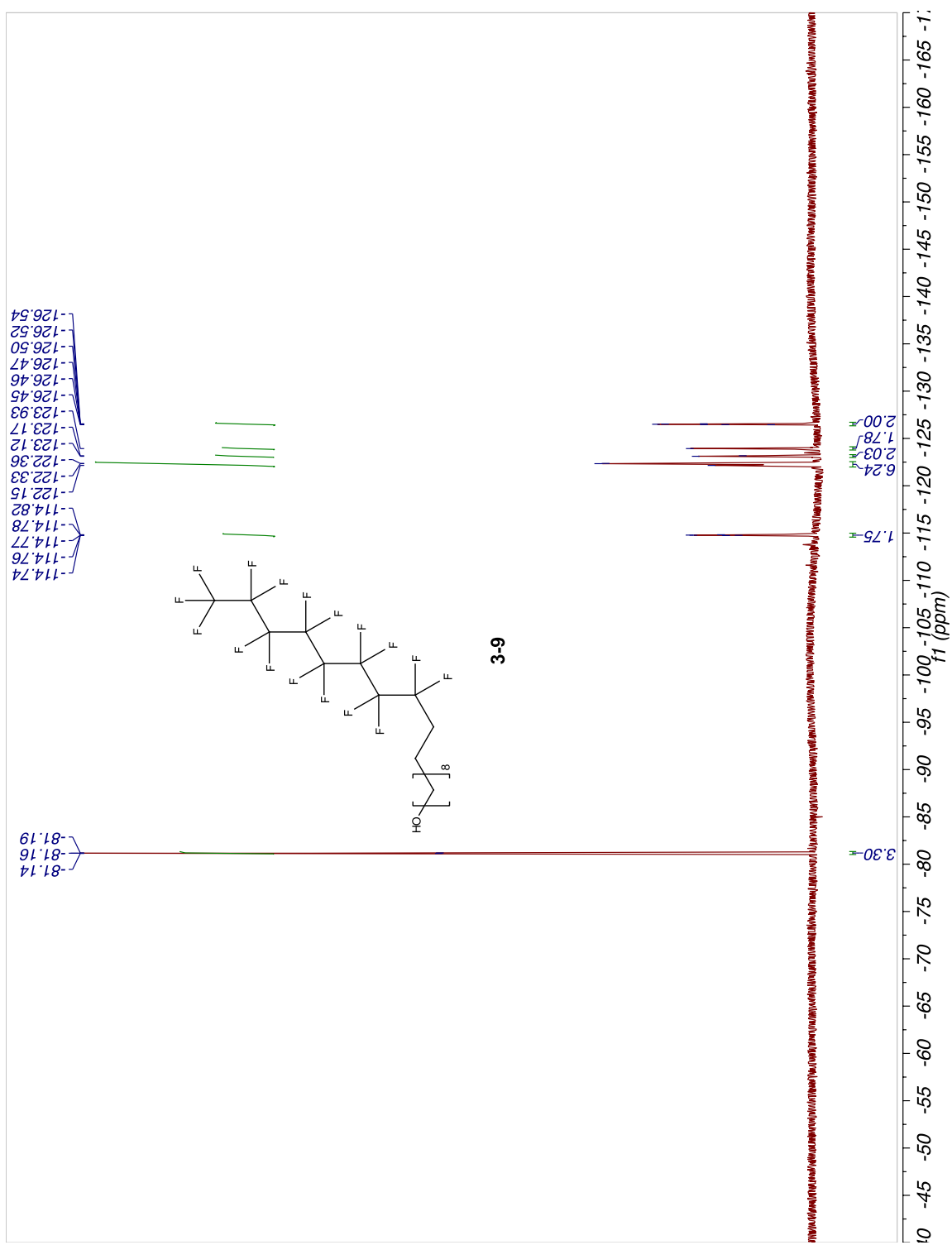


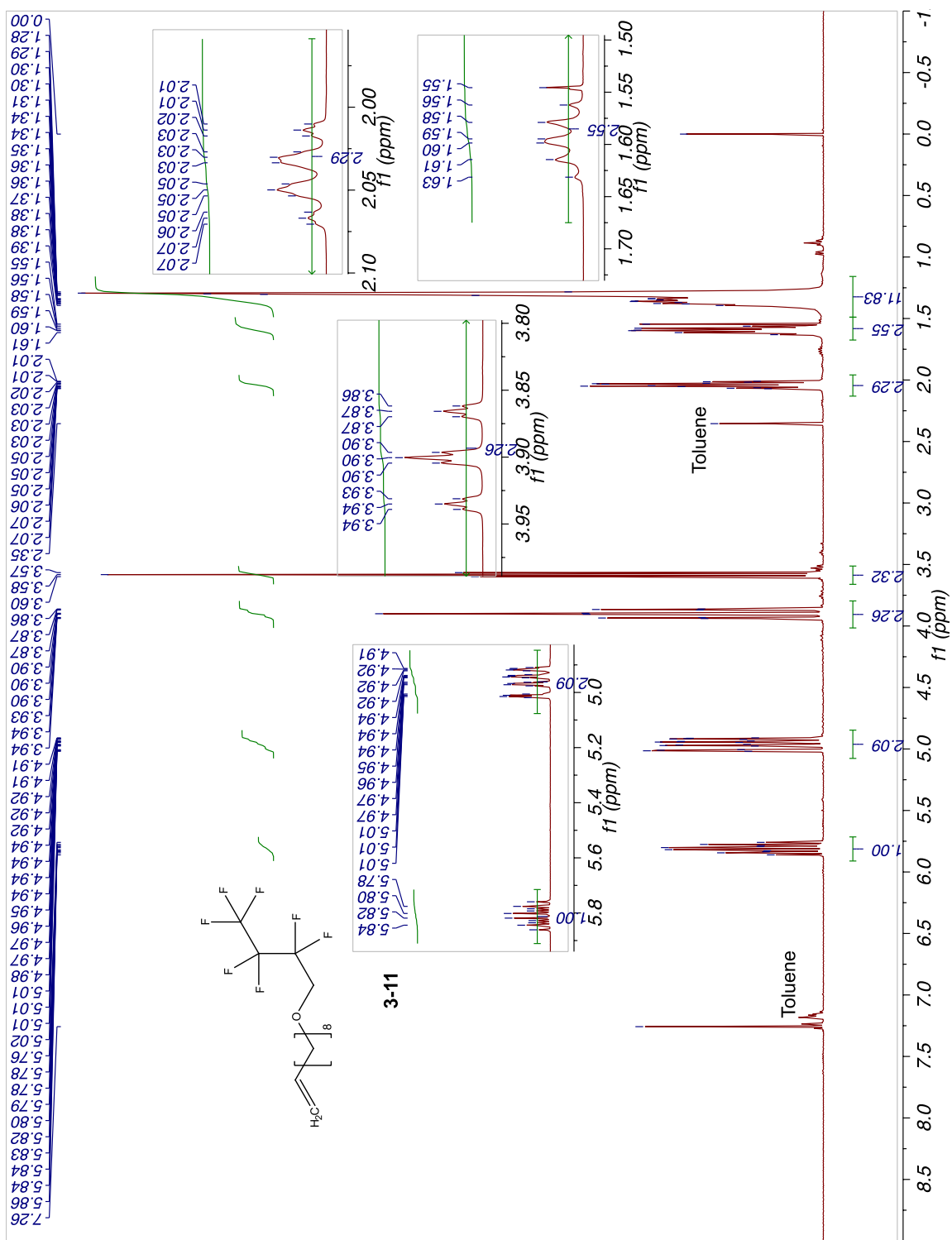


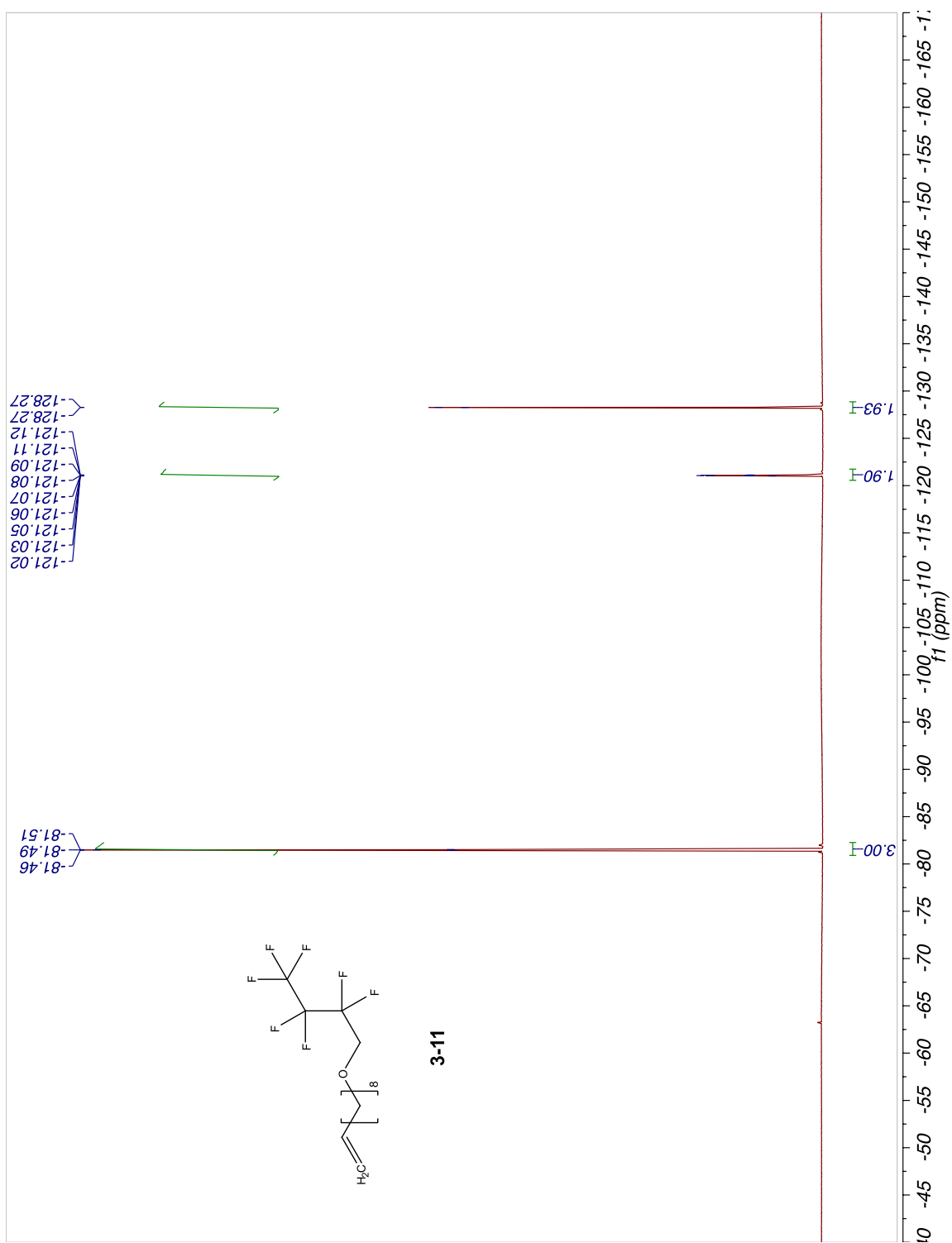


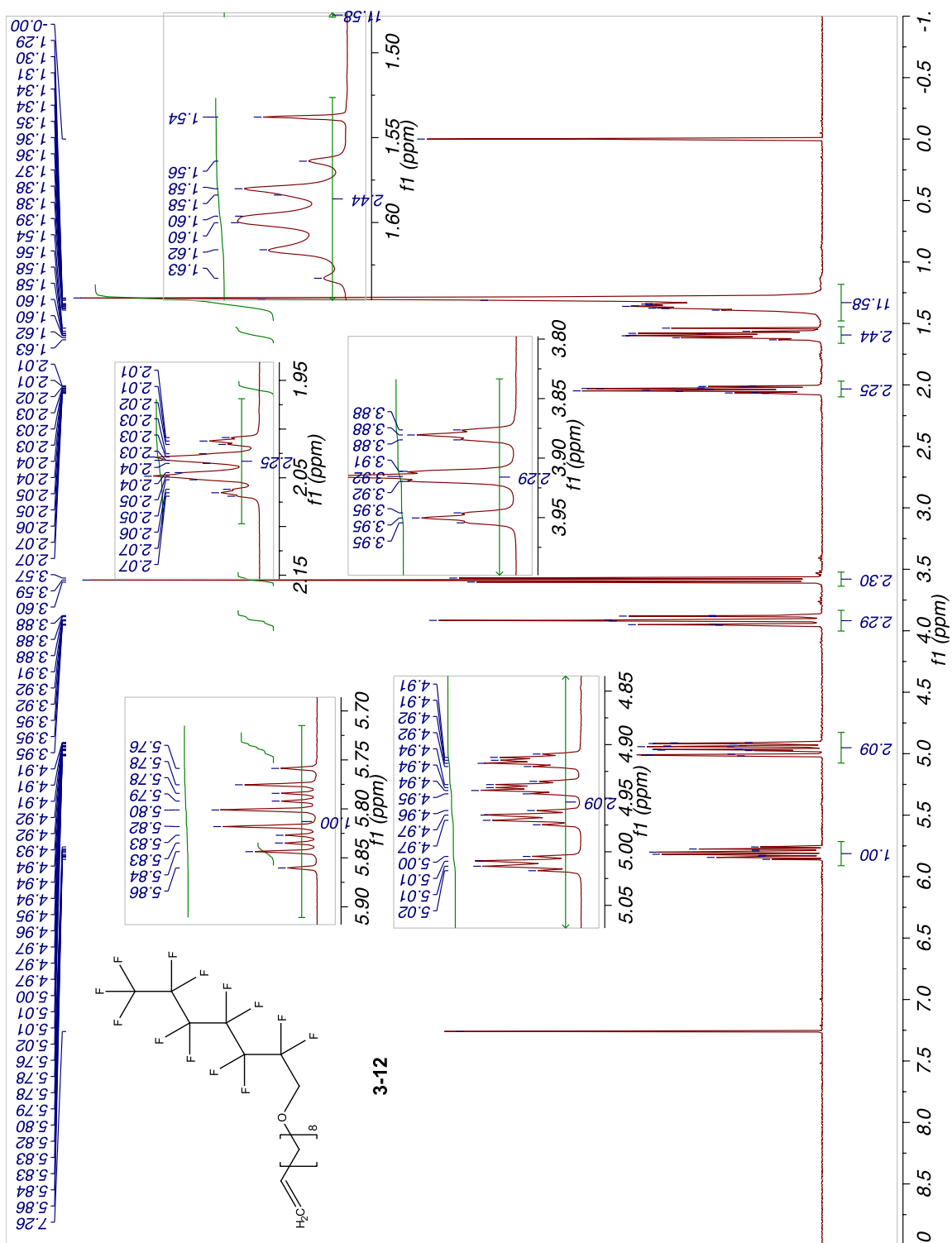


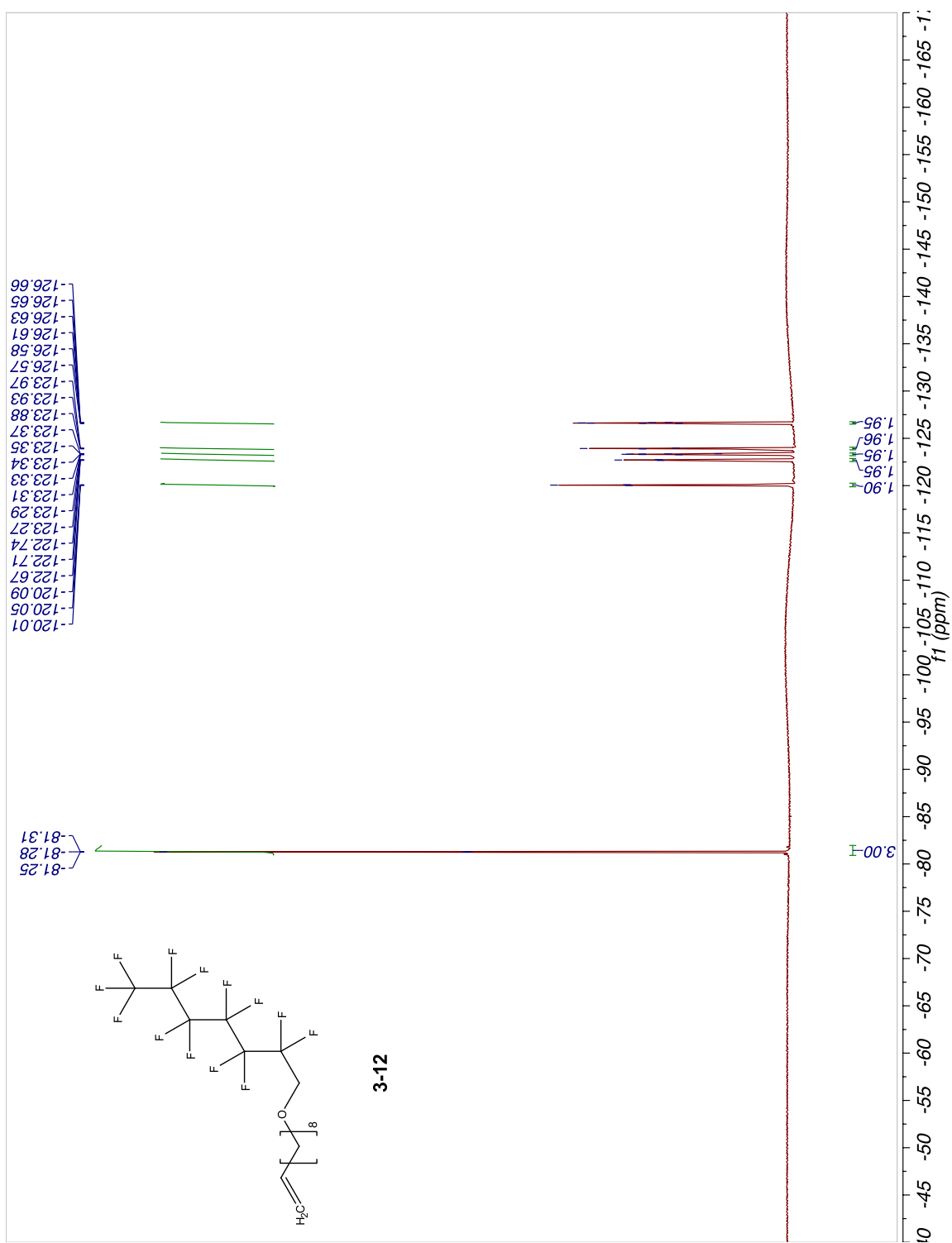


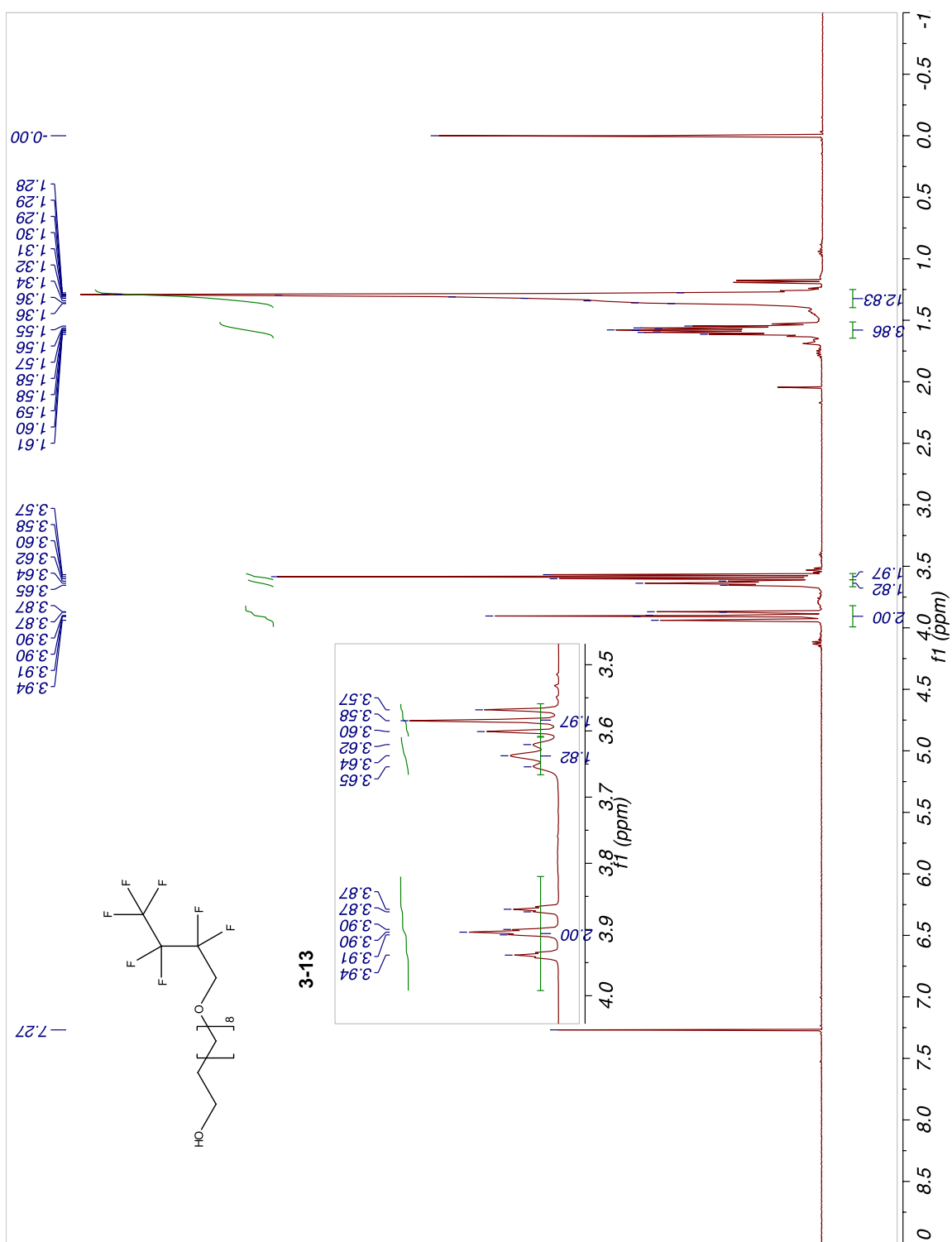


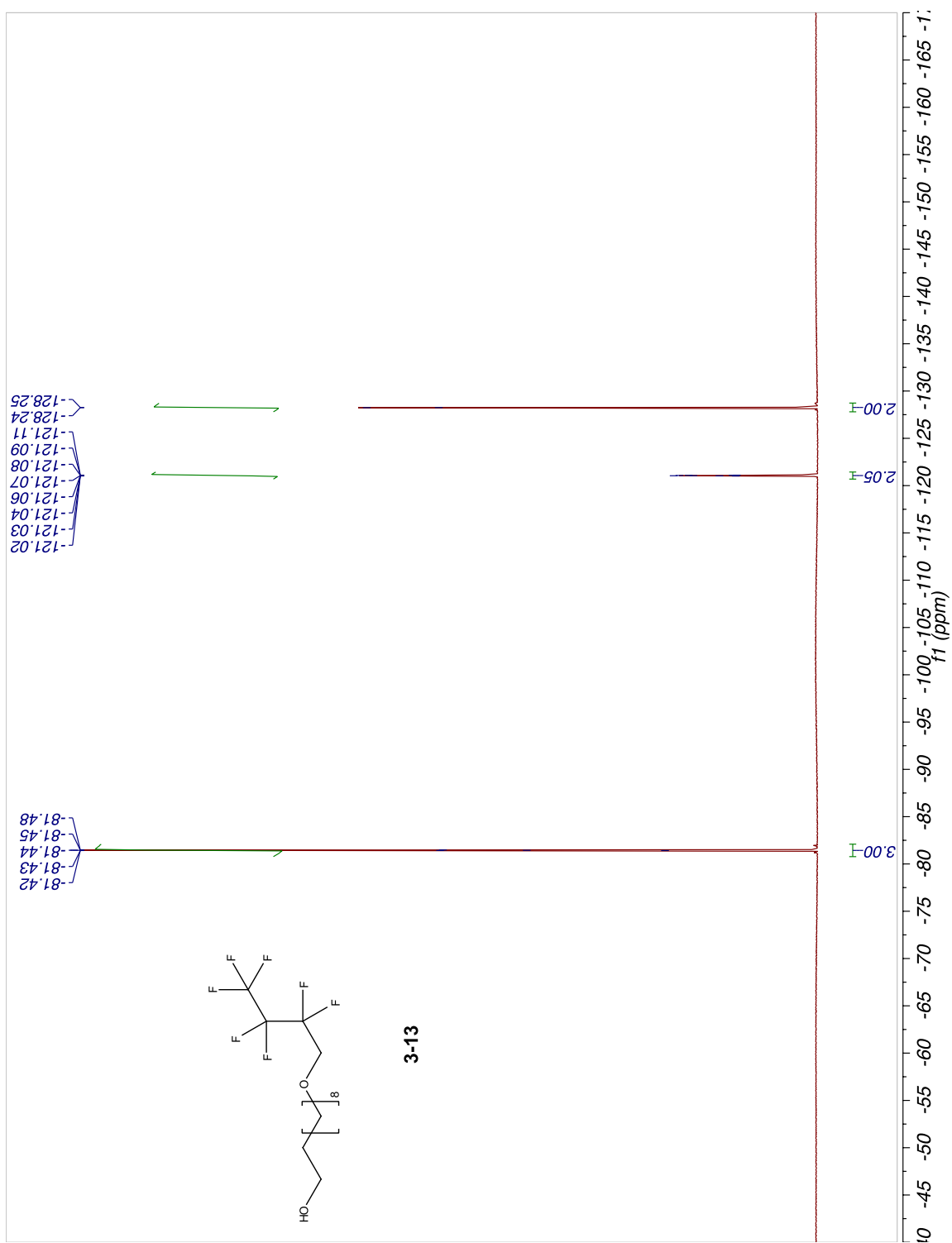


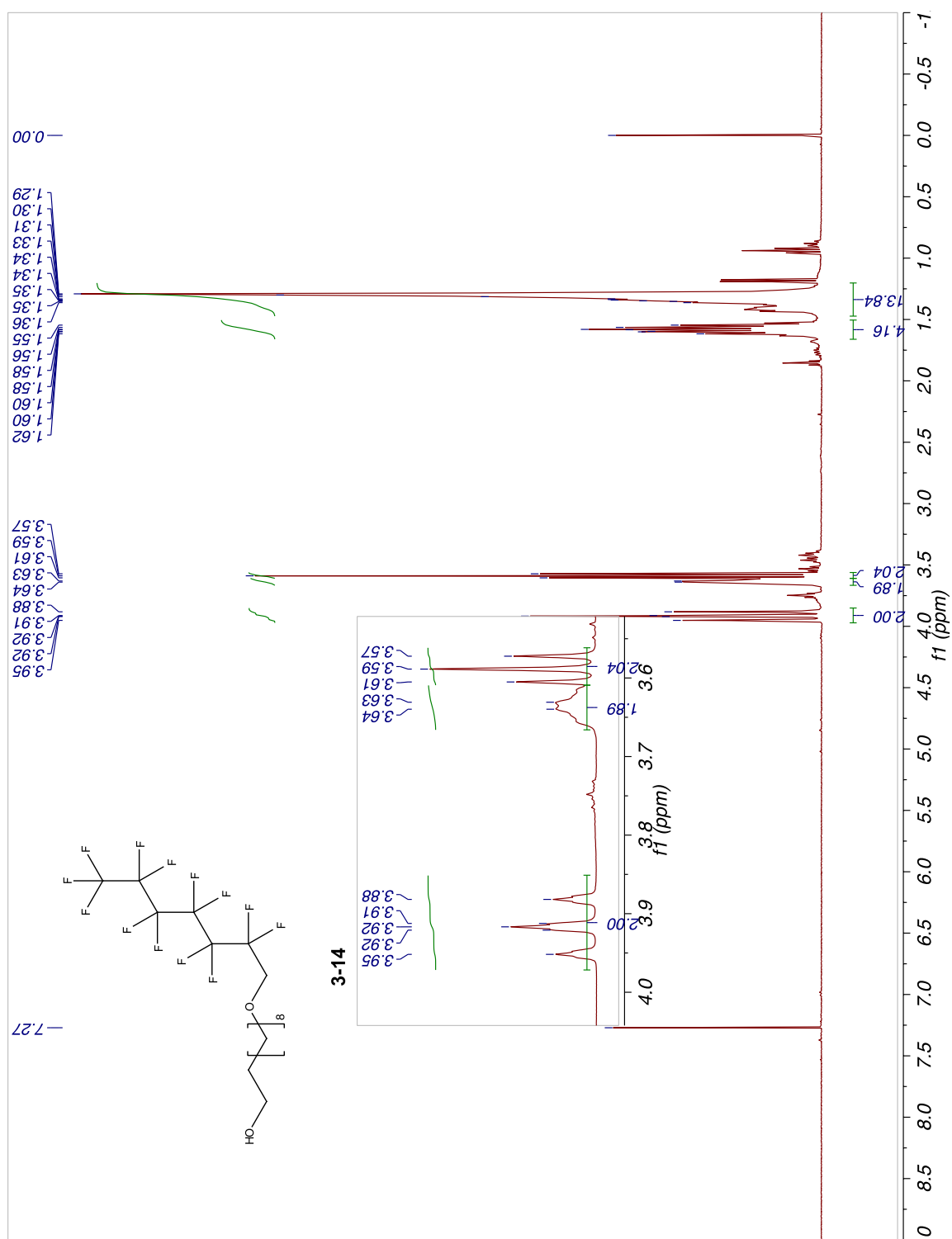


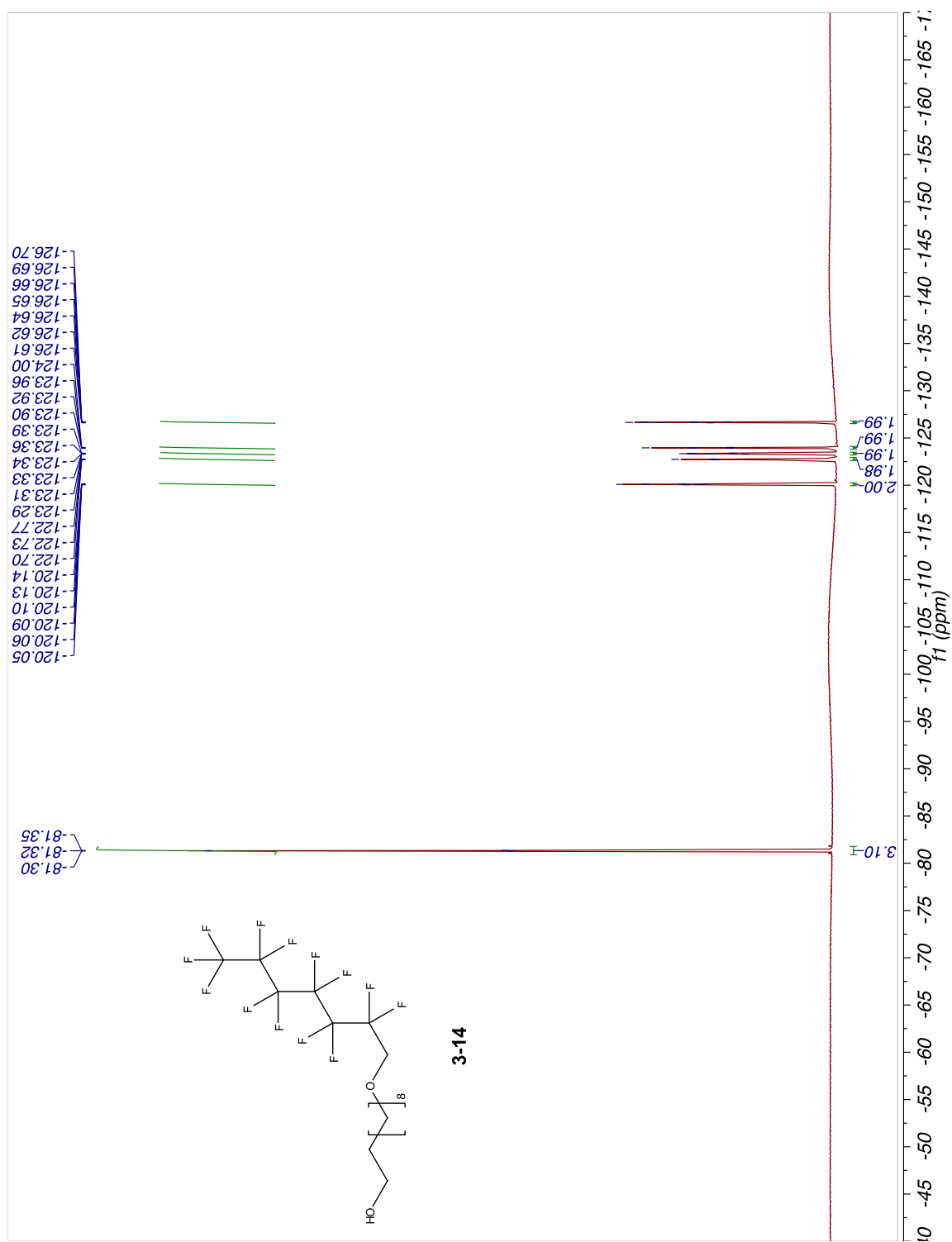


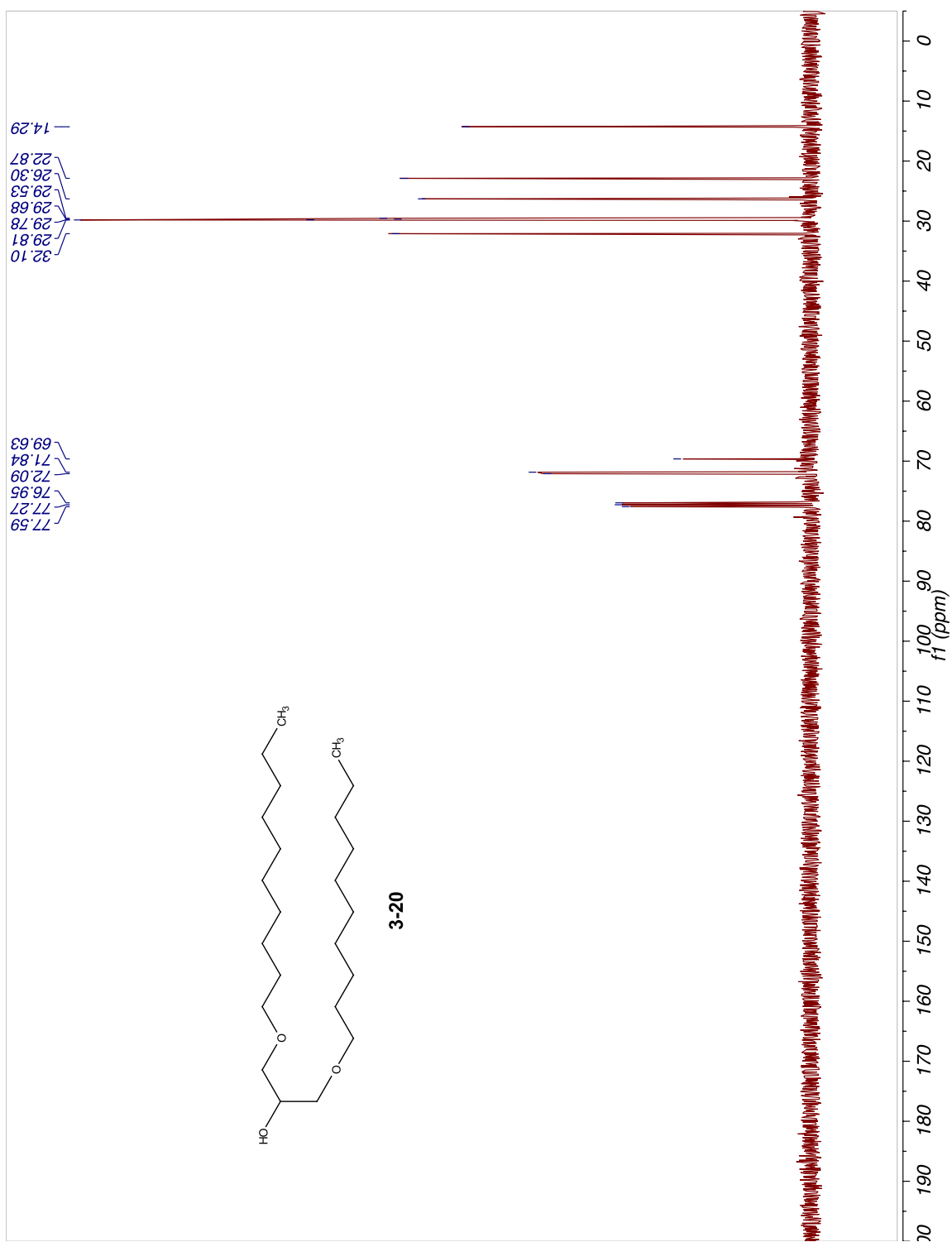


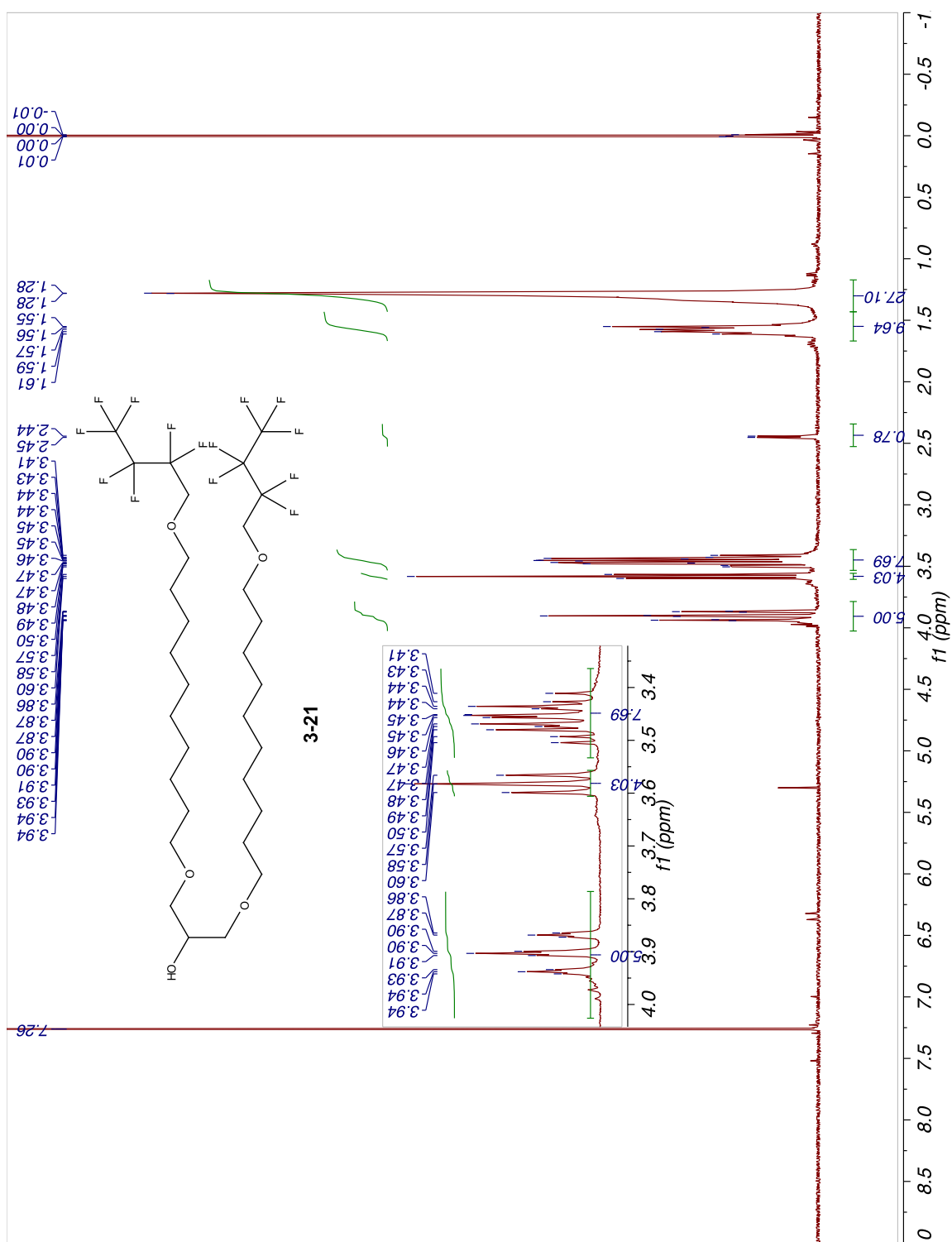


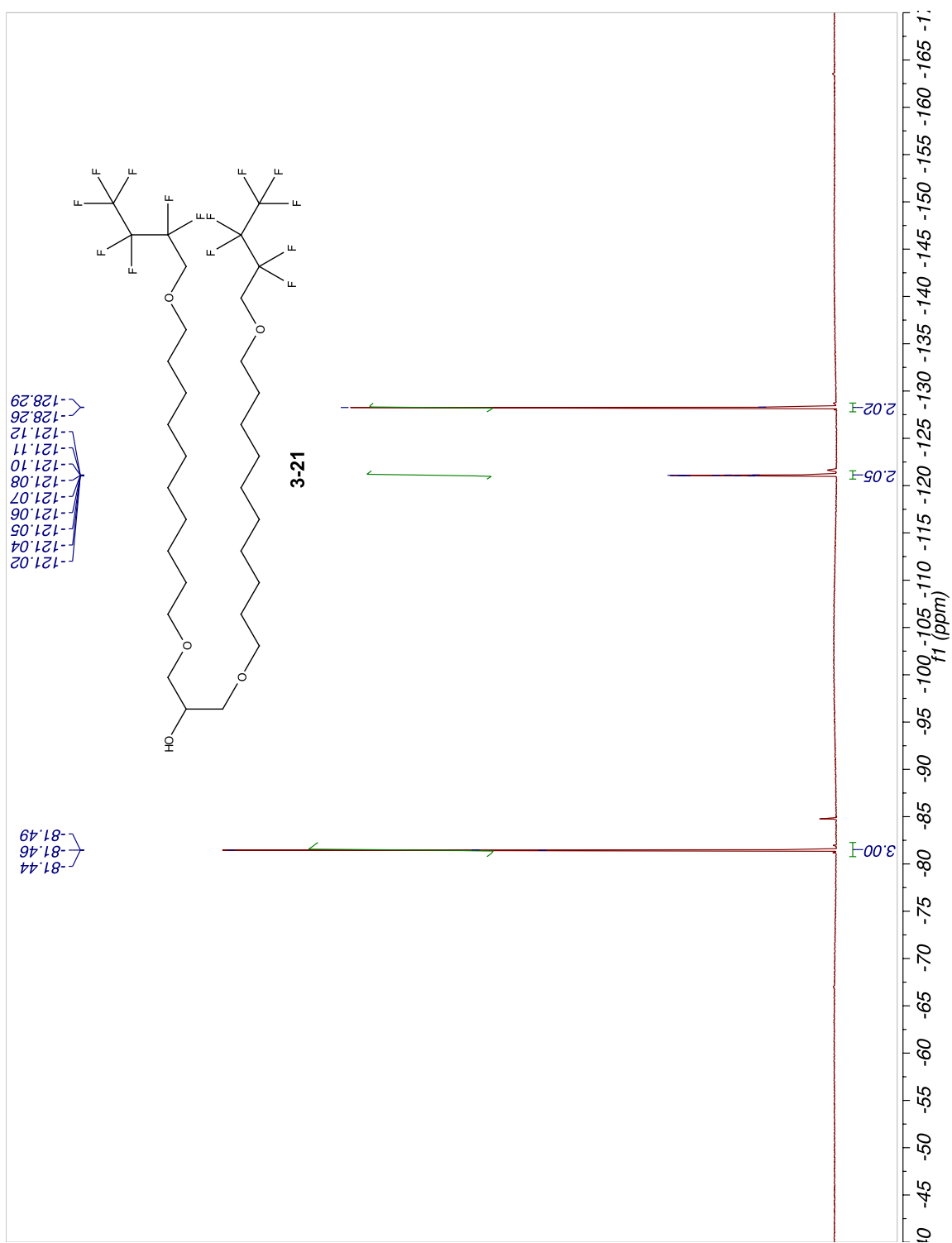


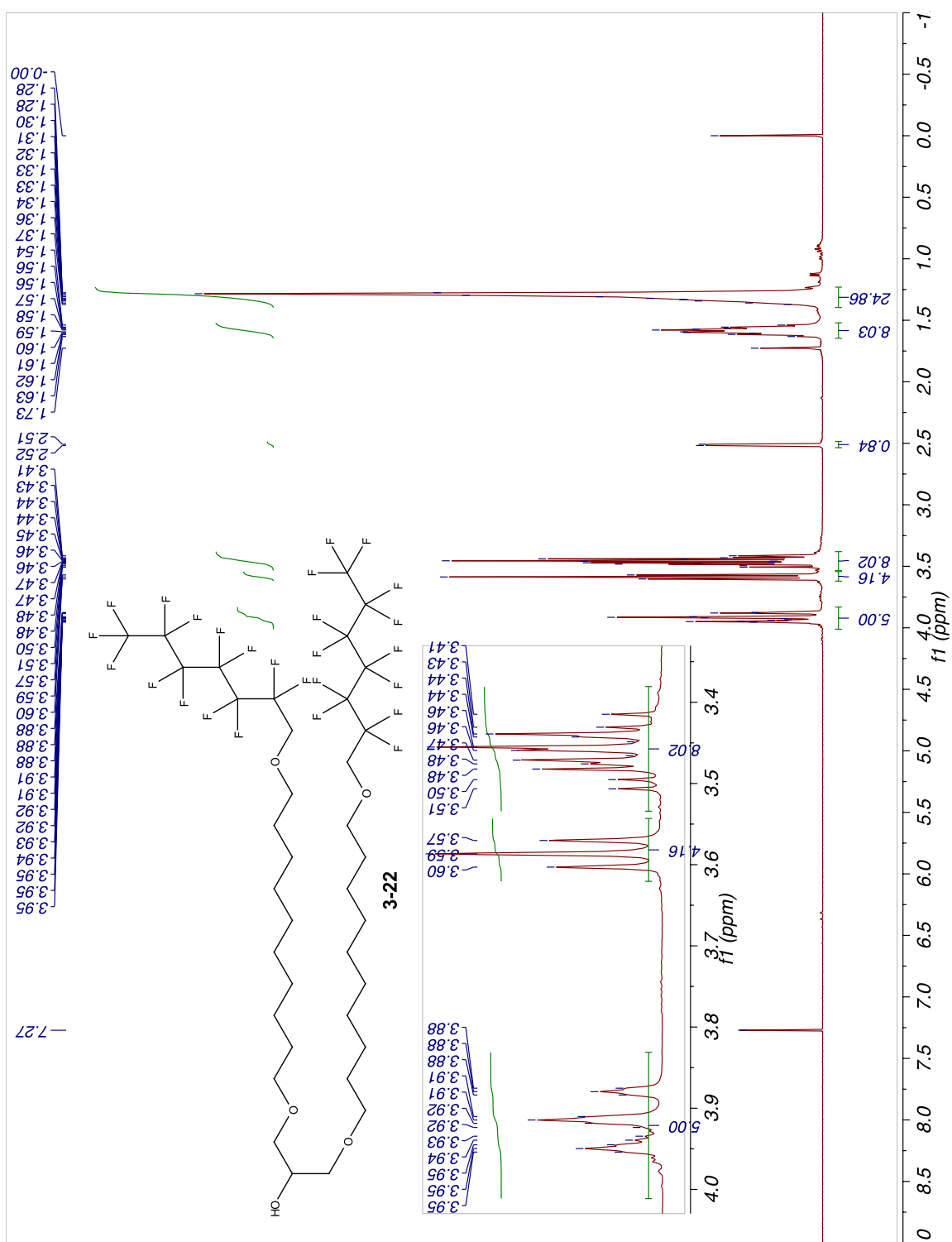


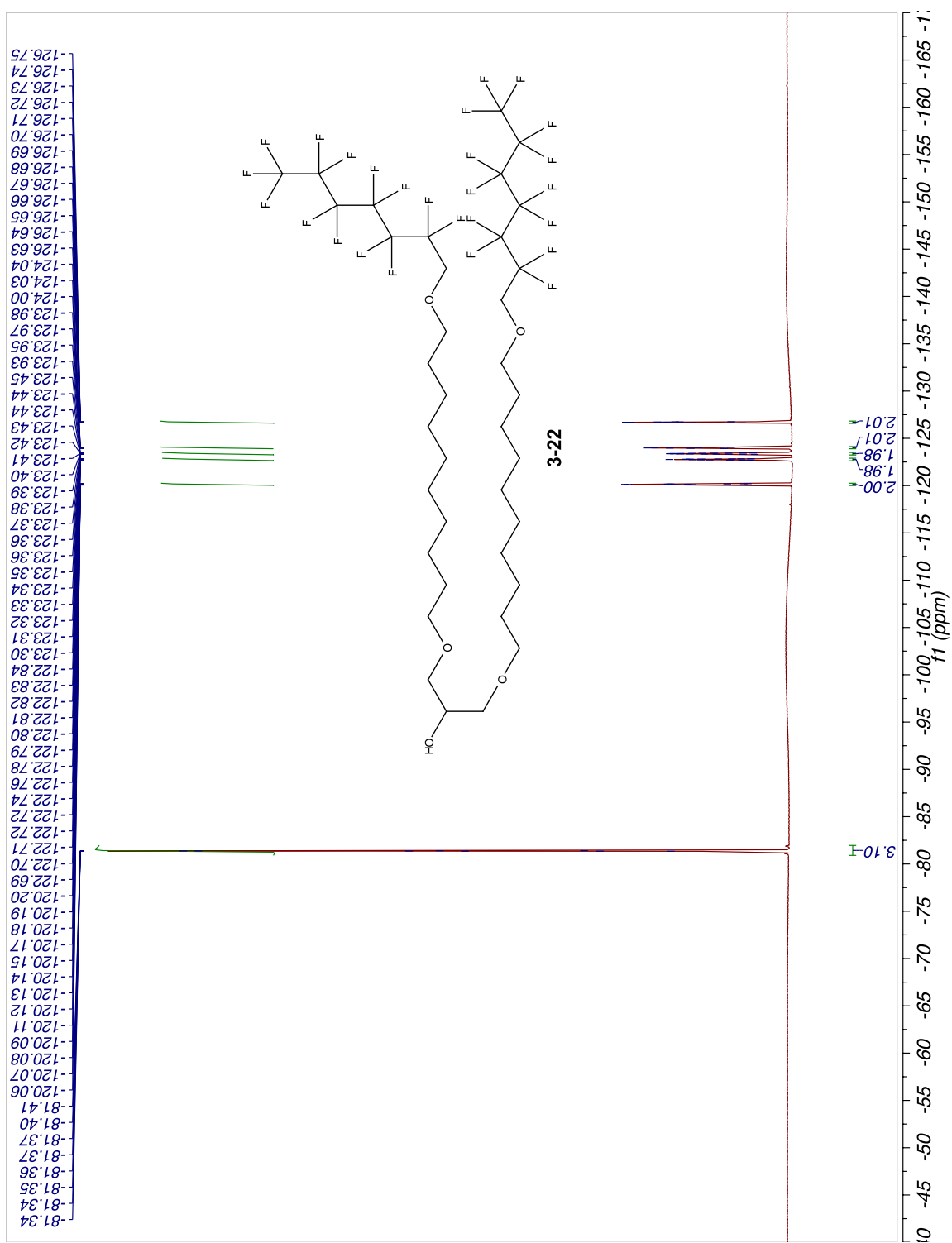


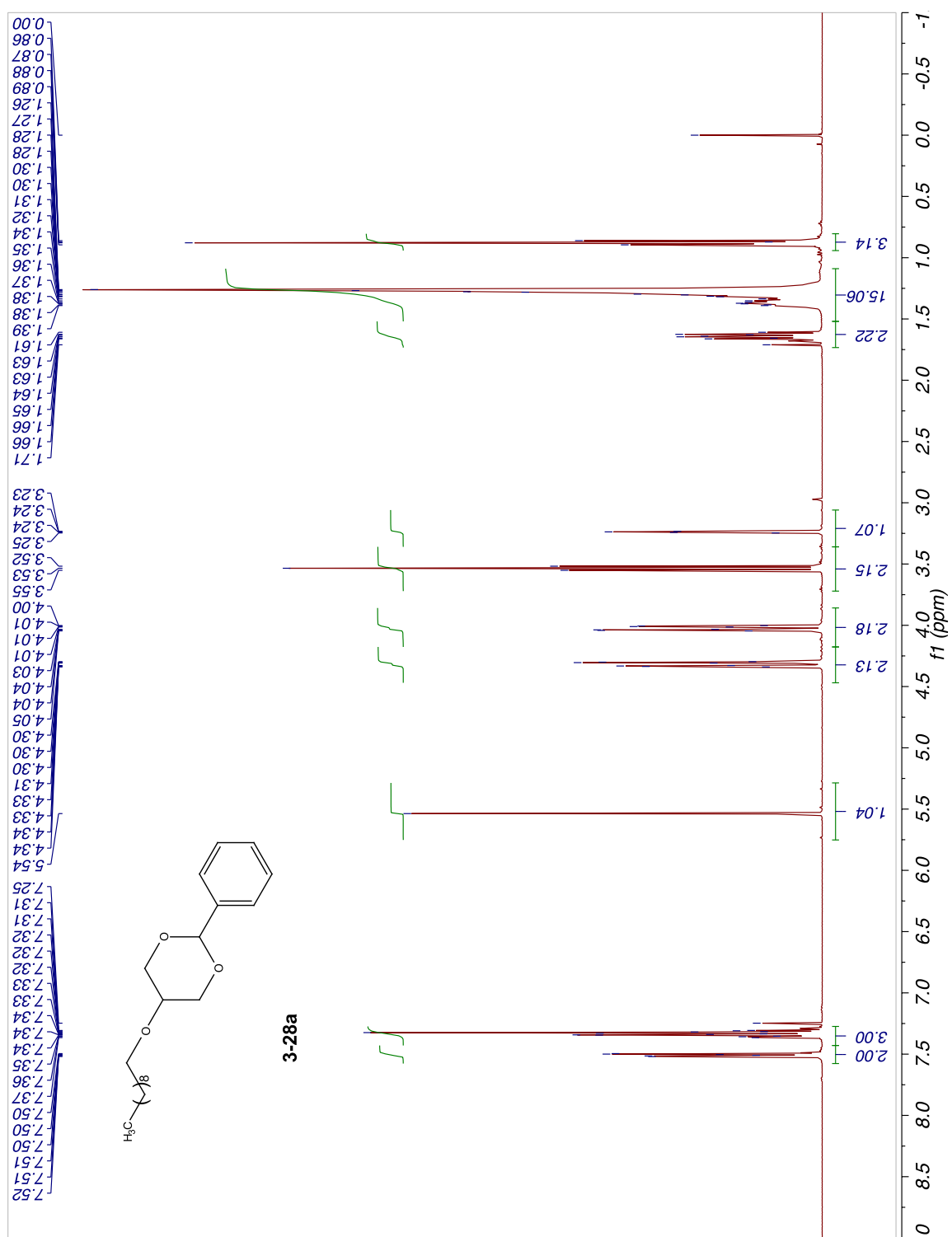


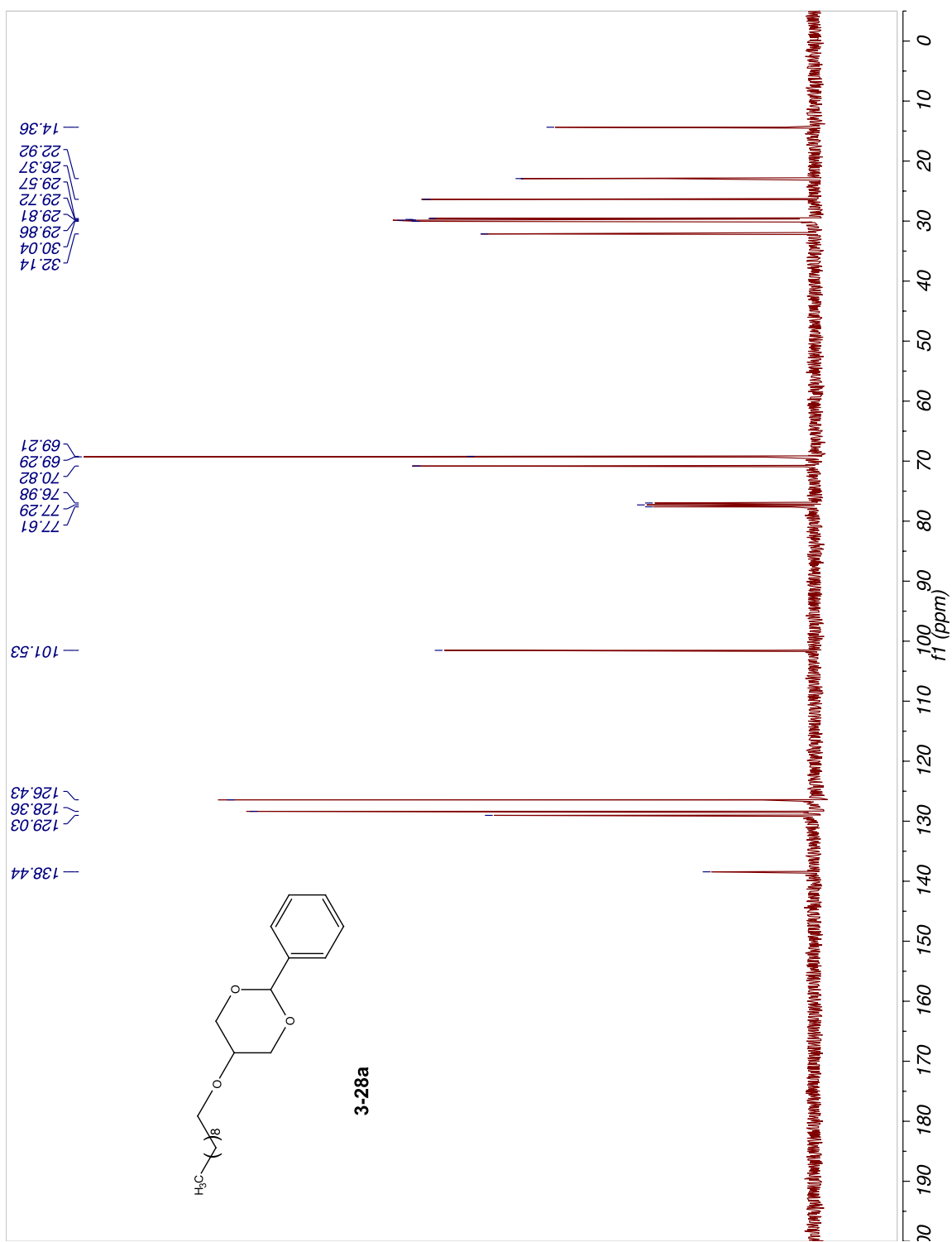


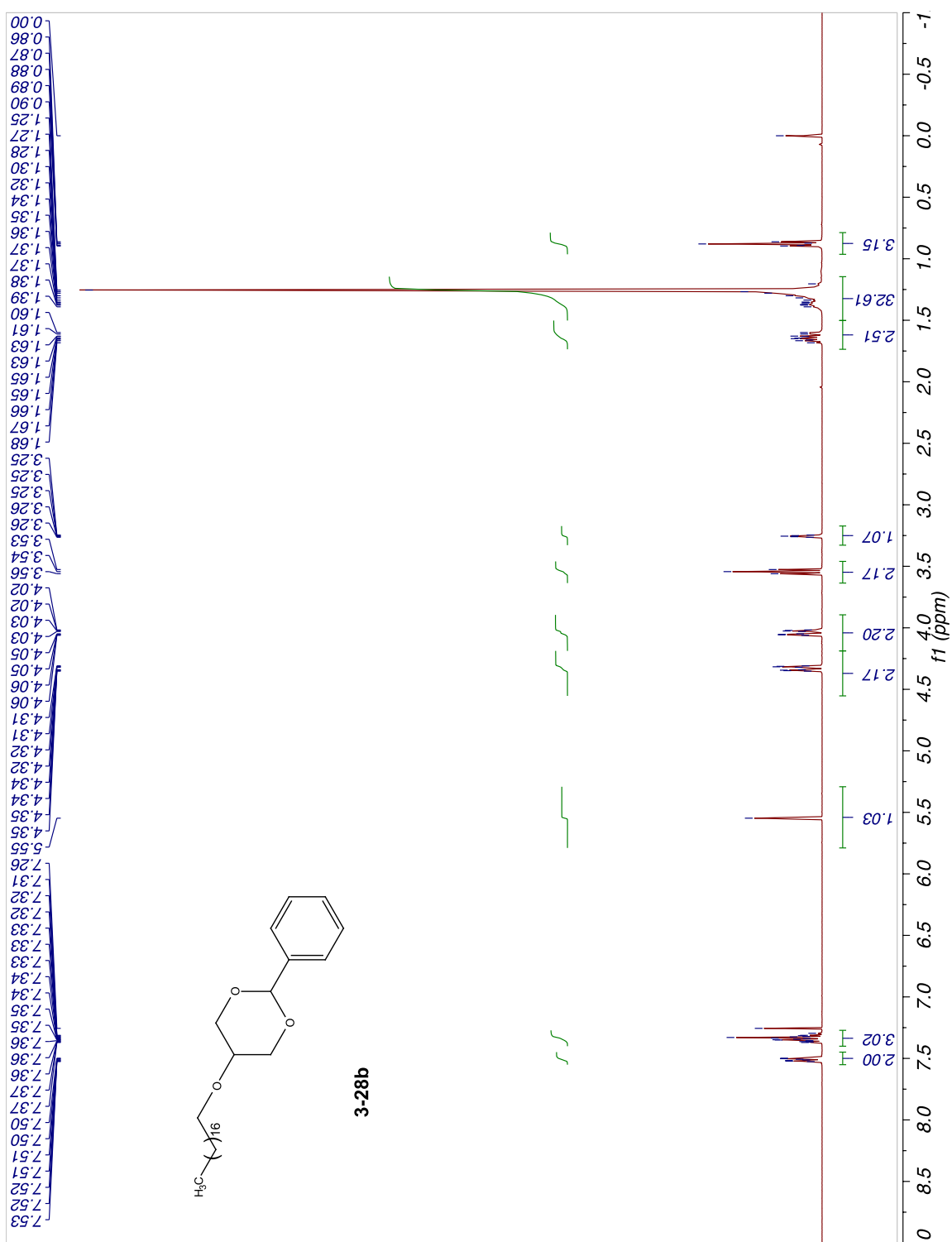


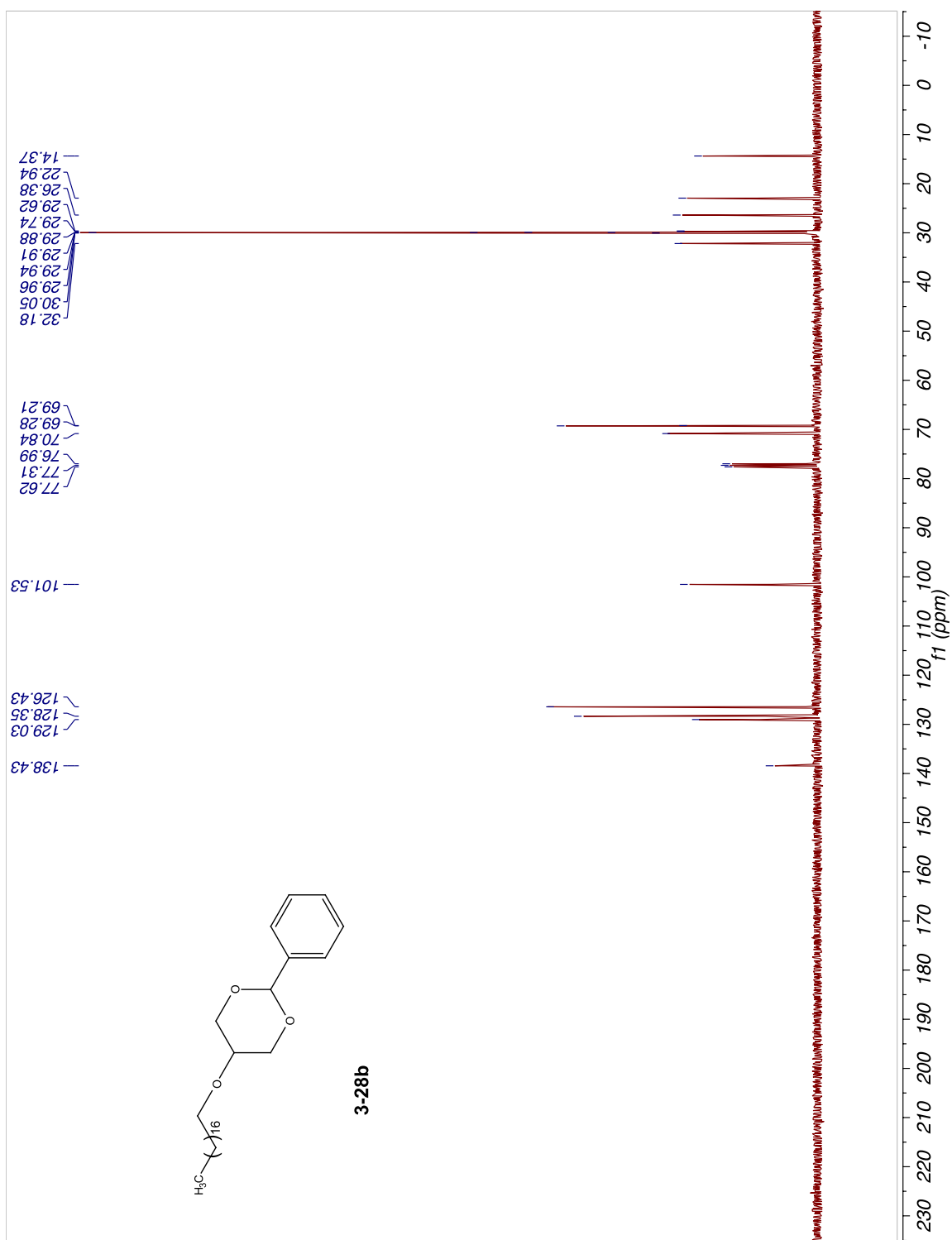


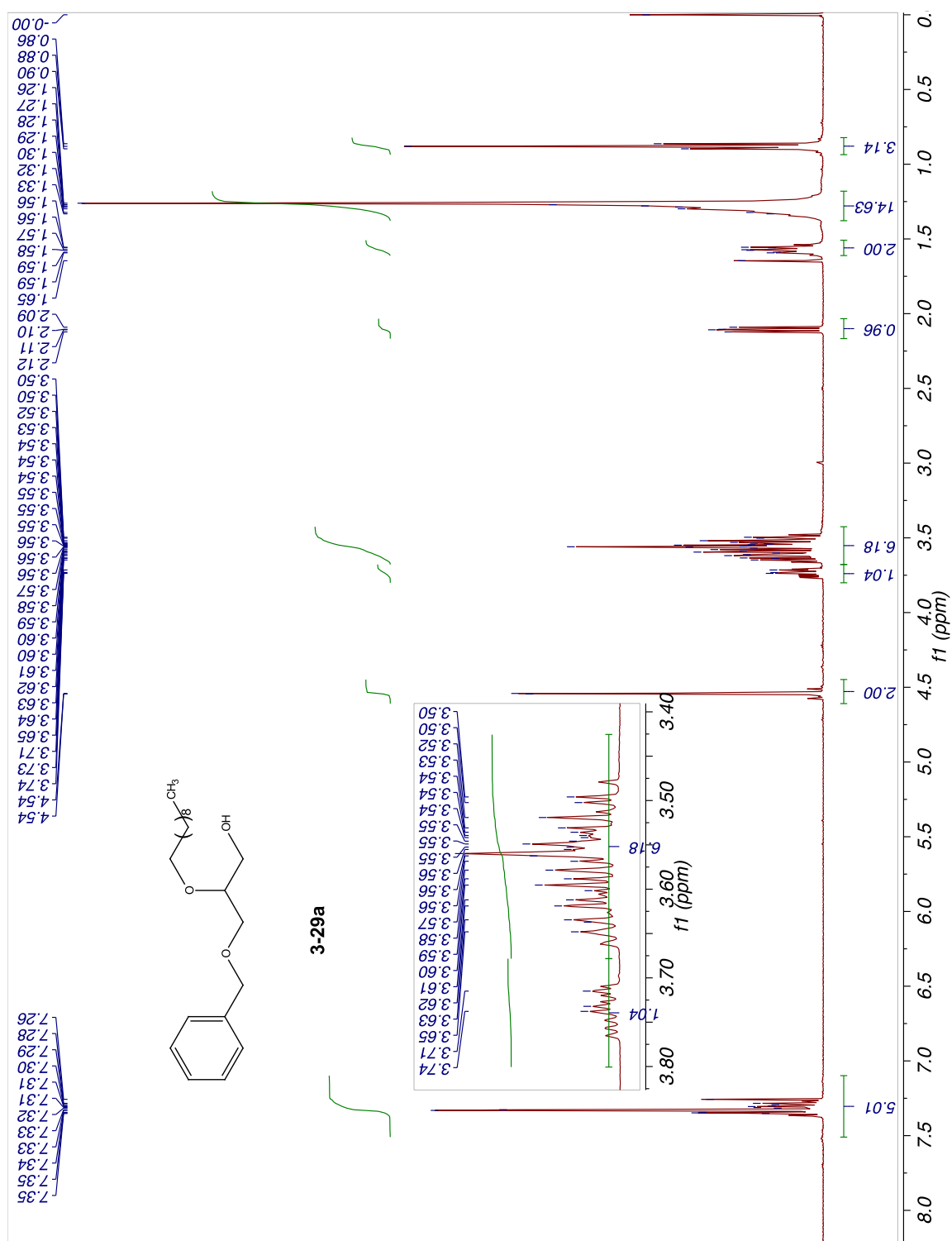


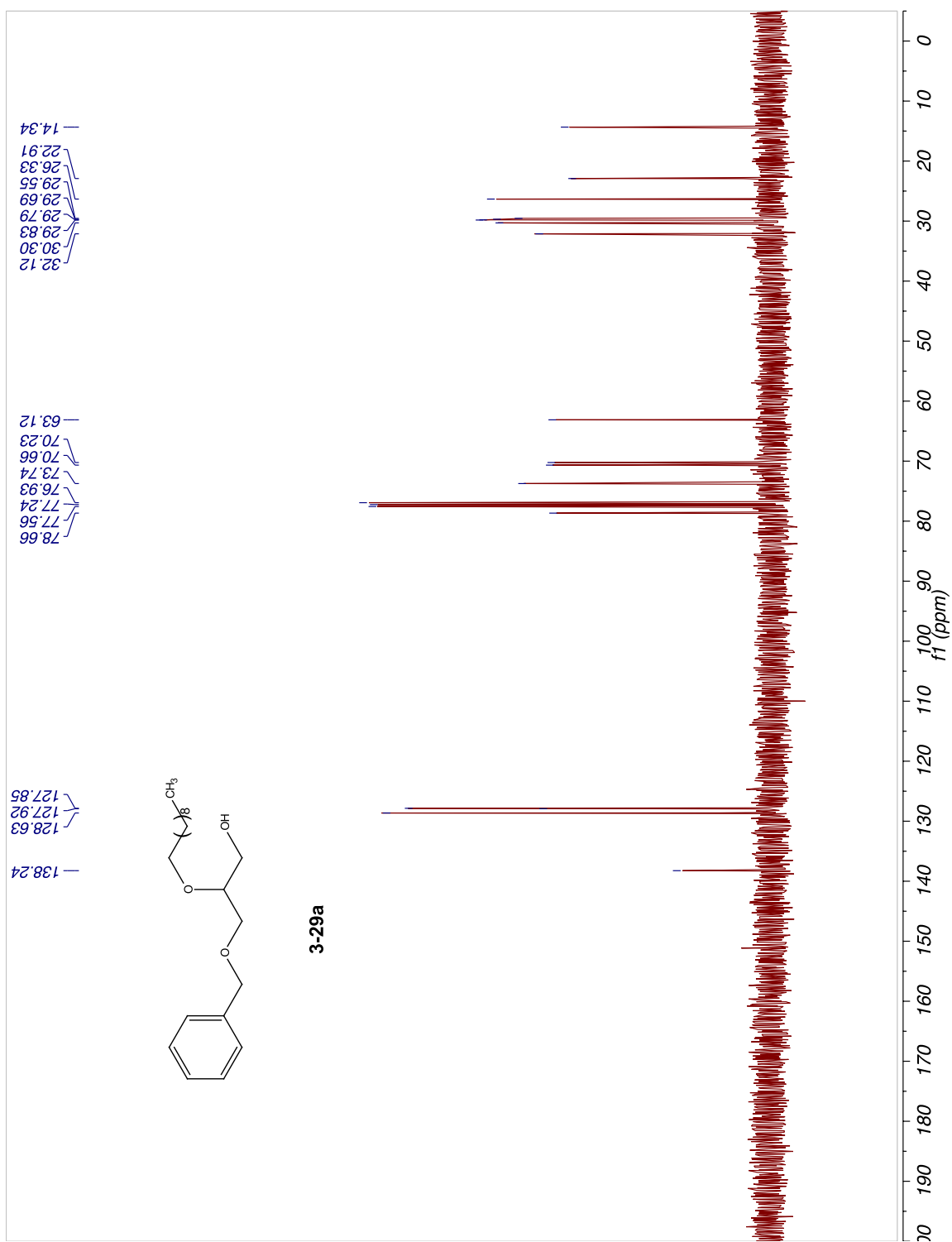


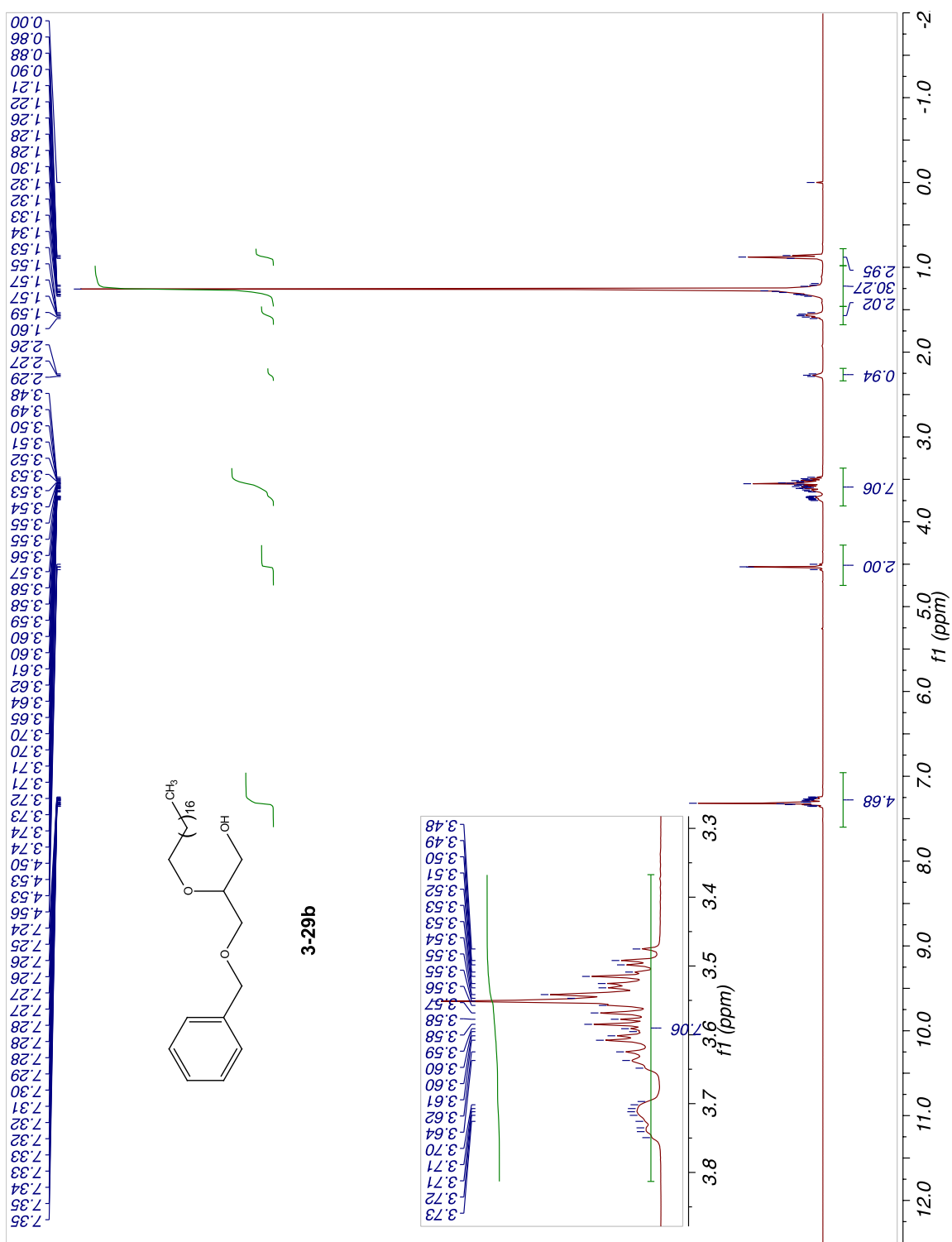


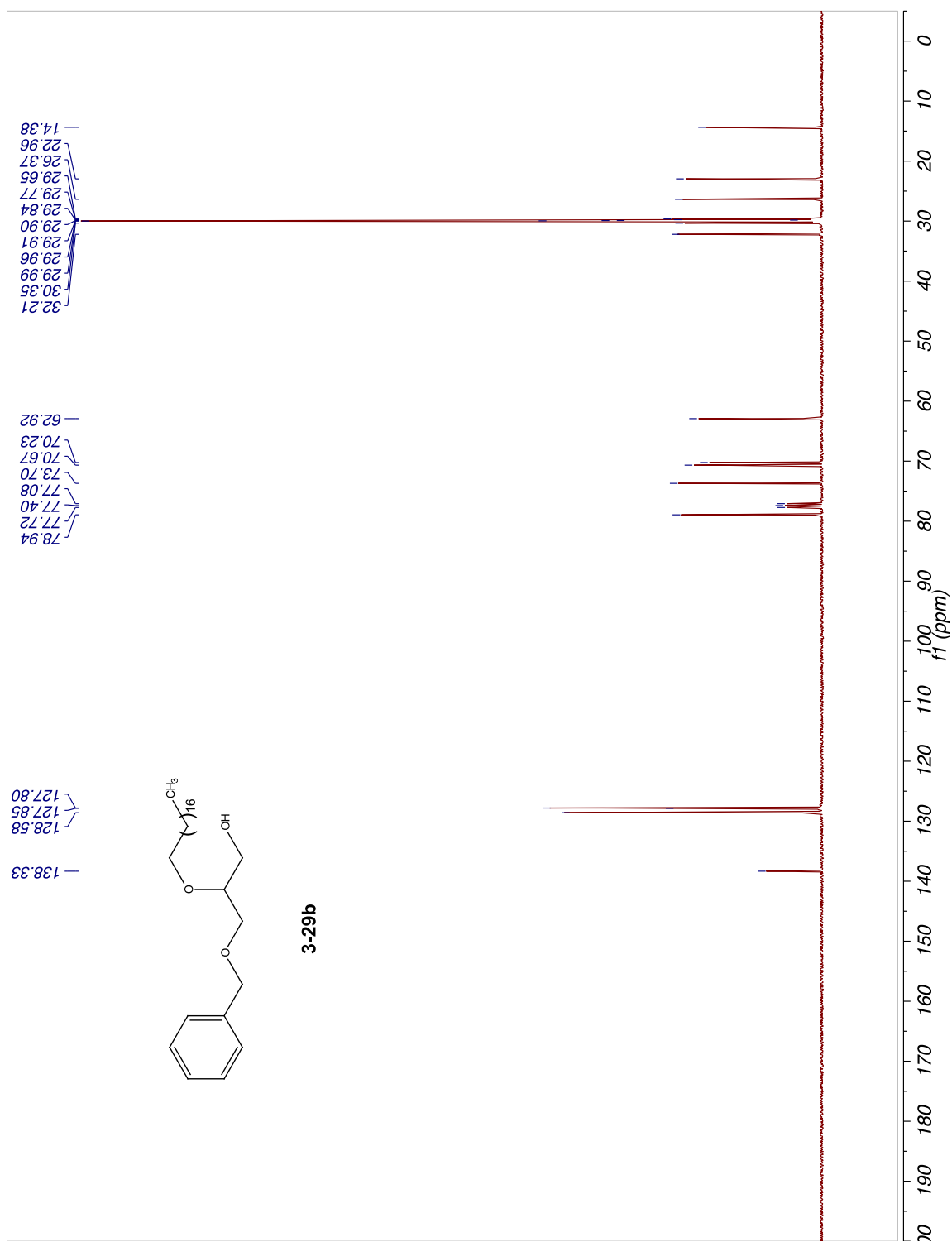


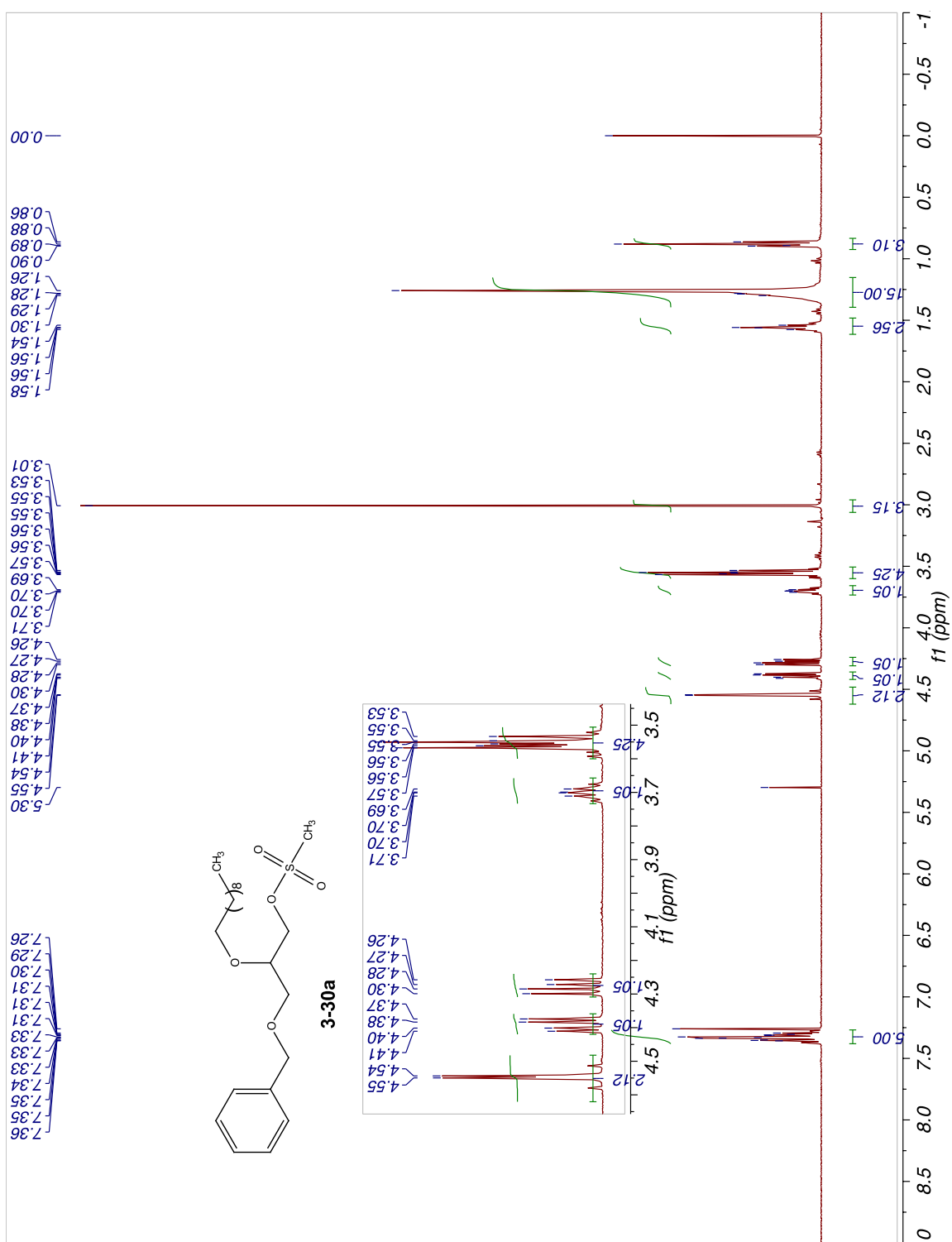


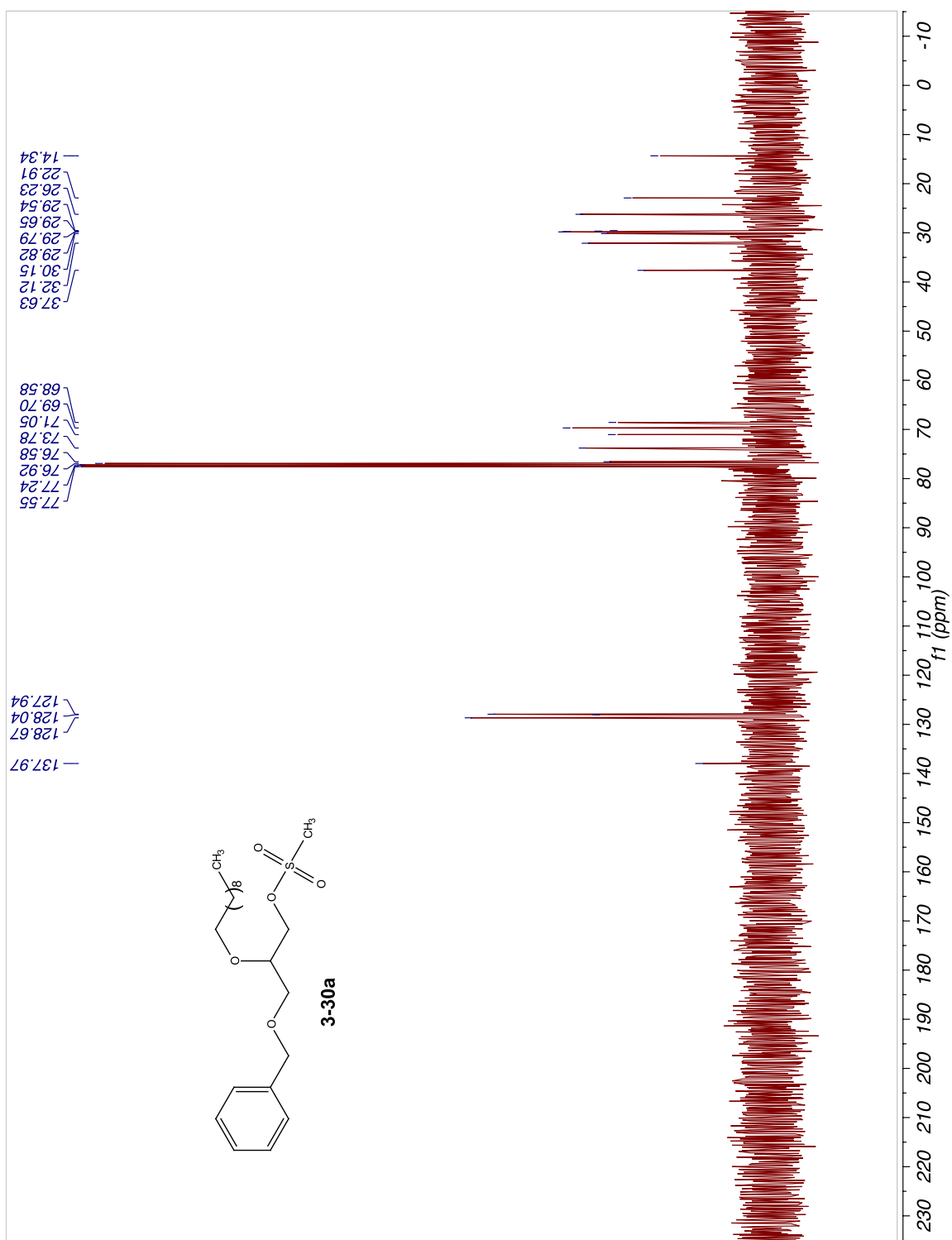


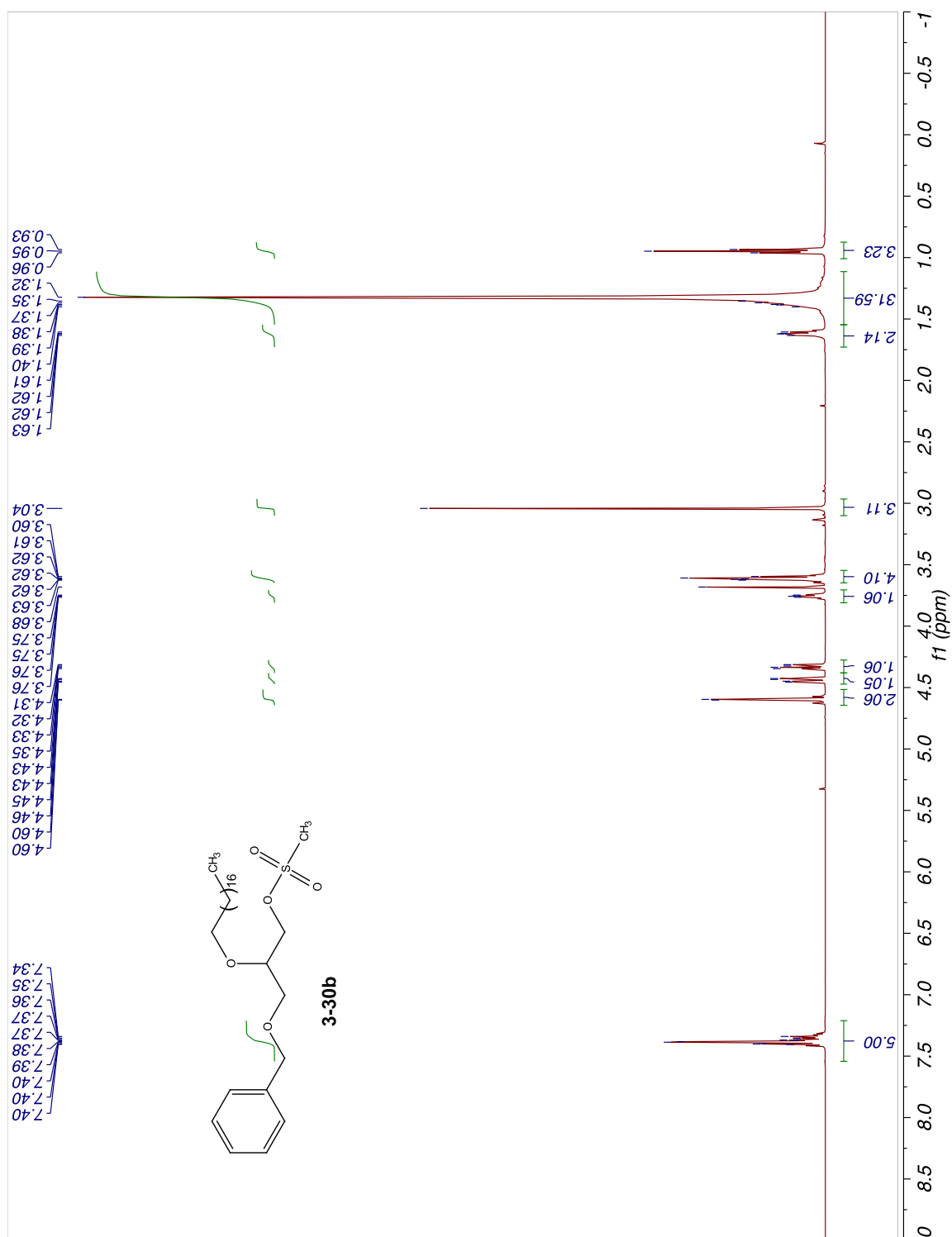


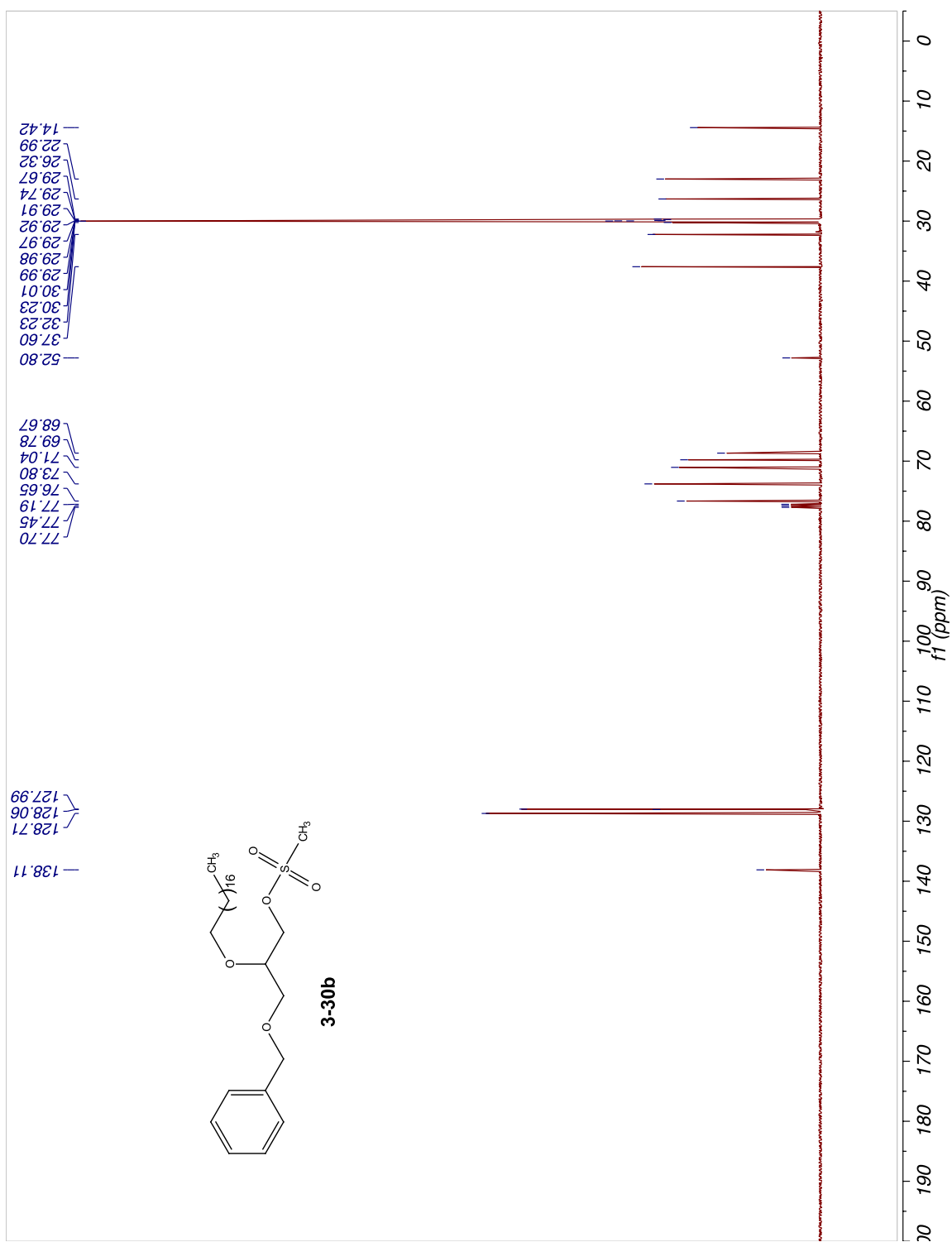


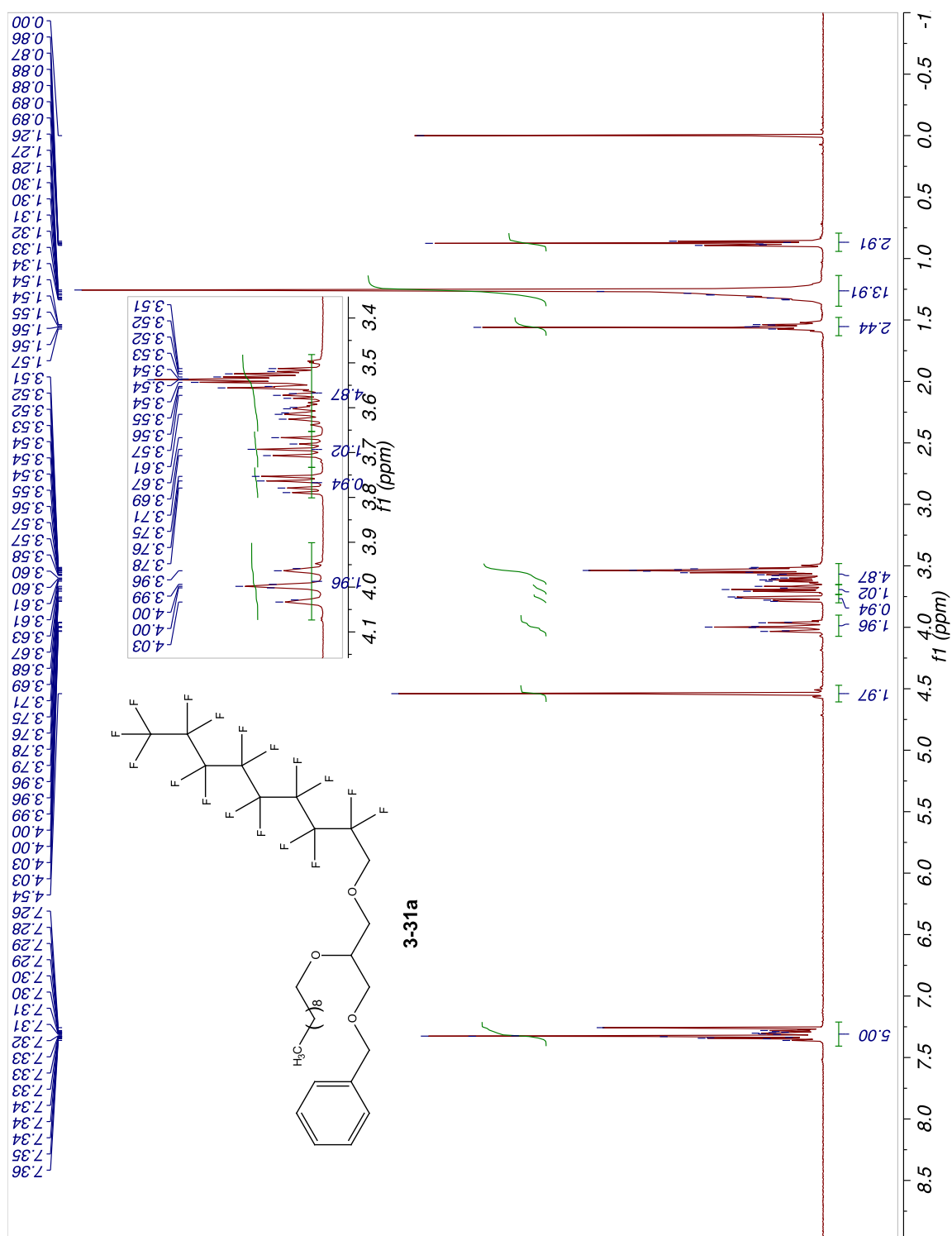


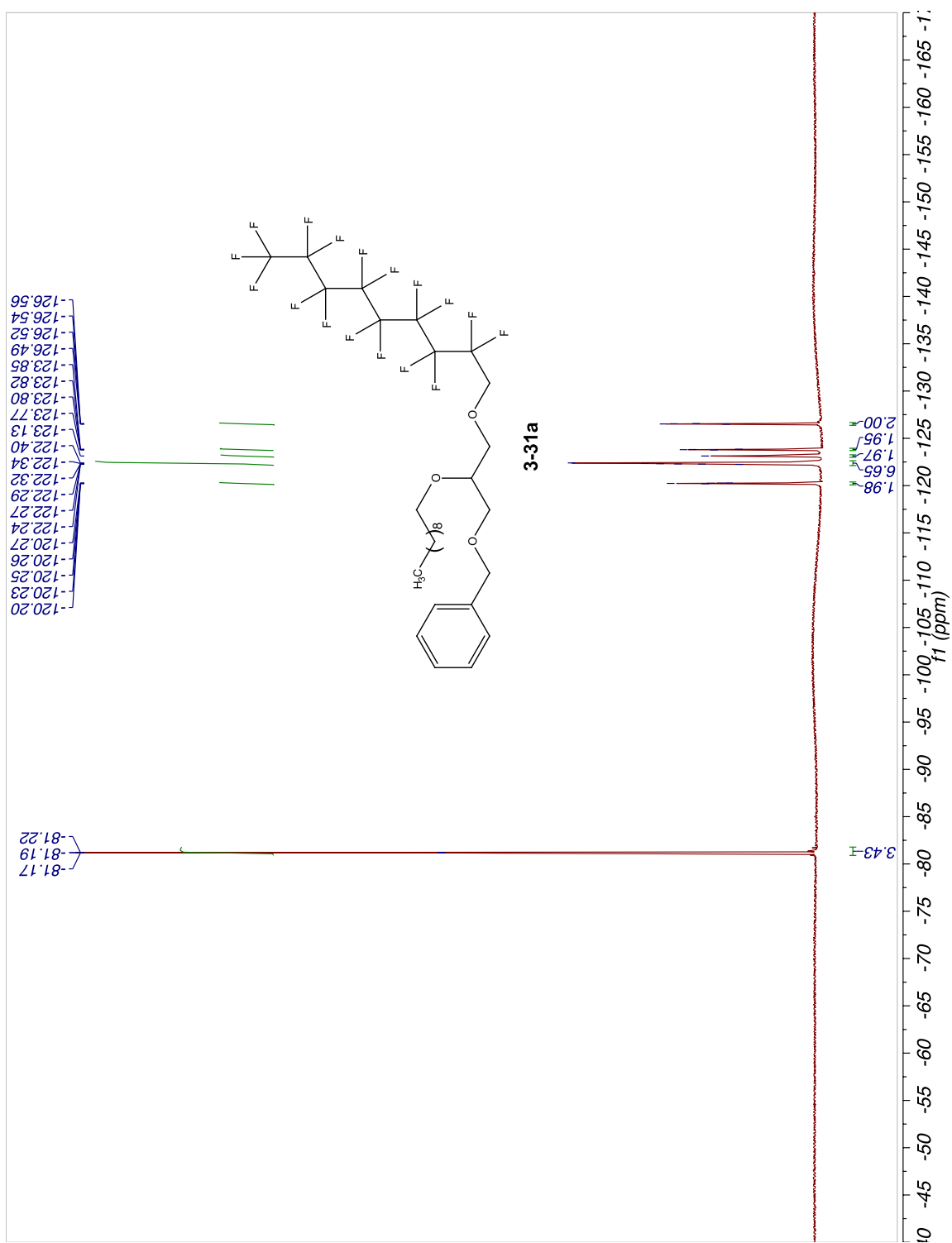


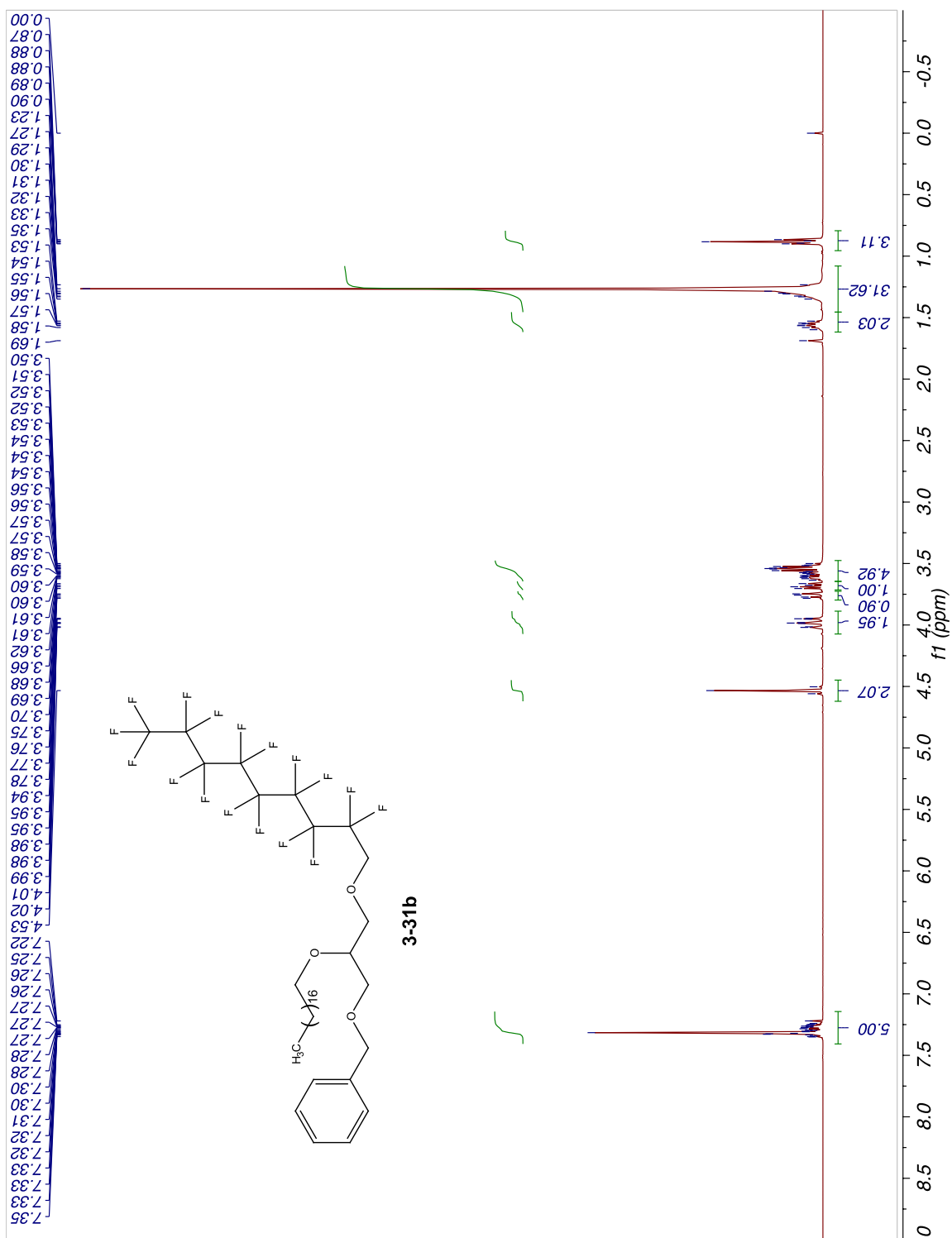


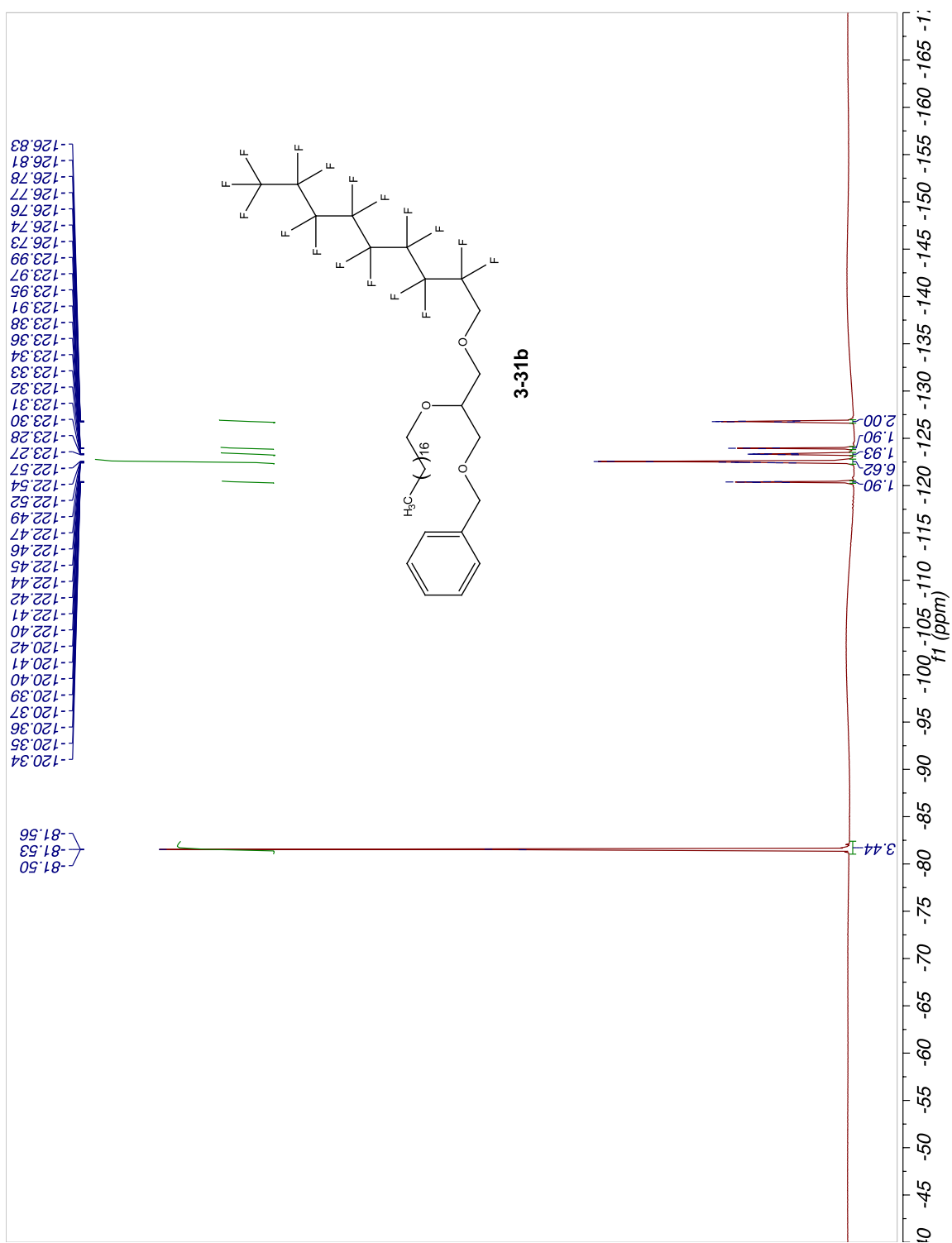


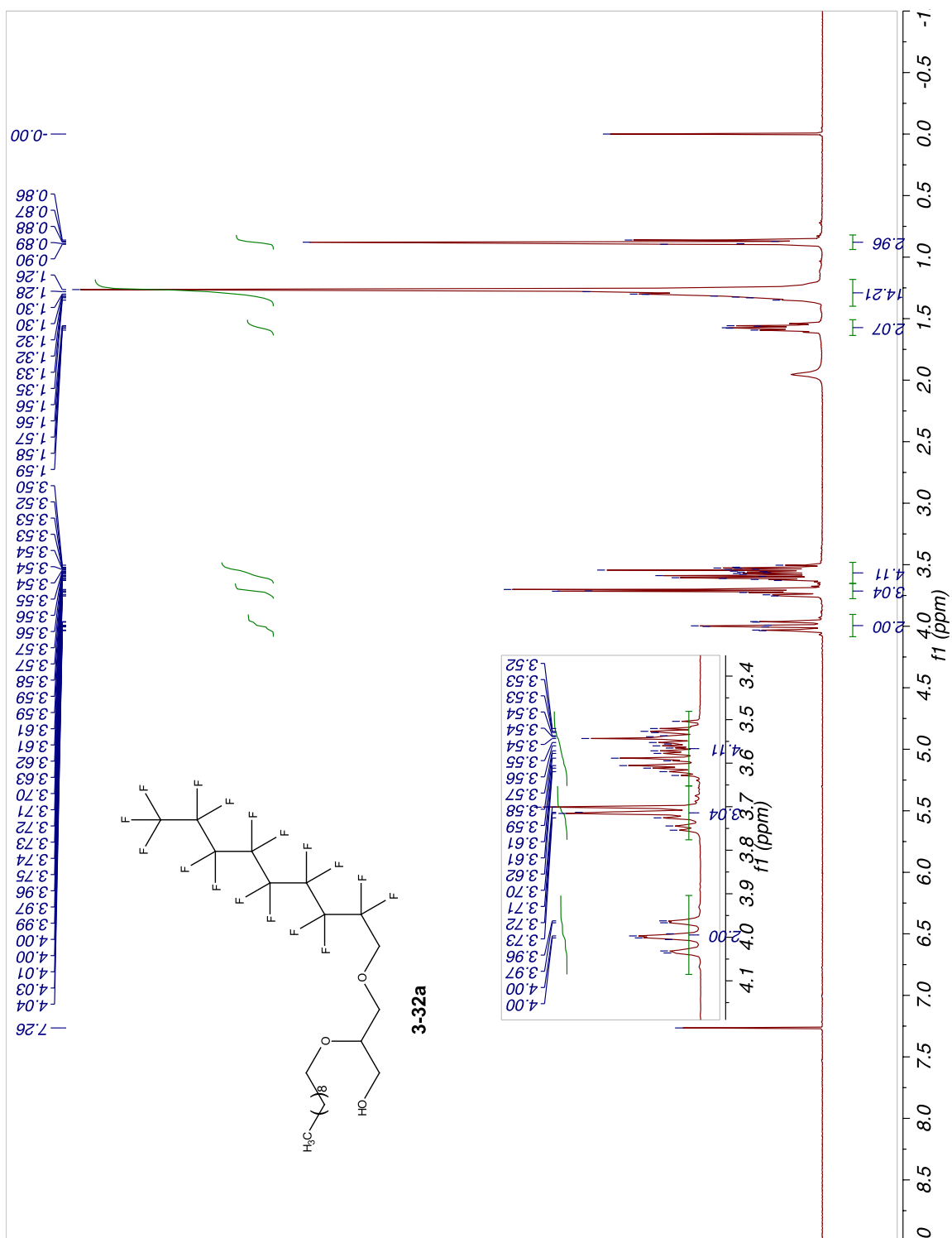


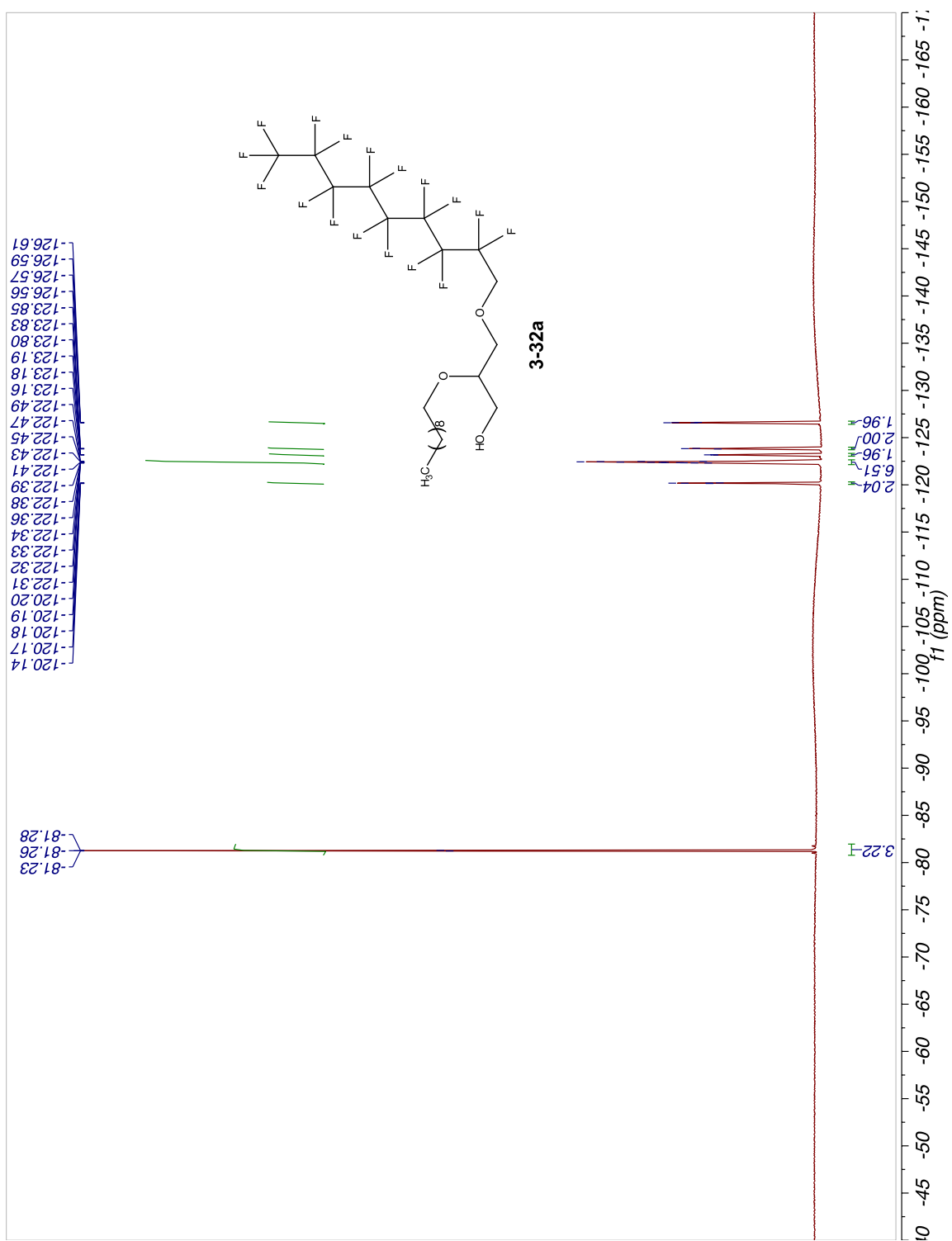


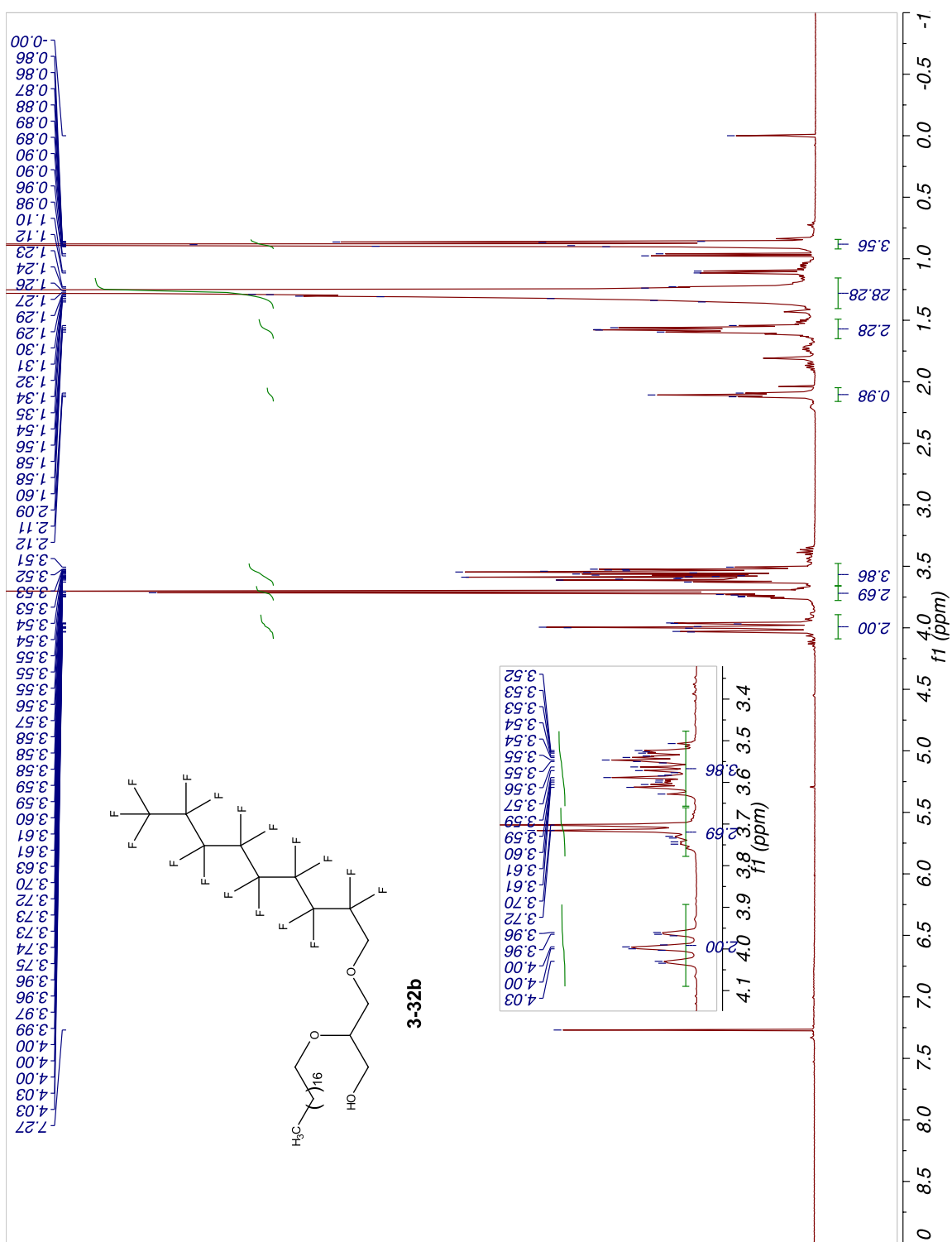


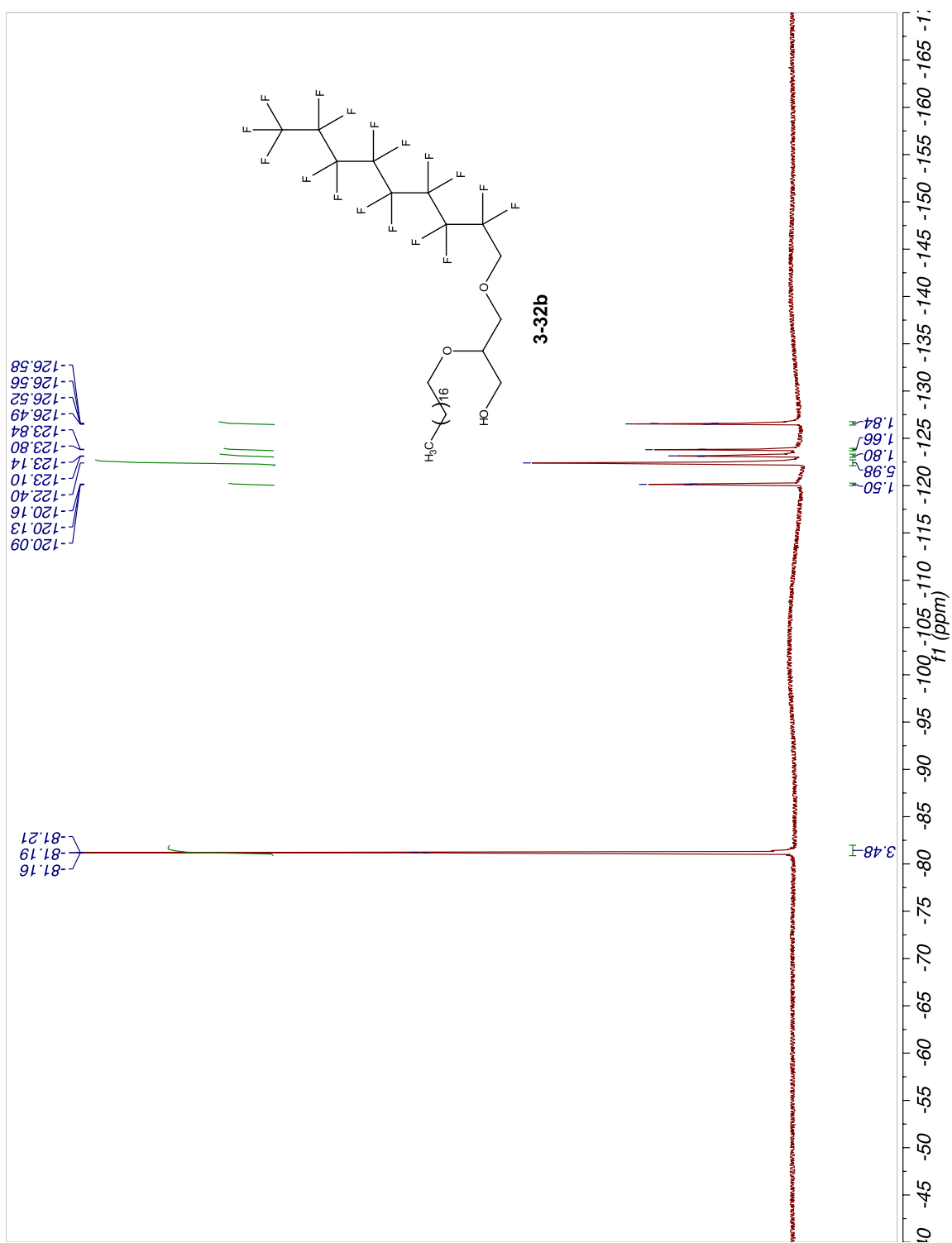


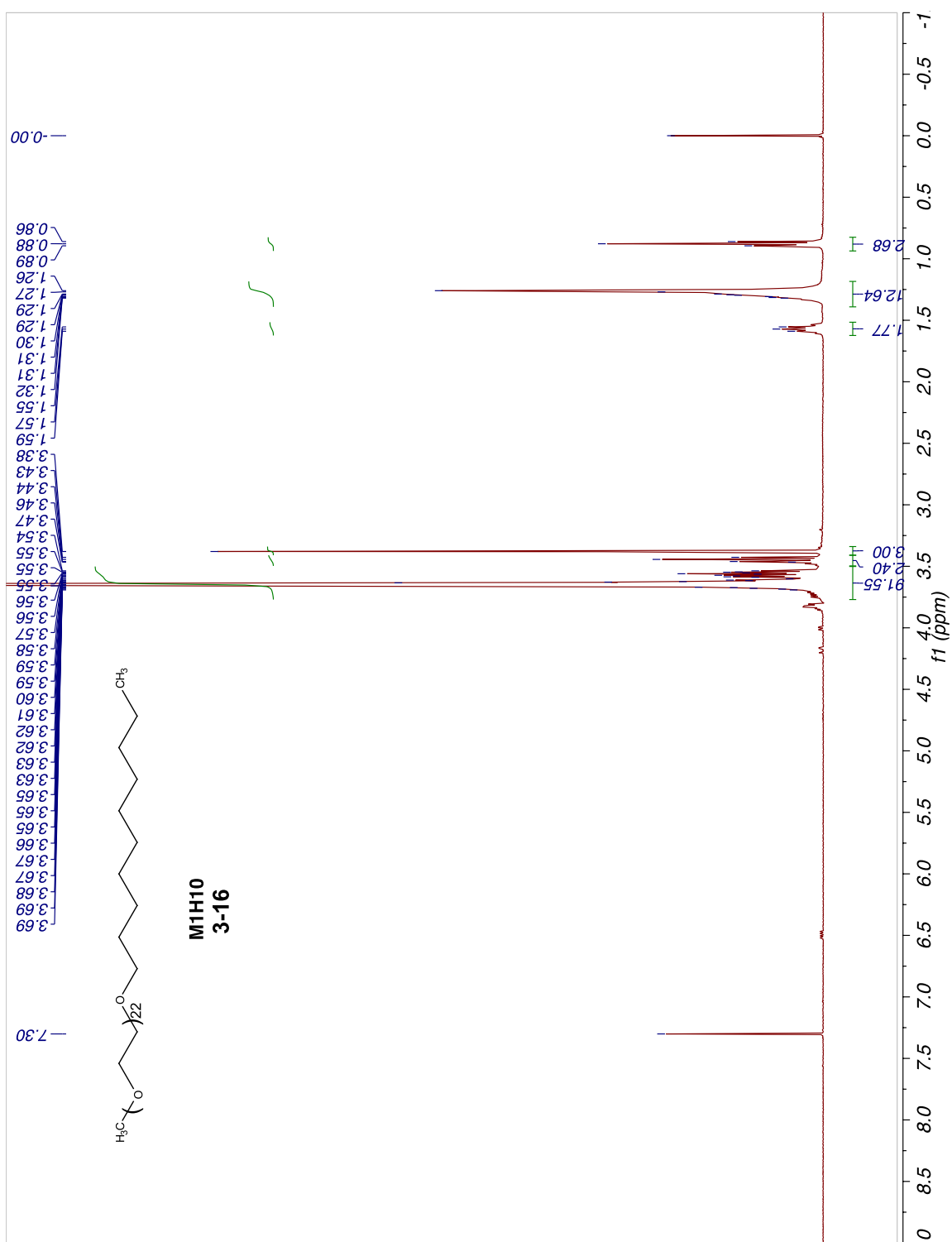


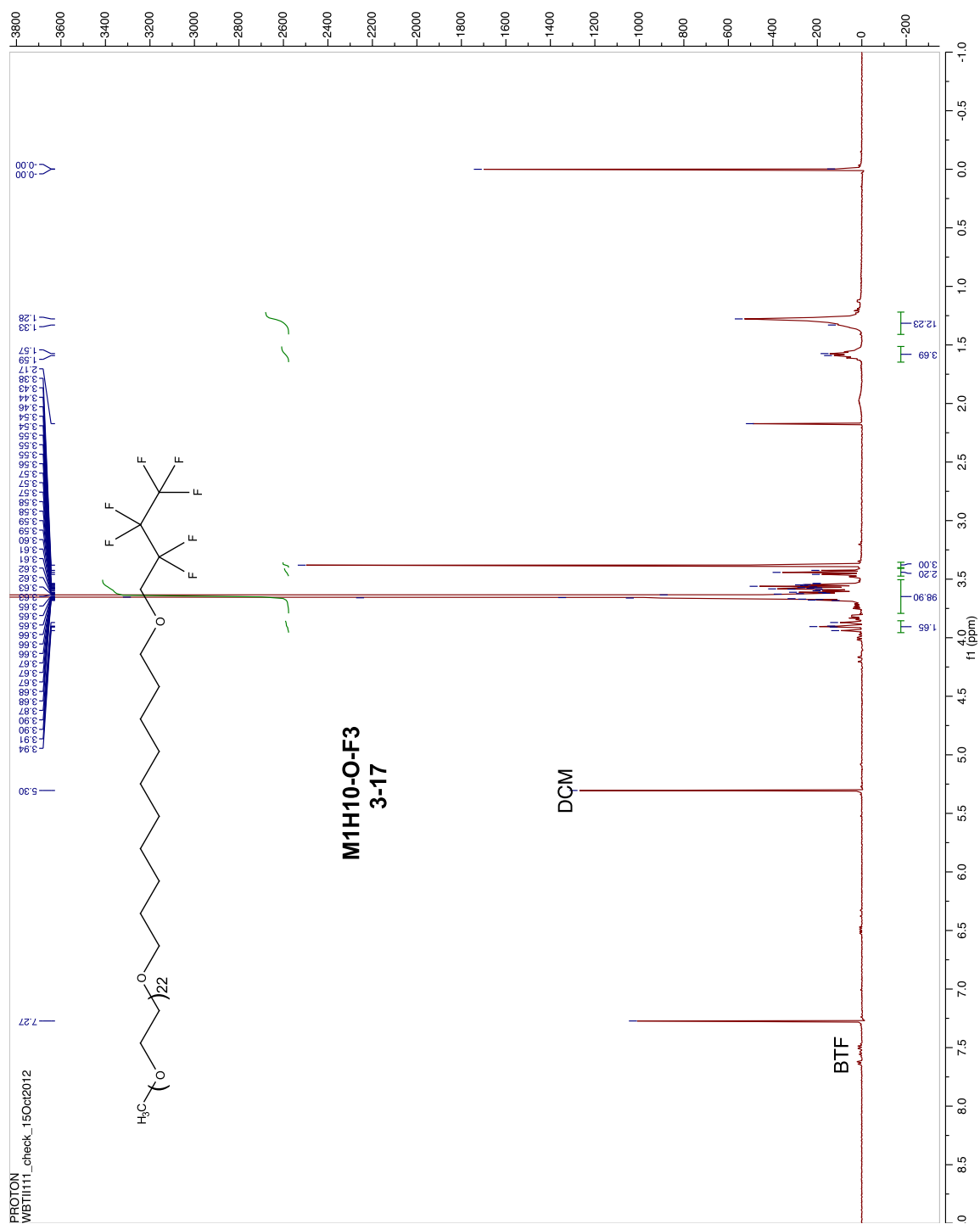


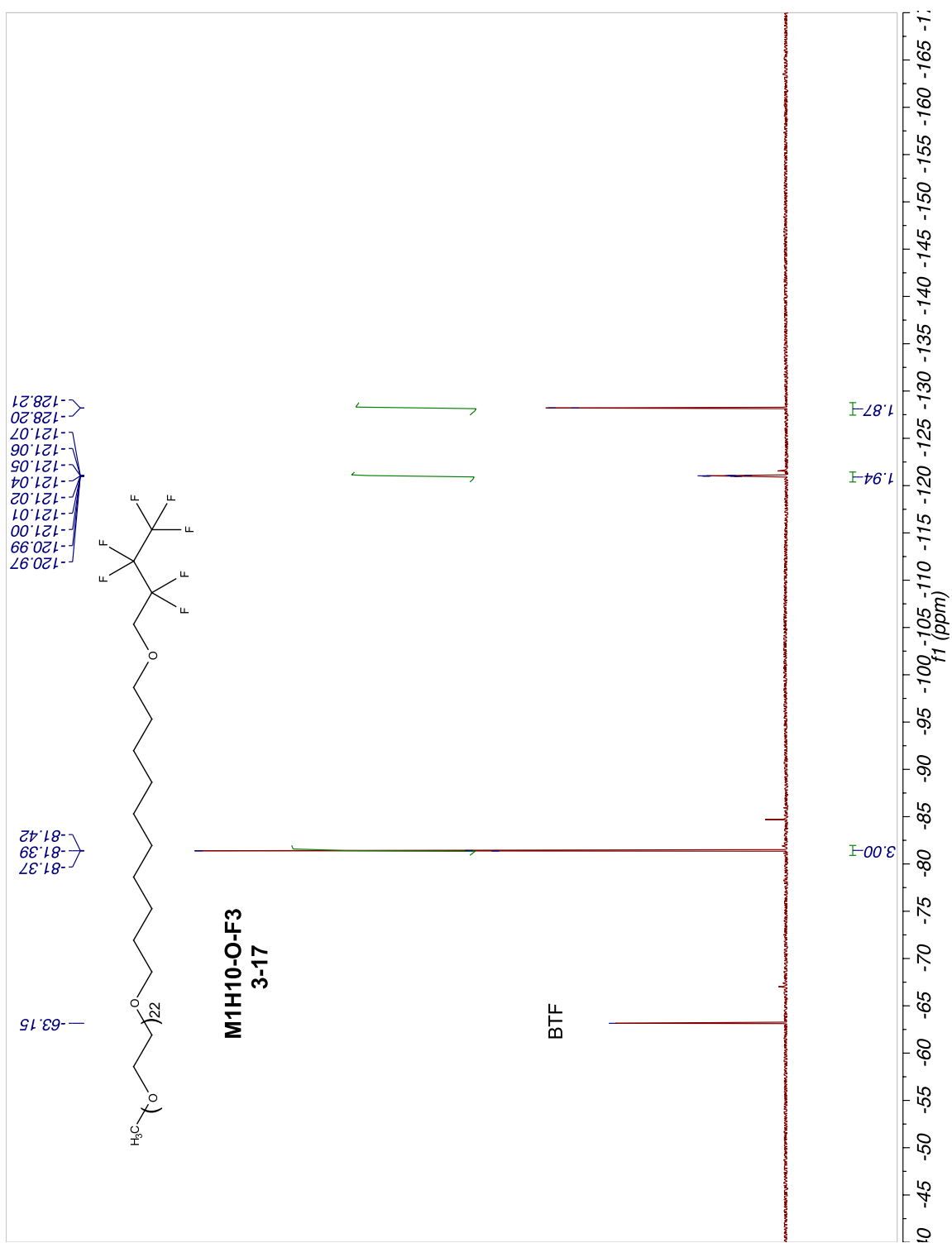


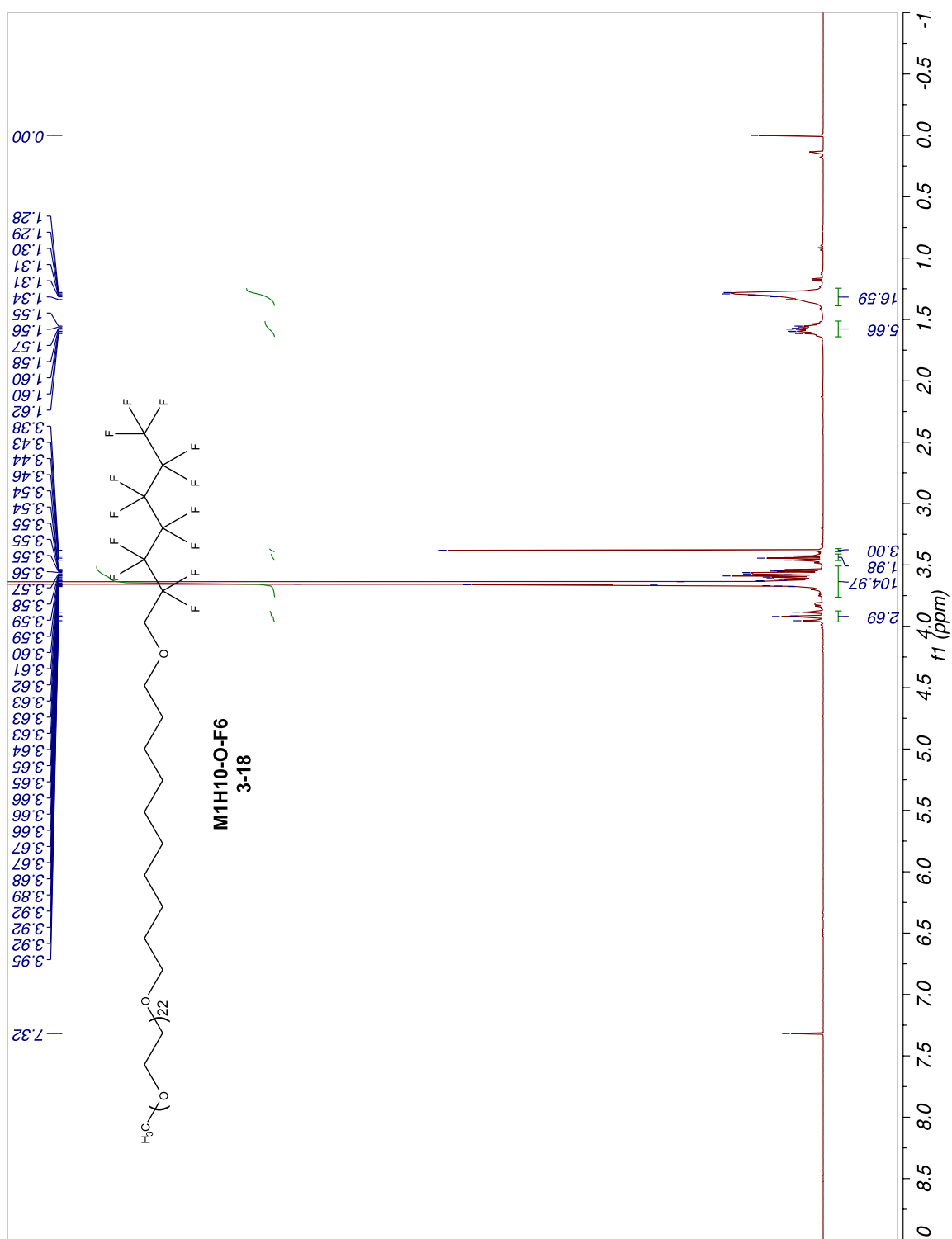


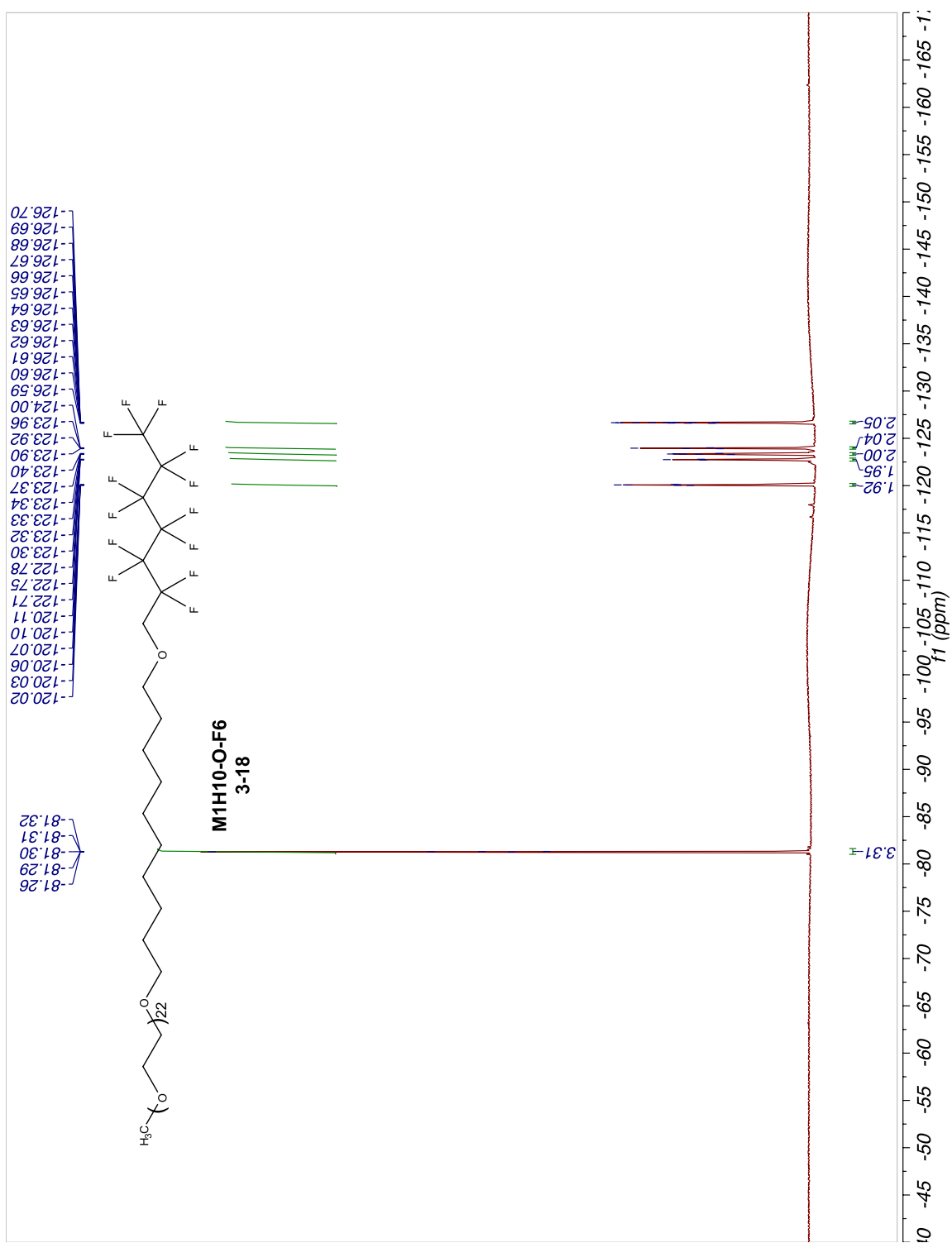


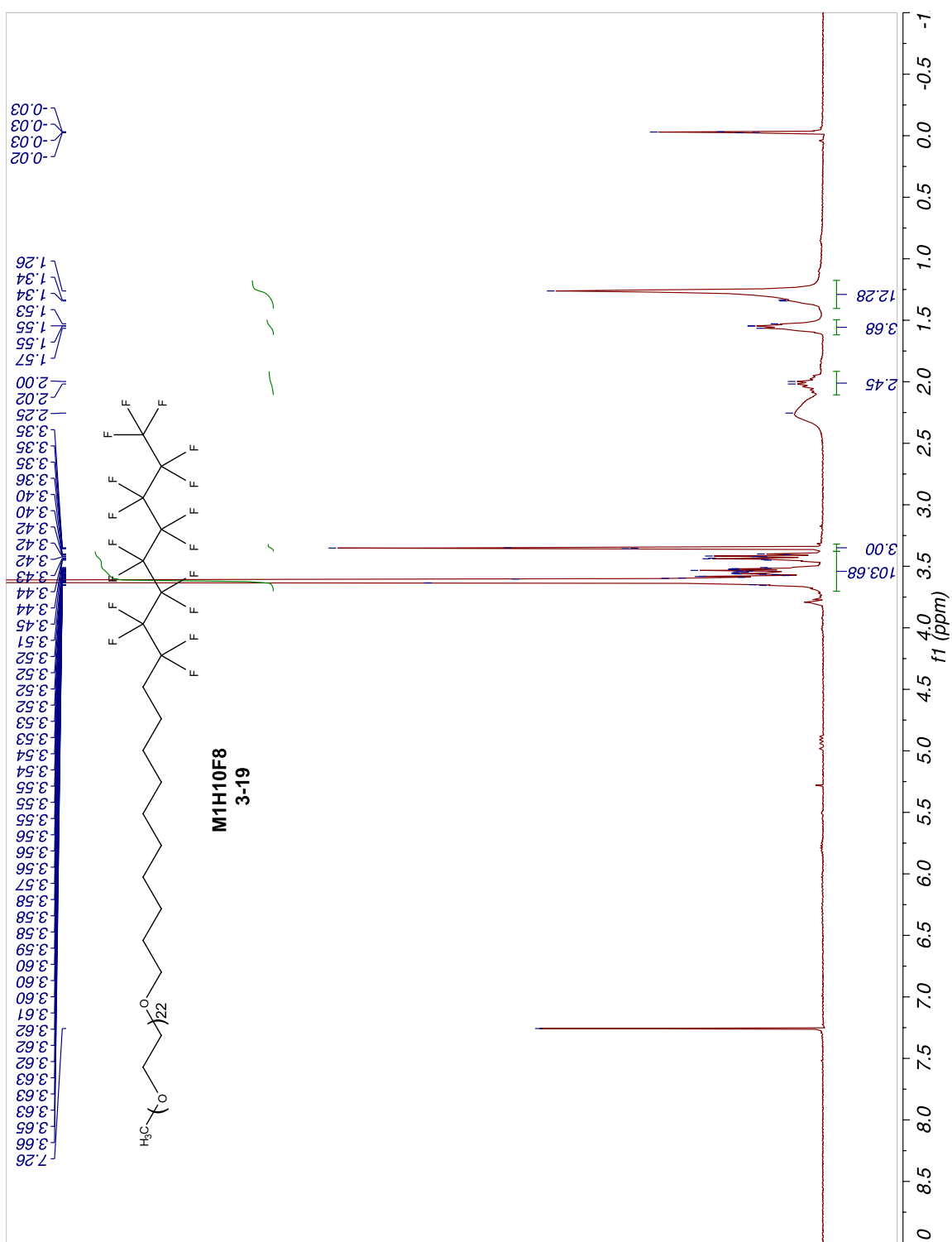


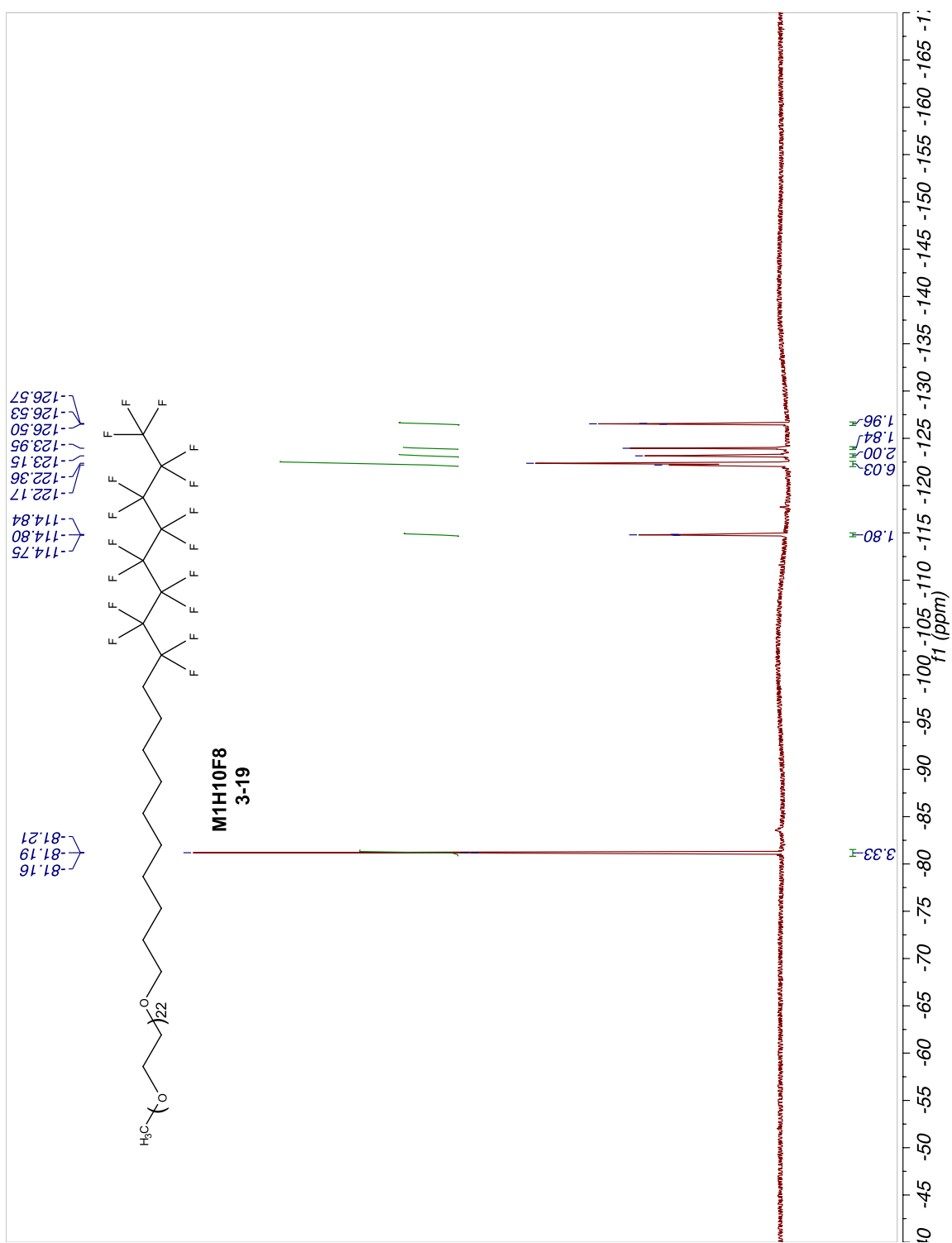


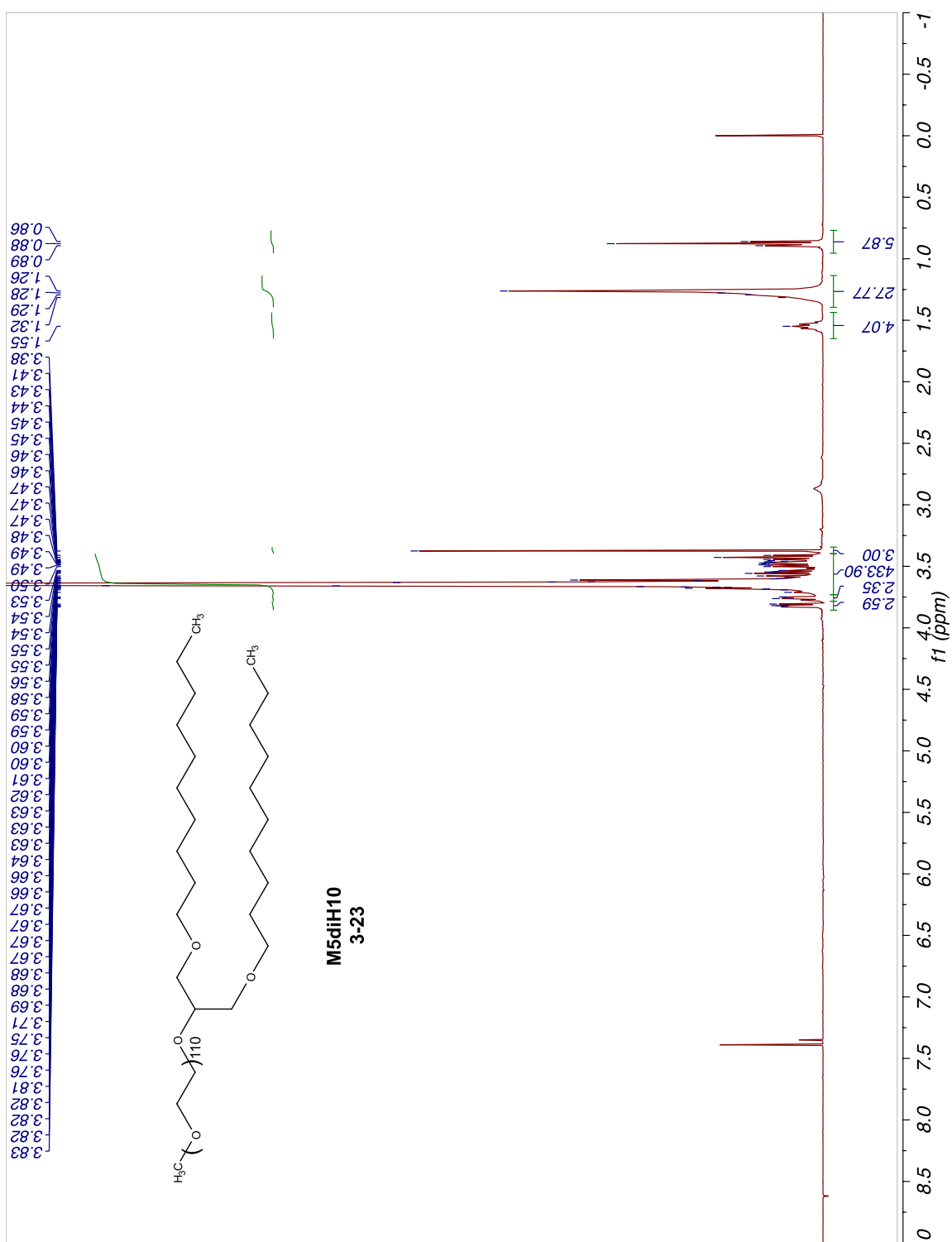


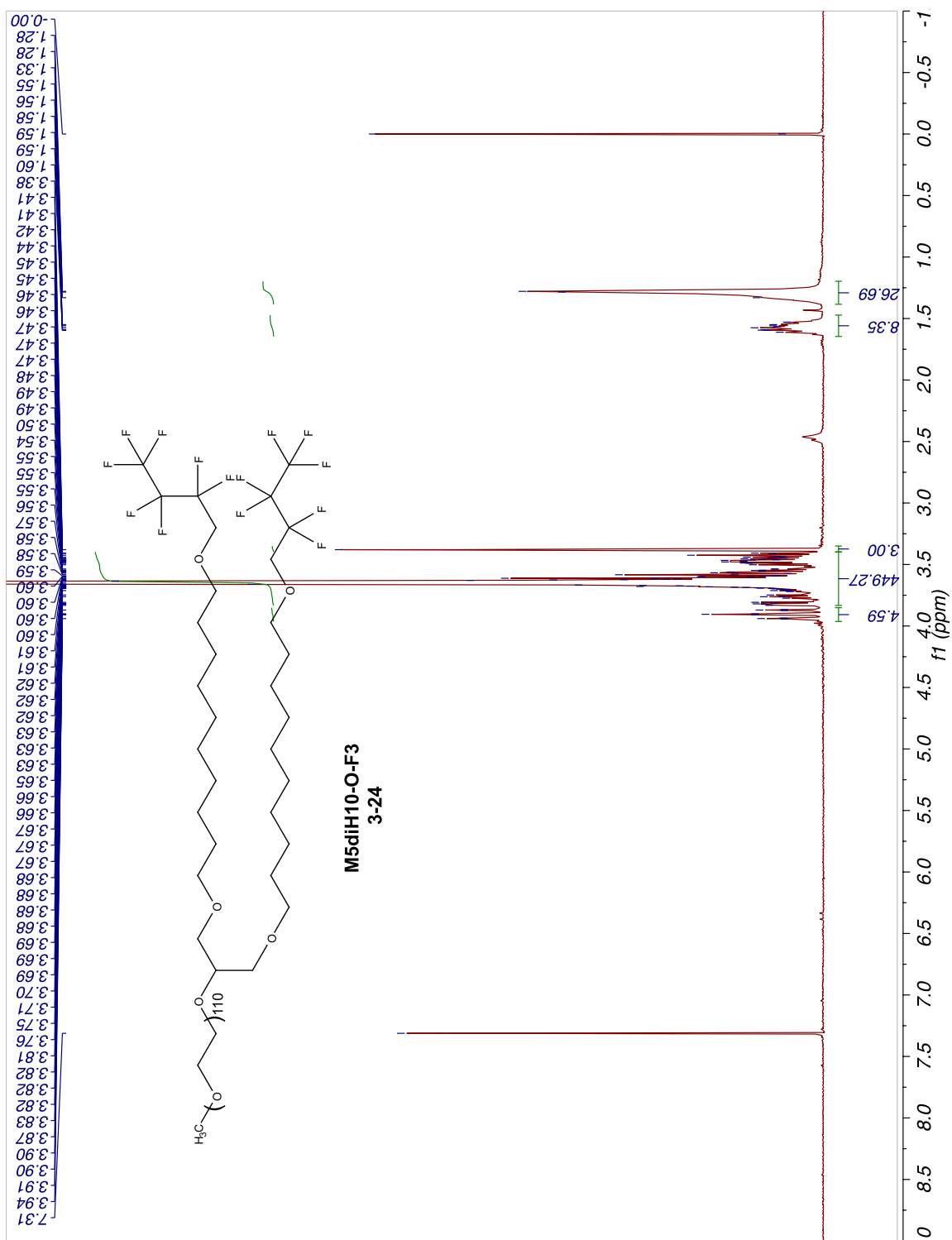


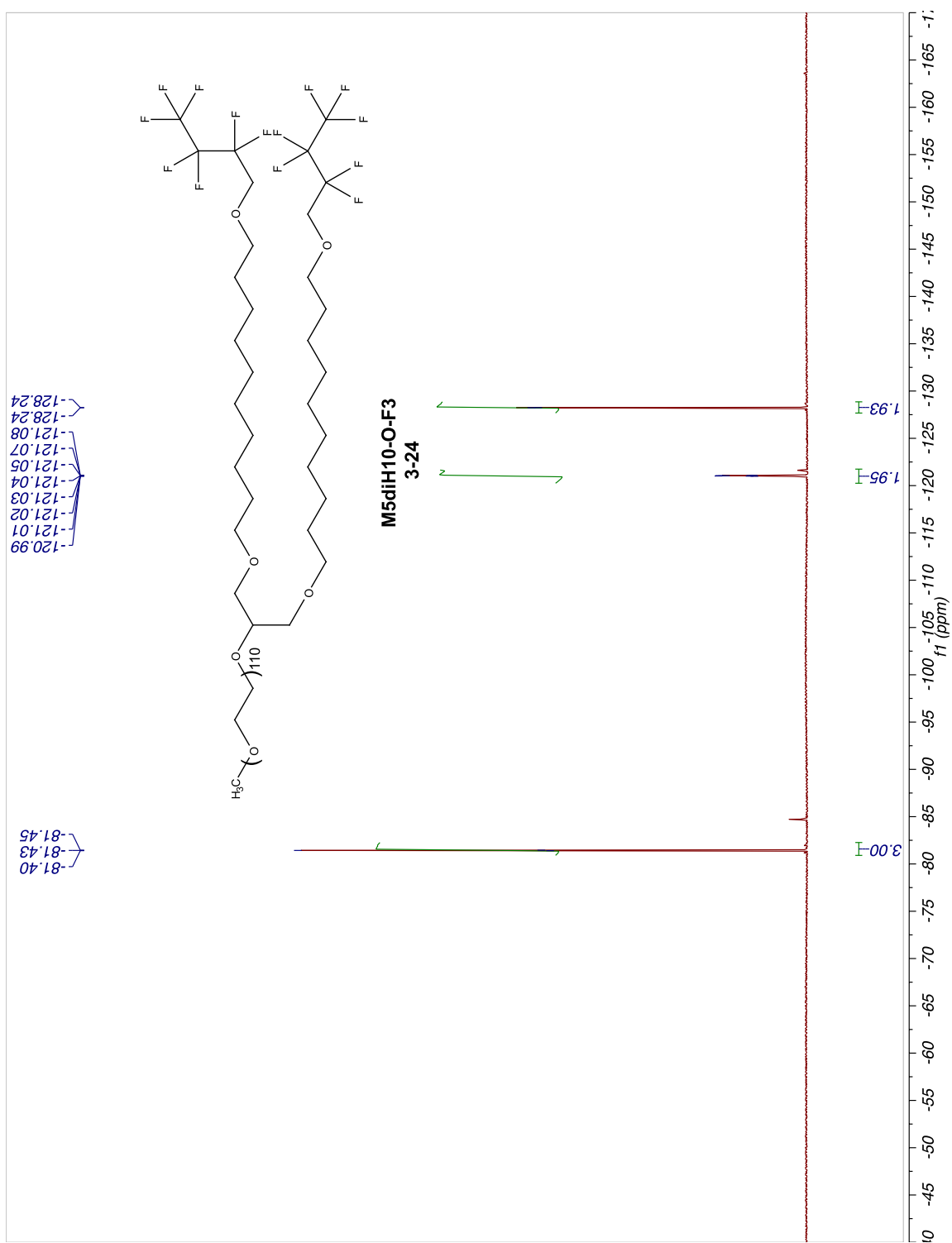


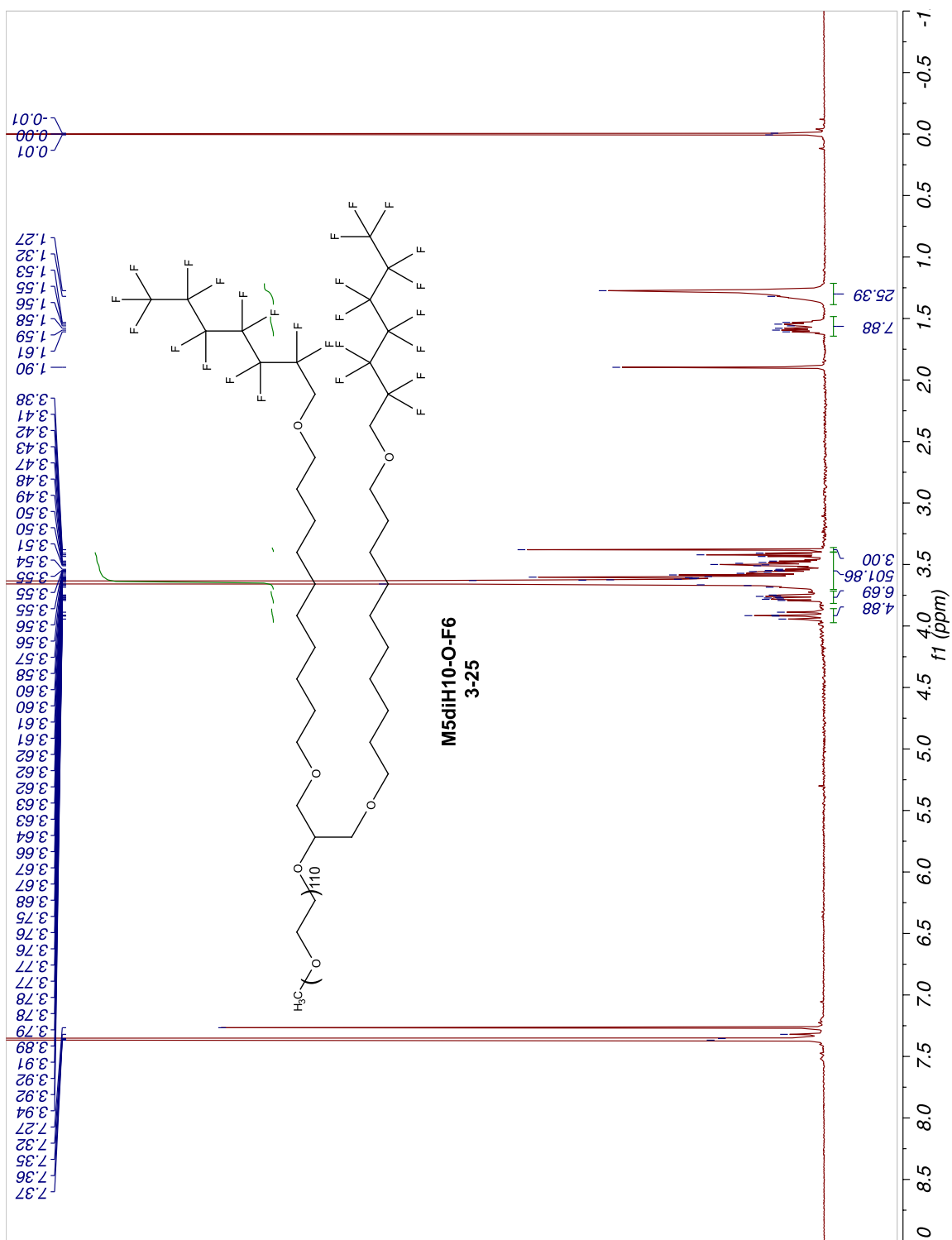


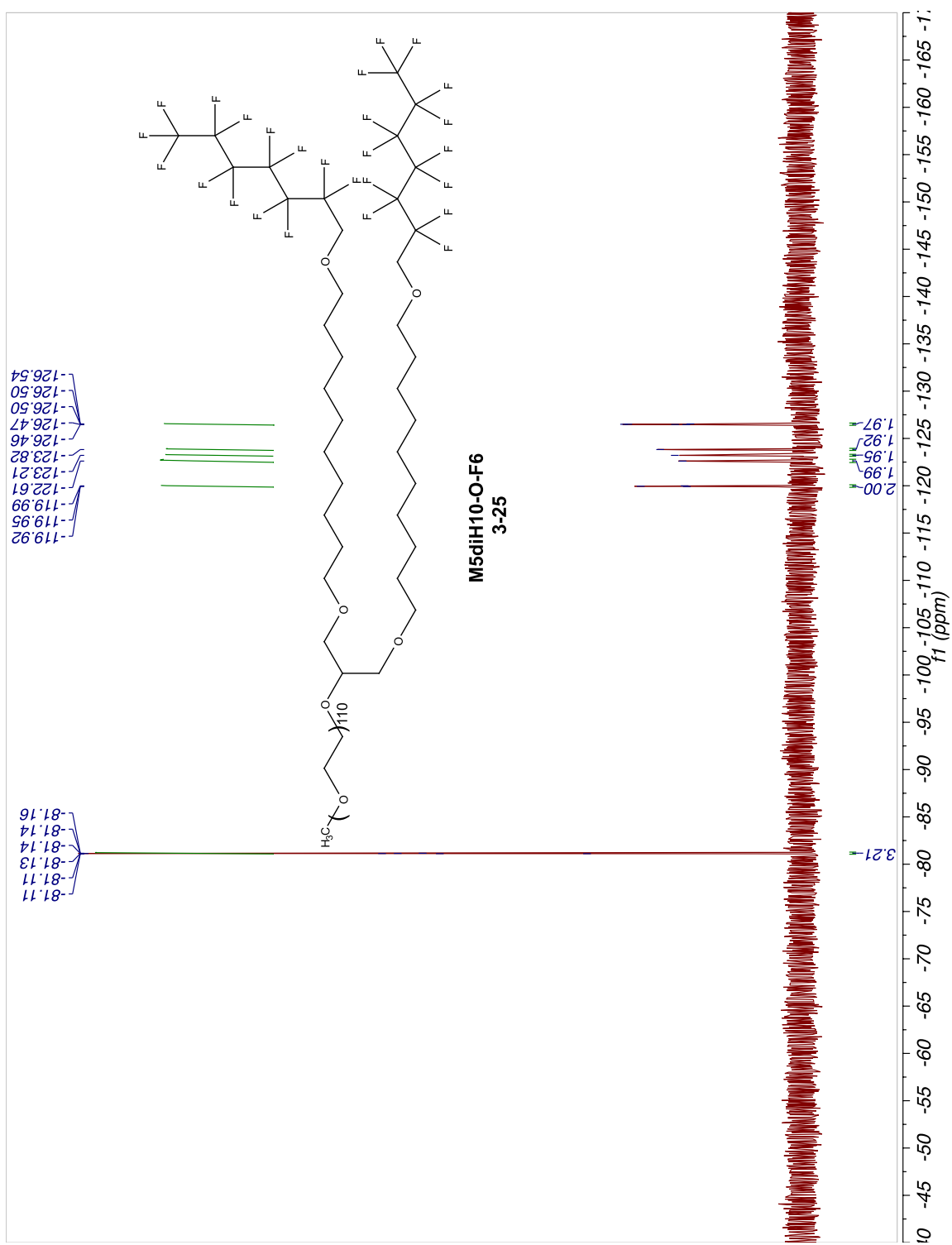


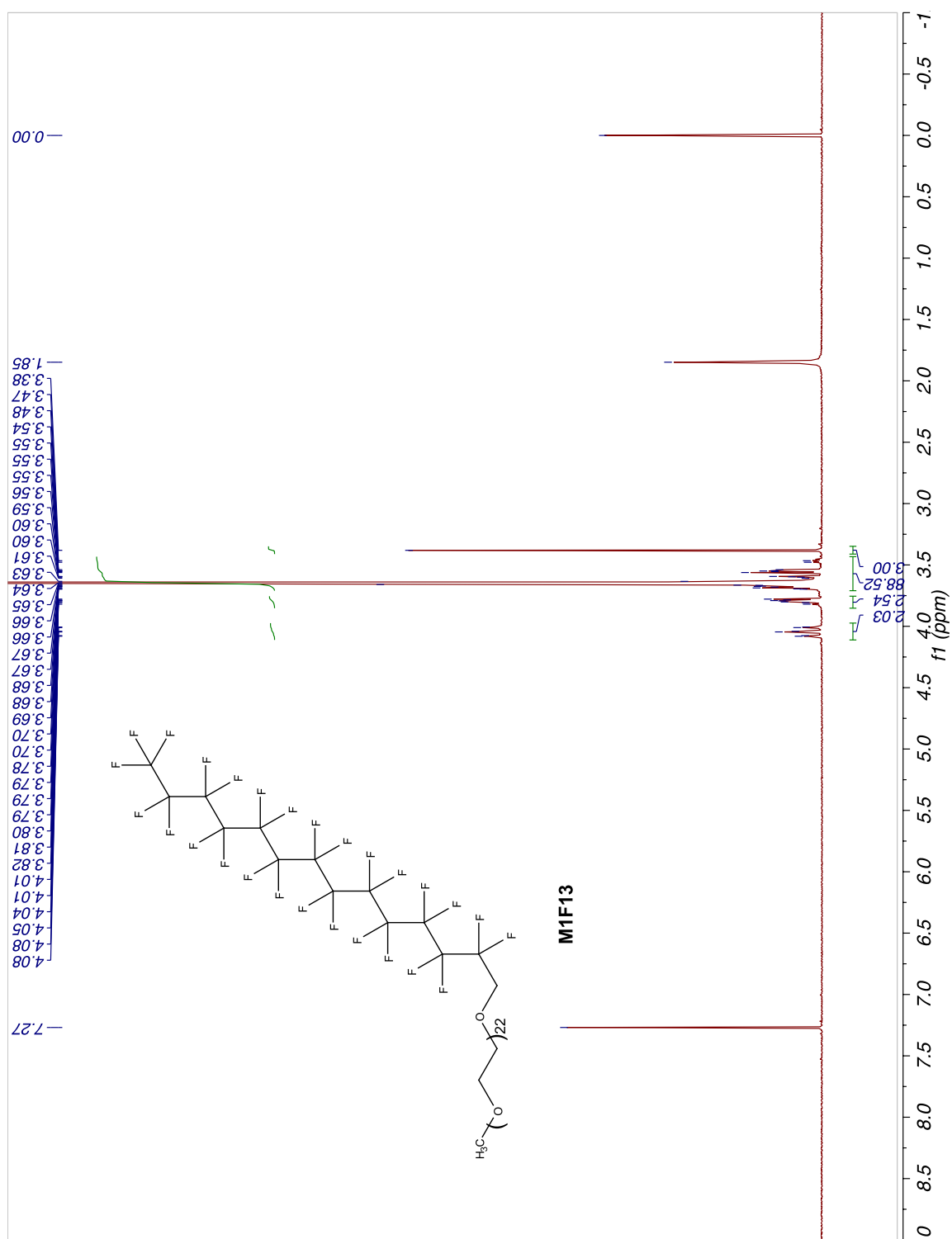


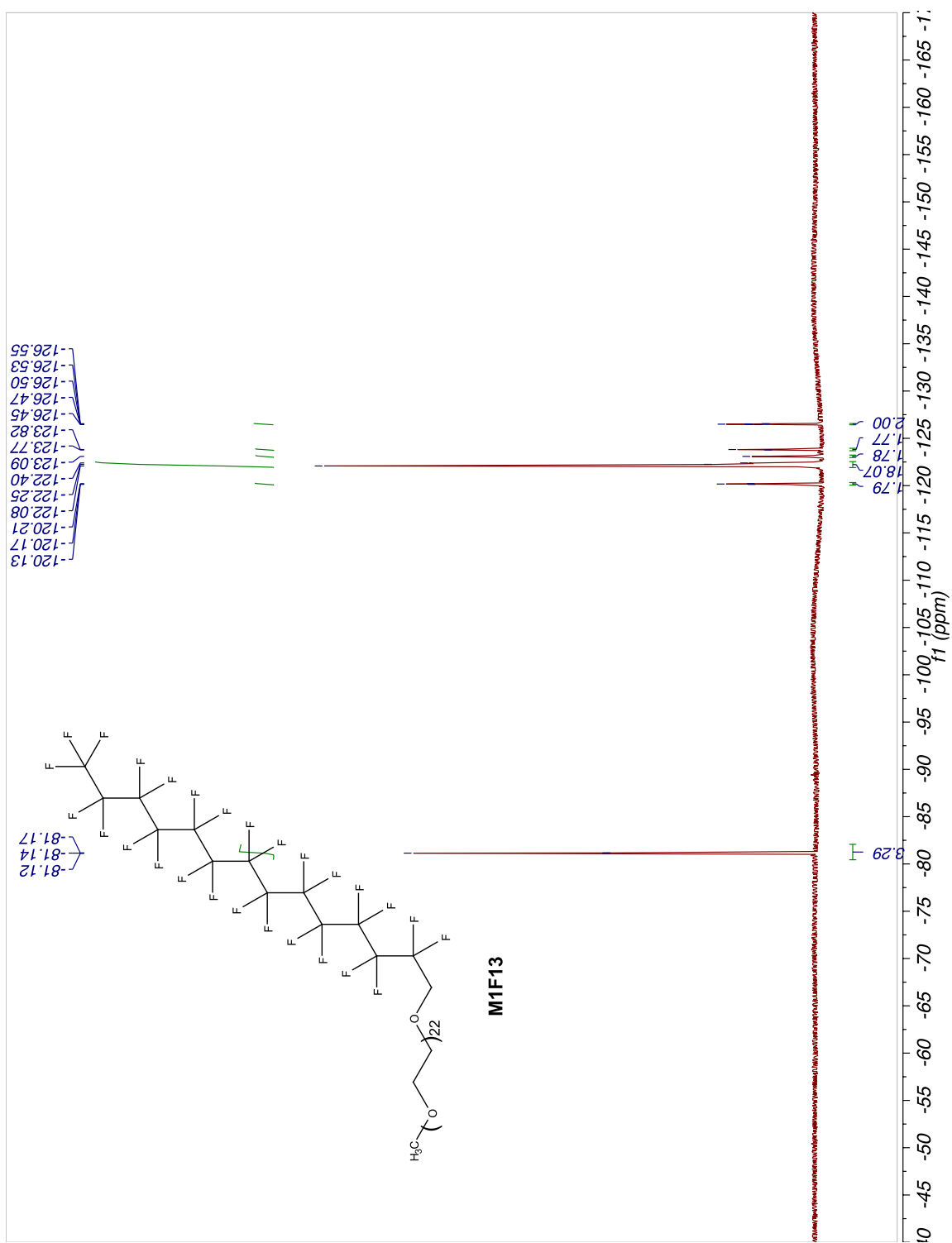


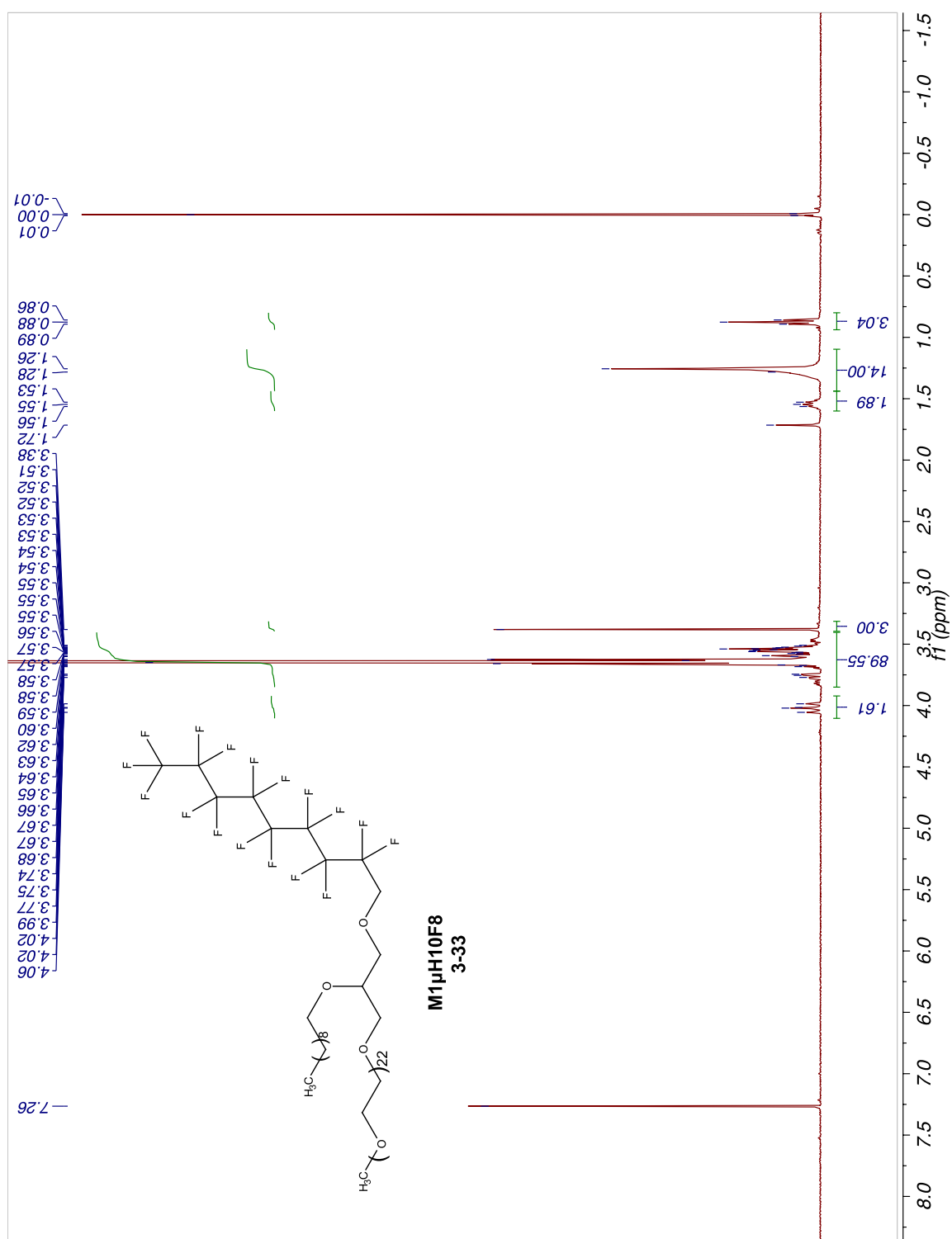


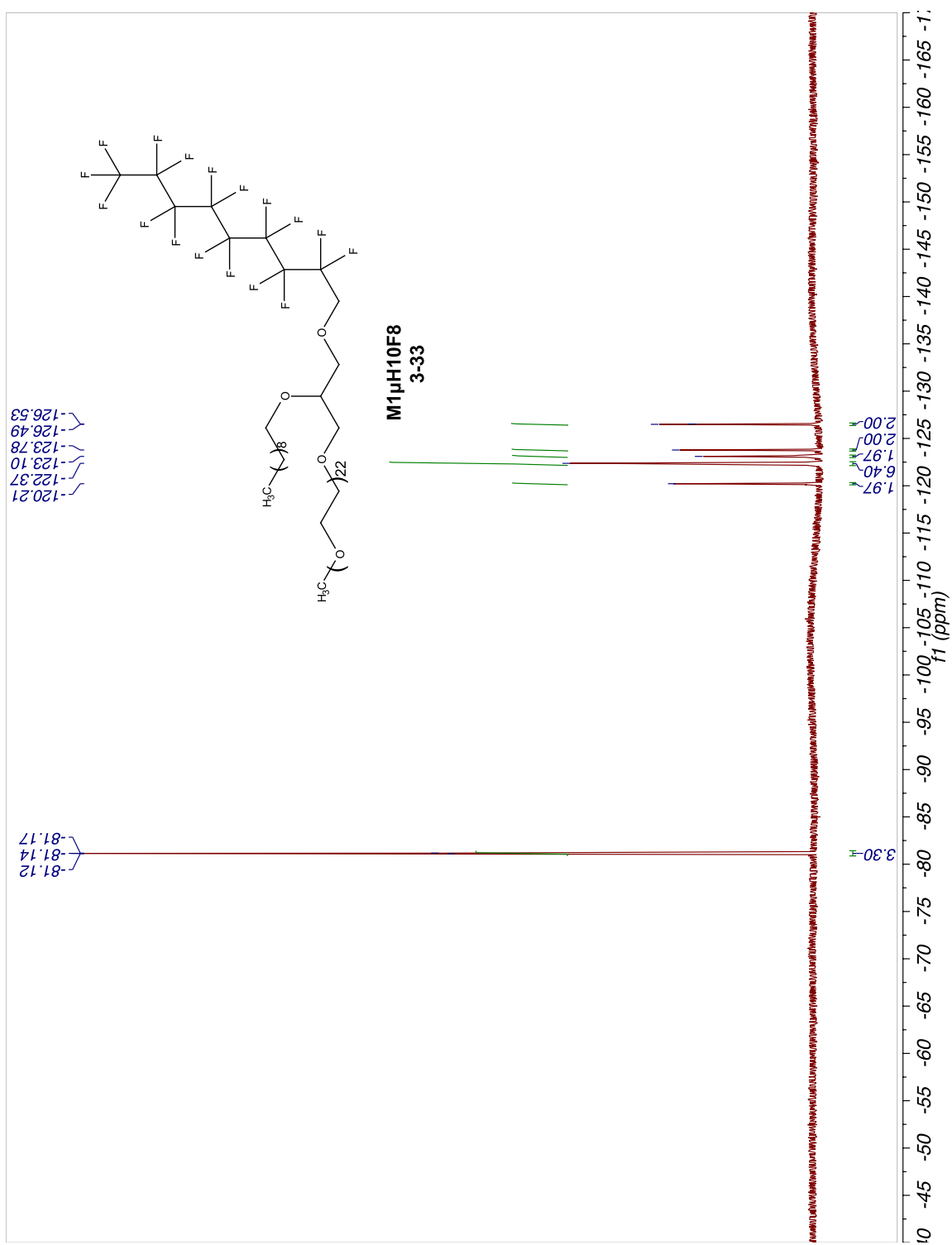


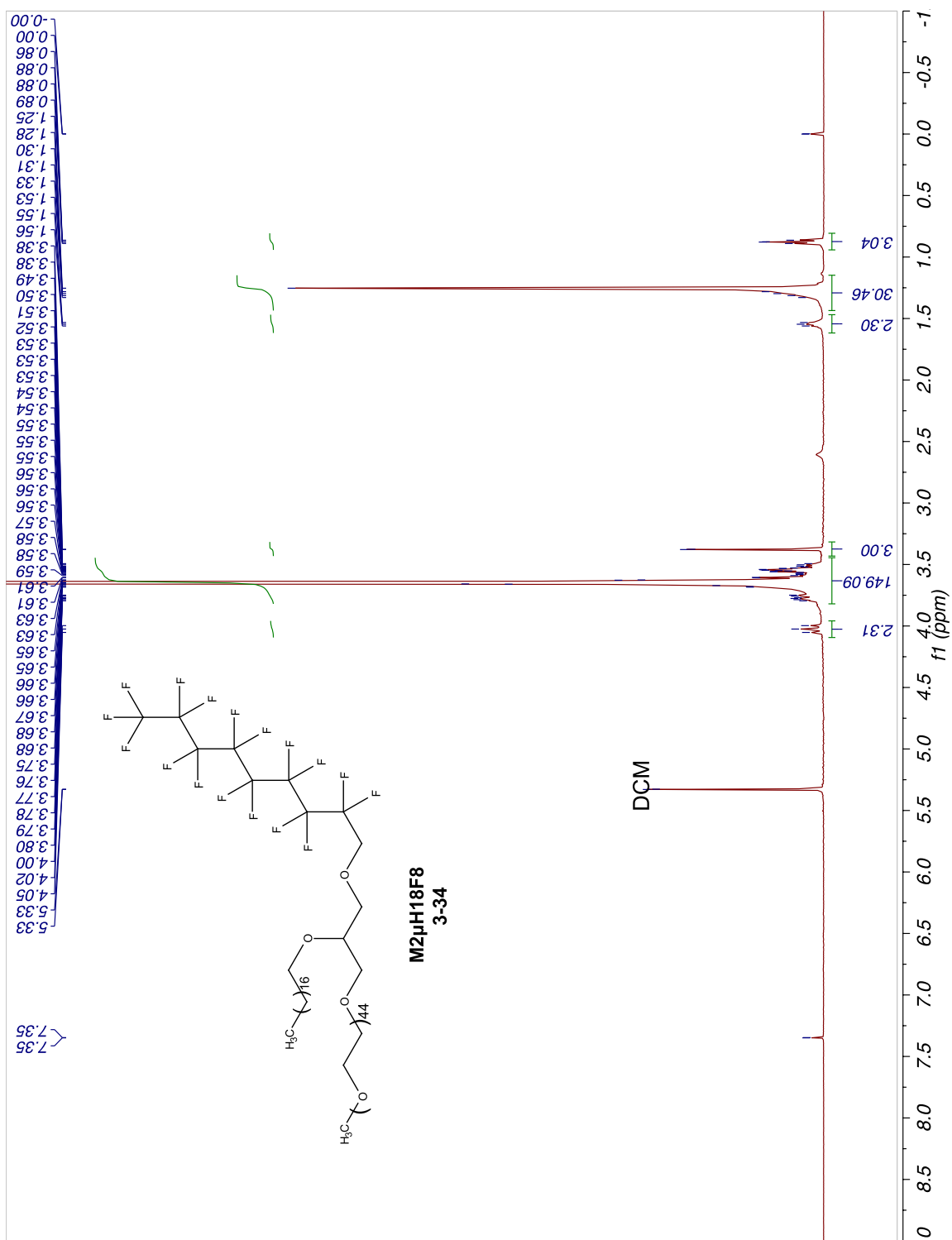


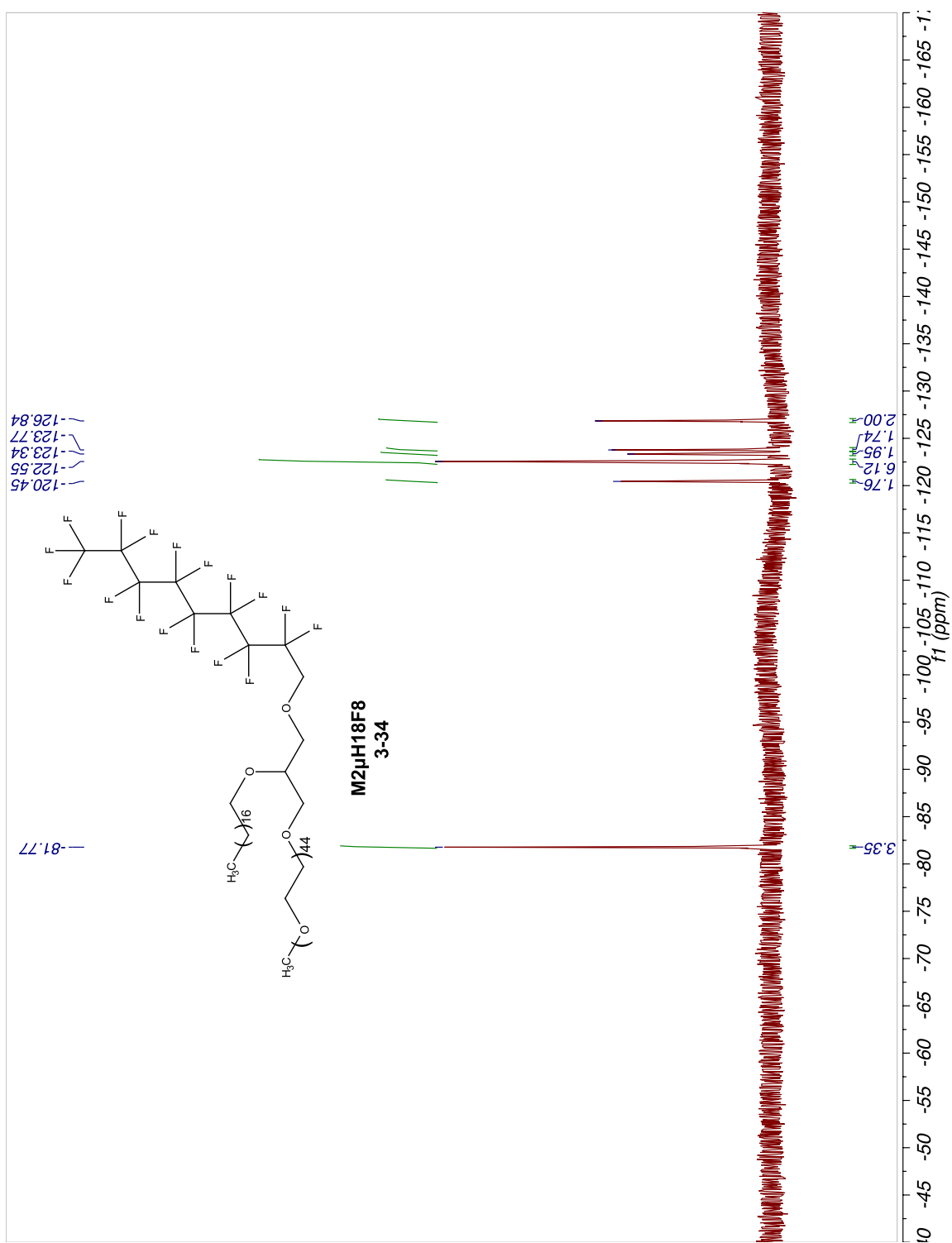


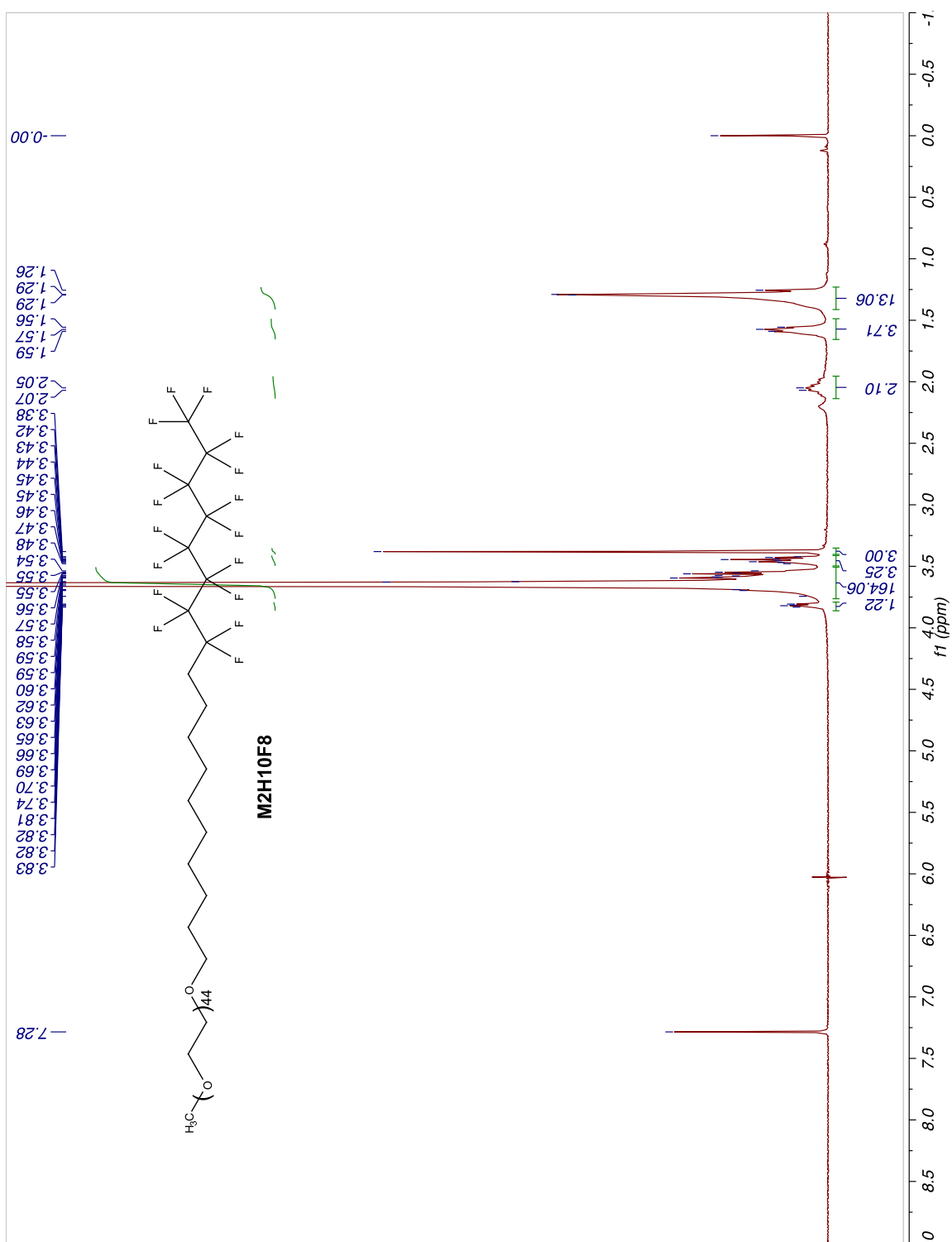


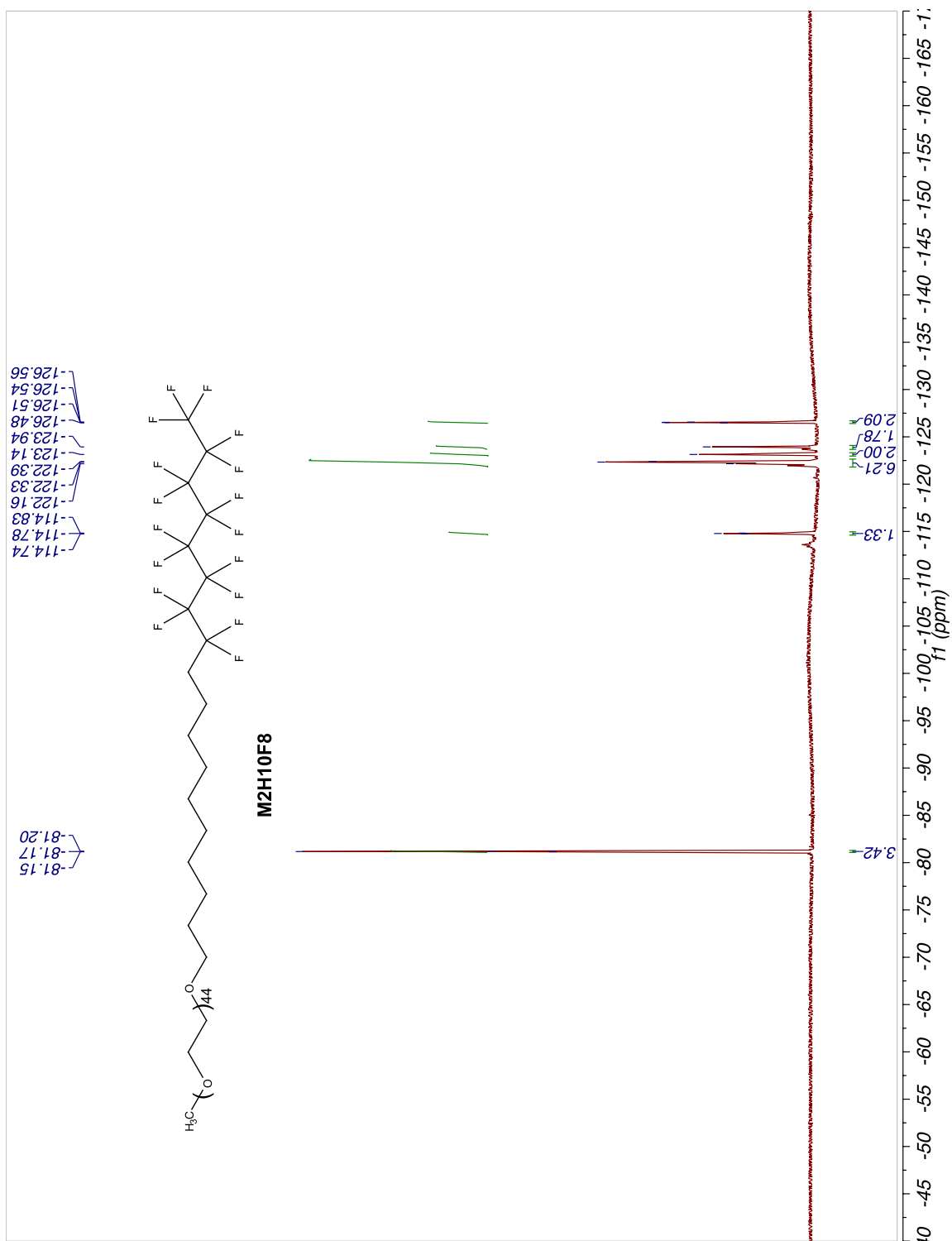


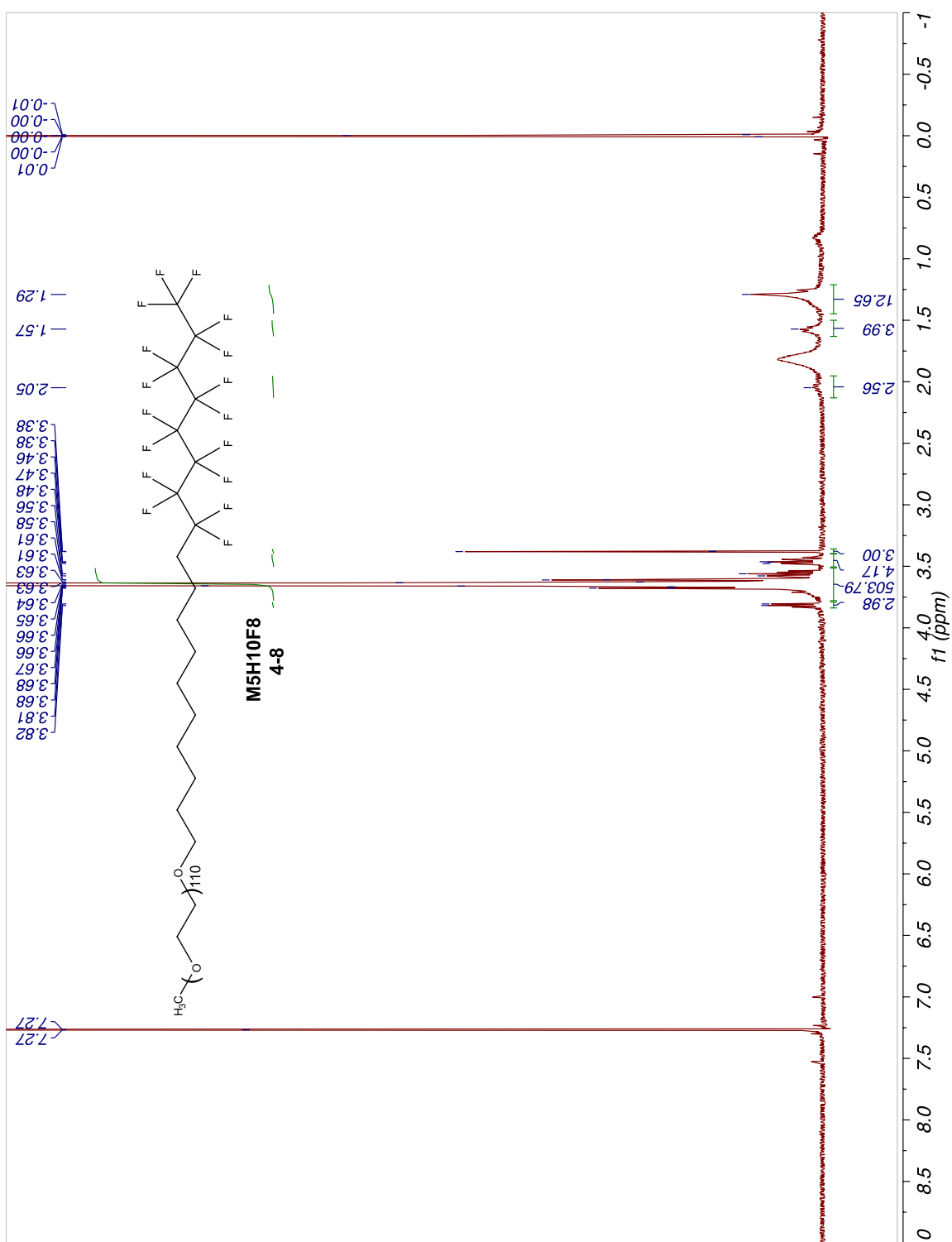


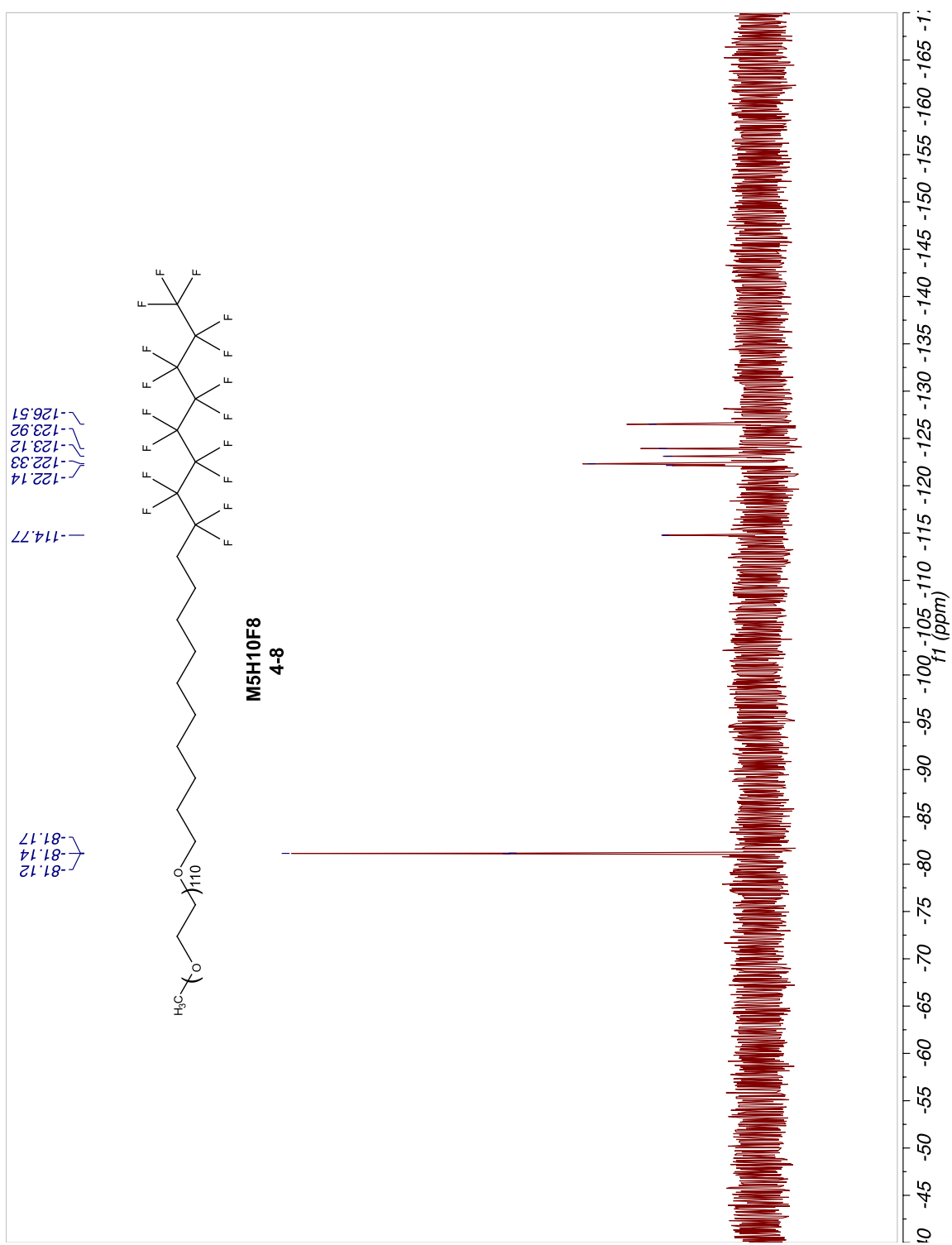


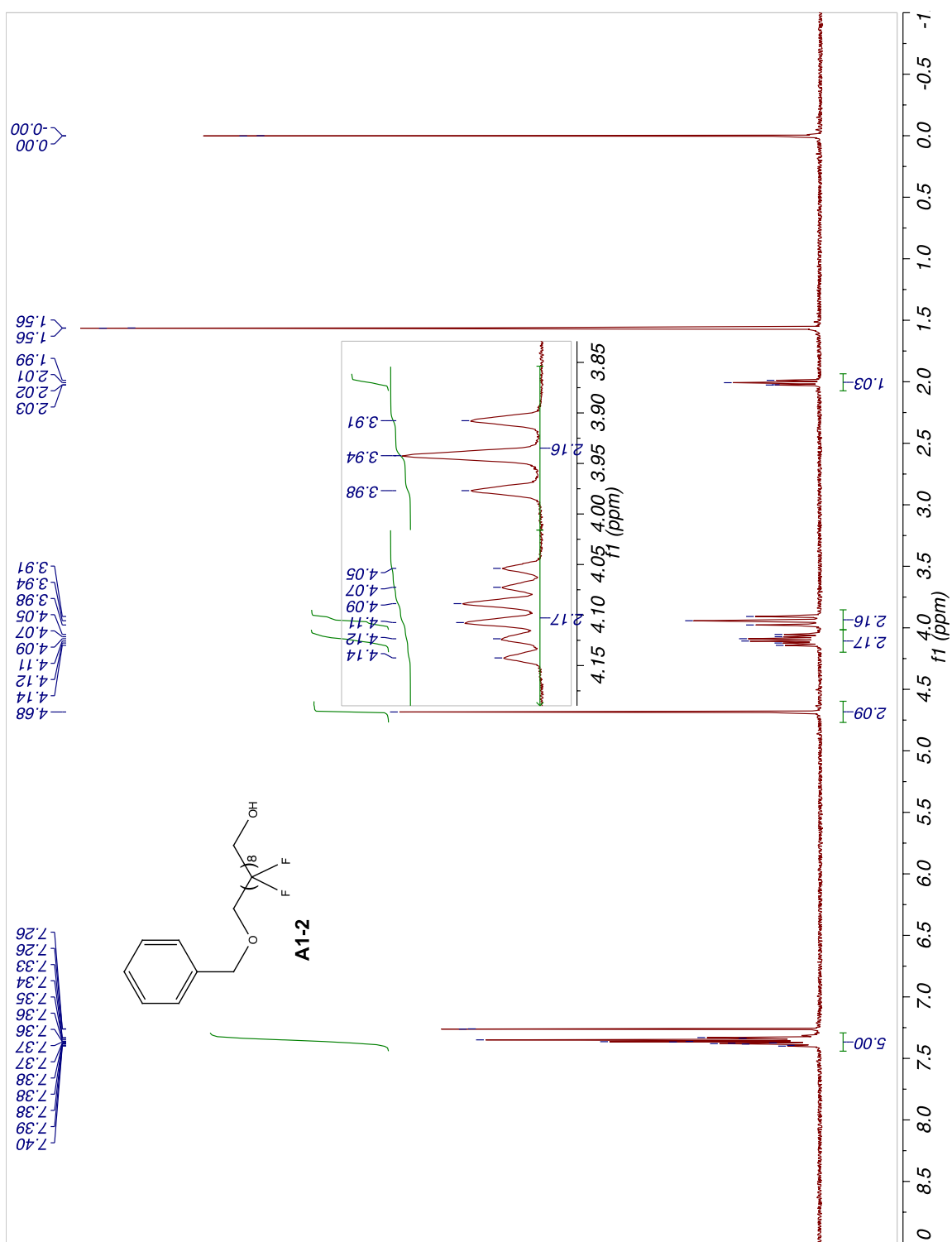


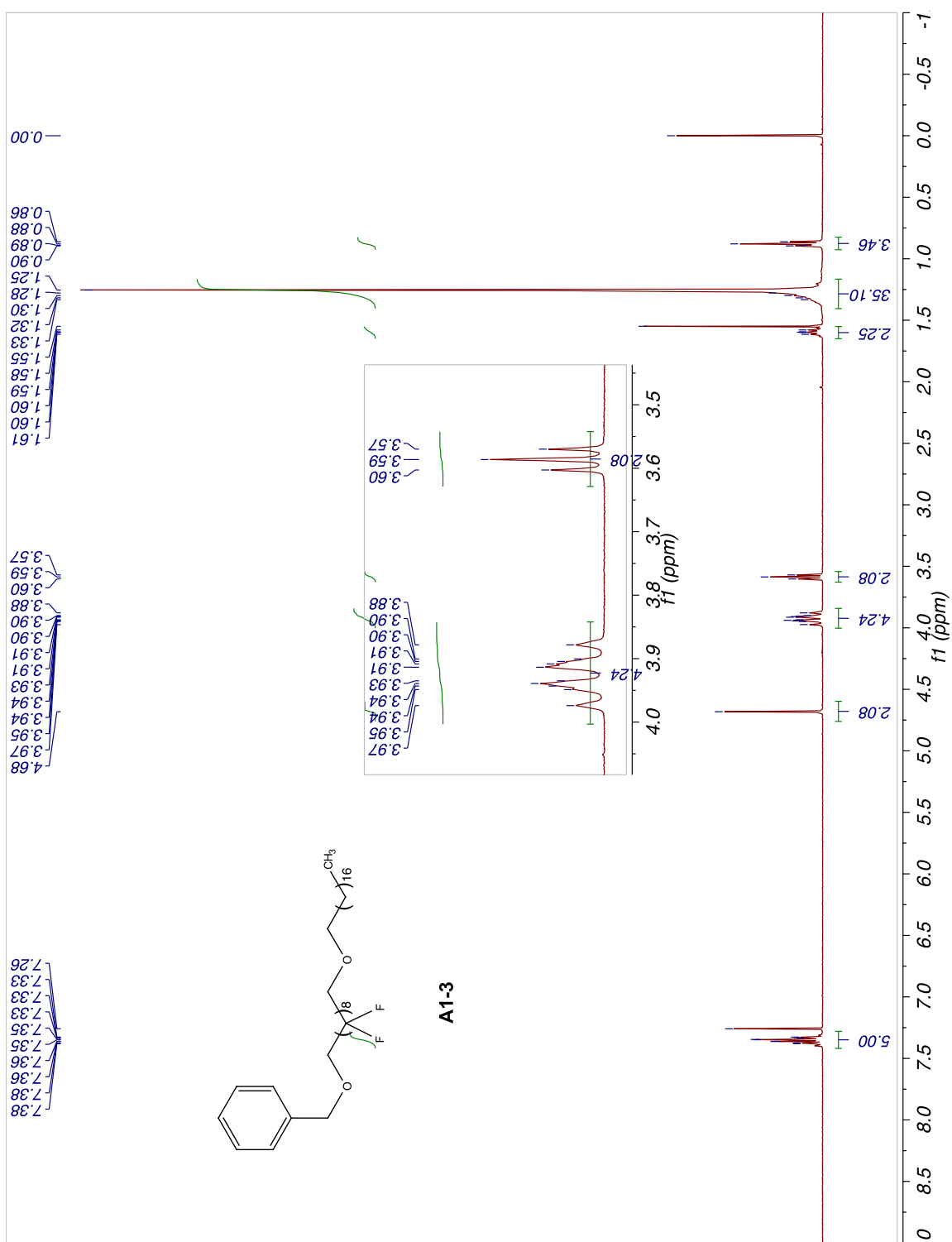


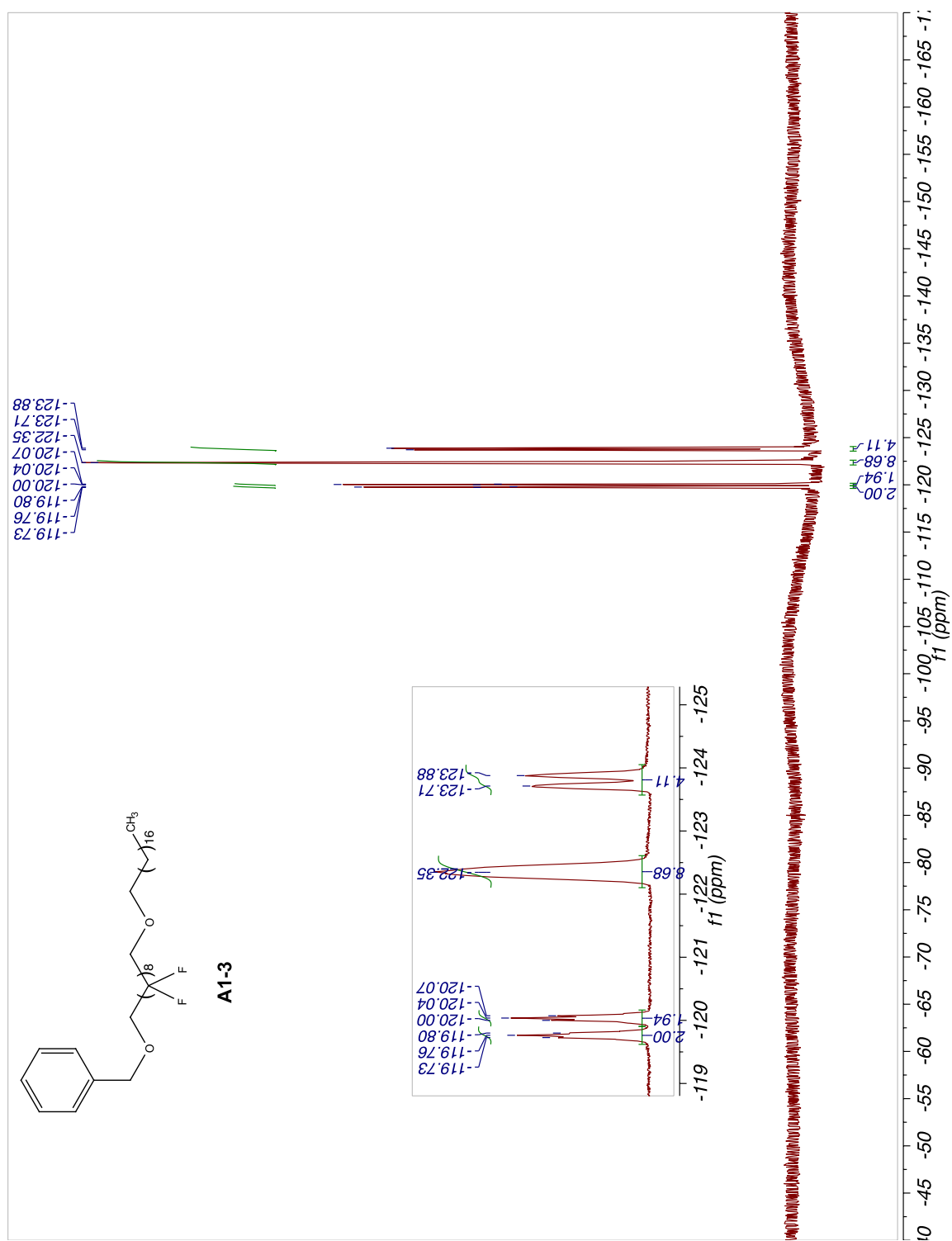


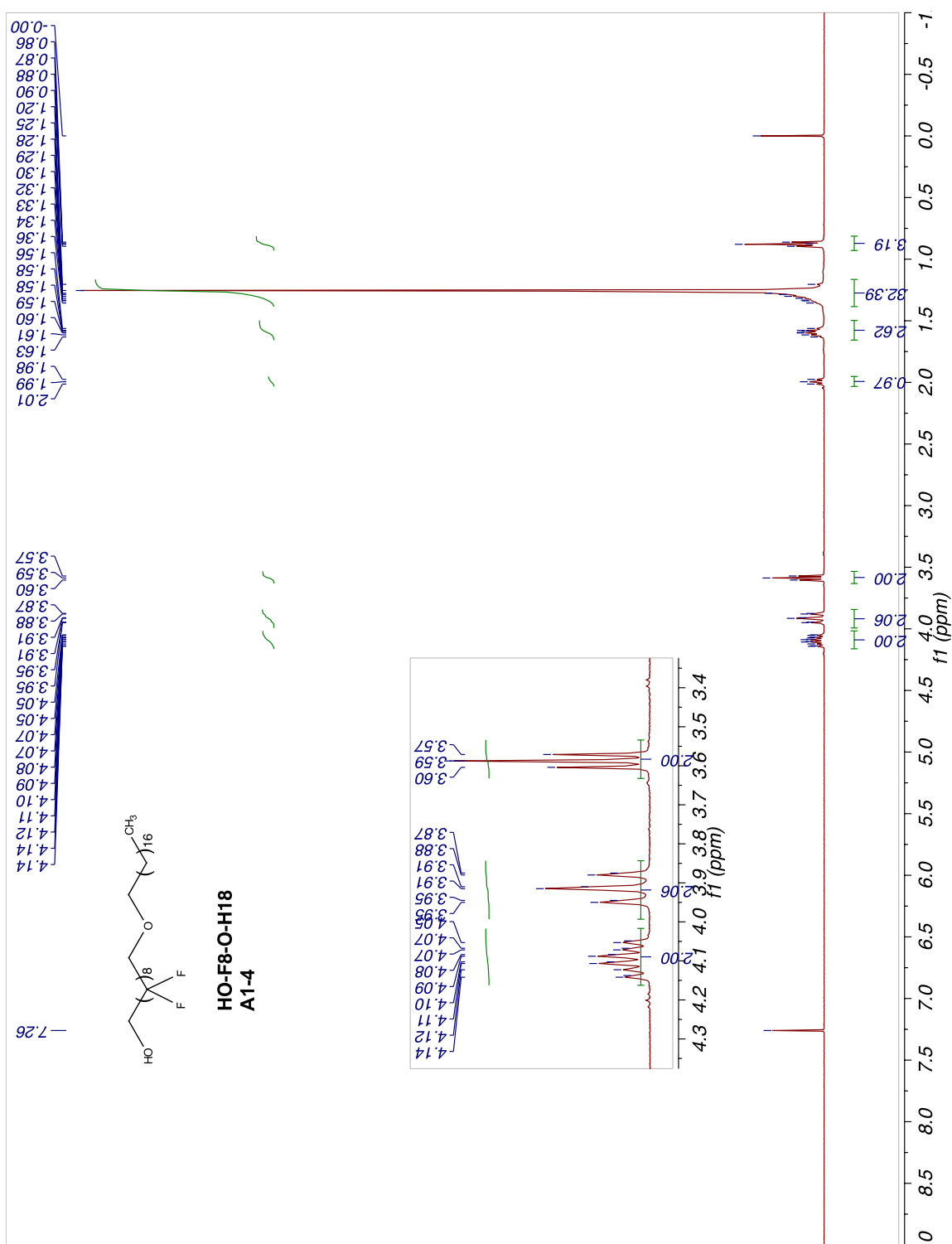


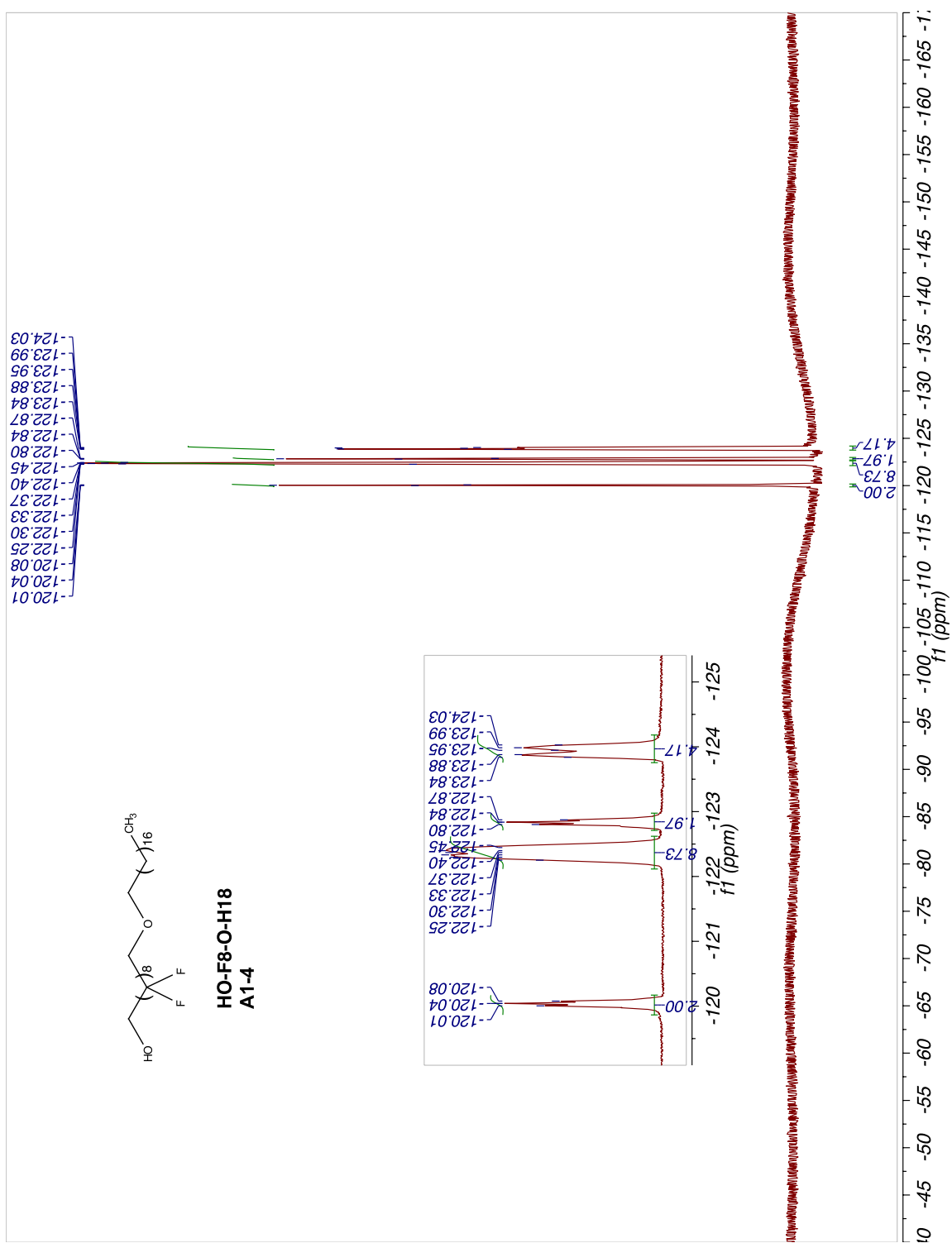


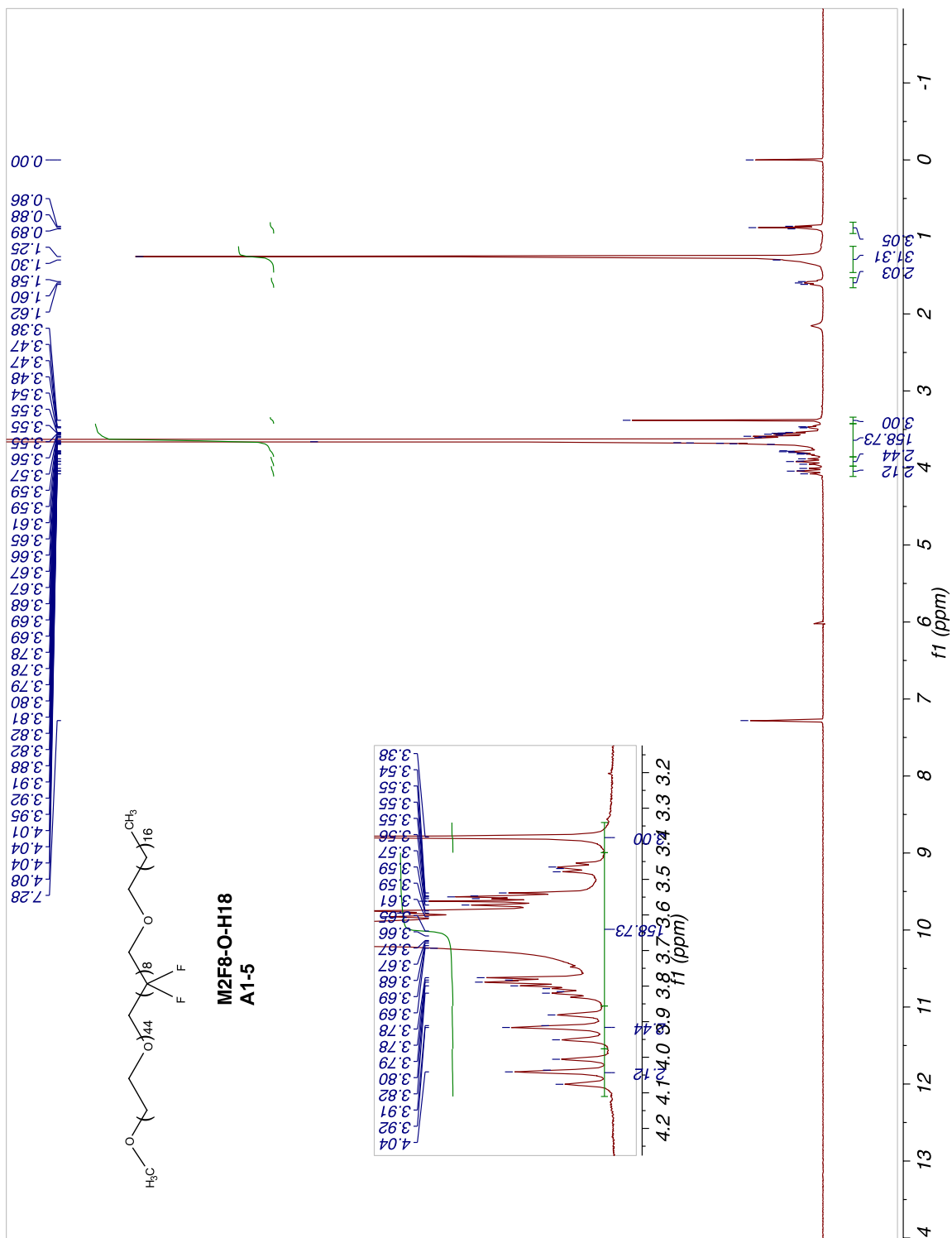


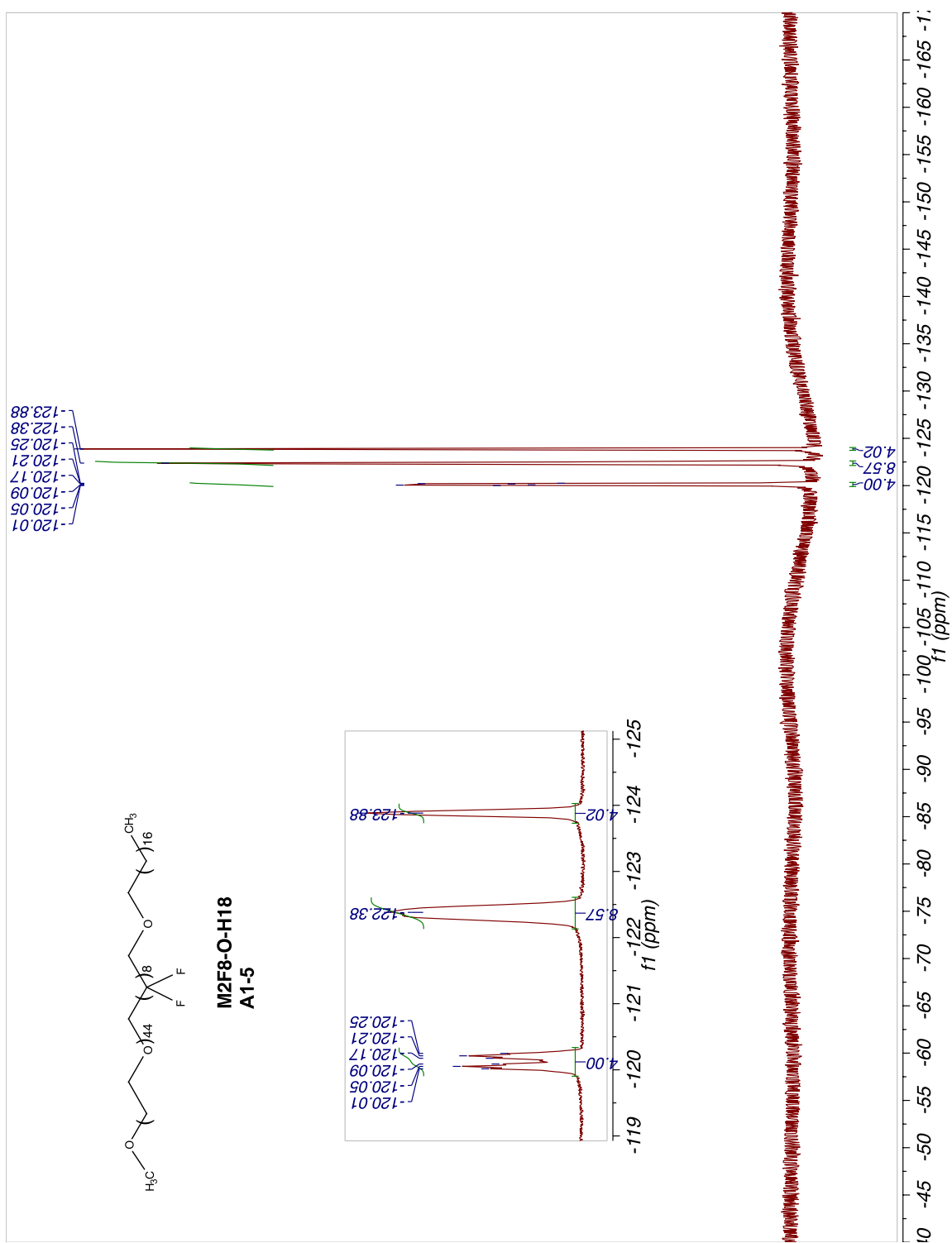








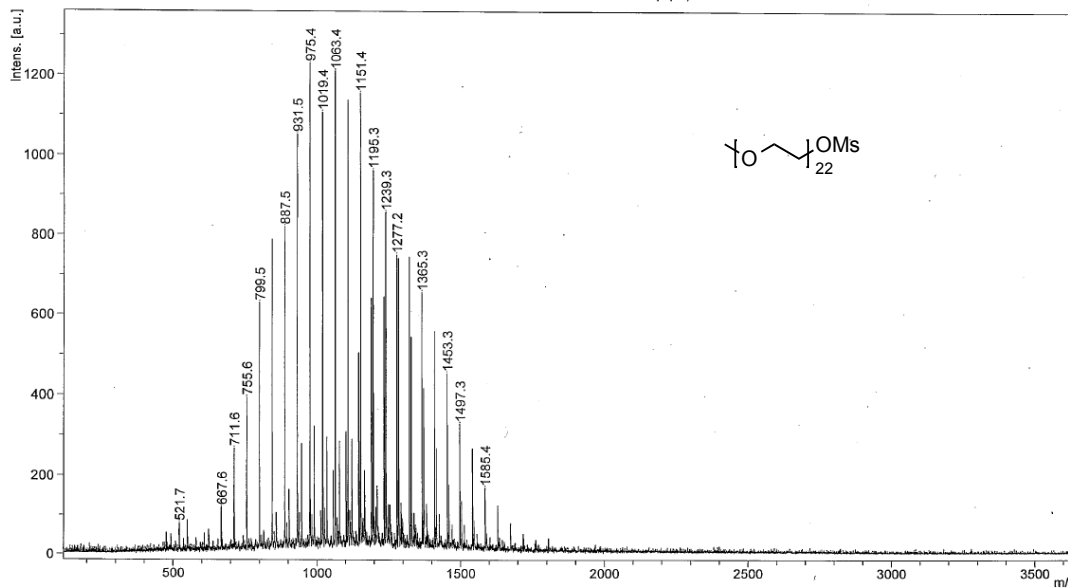




A2.2.2. MALDI spectra

D:\Data\mmv\131002x0210_I11

Comment 1 Decato 3726 // CHCA // RP_PepMix.par
Comment 2 250 shots, 30% lp (74)

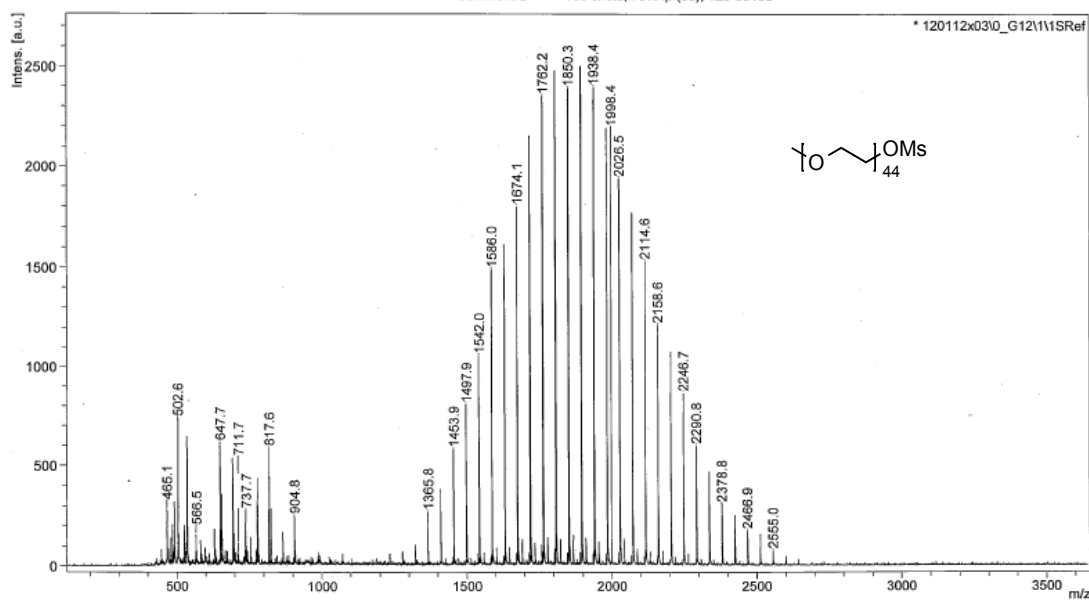


Bruker Ultraflex III, Chem. Dept., Univ. Wisconsin, Cite: NIH NCRR 1S10RR024601-01

printed: 10/2/2013 11:37:06 AM

D:\Data\mmv\120112x0310_G121

Comment 1 Tucker 118 // CHCA // RP_PepMix.par
Comment 2 150 shots, 70% lp (68), 120-3640d



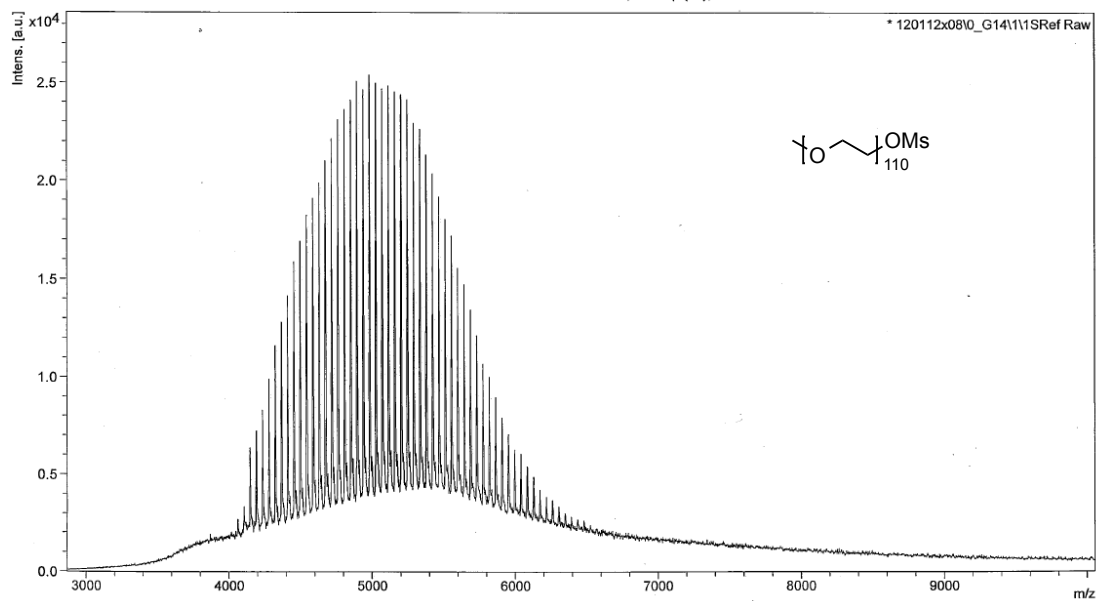
Bruker Ultraflex III, Chem. Dept., Univ. Wisconsin, Cite: NIH NCRR 1S10RR024601-01

printed: 1/12/2012 11:56:35 AM

D:\Data\mmv\120112x08\0_g14\1

Comment 1 Tucker 120 // CHCA // RP_ProtMix.par

Comment 2 350 shots, 45% lp (72), 1920-14859d



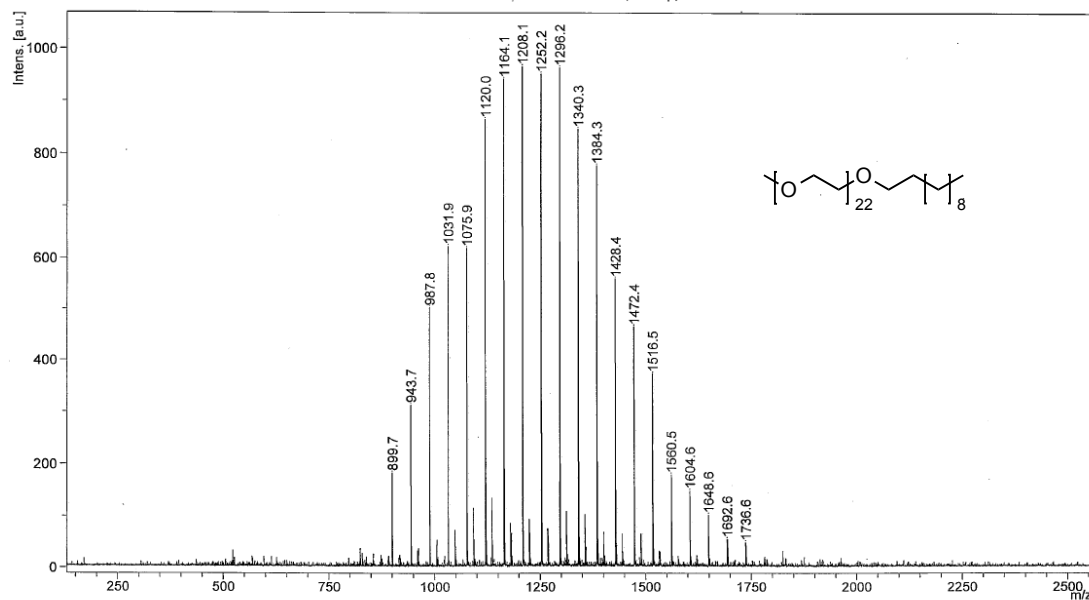
Bruker Ultraflex III, Chem. Dept., Univ. Wisconsin, Cite: NIH NCRR 1S10RR024601-01

printed: 1/12/2012 12:28:14 PM

D:\Data\mmv\130213x01\0_A12\1

Comment 1 Tucker 578 // CHCA // RP_PepMix.par

Comment 2 250 shots, 30% lp, 120-3640d

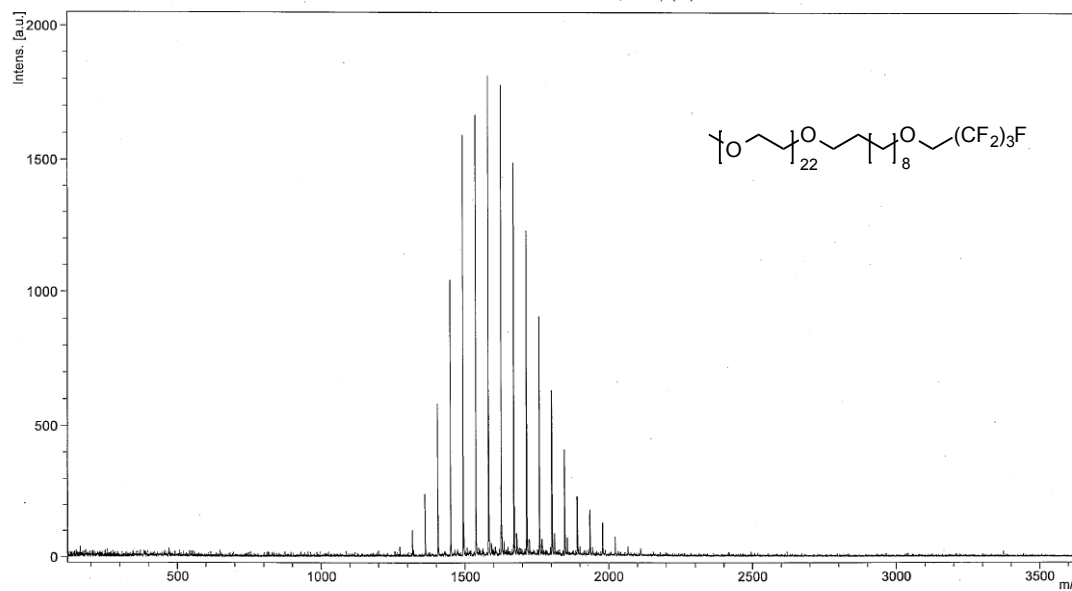


Bruker Ultraflex III, Chem. Dept., Univ. Wisconsin, Cite: NIH NCRR 1S10RR024601-01

printed: 2/13/2013 11:25:12 AM

D:\Data\mmv\130828x0610_E1\1

Comment 1 Tucker 3388 // dnb // RP_PepMix.par
Comment 2 150 shots, 25% lp (74)

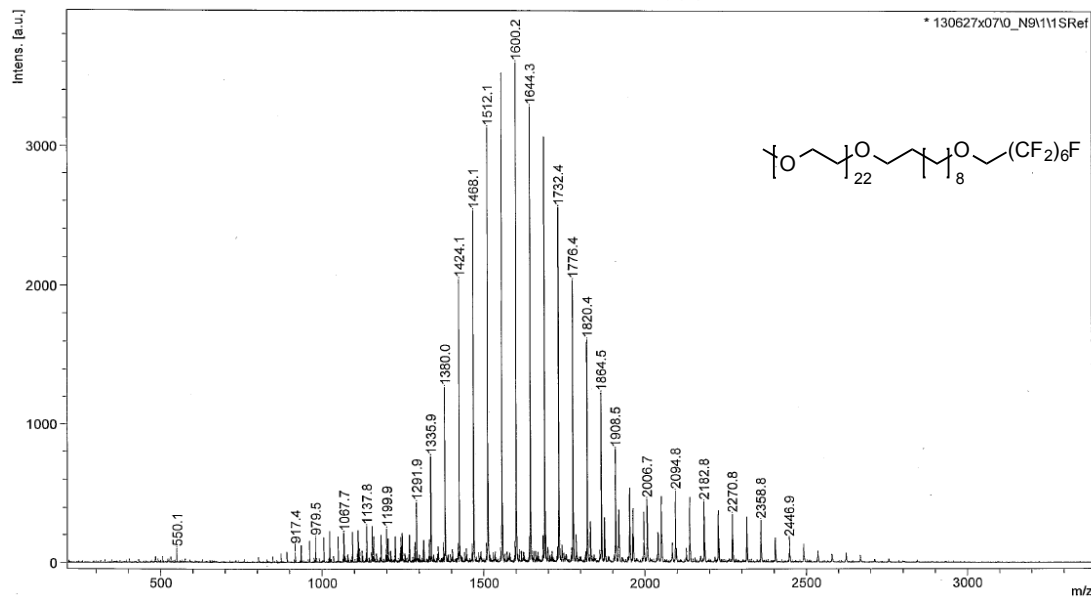


Bruker Ultraflex III, Chem. Dept., Univ. Wisconsin, Cite: NIH NCRR 1S10RR024601-01

printed: 8/28/2013 3:43:05 PM

D:\Data\mmv\130627x0710_n9\1

Comment 1 Tucker 2228 // dnb // RP_PepMix.par
Comment 2 300 shots, 40% lp (72)



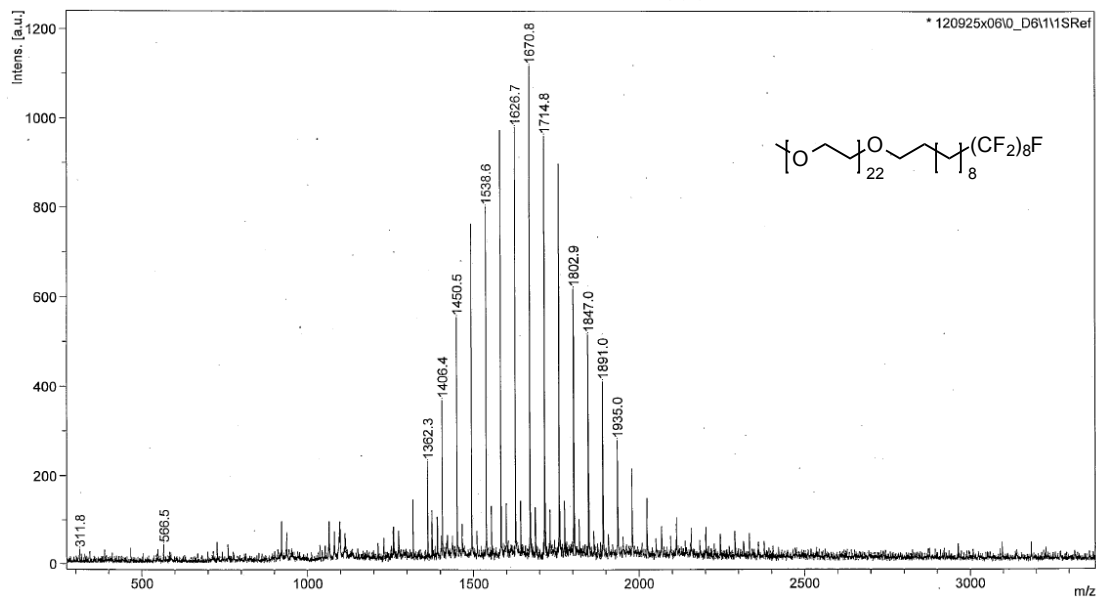
Bruker Ultraflex III, Chem. Dept., Univ. Wisconsin, Cite: NIH NCRR 1S10RR024601-01

printed: 6/27/2013 1:39:32 PM

D:\Data\mmv\120925x06\0_D611

Comment 1 Tucker 4028// dnb // RP_PepMix.par

Comment 2 400 shots, 50% lp (72) d



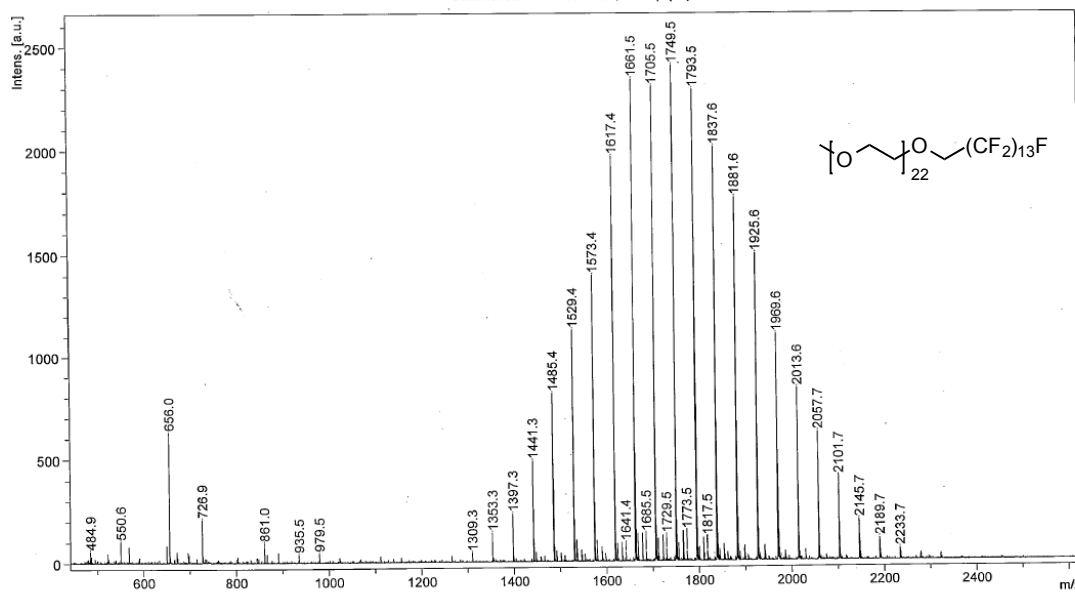
Bruker Ultraflex III, Chem. Dept., Univ. Wisconsin, Cite: NIH NCRR 1S10RR024601-01

printed: 9/25/2012 11:58:32 AM

D:\Data\Mecozzi\140226x01\0_1151

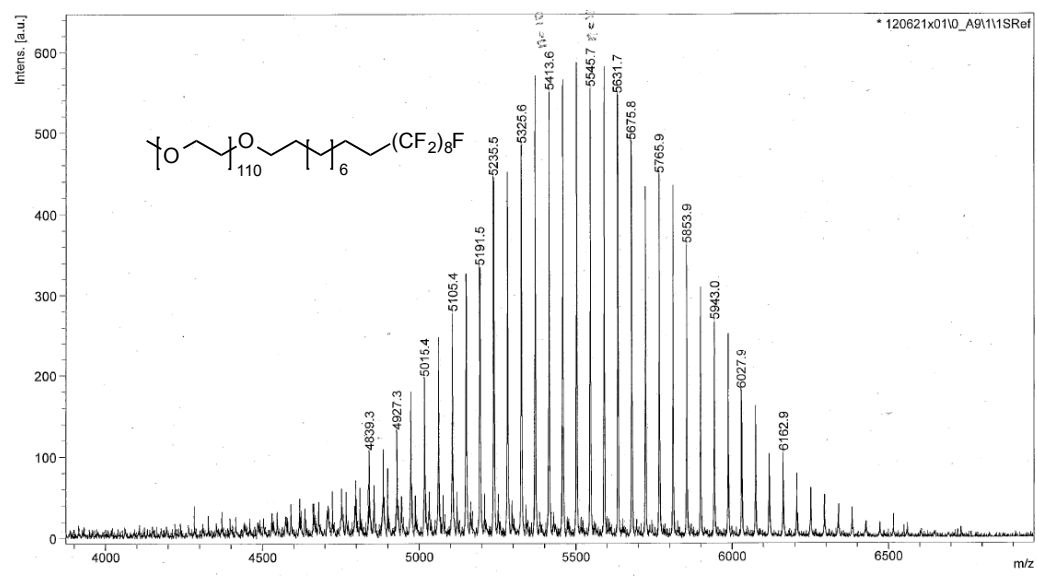
Comment 1 Fleetwood 646 // CHCA // RP_PepMix.par

Comment 2 100 shots, 80% lp (74)



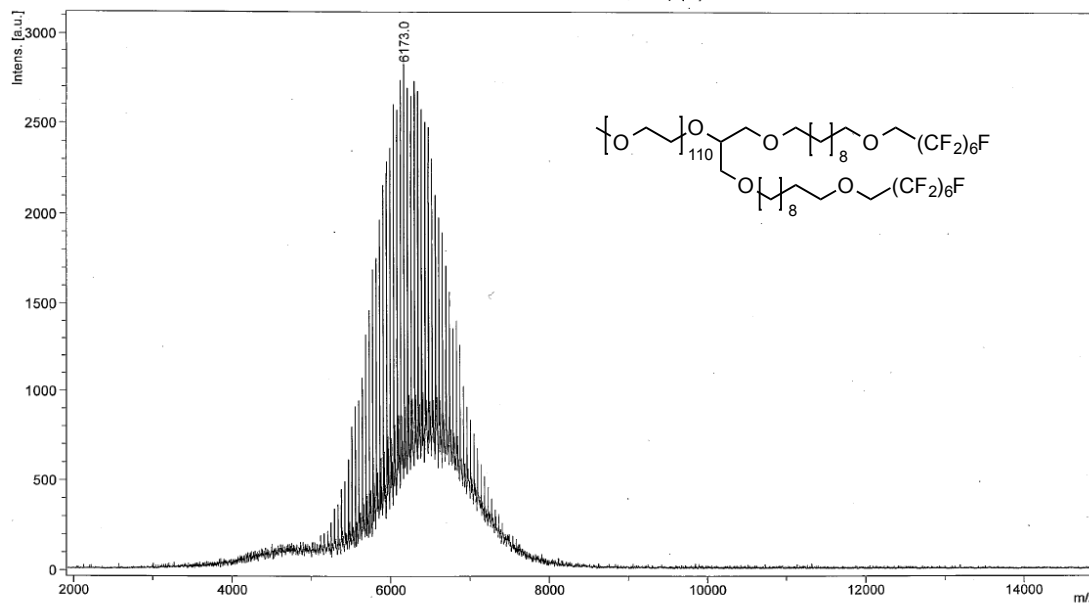
Bruker Ultraflex III, Chem. Dept., Univ. Wisconsin, Cite: NIH NCRR 1S10RR024601-01

printed: 2/26/2014 9:54:29 AM



printed: 5/29/2013 3:35:20 PM

Comment 1 Tucker 1063 // CHCA // RP_ProtMix.par
Comment 2 400 shots, 30% lp (74)

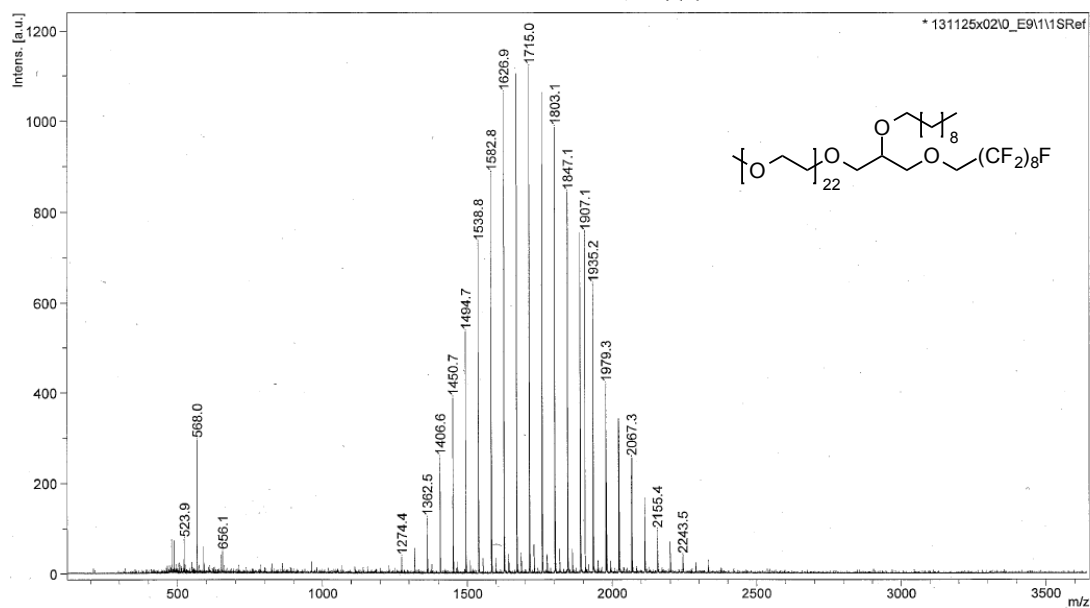


Bruker Ultraflex III, Chem. Dept., Univ. Wisconsin, Cite: NIH NCRR 1S10RR024601-01

printed: 3/27/2014 3:07:58 PM

D:\Data\mmv\131125x02\0 E9\1

Comment 1 McCoy 4266 // CHCA // RP_PepMix.par
Comment 2 100 shots, 70% lp (72)

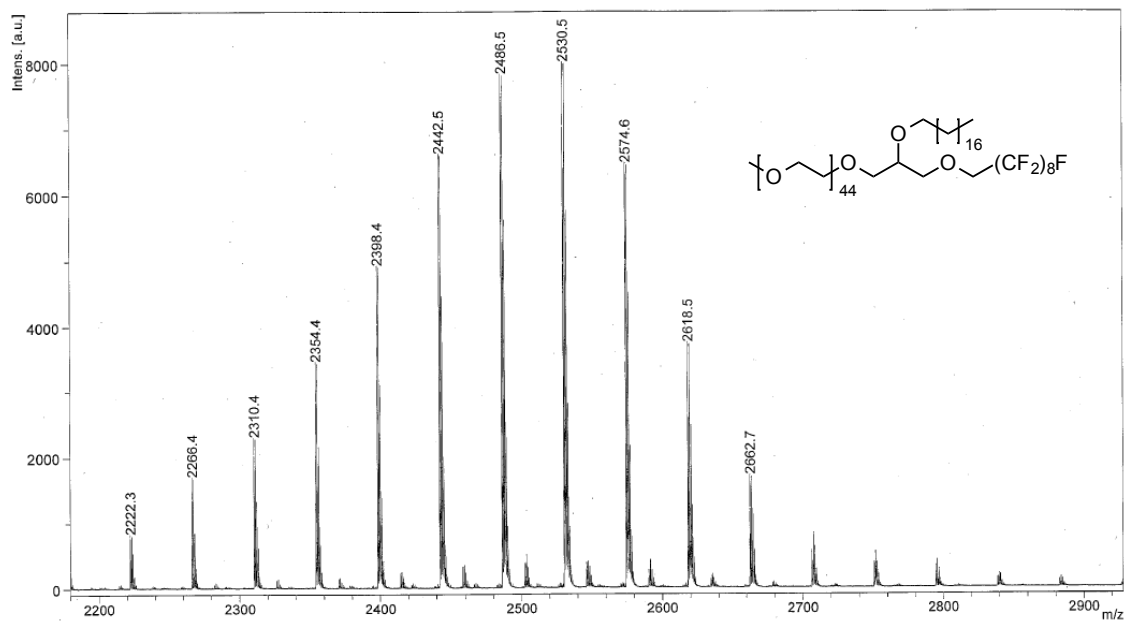


Bruker Ultraflex III, Chem. Dept., Univ. Wisconsin, Cite: NIH NCRR 1S10RR024601-01

printed: 11/25/2013 12:06:25 PM

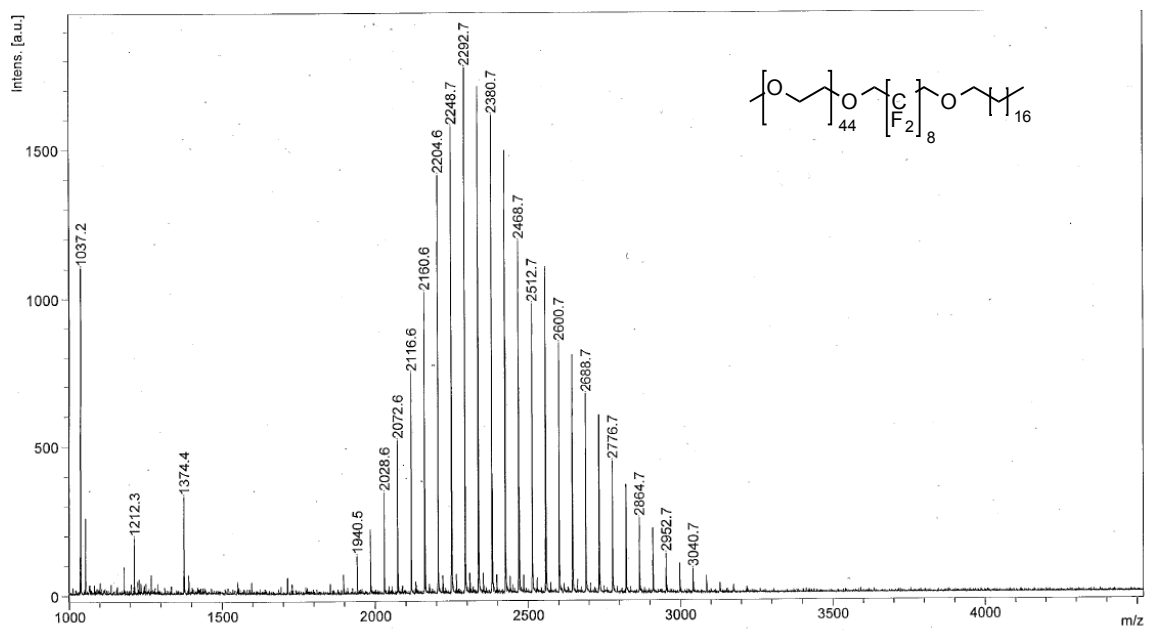
D:\Data\mmv\140218x09\0_E151

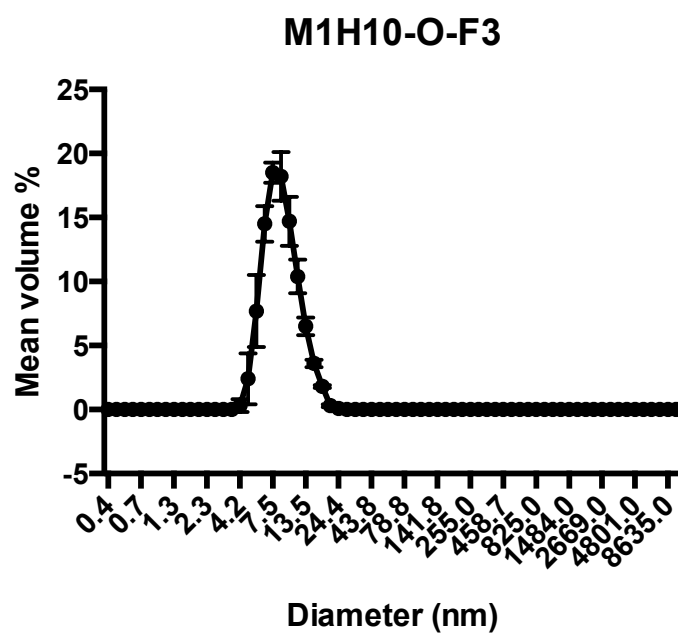
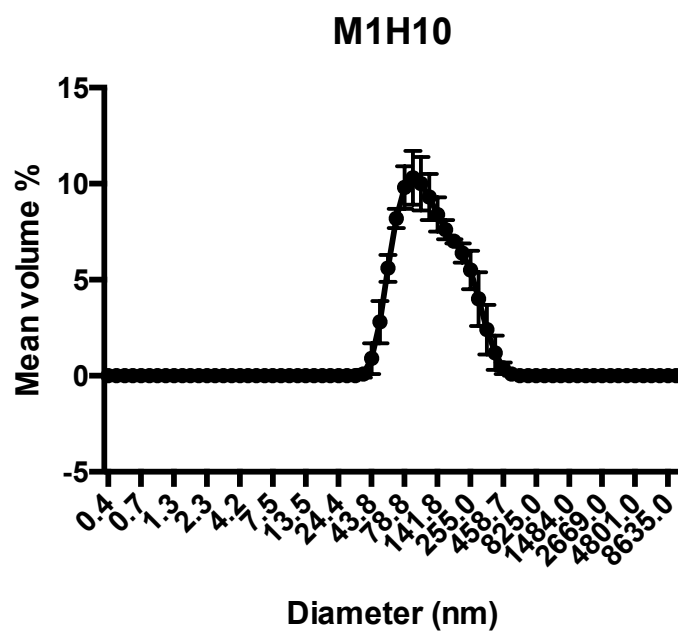
Comment 1 McCoy 549 // CHCA // RP_PepMix.par
Comment 2 150 shots, 45% lp (76)

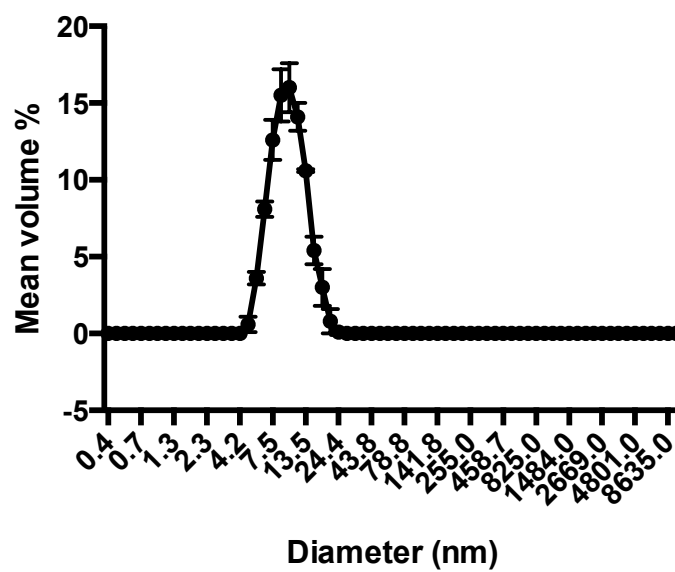
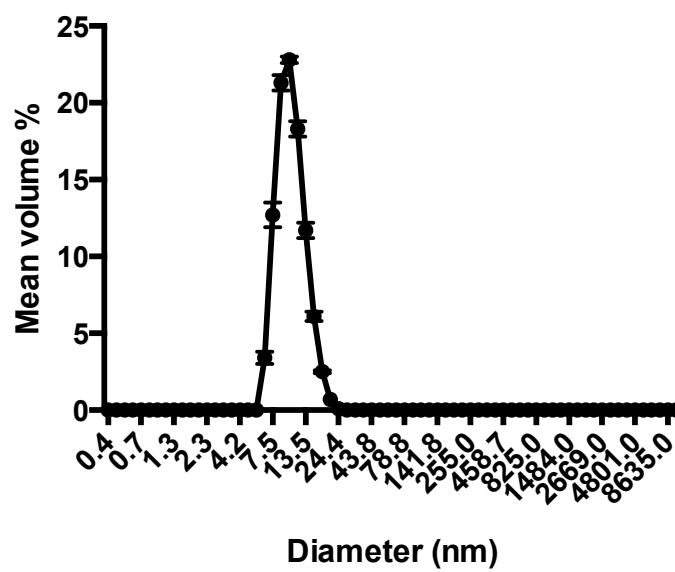


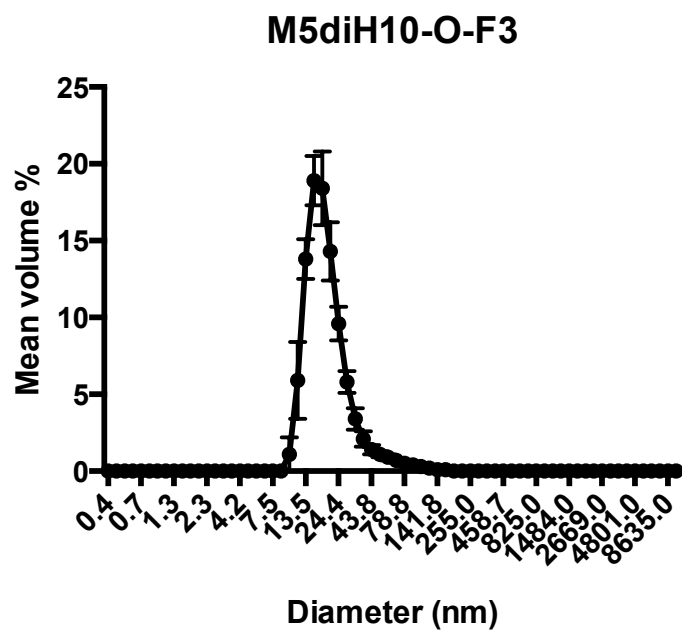
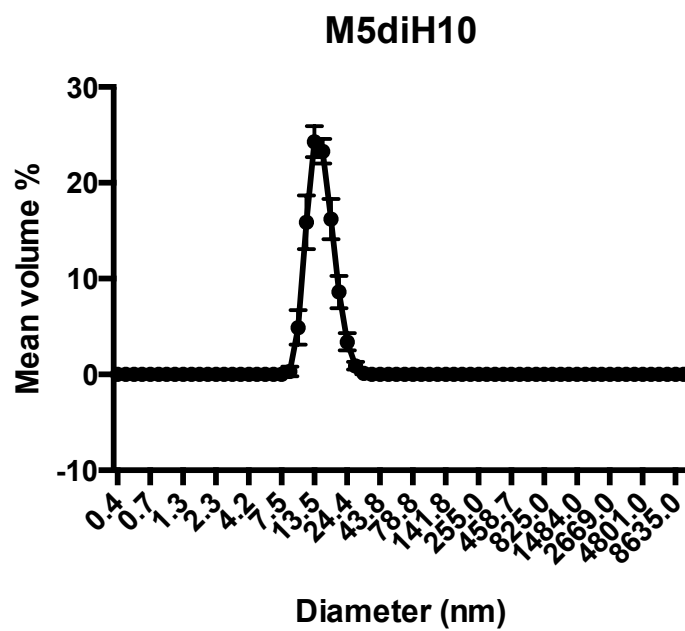
Bruker Ultraflex III, Chem. Dept., Univ. Wisconsin, Cite: NIH NCRR 1S10RR024601-01

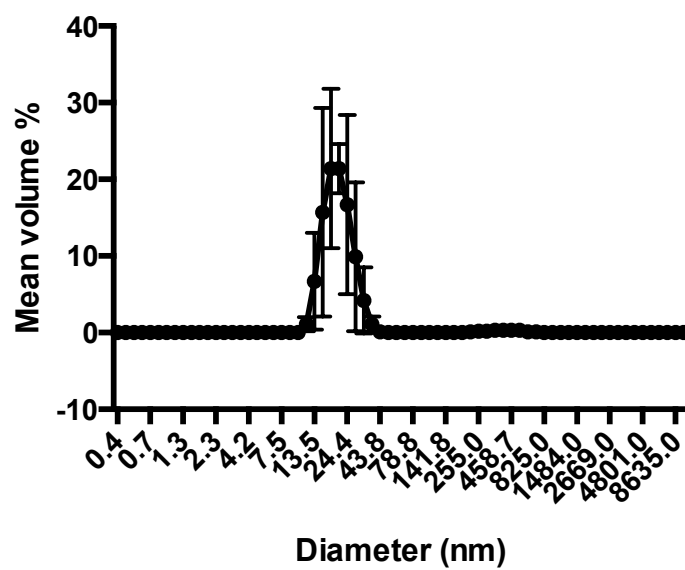
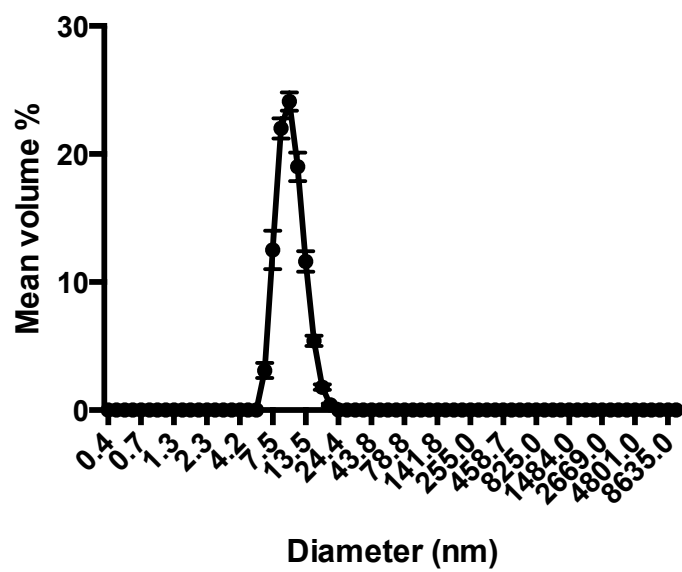
printed: 2/18/2014 11:30:41 AM

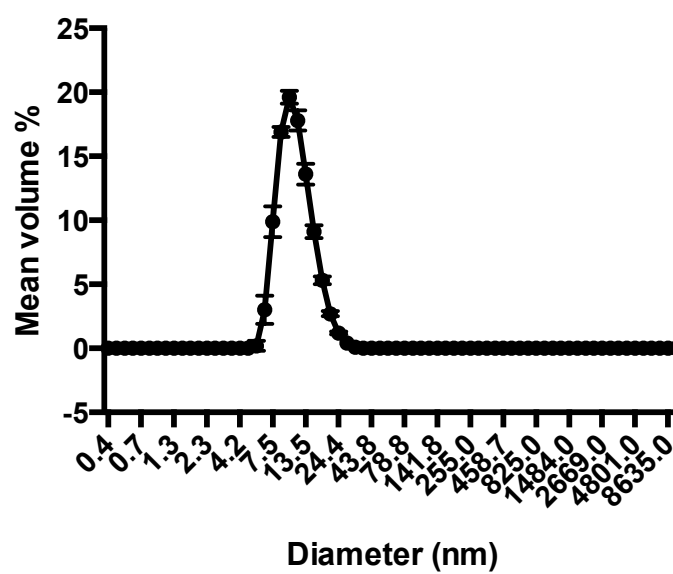
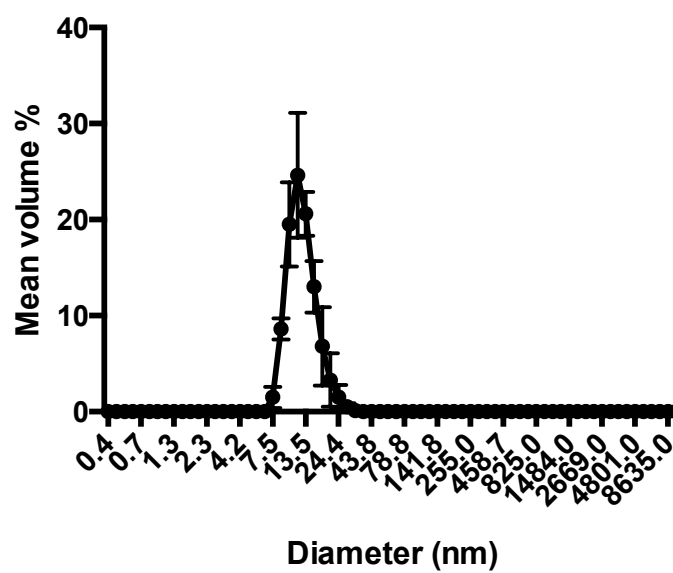


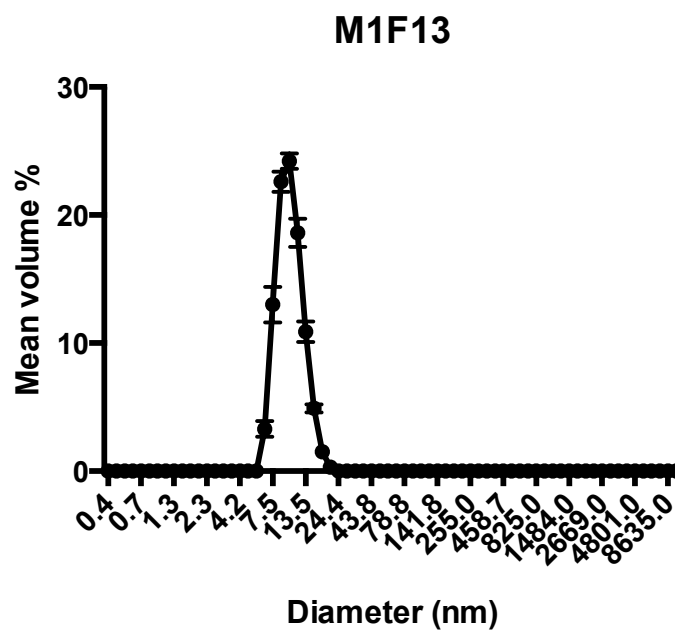
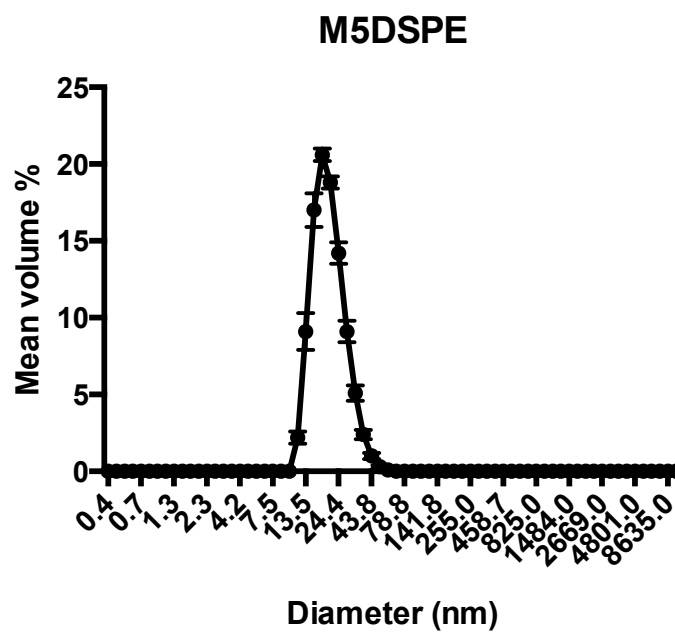
A2.2.3. DLS data

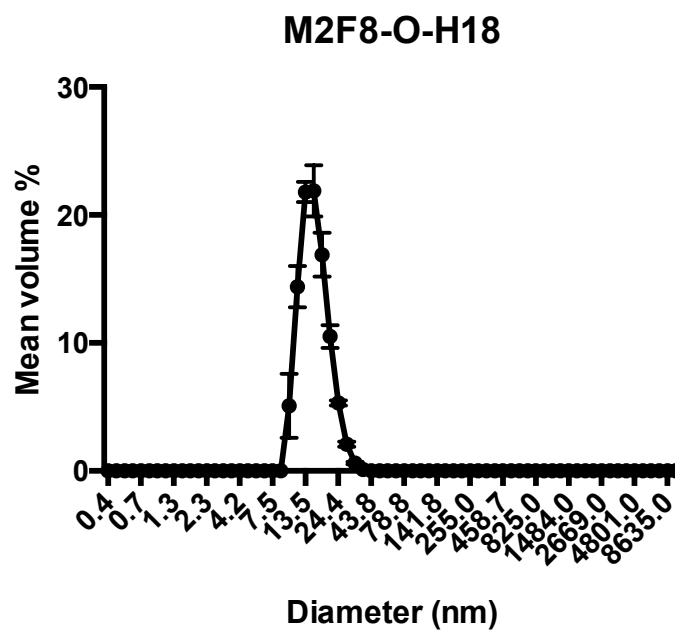
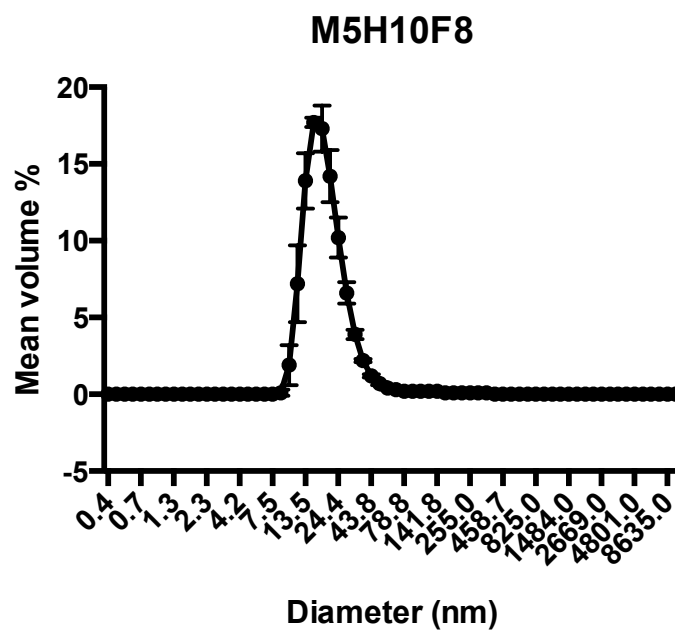
M1H10-O-F6**M1H10F8**



M5diH10-O-F6**M1 μ H10F8**

M2 μ H18F8**M2DSPE**





A2.2.4. CMC data

Each sample was measured in quadruplicate. The average and standard deviation were then calculated. The CMC value was determined from the intersection of the slope at the crossover point and the slope at high concentrations. The error in the CMC measurement was calculated by applying a weighted, least-squares analysis to the linear sections of interest. The individual uncertainties of the two slopes and intercepts produced by the weighted least squares analysis were then propagated through as follows:

$$x_{\log(M)} = \frac{b_2 - b_1}{m_2 - m_1}$$

$$\sigma_{x_{\log(M)}} = \sqrt{x_{\log(M)}^2 \left[\left(\frac{\sigma_{b_2 - b_1}}{b_2 - b_1} \right)^2 + \left[\left(\frac{\sigma_{m_1 - m_2}}{m_1 - m_2} \right)^2 \right] \right]}$$

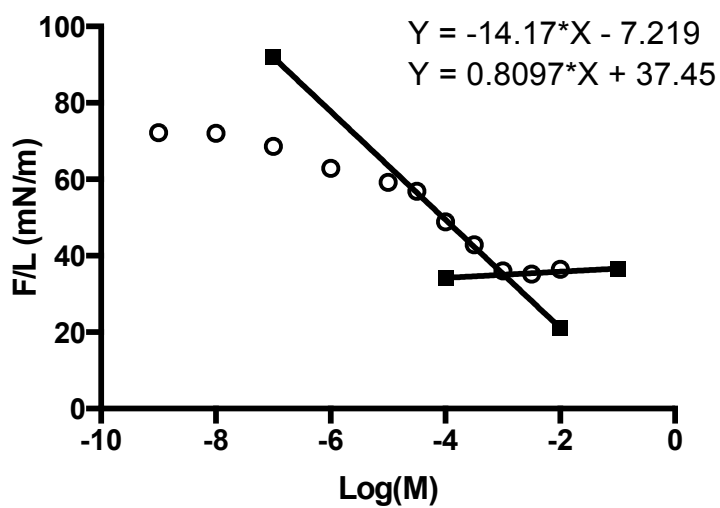
where

$$\sigma_{m_1 - m_2} = \sqrt{\sigma_{m_1}^2 + \sigma_{m_2}^2}, \sigma_{b_2 - b_1} = \sqrt{\sigma_{b_2}^2 + \sigma_{b_1}^2}$$

The weighted, least-squares analysis was chosen because the uncertainty of each individual data point was known.

M1H10

log(M)	Ave. S.T. (mN/m)	Std. Dev.
-2.00	36.491	0.550
-2.50	35.170	0.245
-3.00	36.054	0.689
-3.50	42.887	0.243
-4.00	48.846	0.185
-4.50	56.902	0.204
-5.00	59.178	0.560
-6.00	62.912	0.155
-7.00	68.616	0.147
-8.00	72.051	0.175
-9.00	72.198	0.126

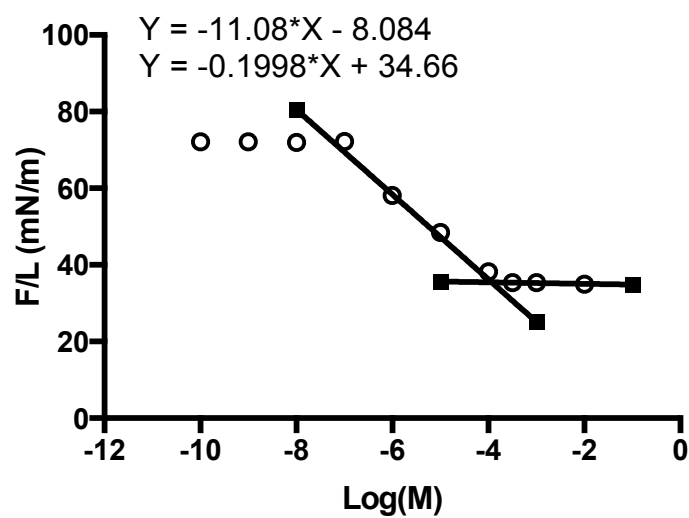


$$\text{CMC (log(M))} = -3.01 \pm 0.25$$

$$\gamma_{\text{CMC}} = 35.0 \text{ mN/m}$$

M1H10-O-F3

log(M)	Ave. S.T. (mN/m)	Std. Dev.
-2.00	34.978	0.227
-3.00	35.366	0.145
-3.50	35.349	0.065
-4.00	38.230	0.149
-5.00	48.457	0.214
-6.00	58.153	0.027
-7.00	72.238	0.117
-8.00	71.986	0.141
-9.00	72.094	0.156

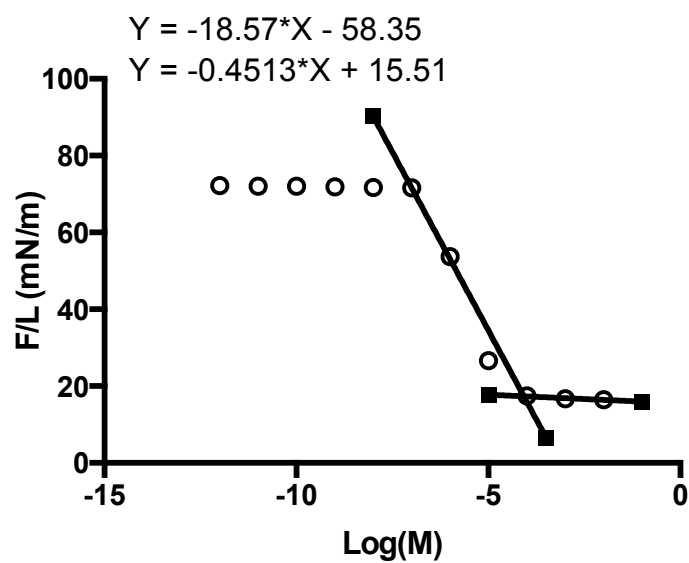


$$\text{CMC} (\log(M)) = -3.82 \pm 0.08$$

$$\gamma_{\text{CMC}} = 35.4 \text{ mN/m}$$

M1H10-O-F6

log(M)	Ave. S.T. (mN/m)	Std. Dev.
-2.00	16.436	0.138
-3.00	16.730	0.263
-4.00	17.441	0.348
-5.00	26.609	1.100
-6.00	53.668	0.210
-7.00	71.598	0.102
-8.00	71.744	0.059
-9.00	71.865	0.051
-10.00	72.065	0.093
-11.00	72.058	0.139
-12.00	72.204	0.571

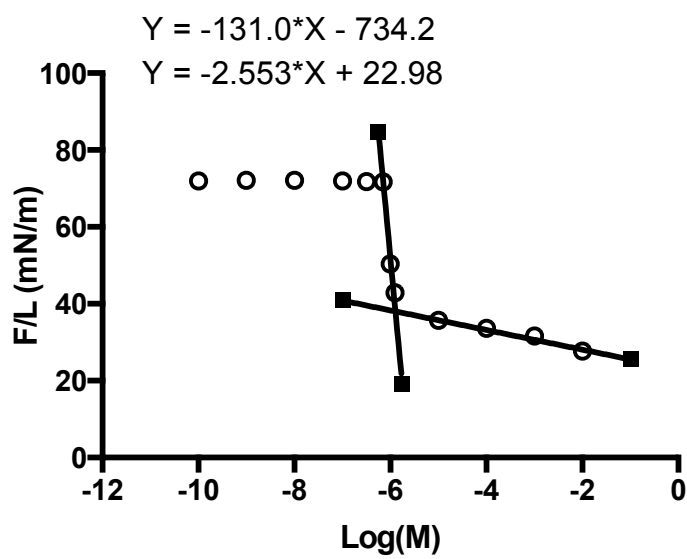


$$\text{CMC} (\log(M)) = -4.53 \pm 0.12$$

$$\gamma_{\text{CMC}} = 17.6 \text{ mN/m}$$

M1H10F8

log(M)	Ave. S.T. (mN/m)	Std. Dev.
-2.00	27.736	0.131
-3.00	31.598	0.203
-4.00	33.664	0.181
-5.00	35.687	0.057
-5.90	42.873	0.365
-6.00	50.397	0.180
-6.15	71.696	0.045
-6.50	71.758	0.150
-7.00	71.993	0.115
-8.00	72.101	0.158
-9.00	72.145	0.139

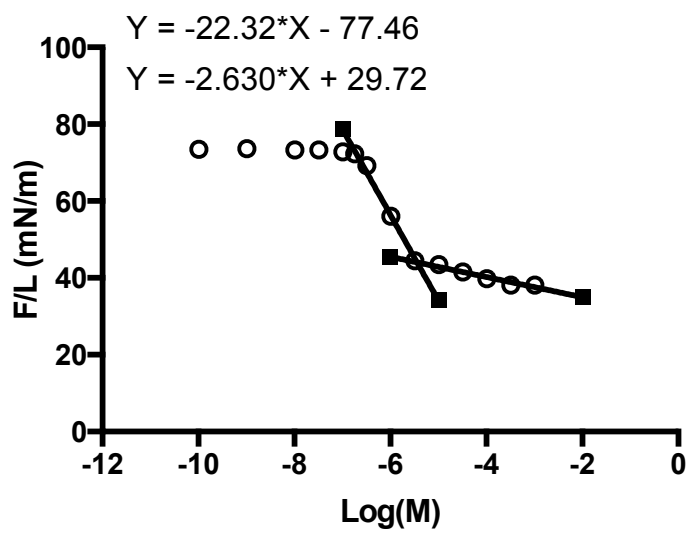


$$\text{CMC} (\log(M)) = -5.85 \pm 0.06$$

$$\gamma_{\text{CMC}} = 38.0 \text{ mN/m}$$

M2H10F8

log(M)	Ave. S.T. (mN/m)	Std. Dev.
-2.99	38.141	0.050
-3.49	38.106	0.057
-3.99	39.786	0.085
-4.49	41.522	0.084
-4.99	43.427	0.133
-5.49	44.479	0.083
-5.99	56.041	0.086
-6.49	69.183	0.150
-6.74	72.255	0.117
-6.99	72.820	0.166
-7.49	73.329	0.120
-7.99	73.257	0.111
-8.99	73.626	0.157
-9.99	73.457	0.125



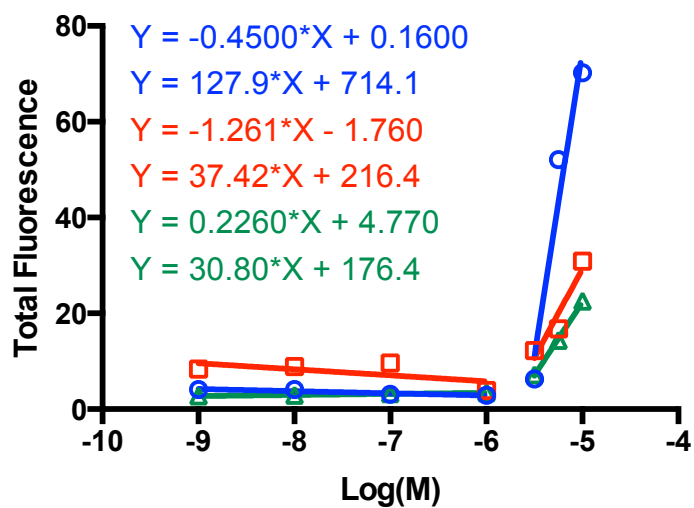
$$\text{CMC} (\log(M)) = -5.44 \pm 0.08$$

$$\gamma_{\text{CMC}} = 44.0 \text{ mN/m}$$

M5H10F8

No CMC was found by surface tension. The CMC was therefore found by pyrene solubilization.

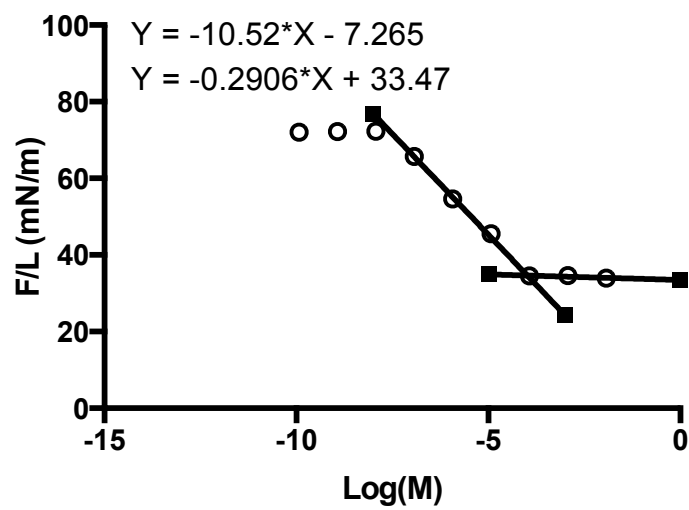
Log(M)	Total Fluorescence	Total Fluorescence	Total Fluorescence
-9	4.08	8.35	2.76
-8	4.07	8.91	2.92
-7	3.08	9.62	3.2
-6	2.91	3.91	3.42
-5.5	6.29	12.22	7.15
-5.25	52.08	16.8	14.34
-5	70.22	30.93	22.55



$$\text{CMC (log(M))} = -5.61 \pm 0.04$$

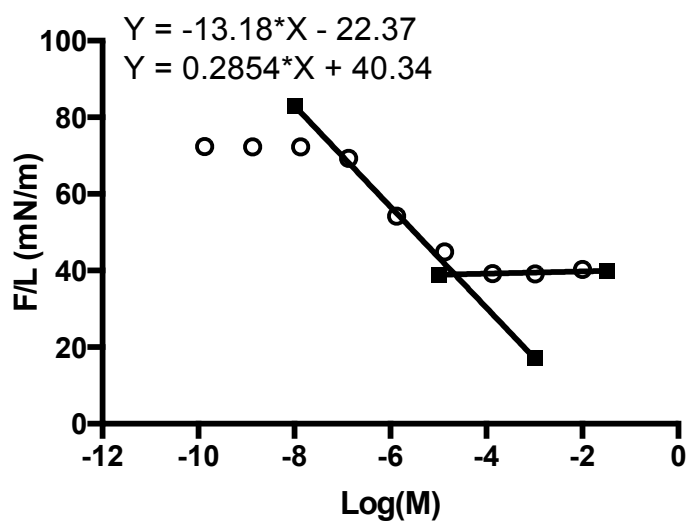
M5diH10

log(M)	Ave. S.T. (mN/m)	Std. Dev.
-1.93	33.968	0.128
-2.93	34.628	0.193
-3.93	34.585	0.087
-4.93	45.578	0.463
-5.93	54.657	0.211
-6.93	65.677	0.132
-7.93	72.330	0.400
-8.93	72.230	0.124
-9.93	72.063	0.100



M5diH10-O-F3

log(M)	Ave. S.T. (mN/m)	Std. Dev.
-2.00	40.300	0.966
-2.98	39.104	0.566
-3.87	39.236	0.049
-4.87	44.913	0.114
-5.87	54.169	0.042
-6.87	69.256	0.067
-7.87	72.245	0.076
-8.87	72.248	0.209
-9.87	72.380	0.108



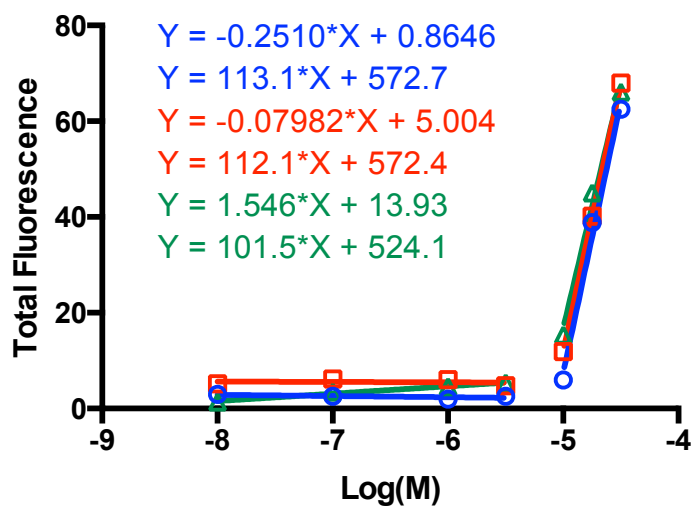
$$\text{CMC (log(M))} = -4.44 \pm 0.18$$

$$\gamma_{\text{CMC}} = 39.1 \text{ mN/m}$$

M5diH10-O-F6

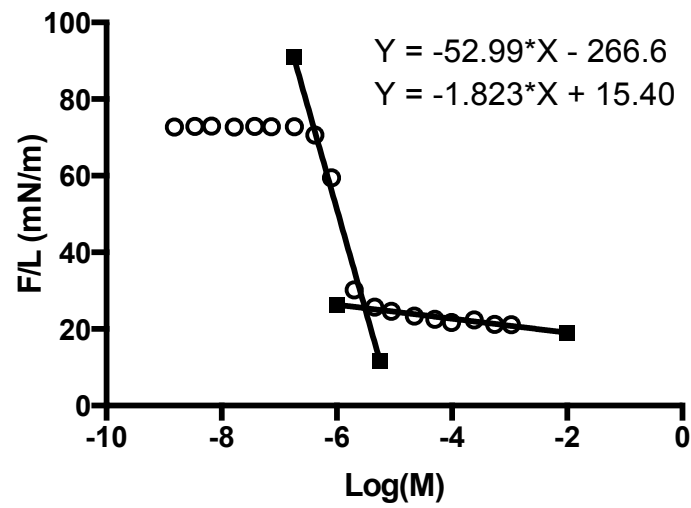
No CMC was found by surface tension. The CMC was therefore found by pyrene solubilization.

Log(M)	Total Fluorescence	Total Fluorescence	Total Fluorescence
-8	2.99	5.16	1.39
-7	2.56	6.18	3.41
-6	1.97	6.04	4.58
-5.499	2.59	4.75	5.36
-4.999	5.96	11.93	15.38
-4.749	38.82	40.16	45.01
-4.499	62.49	67.98	66.12



M1μH10F8

log(M)	Ave. S.T. (mN/m)	Std. Dev.
-2.97	21.138	0.079
-3.26	21.206	0.057
-3.61	22.341	0.059
-4.01	21.708	0.115
-4.30	22.566	0.095
-4.66	23.337	0.102
-5.05	24.638	0.156
-5.34	25.737	0.082
-5.70	30.190	0.205
-6.09	59.424	0.103
-6.38	70.603	0.077
-6.74	72.757	0.197
-7.14	72.805	0.107
-7.42	72.877	0.086
-7.78	72.704	0.420
-8.18	72.922	0.089
-8.46	72.876	0.133
-8.82	72.706	0.153

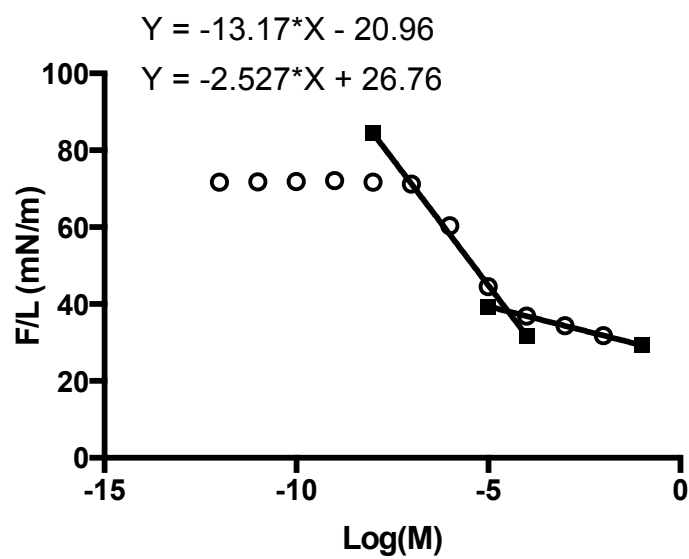


CMC (log(M)) = -5.51 ± 0.05

$\gamma_{\text{CMC}} = 25.4 \text{ mN/m}$

M2 μ H18F8

log(M)	Ave. S.T. (mN/m)	Std. Dev.
-2.00	31.816	0.122
-3.00	34.337	0.230
-4.00	36.876	0.199
-5.00	44.580	0.079
-6.00	60.375	0.140
-7.00	71.180	0.044
-8.00	71.699	0.165
-9.00	72.085	0.126
-10.00	71.891	0.123
-11.00	71.816	0.148
-12.00	71.674	0.150

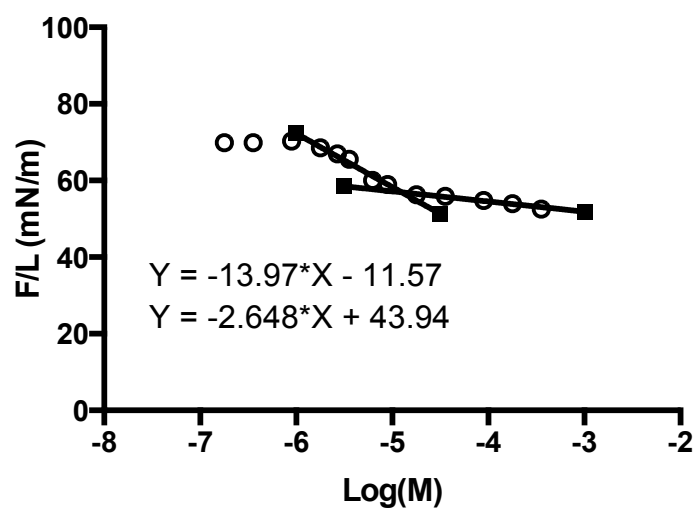


$$\text{CMC} (\log(M)) = -4.61 \pm 0.07$$

$$\gamma_{\text{CMC}} = 38.4 \text{ mN/m}$$

M2DSPE

Log(M)	Ave. S.T. (mN/m)	Std. Dev.
-3.45	52.529	0.236
-3.75	53.942	0.494
-4.05	54.775	0.0845
-4.45	55.891	0.193
-4.75	56.318	0.134
-5.05	58.998	0.047
-5.20	60.028	0.347
-5.45	65.549	0.440
-5.57	66.921	0.281
-5.75	68.566	0.168
-6.05	70.303	0.300
-6.45	69.916	0.121
-6.75	69.882	0.179

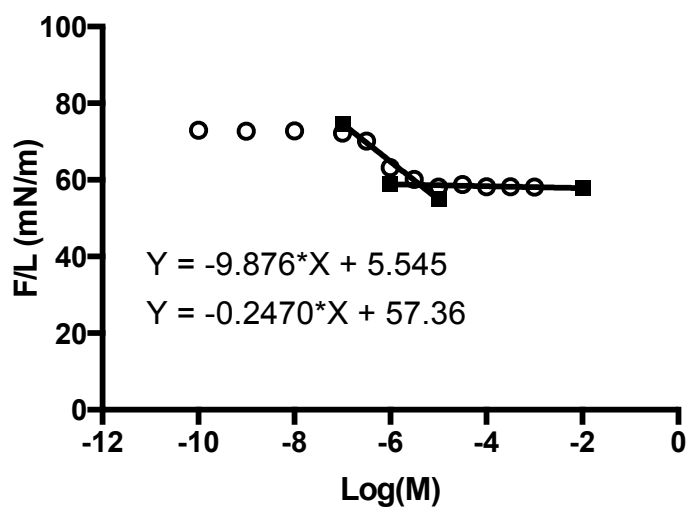


$$\text{CMC} (\log(M)) = -4.90 \pm 0.17$$

$$\gamma_{\text{CMC}} = 56.9 \text{ mN/m}$$

M5DSPE

Log(M)	Ave. S.T. (mN/m)	Std. Dev.
-3.000	58.110	0.090
-3.500	58.190	0.100
-4.000	58.220	0.150
-4.500	58.780	0.130
-5.000	58.160	0.210
-5.500	60.100	0.060
-6.000	63.210	0.110
-6.500	70.160	0.080
-7.000	72.200	0.090
-8.000	72.770	0.150
-9.000	72.730	0.150
-10.000	72.990	0.110

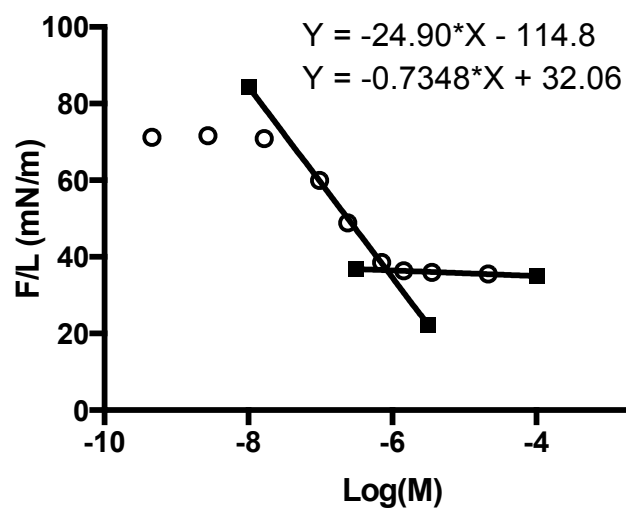


$$\text{CMC (log(M))} = -5.38 \pm 0.10$$

$$\gamma_{\text{CMC}} = 58.7 \text{ mN/m}$$

M1F13

log(M)	Ave. S.T. (mN/m)	Std. Dev.
-4.67	35.509	0.238
-5.45	35.971	0.333
-5.84	36.405	0.305
-6.15	38.529	0.140
-6.62	48.849	0.255
-7.01	59.954	0.131
-7.78	70.854	0.218
-8.56	71.610	0.186
-9.34	71.217	0.165

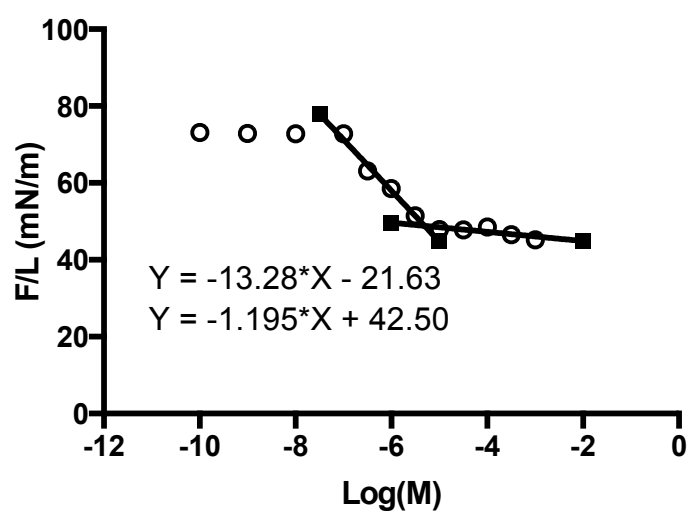


$$\text{CMC} (\log(M)) = -6.08 \pm 0.13$$

$$\gamma_{\text{CMC}} = 36.5 \text{ mN/m}$$

M2F8-O-H18

log(M)	Ave. S.T. (mN/m)	Std. Dev.
-3.00	45.208	0.129
-3.50	46.569	1.504
-4.00	48.568	0.097
-4.50	47.748	0.046
-5.00	47.852	0.172
-5.50	51.489	0.103
-6.00	58.512	0.125
-6.50	63.116	0.132
-7.00	72.752	0.171
-8.00	72.762	0.053
-9.00	72.840	0.134
-10.00	73.104	0.097



$$\text{CMC} (\log(M)) = -5.31 \pm 0.09$$

$$\gamma_{\text{CMC}} = 48.8 \text{ mN/m}$$

A2.2.5. Microviscosity data

M1H10

376	480	I_M/I_E Ratio	
1.95	0.72	2.71	
2.34	0.81	2.89	
2.22	0.83	2.66	
		<hr/>	
		2.75	Ave
		0.11	Std. Dev.

M1H10-O-F3

376	480	I_M/I_E Ratio	
2.77	0.46	6.06	
3.89	0.62	6.28	
3.59	0.64	5.65	
		<hr/>	
		5.99	Ave
		0.32	Std. Dev.

M1H10-O-F6

376	480	I_M/I_E Ratio	
3.53	0.57	6.23	
2.30	0.35	6.47	
2.38	0.39	6.09	
		<hr/>	
		6.26	Ave
		0.19	Std. Dev.

M1H10F8

376	480	I_M/I_E Ratio	
2.55	0.37	6.91	
2.78	0.41	6.81	
2.54	0.38	6.70	
		<hr/>	
		6.81	Ave
		0.11	Std. Dev.

M5diH10

376	480	I_M/I_E Ratio	
1.59	0.47	3.38	
1.48	0.39	3.79	
1.54	0.41	3.76	
		<hr/>	
		3.64	Ave
		0.23	Std. Dev.

M5diH10-O-F3

376	480	I_M/I_E Ratio	
2.83	0.41	6.90	
2.96	0.44	6.73	
2.26	0.34	6.65	
		<hr/>	
		6.76	Ave
		0.13	Std. Dev.

M5diH10-O-F6

376	480	I_M/I_E Ratio	
2.06	0.31	6.68	
2.32	0.33	7.01	
2.47	0.36	6.79	
		<hr/>	
		6.83	Ave
		0.17	Std. Dev.

M1 μ H10F8

376	480	I_M/I_E Ratio	
2.59	0.51	5.12	
2.22	0.44	5.01	
2.31	0.45	5.12	
		<hr/>	
		5.08	Ave
		0.06	Std. Dev.

M2 μ H18F8

376	480	I_M/I_E Ratio	
2.11	0.39	5.45	
2.54	0.48	5.30	
2.28	0.42	5.39	
		<hr/>	
		5.38	Ave
		0.08	Std. Dev.

M2DSPE

376	480	I_M/I_E Ratio	
2.63	0.46	5.72	
3.21	0.60	5.35	
2.53	0.44	5.75	
		<hr/>	
		5.61	Ave
		0.22	Std. Dev.

M5DSPE

376	480	I_M/I_E Ratio	
1.51	0.29	5.21	
2.02	0.39	5.22	
2.32	0.44	5.27	
		<hr/>	
		5.23	Ave
		0.03	Std. Dev.

M1F13

376	480	I_M/I_E Ratio	
1.54	0.44	3.50	
1.50	0.47	3.19	
1.40	0.40	3.50	
		<hr/>	
		3.40	Ave
		0.18	Std. Dev.

A2.2.6. FRET stability data

M1H10 was not analyzed because it did not form micelles. M1F13 was not analyzed because the lipophilic FRET dyes could not be encapsulated. FRET Ratio: $\frac{I_{565}}{(I_{501}+I_{565})}$, where I_{501} = emission of donor dye and I_{565} = emission of acceptor dye

Min.	M1H10-O-F3		M1H10-O-F6		M1H10F8	
	FRET Ratio	Std. Dev.	FRET Ratio	Std. Dev.	FRET Ratio	Std. Dev.
0	0.742	0.017	0.816	0.025	0.813	0.007
15	0.702	0.008	0.811	0.008	0.814	0.012
30	0.692	0.038	0.801	0.004	0.816	0.013
45	0.680	0.014	0.804	0.005	0.815	0.009
60	0.680	0.024	0.784	0.007	0.808	0.008
75	0.669	0.012	0.749	0.006	0.757	0.005
90	0.661	0.003	0.732	0.004	0.750	0.008
105	0.617	0.008	0.728	0.001	0.733	0.003
120	0.587	0.030	0.710	0.005	0.692	0.001

Min.	M5diH10		M5diH10F3		M5diH10-O-F6	
	FRET Ratio	Std. Dev.	FRET Ratio	Std. Dev.	FRET Ratio	Std. Dev.
0	0.642	0.124	0.892	0.064	0.843	0.119
15	0.499	0.081	0.658	0.022	0.800	0.036
30	0.471	0.042	0.531	0.023	0.749	0.016
45	0.459	0.071	0.459	0.010	0.724	0.035
60	0.451	0.042	0.448	0.023	0.673	0.039
75	0.441	0.020	0.446	0.006	0.638	0.029
90	0.439	0.035	0.429	0.025	0.612	0.035
105	0.436	0.039	0.422	0.012	0.609	0.030
120	0.427	0.024	0.415	0.011	0.608	0.049

Min.	M1 μ H10F8		M2 μ H18F8	
	FRET Ratio	Std. Dev.	FRET Ratio	Std. Dev.
0	0.523	0.03	0.658	0.005
15	0.463	0.004	0.596	0.004
30	0.448	0.003	0.565	0.002
45	0.439	0.002	0.519	0.001
60	0.440	0.003	0.494	0.003
75	0.437	0.003	0.476	0.003
90	0.428	0.001	0.452	0.002
105	0.432	0.002	0.423	0.002
120	0.423	0.004	0.430	0.002

Min.	M2DSPE		M5DSPE	
	FRET Ratio	Std. Dev.	FRET Ratio	Std. Dev.
0	0.789	0.013	0.702	0.027
15	0.723	0.018	0.589	0.125
30	0.695	0.011	0.548	0.125
45	0.660	0.014	0.533	0.077
60	0.634	0.010	0.504	0.046
75	0.621	0.016	0.481	0.022
90	0.616	0.013	0.471	0.039
105	0.626	0.003	0.452	0.042
120	0.626	0.011	0.444	0.027

A2.2.7 Paclitaxel encapsulation data

Amphiphile	Initial Encapsulation $\mu\text{g/mL}$ (ave \pm SD, n = 3) PTX	Remaining After 24 h $\mu\text{g/mL}$ (ave \pm SD, n = 3) PTX
M2DSPE	229.61 \pm 5.38	215.83 \pm 6.51
M5DSPE	187.59 \pm 2.93	184.84 \pm 8.08
M1F13	0	0
M5diH10	152.17 \pm 31.21	16.94 \pm 0.67
M5diH10-O-F3	199.86 \pm 5.65	125.94 \pm 26.75
M5diH10-O-F6	208.38 \pm 15.81	157.15 \pm 17.19
M1H10	<i>Not analyzed, did not form micelles</i>	
M1H10-O-F3	152.50 \pm 9.10	19.11 \pm 6.61
M1H10-O-F6	173.43 \pm 5.59	52.10 \pm 8.19
M1H10F8	192.08 \pm 6.25	80.21 \pm 27.53
M1 μ H10F8	188.44 \pm 6.62	47.27 \pm 6.46
M2 μ H18F8	166.13 \pm 23.39	115.13 \pm 8.75

Amphiphile	Initial Encapsulation wt% (ave \pm SD, n = 3) PTX	Remaining After 24 h wt% (ave \pm SD, n = 3) PTX
M2DSPE	3.41 \pm 0.08	3.21 \pm 0.10
M5DSPE	1.35 \pm 0.02	1.33 \pm 0.06
M1F13	0	0
M5diH10	1.25 \pm 0.26	0.14 \pm 0.01
M5diH10-O-F3	1.47 \pm 0.04	0.93 \pm 0.20
M5diH10-O-F6	1.45 \pm 0.11	1.09 \pm 0.12
M1H10	<i>Not analyzed, did not form micelles</i>	
M1H10-O-F3	4.62 \pm 0.28	0.58 \pm 0.20
M1H10-O-F6	4.56 \pm 0.15	1.37 \pm 0.22
M1H10F8	4.80 \pm 0.16	2.00 \pm 0.69
M1 μ H10F8	4.71 \pm 0.17	1.18 \pm 0.16
M2 μ H18F8	2.72 \pm 0.38	1.89 \pm 0.14

Amphiphile	Average surfactant:PTX ratio	Average surfactant:PTX ratio
	Initial	After 24 h
M2DSPE	9	9
M5DSPE	11	11
M1F13	0	0
M5diH10	13	120
M5diH10-O-F3	10	16
M5diH10-O-F6	11	21
M1H10	<i>Not analyzed, did not form micelles</i>	
M1H10-O-F3	13	106
M1H10-O-F6	12	39
M1H10F8	11	26
M1 μ H10F8	11	44
M2 μ H18F8	12	17

A2.3 Anesthetic emulsion data

A2.3.1 Sevoflurane emulsions

Materials: 11.9 mL normal saline, 590 mg M5H10F8, 1.7 mL PFOB, 3.4 mL sevoflurane (20 vol%).

Time (d)	Mean diameter (nm)	SD
0	166.0	15.102
1	213.6	23.929
2	228.8	46.676
3	243.4	35.781
5	274.8	35.454
7	294.0	59.969
14	358.9	83.632
21	411.5	74.069
28	466.4	166.038
35	517.4	172.304
42	643.5	296.645
49	644.4	280.954
56	729.4	322.389
63	787.3	399.14
77	955.4	527.38
84	Phase separated	

A2.3.2 Isoflurane Emulsions

20 vol% Formulations

Materials: 11.9 mL normal saline, 590 mg M5H10F8, 1.7 mL PFOB, 3.4 mL isoflurane.

Time (d)	Mean diameter (nm)	SD
0	220.20	37.442
1	230.46	46.624
2	232.60	42.094
3	243.00	39.849
5	240.40	53.126
7	254.80	81.283
14	301.80	43.756
21	336.10	44.018
28	357.90	45.101
35	376.90	92.706
42	394.90	74.644
49	415.50	114.674
56	433.30	81.890

63	462.00	149.495
77	550.60	238.946
84	572.80	237.719
91	543.00	210.696
98	566.20	250.823
105	577.80	242.669
112	660.70	325.728
119	672.90	300.645
126	Phase separated	

Materials: 11.9 mL normal saline, 180 mg M1H10F8, 1.7 mL PFOB, 3.4 mL isoflurane.

Results: immediate phase separation.

Materials: 11.9 mL normal saline, 300 mg M1H10F8, 1.7 mL PFOB, 3.4 mL isoflurane.

Results: immediate phase separation.

Materials: 13.6 mL normal saline, 680 mg M1H10, 3.4 mL isoflurane.

Results: immediate phase separation.

25 vol% Formulations

Materials: 11.05 mL normal saline, 610 mg M5H10F8, 1.7 mL PFOB, 4.25 mL isoflurane.

Time (d)	Mean diameter (nm)	SD
0	354.9	101.865
1	372.2	67.374
2	363.9	96.445
3	382.7	90.698
5	366.5	76.597
7	399.4	72.694
14	446.8	150.588
21	530.7	169.308
28	551.7	175.487
35	582.6	227.203
42	629.3	264.942
49	607.0	291.963
56	Phase separated	

Materials: 11.05 mL normal saline, 610 mg M1H10-O-F6, 4.25 mL isoflurane, 1.7 mL PFOB.

Results: immediate phase separation.

30 vol% Formulations

Materials: 10.2 mL normal saline, 563 mg M5H10F8, 1.7 mL PFOB, 5.1 mL isoflurane.

Results: initial particle size of 2618.8 nm, phase separated after 24 hours.

Materials: 10.2 mL normal saline, 150 mg M1H10F8, 1.7 mL PFOB, 5.1 mL isoflurane.

Results: immediate phase separation.

Materials: 10.2 mL normal saline, 255 mg M1H10F8, 1.7 mL PFOB, 5.1 mL isoflurane.

Results: immediate phase separation.

Materials: 11.9 mL normal saline, 300 mg M1H10F8, 5.1 mL isoflurane.

Results: immediate phase separation.

Materials: 11.9 mL normal saline, 280 mg M1H10F8, 130 mg Lipoid E80, 5.1 mL isoflurane.

Results: Initial particle size of 469.7 nm. Phase separated within 24 hours.

Materials: 11.9 mL normal saline, 560 mg M1H10F8, 260 mg Lipoid E80, 5.1 mL isoflurane.

Time (d)	Mean diameter (nm)	SD
0	266.0	114.099
1	263.5	115.170
2	256.4	116.169
3	244.5	113.702
5	246.6	113.177

7	242.2	117.705
14	235.8	123.075
21	Phase separated	

Materials: 11.9 mL DI water, 260 mg Lipoid E80, 5.1 mL isoflurane (30 vol%), 0.3 mL glycerol.

Time (d)	Mean diameter (nm)	SD
0	257.4	114.296
1	258.8	125.789
2	Phase separated	

Materials: 10.2 mL normal saline, 567 mg M5diH10-O-F3, 1.7 mL PFOB, 5.1 mL isoflurane (30 vol%).

Results: immediate phase separation.

Materials: 11.9 mL normal saline, 405 mg M1H10, 260 mg Lipoid E80, 5.1 mL isoflurane (30 vol%).

Results: Initial particle size of 257.0 nm. Phase separated after 24 hours.

Materials: 11.9 mL normal saline, 1.73 g M5diH10, 260 mg Lipoid E80, 5.1 mL isoflurane (30 vol%).

Results: Initial particle size of 322.4 nm. Phase separated after 24 hours.

A2.3.3 Propofol Emulsions

No-additive, linear/dibranched formulations

Materials: 16.82 mL normal saline, 420.5 mg M1H10-O-F3, 0.18 mL propofol.

Time (d)	Mean diameter (nm)	SD
0	364.2	177.700
1	738.8	585.107
2	848.4	674.500
3	1709.6	1489.096
5	Phase separated	

Materials: 16.82 mL normal saline, 420.5 mg M5diH10, 0.18 mL propofol.

Time (d)	Mean diameter (nm)	SD
0	202.6	68.685
1	250.3	48.554
2	273.2	71.571
3	292.3	63.724
5	304.1	45.008
7	377.4	122.664
14	449.3	181.905
21	472.6	195.671
28	490.2	198.184
35	432.9	229.44
42	404.6	252.473
49	556.9	284.144
56	600.5	249.822
63	492.1	288.388
70	620.6	270.588
77	656.9	310.708
84	625.1	261.305
91	474.3	327.735
98	549.5	301.655
105	628.8	302.455
112	633.3	298.303
119	622	280.246
126	684.2	291.459
133	693.3	310.129
140	711.4	350.271
147	720.6	377.619
154	739.3	318.652
161	Phase separated	

Materials: 16.82 mL normal saline, 420.5 mg M1H10, 0.18 mL propofol.

Time (d)	Mean diameter (nm)	SD
0	461.6	281.553
1	866.7	718.458
2	1248.5	850.233
3	Phase separated	

Lipoid E80-stabilized Formulations

Materials (“L3” Formulation): 16.82 mL normal saline, 420.5 mg M1H10-O-F3, 204 mg

Lipoid E80, 0.18 mL propofol.

Time (d)	Mean diameter (nm)	SD
0	160.8	74.278
1	170.9	72.991
2	175.7	72.05
3	179.0	72.851
5	178.2	76.457
7	171.5	74.793
14	180.4	78.279
21	183.4	81.067
28	172.7	74.416
35	168.0	74.757
42	182.4	79.717
49	177.0	78.571
56	180.0	78.309
63	170.6	75.086
70	168.9	87.985
77	174.6	81.34
84	183.0	86.934
91	155.8	80.226
98	169.7	83.174
105	167.6	77.914
112	163.5	80.273
119	172.8	89.169
126	176.5	66.906
133	172.1	71.213

140	166.0	80.852
147	173.3	90.625
154	169.4	87.267
161	170.8	102.987
168	176.7	97.733
175	172.4	97.245
182	174.1	97.322
189	169.3	97.27
196	171.6	91.269
203	171.6	105.731
210	171.5	104.438
217	165.7	95.412
224	175.0	95.023
231	180.7	92.9
238	159.8	87.268
245	175.3	93.666
252	189.4	88.703
259	173.8	97.617
266	161.8	81.218
273	171.5	102.042
280	180.0	113.6
287	180.0	94.321
294	172.7	97.722
301	171.0	93.735
308	181.3	95.275
329	180.8	107.558
336	200.2	117.305
343	177.4	97.051
350	177.3	110.661

Materials: 16.82 mL normal saline, 204 mg Lipoid E80, 0.18 mL propofol.

Results: Initial particle size 2106.0 nm, phase separated within 24 hours.

Materials: 16.82 mL normal saline, 420.5 mg M1H10, 204 mg Lipoid E80, 0.18 mL propofol.

Time (d)	Mean diameter (nm)	SD
0	616.6	545.071
1	2998.5	2635.701
2	Phase separated	

Materials: 16.82 mL normal saline, 420.5 mg M1H10-O-F3, 102 mg Lipoid E80, 0.18 mL propofol.

Time (d)	Mean diameter (nm)	SD
0	323.1	186.758
1	872.0	709.787
2	Phase separated	

Materials: 16.82 mL normal saline, 420.5 mg M1H10-O-F3, 152 mg Lipoid E80, 0.18 mL propofol.

Time (d)	Mean diameter (nm)	SD
0	232.5	95.547
1	299.0	178.791
2	289.0	180.636
3	308.0	200.833
5	316.0	212.038
7	320.9	211.123
14	351.7	247.247
21	335.8	234.743
28	323.4	199.213
35	315.3	204.346
42	343.4	240.736
49	344.0	236.000
56	352.6	257.783
63	342.0	224.72
70	318.3	230.467
77	335.7	227.287
84	324.1	225.928
91	338.2	229.285
98	334.2	229.285

105	319.4	212.313
126	334.3	230.022
133	306.1	203.588
140	319.1	215.064
147	296.3	194.946
154	309.4	210.566
161	304.7	204.175
168	312.1	205.766
175	293.3	202.347
182	297.4	200.428
289	291.0	187.689
196	295.1	188.294

Materials: 16.82 mL normal saline, 420.5 mg M1H10-O-F6, 204 mg Lipoid E80, 0.18 mL propofol.

Time (d)	Mean diameter (nm)	SD
0	173.2	82.984
1	217.9	98.07
2	227.7	103.166
3	227.9	108.235
5	230.3	113.081
7	231.5	119.662
14	238.5	121.855
21	240.2	120.821
28	234.6	125.301
35	237	118.99
42	236.6	119.939
49	238.8	120.369
56	237.4	120.347
63	234.9	120.51
70	241.5	114.212
77	236.8	122.411
84	234.5	123.824
91	236.5	124.862
98	232.7	118.686
105	239.2	117.443
126	237.4	114.44

133	235.1	123.88
140	234.8	119.041
147	234.9	122.134

Materials: 16.82 mL DI water, 420.5 mg M1H10-O-F6, 204 mg Lipoid E80, 0.18 mL propofol.

Time (d)	Mean diameter (nm)	SD
0	193.1	88.234
1	215.1	89.917
2	212.8	101.924
3	217.6	107.638
5	218.6	103.378
7	225.6	106.716
14	233.0	107.633
21	223.0	103.013
28	221.5	110.963
35	217.1	111.371
42	230.5	109.723
49	226.4	113.660
56	226.5	112.354
70	225.6	110.683
77	226.2	112.652
84	224.9	113.617
105	230.7	108.673
112	216.3	113.109
119	234.0	126.148
126	225.4	129.580

Materials: 16.82 mL DI water, 204 mg Lipoid E80, 0.18 mL propofol.

Time (d)	Mean diameter (nm)	SD
0	269.2	138.886
1	257.9	132.045
2	288.7	164.007
3	279.4	144.712
5	300.1	183.071
7	319.2	206.194
14	297.9	124.255
21	285.0	166.983

28	275.2	140.340
35	273.4	131.494
42	293.8	168.028
49	320.7	206.212
56	282.0	159.900
63	276.9	147.844
70	297.1	167.948
77	294.5	209.386
84	371.0	277.773
91	303.5	178.487
112	332.6	190.603
119	328.6	192.207
126	373.9	236.310
133	342.3	225.246
140	337.1	199.210
147	348.3	226.038
154	362.1	230.607

Materials (“L80” Formulation): 16.82 mL DI water, 204 mg Lipoid E80, 0.3 mL glycerol, 0.18 mL propofol.

Time (d)	Mean diameter (nm)	SD
0	297.1	176.504
1	275.7	145.277
2	265.4	128.165
3	296.7	181.299
5	252.3	135.995
7	272.4	139.735
14	286.5	169.023
21	271.3	143.262
28	295.0	180.542
35	245.9	116.781
42	290.8	178.255
49	227.9	110.299
56	274.9	148.461
63	303.4	190.542
70	237.3	104.632
77	244.7	99.348
84	254.3	110.252

Materials: 16.82 mL normal saline, 420 mg M5diH10, 204 mg Lipoid E80, 0.18 mL propofol.

Time (d)	Mean diameter (nm)	SD
0	159.7	78.433
1	187.2	95.112
2	184.0	91.434
3	196.1	97.257
5	177.0	97.182
7	192.7	96.732
14	188.5	95.174
21	191.0	89.945
28	187.8	96.707
35	150.1	78.034
42	184.2	94.665
49	190.5	91.447
56	182.1	95.218
63	183.7	91.298
70	182.8	95.227
77	180.1	94.930
84	185.4	92.264

PFOB-stabilized formulations

Materials: 15.97 mL normal saline, 280 mg M1H10F8, 0.85 mL PFOB, 0.18 mL propofol.

Time (d)	Mean diameter (nm)	SD
0	221.2	75.444
1	264.6	79.130
2	285.3	87.296
3	307.1	94.597
5	309.2	103.882
7	315.0	114.339
14	355.6	136.546
21	361.8	151.595
28	376.4	141.907
35	413.7	172.505
42	375.0	135.390
49	384.9	160.514
56	363.6	146.518

63	414.9	174.262
70	394.4	144.748
77	421.8	192.321
84	Phase separated	

Materials: 15.12 mL normal saline, 280 mg M1H10F8, 1.7 mL PFOB, 0.18 mL propofol.

Time (d)	Mean diameter (nm)	SD
0	248.8	83.358
1	277.3	98.174
2	295.0	108.841
3	312.3	127.409
5	276.6	106.755
7	274.7	115.931
14	270.3	94.608
21	285.1	92.378
28	307.0	111.757
35	316.4	93.656
42	306.2	110.243
49	316.7	139.047
56	319.8	82.176
63	326.7	121.209
70	247.7	124.472
77	317.0	153.421
84	418.7	182.559
91	Phase separated	

Materials (“F8” Formulation): 13.42 mL normal saline, 280 mg M1H10F8, 3.4 mL PFOB, 0.18 mL propofol.

Time (d)	Mean diameter (nm)	SD
0	211.6	19.041
1	222.1	26.207
2	232.6	61.397
3	230.7	40.837
5	233.9	48.561
7	232.7	63.518

14	274.0	78.643
21	287.0	59.980
28	300.1	81.635
35	305.7	55.018
42	306.9	68.447
49	325.8	68.092
56	319.2	100.870
63	332.3	78.082
70	314.8	70.199
77	353.0	110.133
84	346.8	97.115
91	398.0	139.685
98	407.4	174.768
105	414.2	177.692
112	420.9	182.661
119	416.2	178.555
126	Phase separated	

Miktoarm surfactant formulations

Materials: 16.82 mL normal saline, 420 mg M2 μ H18F8, 0.18 mL propofol.

Time (d)	Mean Diameter (nm)	SD
0	223.1	95.714
1	212.1	85.698
2	216.3	94.305
3	217.1	95.072
5	223.7	93.716
7	227.7	91.747
14	224.8	98.686
21	224.5	93.407
28	224.2	96.859
35	222.7	92.869
42	225.5	102.813
49	219.5	100.737
56	162.1	77.947
63	227.7	99.723
70	208.7	94.968
77	224.0	102.359
84	231.4	102.755
91	220.9	106.491

98	228.1	111.991
105	233.6	108.377
112	237.7	115.530
119	232.9	108.309
126	237.4	115.594
133	218.0	100.286
140	228.9	106.663
147	240.6	126.820
154	241.1	126.810
160	229.0	106.242
168	233.3	104.292
177	230.2	94.629
182	239.5	117.848
189	246.3	130.796
196	226.1	111.923
203	259.4	140.706
210	248.0	132.172
217	264.6	145.770
224	250.3	127.919
230	248.9	130.947
237	246.0	124.250
244	259.5	131.551
252	261.9	138.794
259	247.2	134.494
266	251.0	133.778
278	270.3	150.829
280	294.5	180.498
287	236.0	115.084
295	237.9	118.722
299	245.9	118.031
306	274.3	151.714
327	256.5	146.202
332	267.9	141.187
338	285.7	170.278
351	292.2	189.325

Materials (“B8” Formulation): 16.82 mL normal saline, 420 mg M1 μ H10F8, 0.18 mL propofol.

Time (d)	Mean Diameter (nm)	SD
0	155.0	73.292
1	180.2	61.099
2	184.5	58.472
5	222.2	55.319

7	200.2	50.462
14	230.6	79.312
21	267.2	98.341
28	307.4	66.094
35	294.2	57.661
42	314.7	59.475
49	Phase separated	

A2.3.4 Propofol Emulsions – in vivo data

Diprivan® Data

Rat Weight (kg)	Dose (mg/kg)	Time at LORR (s)	Time at RORR (s)	Intralipid Dose (mL/kg)
0.263	5	0	0	
0.286	5	0	0	
0.273	5	19	35	
0.286	5	20	44	
0.290	5	22	53	
0.294	5	0	0	
0.259	5	0	0	
0.272	6.25	20	73	
0.289	6.25	19	83	
0.298	6.25	19	77	
0.256	6.25	18	102	
0.260	6.25	20	44	
0.282	6.25	18	84	
0.254	7.5	19	180	
0.289	7.5	18	173	
0.298	7.5	17	209	
0.262	7.5	13	124	
0.285	7.5	19	102	
0.270	10	18	355	
0.286	10	12	445	
0.304	10	10	512	
0.266	10	13	430	
0.278	10	0	0	
0.281	10	13	304	
0.302	15	8	755	
0.252	15	12	669	
0.299	15	10	675	
0.274	15	13	660	
0.288	15	12	585	
0.317	15	9	423	15
0.302	15	9	369	15

0.331	15	9	726	15
0.307	15	10	537	15
0.311	15	9	513	15
0.283	15	12	742	7.5
0.271	15	11	471	7.5
0.292	15	11	610	7.5
0.276	15	12	713	7.5
0.289	15	10	757	7.5
0.279	15	9	638	7.5
0.270	15	12	632	3.75
0.276	15	11	693	3.75
0.275	15	10	470	3.75
0.270	15	9	624	3.75
0.263	15	10	541	3.75
0.267	15	9	622	3.75
0.249	10	14	212	15
0.258	10	15	239	15
0.256	10	14	240	15
0.265	10	14	184	15
0.251	10	15	234	15
0.252	10	12	260	15
0.284	7.5	15	301	15
0.295	7.5	18	135	15
0.292	7.5	17	300	15
0.275	7.5	16	182	15
0.279	7.5	18	137	15
0.287	7.5	18	202	15

B8 Data

Rat Weight (kg)	Dose (mg/kg)	Time at LORR (s)	Time at RORR (s)	Intralipid Dose (mL/kg)
0.273	5	19	35	
0.279	5	0	0	
0.296	5	0	0	
0.293	5	0	0	
0.267	5	0	0	
0.291	5	0	0	
0.280	6.25	23	41	
0.299	6.25	22	56	
0.302	6.25	0	0	
0.296	6.25	24	66	
0.290	6.25	0	0	
0.273	6.25	0	0	

0.305	7.5	16	337	
0.281	7.5	13	336	
0.308	7.5	17	355	
0.265	7.5	0	0	
0.294	7.5	20	53	
0.264	7.5	23	57	
0.294	10	16	135	
0.297	10	18	244	
0.272	10	15	334	
0.291	10	18	150	
0.266	10	18	80	
0.272	15	9	497	
0.291	15	13	472	
0.298	15	10	607	
0.269	15	13	611	
0.289	15	14	556	
0.294	15	10	279	15
0.297	15	11	309	15
0.290	15	12	440	15
0.300	15	12	237	15
0.310	15	11	282	15
0.317	15	14	597	Saline 15 mL/kg
0.316	15	11	501	Saline 15 mL/kg
0.305	15	14	586	Saline 15 mL/kg
0.320	15	13	423	Saline 15 mL/kg
0.342	15	10	622	Saline 15 mL/kg
0.312	15	13	424	7.5
0.316	15	10	488	7.5
0.332	15	10	710	7.5
0.307	15	12	456	7.5
0.315	15	12	445	7.5
0.276	15	10	640	3.75
0.273	15	11	499	3.75
0.280	15	12	638	3.75
0.292	15	10	730	3.75
0.288	15	12	526	3.75
0.282	15	12	733	3.75
0.263	10	16	179	15
0.251	10	17	187	15
0.257	10	14	193	15

0.251	10	16	245	15
0.253	10	15	214	15
0.259	10	14	283	15
0.300	7.5	16	102	15
0.290	7.5	15	120	15
0.294	7.5	19	124	15
0.304	7.5	20	166	15
0.287	7.5	20	131	15
0.304	7.5	16	121	15

L3 data

Rat Weight (kg)	Dose (mg/kg)	Time at LORR (s)	Time at RORR (s)
0.273	5	0	0
0.288	5	0	0
0.290	5	0	0
0.255	5	0	0
0.302	5	21	30
0.272	6.25	0	0
0.276	6.25	0	0
0.294	6.25	0	0
0.295	6.25	0	0
0.297	6.25	23	44
0.263	6.25	0	0
0.283	6.25	0	0
0.264	7.5	21	71
0.293	7.5	19	93
0.294	7.5	17	65
0.294	7.5	18	91
0.261	7.5	0	0
0.257	7.5	0	0
0.283	7.5	19	72
0.278	10	16	204
0.287	10	13	218
0.296	10	13	214
0.261	10	14	300
0.289	10	16	165
0.282	15	9	516
0.296	15	9	558
0.295	15	14	581

0.290	15	12	504
0.270	15	14	614

F8 Data

Rat Weight (kg)	Dose (mg/kg)	Time at LORR (s)	Time at RORR (s)
0.303	5	0	0
0.333	5	0	0
0.288	5	0	0
0.300	6.25	20	37
0.313	6.25	0	0
0.304	6.25	0	0
0.297	7.5	0	0
0.315	7.5	21	45
0.298	7.5	22	54
0.312	10	20	121
0.296	10	16	378
0.291	10	20	185
0.317	15	15	1709
0.297	15	12	560
0.315	15	10	982
0.337	15	13	1002

L80 Data

Rat Weight (kg)	Dose (mg/kg)	Time at LORR (s)	Time at RORR (s)
0.314	5	0	0
0.307	10	0	0
0.259	15	0	0
0.267	15	0	0
0.265	15	0	0
0.263	15	0	0
0.268	15	0	0
0.265	15	0	0

A2.3.5 Paclitaxel Emulsions

Materials: 14 mL normal saline, 401 mg M2F8-O-H18, 3 mL 2-octyldodecan-1-ol, 100 mg paclitaxel.

Time (d)	Mean Diameter (nm)	SD
0	106.4	9.787
1	112.7	15.446
2	117.2	9.377
3	122.1	16.482
5	129.0	24.775
7	133.1	21.688
14	157.4	23.924
21	Phase separated	

